UNIVERSITY OF GHANA

COLLEGE OF BASIC AND APPLIED SCIENCES

PETROLOGY AND GEOCHEMISTRY OF CLASTIC ROCKS OF THE TAMALE-OBOSUM AND OTI-PENDJARI GROUPS, VOLTAIAN SUPERGROUP, GHANA: IMPLICATIONS FOR PROVENANCE

BY

JENNIFER EDZORDZINAM AGBETSOAMEDO

(ID. NO.10247055)

THIS THESIS IS SUBMITTED TO THE UNIVERSITY OF GHANA, LEGON IN PARTIAL FULFILLMENT OF THE REQUIREMENT FOR THE AWARD OF PHD IN EARTH SCIENCE DEGREE

(NOVEMBER 2024)

DECLARATION

I affirm that this thesis represents my own work and research, carried out under guidance and supervision of the underlisted signatories. I assert that it does not contain any unauthorized or previously published material, except where acknowledged.

November 05, 2024

Jennifer E. Agbetsoamedo **…….** **Date**

(Student) **Signature**

November 05, 2024

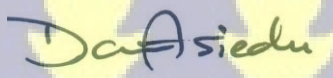

Prof. Daniel Asiedu **……** **November 05, 2024**

(Principal Supervisor) **Signature** **Date**

November 05, 2024

Prof . Chris Yao Anani **……** **Date**

(Co-Supervisor) **Signature**

November 05, 2024

Dr. Zubair Jinnah **……** **Date**

(Co-supervisor) **Signature**

ABSTRACT

The Voltaian Basin of Ghana, one of the largest Neoproterozoic sedimentary basins in West Africa, preserves a thick stratigraphic succession that remains poorly constrained in terms of provenance, depositional history, and tectonic evolution. In particular, the Oti-Pendjari and Tamale-Obosum Groups are minimally studied, limiting their integration into models of West African craton evolution and Pan-African orogenesis. This study addresses these uncertainties by applying an integrated petrographic, geochemical, heavy mineral, and isotopic approach to reconstruct provenance, weathering intensity, and tectonic setting, thereby refining the geodynamic framework of the Voltaian Supergroup.

Petrographic data from twelve lithostratigraphic units reveal that the Tamale-Obosum Group consists largely of quartzose sandstones with subordinate litharenites, while the Oti-Pendjari Group is dominated by arkosic and lithic sandstones. Provenance analysis indicates that Tamale-Obosum sediments were derived mainly from felsic plutonic rocks with minor metasedimentary inputs, whereas the Oti-Pendjari Group records contributions from volcanic arcs, recycled terranes, and glaciogenic successions. Detrital compositions suggest transitional arc, cratonic interior, and recycled orogenic sources for different formations.

Whole-rock geochemistry highlights significant compositional variation. Quartz arenites are SiO_2-rich and chemically mature, reflecting intense weathering. Wackes and litharenites display higher Al_2O_3, Fe_2O_3, and alkali contents, consistent with feldspathic and mafic inputs. Major oxide correlations confirm quartz–clay trade-offs, while depletion and enrichment trends relative to Upper Continental Crust (UCC) distinguish feldspathic versus mafic contributions. Weathering intensity assessed using the Chemical Index of Alteration (CIA), ranges from strong alteration in the Tamale Sandstone and Undivided Obosum formations to weaker weathering in the Densubon

Sandstone and Sang Conglomerates. Combined CIA–Index of Compositional Variability (ICV) values reveal that the Tamale Formation was derived from uniform felsic sources under intense weathering, whereas other units reflect mixed sources and moderate alteration.

Trace and rare earth element (REE) patterns further refine provenance. Enrichment in light REEs (LREEs) and large ion lithophile elements (LILEs) indicate felsic inputs, whereas localized enrichment in ferromagnesian trace elements (Cr, Ni, Co) suggests mafic or recycled sedimentary contributions. Negative Eu anomalies in most formations reflect feldspar depletion, while occasional positive anomalies in younger units suggest feldspar input or sediment mixing.

Tectonic discrimination diagrams differentiate depositional settings: the Tamale and Undivided Obosum formations plot within passive margin fields, while the Densubon and Sang Conglomerates display signatures of active continental margins or island arcs. The Oti-Pendjari Group records a transition from stable continental sedimentation in its older members to arc- and rift-influenced deposition in younger units.

Isotopic analyses provide additional constraints. Nd and Sr isotopic compositions confirm continental crustal derivation, with the Tamale-Obosum Group reflecting upper crustal sources linked to Birimian and Kwahu- terranes. The Oti-Pendjari Group, by contrast, records mixed contributions from Proterozoic crust and Pan-African belt rocks, consistent with foreland basin development during the Dahomeyide orogeny (\~590 Ma). Sm–Nd depleted mantle model ages (TDM) support derivation from Proterozoic sources and indicate sediment recycling during Pan-African tectonism.

Overall, the Oti-Pendjari and Tamale-Obosum Groups represent complementary tectono-sedimentary records within the Voltaian Basin. The Tamale-Obosum Group reflects felsic plutonic sources, strong weathering, and deposition in mixed passive and active margin environments, whereas the Oti-Pendjari Group captures volcanic arc erosion, rift tectonism, and foreland basin sedimentation. These results demonstrate that the Voltaian Basin evolved through dynamic interactions between the West African Craton and Pan-African mobile belts, contributing to regional models of crustal recycling, sedimentary basin development, and Neoproterozoic geodynamics.

DEDICATION

I dedicate this thesis to God Almighty, to my parents, Comfort Ami Kuevogah and Godwin L.K. Agbetsoamedo; and to my husband and children, Nunana, Elinam and Kekeli, for commencing and completing the journey with me.

ACKNOWLEDGEMENT

First and foremost, I would like to thank God Almighty for his guidance and support throughout the whole PhD journey. I am grateful for His provision, sustenance and the strength to successfully complete the program. I am most grateful to my sponsors: University of Ghana Faculty Development Fund, Building a New Generation of Academics in Africa" (BANGA-Africa) Project II., West African Exploration Initiative (WAXI) III and PGS through the GNPC Research Chair at the University of Ghana, for the funding opportunities made available to me throughout the research program. I am eternally grateful for their immense support, without which this research program would have been unsuccessful.

I am deeply grateful to the many scholars and researchers whose works have been essential to this study. Their contributions, referenced throughout this thesis, have significantly shaped my understanding of geochemical and petrological contributions to understanding provenance implications of sedimentary rocks. I would also like to thank my supervisors for their invaluable support and guidance, which has been crucial to the successful completion of this project.

Furthermore, I would like to acknowledge the immense support of my family throughout the timeline of the PhD program. They have been my strong pillar and backbone, and I appreciate all the sacrifices made to help me find time to study for my PhD program. I acknowledge all my friends and colleagues for their counsel and assistance which came in diverse forms and times.

Finally, I would like to acknowledge the Department of Earth Science for granting me the opportunity to study for this program and providing some analytical instruments for the research undertaken. I am grateful to the technicians for their immense support and guidance during all the laboratory sessions run at the department.

1. Table of Contents

LIST OF FIGURES

LIST OF TABLES

CHAPTER 1

INTRODUCTION

1.1 Background

Petrology, the scientific study of rocks, is a cornerstone of geological research that provides critical insights into the Earth's formation, evolution, and composition. By examining the mineral assemblage, texture, and formation conditions of rocks, petrologists can decipher the complex geological processes that have shaped our planet, including plate tectonics, magmatism, metamorphism, and sedimentation (Blatt et al., 1980; Boggs, 2009). Petrological investigations are essential for understanding the origin and distribution of valuable mineral resources, such as ore deposits and gemstones (Winter, 2010; Rollinson, 2021).. Additionally, petrological studies contribute to the development of new materials and technologies, such as ceramics, construction materials, and energy resources (Deer et al. 1992). Petrology plays a pivotal role in advancing our knowledge of the Earth's dynamic systems and informing sustainable resource management.

Provenance studies, which aim to determine the source region of sedimentary materials, are fundamental in understanding the geological evolution of sedimentary basins (Dickinson & Suczek, 1979; Weltje & von Eynatten, 2004). Petrology and geochemistry, as interrelated disciplines, provide essential tools for unraveling the complex processes involved in sediment production, transportation, and deposition (Taylor & McLennan, 1985; Cullers, 1995). By examining the mineralogical, petrographic, and geochemical characteristics of sedimentary rocks, researchers can reconstruct the nature of the source terrain, the weathering and erosion processes, and the depositional environments of the study interval (McLennan et al., 1993; Garzanti et al., 2007; Moradi et al., 2016).

Petrology, the study of rocks, offers invaluable insights into sediment provenance (Dickinson, 1985; Pettijohn et al., 1987). The analysis of mineral composition, texture, and structure of sedimentary rocks provides crucial information about the source lithologies (Blatt, Middleton & Murray, 1980). For instance, the presence of specific minerals such as zircon, tourmaline, and garnet can indicate the erosion of granite, igneous, or metamorphic rocks, respectively (Morton, 1985; Mange & Maurer, 1992). Moreover, the study of sedimentary structures and textures can help decipher depositional environments and transport processes, which can indirectly provide clues about the source region (Reading, 1996; Nichols, 2009).

Geochemistry plays a vital role in petrology, particularly in provenance studies of sedimentary rocks. By analyzing trace elements and isotopes, researchers can effectively trace the origins of sediments and understand their geological history. Trace elements and rare earth elements (REEs), consist of high field strength elements (HFSEs), which are all relatively immobile during weathering, making them reliable indicators of source rock composition(Gurumurthy, 2024). Studies have shown that the geochemical signatures of sediments can reveal their provenance, as demonstrated in the Nethravati River, where elemental compositions indicated a homogenous lithology from Peninsular Gneiss(Gurumurthy, 2024). Isotope geochemistry, particularly Sr and Nd isotopes, provides insights into the age and tectonic setting of source terrains, enhancing the understanding of sedimentary processes(Babu et al., 2023). The integration of isotopic data with trace element analysis allows for a more robust provenance determination, as seen in various sedimentary systems(Babu et al., 2023)(Zhu, 2023). While geochemistry significantly aids in provenance studies, it is essential to consider the complexities introduced by post-depositional processes, which can alter the original geochemical signatures of sediments (Babu et al., 2023).

The integration of petrological and geochemical approaches is essential for effective provenance studies, as each method provides complementary insights into sediment characteristics and origins (Taylor & McLennan, 1985; Rollinson, 1993; Cox & Lowe, 1995). Petrographic analysis serves as a qualitative framework, allowing for the detailed examination of mineral assemblages and sedimentary structures (Dickinson, 1985; Pettijohn et al., 1987; Boggs, 2009). This qualitative data is crucial for understanding the physical characteristics of sediments, such as grain size and sorting, which can indicate the energy conditions of the depositional environment (Maravelis et al., 2020). On the other hand, geochemical data provides quantitative constraints that are vital for interpreting source rock composition and tectonic settings. For instance, the chemical signatures of sediments can reveal the nature of their source rocks, including their mineralogical composition and the processes they have undergone during weathering and transport (Li et al., 2016; Abubakar et al., 2019).

A notable example of the synergy between petrographic and geochemical methods is the identification of detrital zircon grains with specific age populations. Petrographic analysis can effectively isolate these zircon grains, while U-Pb geochronology can be employed to determine the timing of source rock formation, thereby providing a temporal context for sediment provenance (Spalletti et al., 2008; Armstrong-Altrin et al., 2018). This dual approach not only enhances the accuracy of provenance assessments but also allows for a more nuanced understanding of the geological history of sedimentary deposits. For instance, studies have shown that the combination of detrital zircon dating and geochemical analysis can elucidate the tectonic evolution of sedimentary basins, revealing insights into past tectonic events and sedimentation processes (Armstrong-Altrin et al., 2018).

While petrology and geochemistry have made significant contributions to provenance studies, several challenges remain. These include the complexities of weathering and diagenesis, which can alter the primary geochemical signature of sediments (Nesbitt & Young, 1982; McLennan, 1989; Taylor & McLennan, 1985), and the potential for multiple sources contributing to a single sedimentary deposit (Dickinson, 1985; Cox & Lowe, 1995; Garzanti et al., 2007). Additionally, the development of new analytical techniques, such as heavy mineral varietal studies and radiogenic isotopic studies (i.e. Samarium neodymium and rubidium strontium isotopic studies), offers exciting opportunities for research (Lubbe et al., 2016; Mantovanelli et al., 2018).

Heavy minerals, such as zircon, rutile, garnet, and tourmaline, are known for their resistance to weathering and transport processes, making them valuable indicators in provenance studies (Morton, 1985; Mange & Maurer, 1992; Garzanti & Andò, 2007). The analysis of these minerals provides critical insights into the source rocks and the transport mechanisms that have influenced sediment deposition. Each rock type is characterized by distinct heavy mineral assemblages, which can be identified to infer the types of rocks contributing to the sedimentary deposits (Morton & Hallsworth, 1994; Garzanti et al., 2009). For instance, the presence of specific heavy minerals can indicate the geological environments from which the sediments were derived, such as metamorphic or volcanic terrains (Morton & Chenery, 2009; Mahanta et al., 2019).

The composition and abundance of heavy minerals are particularly informative regarding the distance and direction of sediment transport. Variations in mineral stability and hydraulic sorting can be used to estimate transport pathways, with more stable minerals like zircon and tourmaline often surviving long-distance transport (Morton, 1985; Morton & Hallsworth, 1999). Certain minerals, such as tourmaline, are also associated with specific geological settings (e.g., granitic and metamorphic terranes), making them especially useful for reconstructing sediment provenance

and depositional history (Deer et al., 1992; Mange & Wright, 2007). For example, studies have shown that heavy mineral assemblages can reflect the geological characteristics of their source areas, as these minerals retain their chemical signatures through weathering and transport (Yang et al., 2009; Zhu & Zeng, 2021). This stability allows researchers to utilize heavy minerals as proxies for understanding sediment provenance, as they can indicate not only the source rock types but also the processes involved in sediment transport and deposition (Wong et al., 2013; Hussain et al., 2004).

Moreover, the analysis of heavy minerals can reveal the degree of weathering that sediments have undergone, which is crucial for interpreting their geological history. The relative abundance of angular versus rounded heavy minerals provides valuable insights into transport processes and source-to-sink relationships. Angular minerals typically suggest derivation from a proximal source with minimal reworking, whereas rounded minerals indicate longer transport distances and extended sediment recycling (Hubert, 1962; Morton, 1985; Morton & Hallsworth, 1994). In addition, the degree of abrasion and dissolution of less stable minerals such as garnet and amphibole can be used as indicators of both transport distance and intensity of chemical weathering (Morton & Hallsworth, 1999; Mange & Wright, 2007; Bela, 2024). Additionally, the study of heavy mineral assemblages can help identify changes in sedimentary environments over time, thereby contributing to a more comprehensive understanding of past geological processes (Mahanta et al., 2017; Solís-Castillo et al., 2013; Akaram et al., 2015).

Framework grains, including quartz, feldspar, and lithic fragments, constitute the bulk of sandstones and are central to provenance studies. Petrographic analysis of these grains provides valuable information about sediment sources and post-depositional history. Identification of framework minerals allows determination of source rock types, such as igneous, metamorphic, or

sedimentary origins (Folk, 1980; Pettijohn et al., 1987). Grain size, shape, and sorting provide insights into transport history, distinguishing between long-distance transport and more proximal sources (Blatt et al., 1972; Boggs, 2009). Furthermore, petrography helps evaluate diagenetic changes such as cementation and compaction, which can significantly alter the original textural and compositional signatures of sandstones (Worden & Burley, 2003; Morad et al., 2000).

Radiogenic isotopes, particularly Sm–Nd and Rb–Sr systems, are powerful tools in provenance studies because they provide age constraints and trace the evolution of source rocks. Sm–Nd and Rb–Sr isotopic data help determine the crustal residence ages of sediments, thereby constraining the age of the source rocks and the timing of crustal growth (DePaolo, 1988; McCulloch & Wasserburg, 1978). Different rock types, such as felsic continental crust versus mafic oceanic crust, display distinct isotopic signatures, which can be compared with sandstone data to pinpoint source terranes (Taylor & McLennan, 1985; Faure & Mensing, 2005). Isotopic ratios also provide insights into tectonic settings, distinguishing sediments derived from evolved continental crust, juvenile arc terranes, or reworked orogenic belts (Dickin, 2005; Goldstein et al., 1984).

In summary, combining heavy mineral studies, framework grains petrology, and isotopic geochemistry provides a comprehensive approach to unravel the provenance of the Voltaian Supergroup. These methods allow us to reconstruct the geological history, paleoenvironments, and tectonic processes that shaped this intriguing sedimentary sequence.

1.2 Problem Statement

Despite numerous studies on the Voltaian Supergroup, a comprehensive understanding of its provenance remains elusive. While previous investigations have provided valuable insights into the lithological composition and depositional environments of the succession, the precise nature

and evolution of the source terrane remain poorly constrained. In addition, majority of the research carried out on the Voltaian Supergroup has focused on the very exposed lower Kwahu-Bombouka group of the Supergroup, leaving very limited to no research outcomes on the Middle (Oti-Pendjari) and Upper (Tamale-Obosum) Groups. Thus, there exists a gap of information in terms of the geochemistry and petrology of the sediments that constitute these groups.

The limited application of advanced geochemical and petrological techniques, coupled with the complex geological history of the region, has also hindered the development of a robust provenance model for the Voltaian Supergroup. Consequently, there is a critical need for more detailed and integrated studies to elucidate the provenance of these sediments and to unravel the tectonic and climatic conditions that prevailed during their deposition. Addressing these challenges through a comprehensive and multidisciplinary approach is essential for advancing our knowledge of the Voltaian Supergroup and its implications for the regional geological evolution.

1.3 Justification

Petrographic analysis of framework grains and heavy minerals offers a fundamental approach to unraveling the provenance of sedimentary rocks such as those within the Voltaian Supergroup. This methodology provides crucial insights into the nature of the source rocks, the intensity of weathering, and the transportation processes involved. Framework grain analysis allows for the identification of lithological components like quartz, feldspar, and lithic fragments, providing direct clues about the source rock composition (Marsaglia et al. 1995; Augustsson, 2021; Sahraeyan, M. and Bahrami, M., 2012). The textural characteristics of these grains, such as roundness and sphericity, can offer additional information about the sedimentary processes and transport distances (Chmielowska et al. 2021). Baiyegunhi et al. 2020; Lupin & Hampson, 2020). Heavy mineral analysis complements framework grain studies by focusing on resistant minerals

that retain information about the source rock environment (Mange & Wright, 2007; Mange & Maurer, 2012; Garzanti & Andò, 2007). The presence or absence of specific heavy minerals, such as zircon, tourmaline, and garnet, can be used to discriminate between different source rock lithologies and tectonic settings (Mange & Morton, 2007). By integrating both framework grain and heavy mineral analysis, a more comprehensive understanding of the Voltaian Supergroup's provenance can be achieved (Kwayisi et al. 2022; Kuchenbecker et al. 2016; Osae et al. 2006).

Sm-Nd and Rb-Sr isotope systems offer powerful tools for unraveling the provenance of sedimentary rocks such as those found in the Voltaian Supergroup. These isotopic systems provide critical insights into the age, tectonic setting, and weathering history of the source rocks. By analyzing the Sm-Nd isotopic composition of whole-rock samples, it is possible to estimate the age and crustal residence time of the source materials (DePaolo, 2012; Chen & Yang, 2000; Brems et al. 2013). The Nd isotope ratio (εNd) can differentiate between crustal and mantle-derived materials, providing valuable constraints on the tectonic setting of the source region (Zhang et al. 2007; Kaur et al. 2009).

Similarly, Rb-Sr isotope analysis can be used to assess the degree of weathering and the influence of marine environments on the sedimentary system (McDougall & Watkins, 2006). By comparing the isotopic composition of sedimentary rocks to potential source rocks, it is possible to reconstruct the evolution of the source terrain and the processes that affected the sediment during transportation and deposition. Integrating Sm-Nd and Rb-Sr isotope data with other geochemical and petrological information will provide a comprehensive understanding of the Voltaian Supergroup's provenance.

1.4 Objectives of the study

The Voltaian Supergroup, the primary geological unit within the Volta basin, exhibits complex stratigraphy with three main groups: the Kwahu-Bombouaka, Oti-Pendjari and Tamale-Obosum Groups (Carney et al,2008, 2010; Abu et al. 2020; Vignoli et al. 2020). Irrespective of the economic potential of the basin, its development is hindered by stratigraphic uncertainties, poor outcrop exposure, and limited exploration data. To address these challenges, an integrated approach combining mineralogical (heavy mineral studies) and geochemical (whole-rock and isotopic) analyses is proposed.

The overarching aim of this research is to reconstruct the provenance of the Tamale-Obosum and Oti-Pendjari Groups of the Voltaian Supergroup to refine interpretations of the basin's depositional and tectonostratigraphic evolution.

To achieve this goal, the study pursued the following specific objectives:

1. To characterize and classify the sedimentary rocks of the Tamale-Obosum and Oti-Pendjari Groups using petrographic and geochemical approaches.
2. To identify and constrain the nature of the source lithologies that supplied detritus to these formations.
3. To interpret the depositional and tectonic settings of the formations based on integrated petrographic, geochemical, and isotopic evidence.
4. To determine the crustal residence ages and temporal framework of the source rocks through Sm-Nd and Rb-Sr isotopic systematics.

1.5 The study area

1.5.1 Location

The study area falls within the Voltaian Basin, which is centrally located in Ghana, covering about 40% of the country's land area and extending into parts of Togo and Burkina Faso. It occupies much of central and northern Ghana (Figure 1.2), bounded by the Birimian terranes of the West African Craton to the west and south, and by the Pan-African Dahomeyide and Togo orogenic belts to the east. The basin stretches from the Volta Region in the south through the Northern and Upper Regions, with the White and Black Volta rivers draining much of its interior.

Ghana is bordered to the northwest and north by Burkina Faso, to the east by Togo, to the south by the Atlantic Ocean, and to the west by Côte d'Ivoire. The study area covers parts of the following regions: Ashanti (Capital: Kumasi), Brong Ahafo (capital: Sunyani), Eastern (capital: Koforidua), Northern (capital: Tamale), Volta (capital: Ho), Savannah (capital: Damongo), Bono East (capital: Techiman), Oti (Capital: Dambai), North-East (capital: Nalerigu).

1.5.2 Climate and vegetation

In the savanna, north of the Kwahu Plateau, there are two seasons—a dry season from November to March, with hot days and cool nights under clear skies, and a wet season that reaches its peak in August and September. The mean annual precipitation is between 40 and 55 inches (1,020 and 1,400 mm), but there is a marked moisture deficit because of the long, intensely dry season that follows. In the southern forest country, where the annual mean precipitation from north to south has a range of about 50 to 86 inches (1,270 to 2,180 mm), there are two rainy seasons—one from April to July and a lesser one from September to November—and two relatively dry periods that

occur during the harmattan season, from December to February, and in August, which is a cool, misty month along the coast (https://www.britannica.com/place/Ghana).

1.5.3 Drainage

Ghana's primary drainage system is the Volta River basin, featuring Lake Volta and its tributaries: the Black, White, and Oti rivers. Separated from this system by the Kwahu Plateau, the country's southern region is drained by rivers like the Pra, Ankobra, and Tano, which flow directly into the Atlantic Ocean. A unique feature is Lake Bosumtwi, a crater lake south of Kumasi with no river outlet. Coastal lagoons, formed at the mouths of smaller rivers, are prevalent along the Ghanaian coastline (https://www.britannica.com/place/Ghana).

1.5.4 Geology of the study area

The Neoproterozoic Voltaian sedimentary basin of Ghana is a much smaller version of the sedimentary cover sequences of the West African craton (Figure 1.1). The basin is located on the eastern margin of the Man-Leo Shield and has a thickness of ~5 km, made of variations of sandstones, mudstones and some surbodinate limestone units (Junner and Hirst, 1946; Bozhko, 2008; Annan- Yorke, 1971; Affaton et al., 1980; Affaton, 1990). The Voltaian strata generally are undisturbed, however, the eastern margin of the basin has been affected by Pan-African (~600 Ma) deformation thus resulting in much steeper dips. Some portions of the rocks of the Volta basin have been overthrust by metasedimentary rocks of the Buem and Togo (or Atacora) structural units that belong to the Dahomeyide orogen. The Togo and Buem structural units however are strongly deformed and thus show variable grades of metamorphism in their textural fabrics. Typical of the higher-grade metamorphism is the occurrence of large tectonic lenses of mafic and ultramafic rocks, of eclogite and granulite facies. (Affaton, 1990; Attoh, 1998; Attoh, 1990; Trompette, 1994;

Agbossoumondé et al., 2001, 2004). The higher-grade rocks form part of the Trans-Saharan suture zone that separates the West African craton from the Pan-African orogen to the east (Deynoux et al., 2006). Over the years, the detailed stratigraphy of the Volta basin has been under varying debates due to the limited exposure of the rocks of the Voltaian Supergroup. Notwithstanding, a three-group division has generally been accepted over the years with slight variations in the names resulting from the francophone and Anglophone authors. The lower, Kwahu-Bombouaka Group (estimated maximal thickness ~1500 m) consists mainly of coarse-grained quartzitic and feldspathic sandstones. It is unconformably overlain by the Oti-Pendjari Group (~3000 m) which has tilloid beds and limestone at its base and consists mainly of shales and greywackes. The Oti Group is unconformably overlain by the Tamale-Obosum Group (~1000 m) which is largely composed of quartzitic and feldspathic sandstones of variable grain sizes (Carney et al., 2010). The three groups have been differently subdivided into formations by different authors.

Geochronological studies have yielded varying age estimates. Rb-Sr and K-Ar dating suggest depositional ages of around 1000 Ma for the Bombouaka Group, 660 Ma for the Oti Group, and 620 Ma for the Obosum Group (Clauer, 1976; Bozhko et al., 1971). However, more recent Lu-Hf dating on phosphorites from the Oti Group indicates a younger age of 576 ± 13 Ma (Barfod et al., 2004). The peak of Dahomeyide metamorphism is dated at approximately 612 ± 1 Ma (Affaton et al., 2000) and 603 ± 5 Ma (Hirdes and Davis, 2002), with thrusting and exhumation of the suture zone nappes occurring around 580 Ma (Attoh et al., 1997).

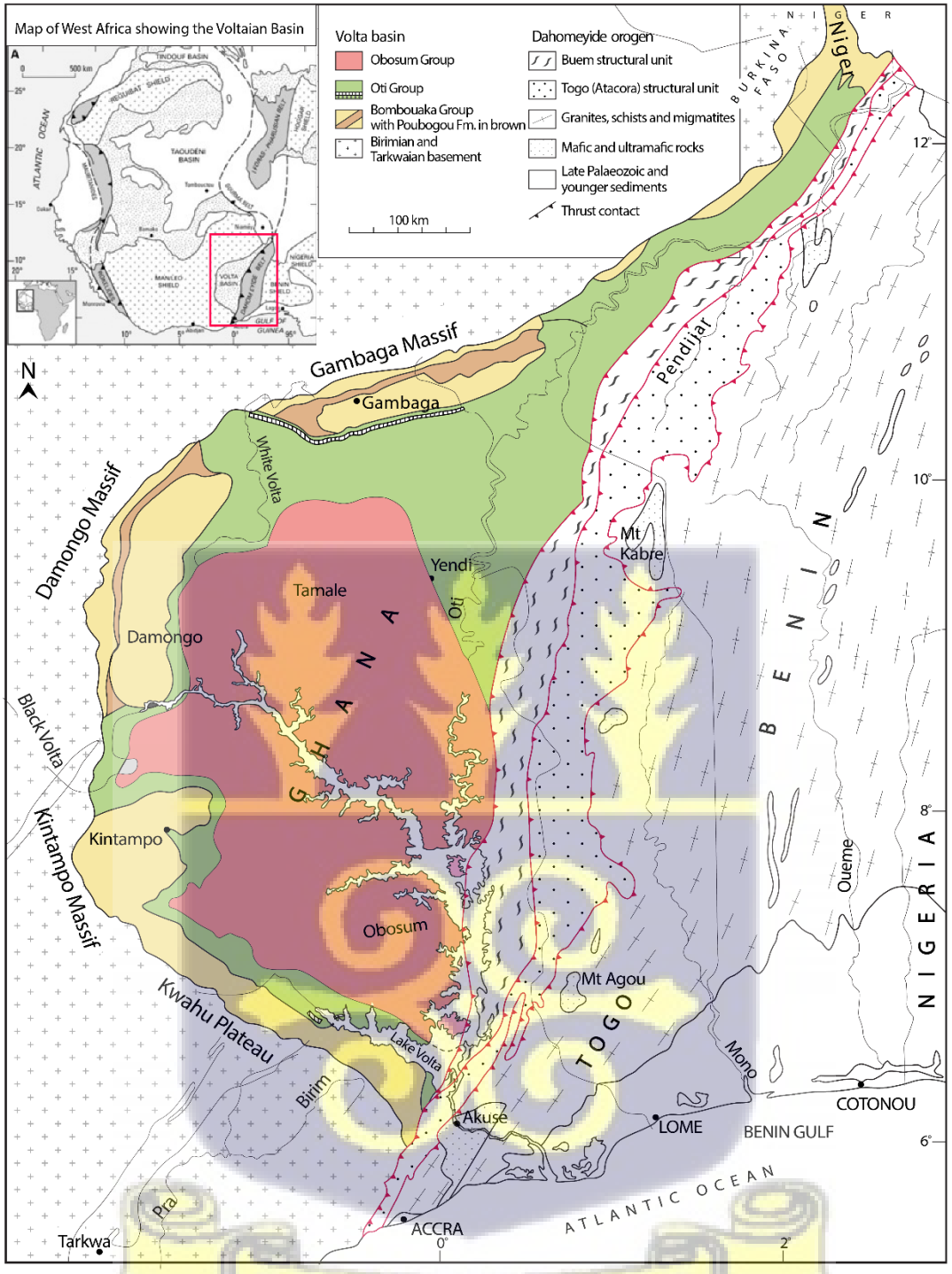

Figure 1.1. Geological sketch map of West Africa showing the Voltaian Supergroup in the Volta sedimentary basin (After Carney 2010).

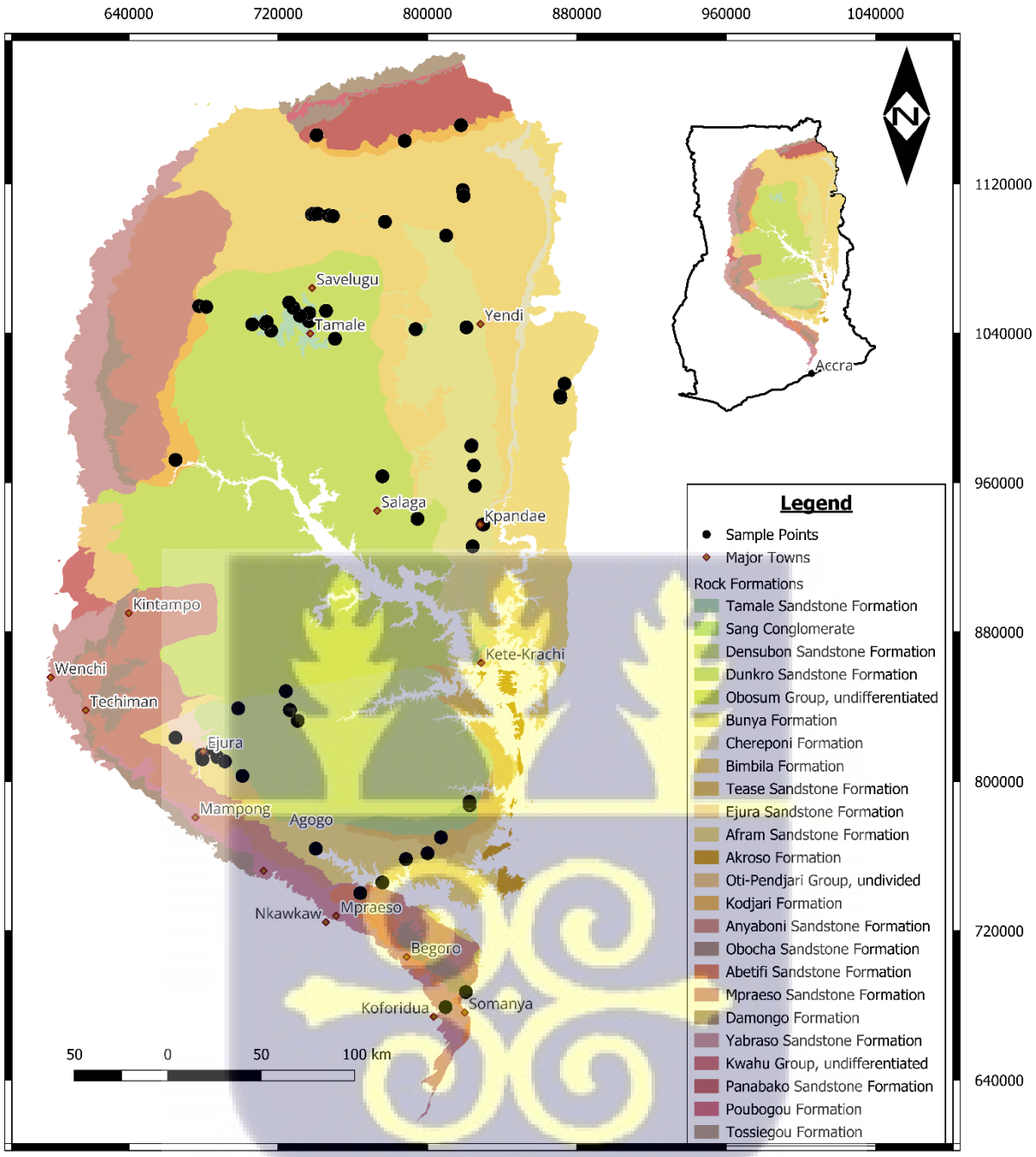

Figure 1.2. Simplified geological map of the Voltaian Supergroup of the Volta Sedimentary Basin in Ghana after Carney 2010, showing sample location points.

1.6 Outline of the chapters

Chapter 1 introduces the background of this study, outlining some previous findings and reportage leading to interest in the research area and further speaks to the scope of the research by identifying the objectives to be undertaken.

In the second chapter, literature on stratigraphy, tectonic evolution and paleoclimate is reviewed substantively leading to a buildup of the conceptual and theoretical framework of the study. Pertinent literature on the methodological approaches of employing heavy mineral analyses, whole rock and isotopic geochemistry for provenance studies is also to be reviewed.

Further in Chapter 3, the various methods adopted for the research study, commencing with the study area selection through sample collection, preparation and analyses using the gravity method separation of heavy minerals, identification of mineral phases using the XRD, SEM, optical microscopes, measurements of the major, minor, trace and rare earth elements using the ICP-MS & XRF instruments, measurements of the isotopic compositions using the LA-ICP-MS and SHRIMPS and finally analyzing the data employing the use of softwares such as Geosoft, Deltagraph, Pelcon-pointcounter and Microsoft excel .

Chapter 4 elaborates the results obtained from the various methodologies adopted in the previous chapter. The results for all the analyses carried out on the raw data obtained from the instrumental measurements will also be captured in this chapter.

Chapter 5 presents discussions on all the data gathered from the instrumental measurements and analytical plots (i.e. discrimination diagrams and charts). This chapter highlights the deductions and reasonings behind all the datasets collected from the various analyses. The efficacy of the

varied methodologies as tools for investigating the provenance of the formations of the Voltaian Supergroup is approved or disproved in this chapter.

Chapter 6 concludes on the discussions tailored in the previous chapter. It also enumerates the limitations encountered during this research project and further goes on to suggest some recommendations for subsequent or follow-up research projects in line with this research area.

CHAPTER 2

2. LITERATURE REVIEW

2.1 Whole-Rock Geochemistry

Whole-rock geochemistry is a fundamental analytical technique in Earth Sciences that involves determining the elemental composition of rock samples. By quantifying major, minor, and trace elements, geochemists can decipher the petrogenetic processes, provenance, and geological history encoded within rocks (Castro et al. 2003; Hamann et al. 2016; Urrutia-Fucugauchi et al. 2021). Advanced instrumental methods are employed for modern whole-rock geochemical analysis. Some examples of these methods are outlined below:

X-Ray Fluorescence (XRF) is a non-destructive analytical technique that employs X-ray bombardment to excite electrons in atoms within a sample, causing the emission of characteristic fluorescent radiation. The energy and intensity of this radiation are then measured to quantify the abundance of major and some minor elements within the rock sample (Potts & Webb, 1992; Jenkins, 1999; Van Grieken & Markowicz, 2002).

Inductively Coupled Plasma–Mass Spectrometry (ICP-MS) is a highly sensitive technique in which rock samples are dissolved and introduced into an inductively coupled plasma (ICP) source. The extremely high temperatures of the plasma cause element ionization, and the resulting ions are separated and measured by a mass spectrometer. ICP-MS enables precise determination of trace element abundances in rock samples, offering unparalleled sensitivity for a wide range of elements (Houk, 1986; Jarvis, 1988; Eggins, 2003).

Instrumental Neutron Activation Analysis (INAA) utilizes neutron irradiation of the rock sample to induce radioactivity in specific elements. The characteristic decay patterns and energies of the emitted radiation are then measured to identify and quantify elemental abundances. INAA provides a complementary approach, especially valuable for elements that are difficult to analyze using other techniques such as XRF or ICP-MS, either because of low abundance or spectral interferences (De Corte, 1987; Glascock, 1992; Magyari et al., 1994).

Whole-rock geochemistry finds application in a broad range of geological investigations, providing valuable constraints on various processes:

- Magma Genesis and Differentiation**:** By analyzing the major and trace element compositions of igneous rocks, researchers can infer the composition of their parental magmas and the differentiation processes (e.g., fractional crystallization) that led to their formation (Wilson, 1989; Spandler et al. 2003; Asmerom et al. 2005; Hartono et al. 2008**).** For example, enrichment of incompatible elements (elements less readily incorporated into crystal structures) can be used to fingerprint these differentiation processes.
- Tectonic Setting Discrimination: The geochemical signatures of igneous rocks can be used to discriminate between different tectonic settings, such as mid-ocean ridges, subduction zones, and continental rift zones **(**Pearce et al., 1984; Petrelli & Perugini, 2016; Ueki et al. 2018; Han et al. 2019; Khassen et al. 2020;**).** Specific element ratio plots, like La/Yb or Nb/Ta, have been established to fingerprint the tectonic environment where the magma originated.
- Metamorphic Processes: The chemical changes associated with metamorphism can be traced by analyzing the whole-rock geochemistry of metamorphic rocks. For example, the

mobility of certain elements during metamorphic dehydration reactions can provide valuable information about the metamorphic grade and pressure-temperature conditions experienced by the rock (Winter, 2001; McLellan et al. 2005; Spear & Pyle, 2010).

- Sedimentary Provenance: The geochemical signature of a sedimentary rock can reflect the composition of its source region. By comparing the major and trace element abundances of sediments with potential source rocks, researchers can gain insights into the provenance and weathering history of the sediments (McLennan, 2001; Taylor & McLennan, 1985; 2001**).**
- Paleoenvironmental reconstruction can be achieved through trace element compositions of sedimentary rocks, with specific ratios and enrichments serving as proxies for salinity, redox state, and productivity (Algeo & Lyons, 2006; Tribovillard et al., 2006; Ikhane et al. 2014; Wei & Algeo, 2020; Gregory, 2020; Yao, 2023).

Whole-rock geochemistry remains a cornerstone of Earth Science research due to its versatility and quantitative nature. Techniques such as XRF and ICP-MS provide precise elemental data enabling rigorous comparative studies and quantitative petrogenetic modeling (Rollinson, 1993; Jenner, 1996; Pearce, 2014; Rollinson & Pease, 2021). Applicable to a wide range of rock types, this approach yields invaluable insights into diverse geological processes. By deciphering the geochemical signatures preserved within rocks, whole-rock geochemistry offers a powerful tool for reconstructing past geological environments and unraveling Earth's history, even in the absence of direct observation. (Ahmed et al., 2013; Norman et al. 2003; Göçmengil et al. 2021).

2.2 Provenance Studies

Provenance in geoscience refers to the origin of sedimentary materials, including the nature of the source rocks, their geographic location, and the processes of transport and deposition, which together allow reconstruction of paleogeography, tectonic setting, and weathering conditions (Dickinson & Suczek, 1979; Dickinson, 1985; Garzanti et al., 2009; Vermeesch & Garzanti, 2015). To determine provenance, geologists often employ a variety of techniques, including petrographic analysis, geochemical analysis (e.g., trace element and isotope geochemistry), and detrital zircon geochronology. These methods help to identify the characteristic signatures of different source rock types and to trace the sediment transport pathways (Ershova et al. 2016; Stuut, 2005; Wang et al. 2018; Sawakuchi et al. 2020).

Provenance studies often analyze whole-rock or size-fraction samples as well as single detrital grains, using techniques such as petrographic modal analysis, geochemical characterization, and isotopic methods (Dickinson, 1985; Zuffa, 1985; Garzanti et al., 2009; Vermeesch & Garzanti, 2015). Heavy mineral analysis, which involves identifying and quantifying heavy minerals, is another useful tool. For single grains, detailed mineralogical and geochemical analysis, along with geochronological dating (e.g., U-Pb dating of zircon), can provide valuable insights into the source rock and its age. (Morton & Hallsworth, 1994; Garzanti et al., 2009; Vermeesch & Garzanti, 2015)

Understanding the provenance or origin of sedimentary rocks is highly beneficial in economic geology and in establishing the sequence of geological events. For instance, identifying that a sandstone originated from a specific type of granite known for its porphyry copper potential can be valuable. Alternatively, determining that a sediment of interest has undergone metamorphism and melting to become the igneous rock in question can provide important insights (Dickinson & Suczek, 1979; Ingersoll, 1987; Dickinson, 1988; Garzanti, 2000). Sedimentary rocks are an

important source of information about previous orogenic conditions and the composition of which may describe the evolution of provenance and tectonic setting. As the sediment composition changes through time, the geochemical characteristics of the sediment can be used to understand its geologic history (Li et al. 2011; Pandita et al. 2014; Tegan, 2023).

The study of sedimentary provenance interfaces several of the mainstream geological disciplines (mineralogy, geochemistry, geochronology, sedimentology, igneous and metamorphic petrology). Its remit includes the location and nature of sediment source areas, the pathways by which sediment is transferred from source to basin of deposition, and the factors that influence the composition of sedimentary rocks (e.g. relief, climate, tectonic setting) (Boulter et al. 2004; Luo et al. 2007; Zaid & Gahtani, 2015).

On Earth, sedimentation is governed primarily by tectonic activity, with secondary influences from climate and eustatic sea-level changes, and minor contributions from impact processes; detrital sediments thereby preserve records of eroded crustal material (Dickinson, 1974; Potter & Pettijohn, 1977; Blatt et al., 1980; Nichols, 2009). Knowledge of crusts of the past is gleaned from provenance studies. Tracking the immediate and ultimate sources and origins of sediments, principally of siliciclastic sediments, is the domain of provenance studies. In addition, estimating amounts, proportions, and rates of supply of sediments from multiple sources is also within the purview of provenance studies (Smith et al. 2014; Sharman et al. 2019; Jiang & Yang, 2019; Joshi et al. 2021).

Provenance studies in sedimentary geology focus on determining the source areas of sediments and understanding the processes that transported and deposited them. Sedimentary transport significantly alters the physical and chemical properties of sediments. Mechanical weathering breaks down rocks into smaller particles, while chemical weathering alters the mineral

composition (Haughton et al., 1991). Sorting processes, such as those in streams, separate minerals based on density. Diagenetic processes that occur after sediment deposition can further modify the mineral composition and texture of sedimentary rocks (Sang et al. 2018; Oghenekome et al. 2018; Ogbahon & Olujinmi, 2019). Therefore, provenance studies require careful interpretation and visualization of the original sedimentary materials.

Sedimentologists conduct provenance studies to identify the source areas of sediments and understand their depositional history, information which is critical for predicting basin characteristics and constructing reservoir models (Weljte & von Eynatten, 2004; Weltje, 2012). These studies primarily focus on the coarse silt to fine sand fraction (40-250 μm) of sedimentary rocks to ensure the analyzed grains are representative of the source and not heavily altered by chemical weathering (Garzanti et al., 2009). These techniques include:

Heavy mineral analysis: Examining the composition and abundance of heavy minerals like zircon, magnetite, and garnet to determine their source rocks (Dickinson & Suczek, 1979).

Petrographic analysis: Studying the composition and texture of sedimentary grains to identify their provenance (Ingersoll, 1987).

Detrital zircon geochronology: Dating detrital zircons to constrain the age of the source rocks (Garzanti, 2000).

Trace element geochemistry: Analyzing the concentration of trace elements in sedimentary grains to identify their source rocks (Garzanti, 2000).

2.2.1 Conglomerate Clast Provenance

The large, often distinctive clasts within conglomerates act as direct evidence of their source terrain. As Potter (1978) noted, these phenoclasts serve as geological proxies for ancient landscapes, akin to the fossilization of living organisms, providing a tangible record of rocks that have often since been eroded away. Just as boulders in a riverbed reflect the upstream topography, conglomerate clasts generally provide insights into the nearby provenance of sediments. While it is unsurprising to find clasts derived from nearby hills in river gravels, the presence of these clasts within conglomerates can be particularly revealing, especially in regions affected by faulting (Blatt et al., 1980; Dickinson, 1985; Boggs, 2009). The discovery of identical clast assemblages in widely separated conglomerate outcrops constitutes strong evidence for their former proximity, suggesting that the intervening landscape has undergone significant tectonic deformation (Howard, 1992; Gallastegui et al. 2014; Quick et al. 2019).

2.2.2 Simple Petrographic Provenance

A popular approach for analyzing well-preserved sandstones pioneered around 1980 is to sort the different kinds of grains into three classes and plot them by their percentages on a triangular graph, a ternary diagram (Dickinson & Suczek, 1979; Dickinson et al., 1983; Pettijohn et al., 1987). One point of the triangle is for 100% quartz, the second is for 100% feldspar and the third is for 100% lithics: rock fragments that haven't fully broken down into isolated minerals (Drummond, 2023).

Sedimentary rocks derived from different tectonic settings display characteristic compositional trends on QFL ternary diagrams; for example, sandstones from continental interiors are generally quartz-rich with few lithic grains (Dickinson & Suczek, 1979; Dickinson et al., 1983; Pettijohn et

al., 1987). Conversely, sandstones from volcanic arcs are characterized by a low quartz content, while those derived from recycled orogenic terranes exhibit a deficiency in feldspar.

To refine this classification, it is essential to distinguish between monocrystalline quartz grains and lithic fragments (quartzite or chert). By incorporating this distinction, a QmFLt diagram (monocrystalline quartz–feldspar–total lithics) can be employed to more accurately determine the plate-tectonic setting of the source region for a given sandstone (Garzanti, 2019, Anani et al. 2020, Abu & Sunkari, 2020).

2.2.3 Heavy Mineral Provenance

In addition to quartz, feldspar, and lithic fragments, sandstones often contain accessory detrital minerals, many of which are denser than the host rock and thus classified as heavy minerals (Pettijohn, 1975; Blatt et al., 1980; Boggs, 2009). The high density of heavy minerals allows their separation from the sandstone matrix, and their composition provides valuable insights into sandstone provenance (Morton, 1985; Mange & Maurer, 1992; Morton & Hallsworth, 1999; Garzanti & Andò, 2007). For example, extensive igneous source areas are likely to contribute grains of robust primary minerals such as augite, ilmenite, or chromite. Metamorphic terranes, on the other hand, may shed minerals like garnet, rutile, and staurolite. Other commonly encountered heavy minerals, including magnetite, titanite, and tourmaline, can originate from either igneous or metamorphic source rocks (Hussain et al. 2004; Smale, 1997; Cascalho, 2019).

Zircon stands out amongst the suite of heavy minerals due to its exceptional resilience and chemical inertness (Hoskin & Schaltegger, 2003). This remarkable durability allows zircon grains to persist for billions of years, undergoing multiple cycles of sedimentation and erosion, a process likened to coins perpetually circulating (Veizer, 1988). The remarkable persistence of these detrital

zircons has fueled a highly active field of research known as provenance analysis (Cawood et al., 2012; Gehrels, 2014; Hu et al. 2024). Detrital zircon analysis involves separating hundreds of zircon grains and determining their ages using isotopic methods, with the age distribution being more significant than individual ages (Gehrels, 2014; Spencer et al., 2016; Vermeesch, 2018). Each rock body exhibits a characteristic zircon age spectrum that can be traced into its derived sediments, making detrital zircon (DZ) studies a powerful tool for reconstructing basin histories (Gehrels, 2014; Spencer et al., 2016; Vermeesch, 2018; Hart et al., 2016).. However, these techniques necessitate access to expensive laboratory equipment and specialized preparation procedures, thus typically being reserved for high-impact research endeavors. Fortunately, the traditional methods of mineral separation, sorting, and grain counting remain valuable tools within the geoscientist's arsenal (Kumar et al. 2021; Andersen et al. 2022; George et al. 1995).

2.2.3.1 Heavy mineral abundances

The initial technique focuses on determining the composition of the heavy mineral assemblage within a given sample (Mange and Maurer, 1992). Heavy minerals are accessory minerals, typically comprising less than 1% of the total rock volume, and include examples like garnet, apatite, zircon, and chrome spinel (Hubert, 1962). While these dense minerals are diagnostically useful, sandstones are frequently dominated by more abundant light minerals such as quartz, feldspars, and micas. Quartz, in particular, exhibits exceptional resistance to both abrasion and chemical weathering, leading to its concentration within sediments (Boggs, 2009). Furthermore, quartz can undergo multiple cycles of deposition and exhumation, rendering it uninformative for provenance studies. In contrast, heavy minerals can be diagnostic of specific igneous and metamorphic rock sources, and distinct assemblages of these minerals can be linked to particular source terranes (Tangari et al., 2024; Sun et al., 2022; Ali, 2021; Zhu & Zeng, 2021).

Heavy mineral analysis involves the separation of these denser minerals from the lighter minerals within the sandstone matrix. This separation is typically achieved using heavy liquids (Mange and Maurer, 1992). Following separation, the heavy minerals are mounted onto a petrographic slide for microscopic examination. The abundance of each heavy mineral species within a sample is then determined by statistically analyzing a representative population (typically at least 200 non-opaque and non-micaceous grains) through identification and counting (Galehouse, 1971; Mange and Maurer, 1992). This process yields a quantitative dataset, often presented in tabular form. The overall abundance and composition of the heavy mineral assemblage can vary over time, reflecting the progressive geological evolution of the source terrane. These variations can be effectively tracked within a stratigraphic section.

2.2.3.2 Heavy mineral morphologies

Microscopic analysis of the coarse silt and fine sand fraction extends beyond simply quantifying the proportion of heavy minerals present (Mange and Maurer, 1992). Grain morphology, a term referring to the shape and surface features of grains, also provides valuable insights into the transport history experienced by the sediment (Garzanti and Andò, 2007). This information can be used to subdivide the population of a single heavy mineral species into sub-populations. The characteristics of these sub-populations can then be linked to the duration of transport, potentially allowing estimation of the source terrane's relative proximity or distance (distal) to the basin (Garzanti et al., 2009). This approach can be particularly useful in differentiating between two potential source terranes identified based on their similar heavy mineral compositions but situated at varying distances from the depositional site within the basin. Morphological analysis typically categorizes grains based on a spectrum ranging from well-rounded to euhedral (sharp-edged

crystals). Euhedral grains are more likely to originate from a proximal source area due to minimal mechanical abrasion during transport (Garzanti and Andò, 2007; Weltje and von Eynatten, 2004).

2.2.3.3 Dating sediments using Heavy minerals

U-Pb dating of zircon and apatite crystals represents a third, commonly employed technique within the realm of heavy mineral analysis (Gehrels, 2014; Vermeesch, 2018). This technique leverages isotopic ratios to determine the age of these minerals. Specifically, it measures the relative abundance of parent and daughter isotopes within the crystal lattice. In the case of U-Pb dating, the parent isotope is uranium (U), which undergoes radioactive decay over time to form the daughter isotope, lead (Pb). The known decay rates of specific uranium isotopes allow scientists to calculate the age of the mineral based on the measured ratio of parent to daughter isotopes (Dickin, 2018; Faure & Mensing, 2005). This analysis typically involves a population of zircon or apatite grains, yielding a range of individual ages, which is then interpreted as a detrital age spectrum to fingerprint source terrains (Gehrels, 2014).

Each obtained age represents the time elapsed since the crystal's formation within a magma chamber (Hoskin & Schaltegger, 2003). During crystallization, both uranium and its lead daughter isotope become trapped within the mineral structure. Over time, uranium undergoes radioactive decay, releasing energy and transforming into lead isotopes that remain trapped within the mineral (Dickin, 2018). The resulting population of grain ages is often visualized using a frequency histogram or a probability density function plot (Vermeesch, 2012). These plots frequently exhibit broad peaks with higher frequencies, which are interpreted as representing orogenic (mountain-building) events (Cawood et al., 2012). During these events, rocks typically residing deeper within the Earth's crust, including solidified magma chambers, are exhumed. This process leads to an

influx of zircons and apatites derived from these exhumed rocks into the sedimentary basin. Orogenic events also coincide with periods of increased volcanic activity, further contributing zircons and apatites to the sedimentary record through volcanic ashfall and extrusive events (Cawood et al., 2012; Fedo et al., 2003).

2.2.3.4 Composite heavy mineral suite

The synergistic application of these three techniques offers a powerful toolkit for deciphering sediment provenance and transport pathways. Consider a scenario where multiple potential source terranes exhibit heavy mineral assemblages resembling those observed in the study sediments. However, only one of these sources may have been active during the same time period as indicated by the age distribution of detrital zircons within the basin and may also be situated at the appropriate distance from the basin as inferred from grain morphology analysis. In such a situation, through a process of elimination, only a single source area emerges as a viable candidate that satisfies all criteria (Morton & Hallsworth, 1999; Garzanti & Andò, 2007; Gehrels, 2014; Vermeesch, 2018). Provenance data not only identify likely sources but also help exclude nearby cratons that might otherwise be assumed to supply sediments based on geographic proximity alone (Dickinson, 1985; Ingersoll, 1990; Gehrels, 2014; Vermeesch, 2018). The power of provenance analysis is further amplified when these techniques are applied iteratively throughout a stratigraphic section. This approach allows for the identification of variations in provenance over time, which can then be used to explain changes in other parameters such as sedimentary architecture. Furthermore, these variations can be integrated with paleogeographic analysis to elucidate broader-scale tectonic processes operating over extended timeframes (Dickinson, 1985; Morton & Hallsworth, 1999; Gehrels, 2014; Romans et al., 2016; Vermeesch, 2018).

2.3 Radiogenic isotopes and isotope geochronology

Radiogenic isotopes are nuclides formed through the radioactive decay of parent isotopes. A common example is the production of radiogenic strontium-87 (^{87}Sr) from the decay of rubidium-87 (^{87}Rb). In geochronology, the abundance ratios of radiogenic isotopes relative to their stable, non-radiogenic counterparts (e.g., $^{87}Sr/^{86}Sr$) are used to determine the timing and duration of geological events. Additionally, these ratios can serve as tracers for past geochemical fractionations involving parent and daughter elements, such as those that occurred during the Earth's differentiation (Faure & Mensing, 2005; Dickin, 2005; Rollinson, 2007; Stracke, 2012).

2.3.1 Principles of Isochrons

Consider the scenario of an intermediate magma undergoing fractional crystallization, progressively evolving into a series of more felsic liquids. This process alters the parent-daughter ratios of various radioactive decay systems within the magma due to the differing compatibilities of parent and daughter elements within crystallizing minerals. For instance, rubidium (Rb) tends to be enriched in more evolved magmas (e.g., granites) relative to strontium (Sr), compared to their parental andesite which exhibits a lower Rb/Sr ratio (Faure & Mensing, 2005; Dickin, 2005; Winter, 2010). Because crystallization proceeds on timescales far shorter than the half-life of ^{87}Rb, all minerals and melts in a magmatic system inherit the same initial $^{87}Sr/^{86}Sr$ ratio at the time of solidification, even though their Rb/Sr ratios may vary; crystallization thus does not significantly alter isotopic compositions (Faure & Mensing, 2005; Dickin, 2005; Winter, 2010; Vukmanovic et al., 2019; Li et al., 2024; Zhang et al., 2024). Applying this principle to a single rock, such as a granite composed of quartz, feldspar, and biotite, each mineral incorporates different amounts of trace elements (Rb and Sr), but all share the same initial $^{87}Sr/^{86}Sr$ ratio at crystallization. Feldspars typically contain high concentrations of both Rb and Sr, biotite exhibits lower overall abundances

but a higher Rb/Sr ratio, while quartz contains negligible Rb and Sr and thus shows very low Rb/Sr ratios (Vukmanovic et al., 2019; Li et al., 2024; Zhang et al., 2024). The intermediate Rb/Sr ratio of a whole-rock powder is a product of averaging the high ratio of biotite with the low ratios of feldspar and quartz (Dickin, 2018).

2.3.2 The Rb-Sr Isotope System

The Rb-Sr system stands out as one of the pioneering and enduring workhorses in both geochronology (determining rock ages) and geochemical tracing (Dickin, 2018; Li et al., 2020). A key advantage of this system lies in the substantial variations observed in Rb/Sr ratios across different rock types. These variations can span several orders of magnitude due to the inherently contrasting geochemical behaviors of rubidium (Rb) and strontium (Sr) during magmatic and metamorphic processes (Bosch et al., 2022). The accuracy of age determinations using the Rb-Sr system is heavily influenced by the spread of measured isotopic ratios, a principle that underpins both traditional whole-rock analysis and modern in-situ techniques (Zhou & Li, 2021; Reddy et al., 2020). Therefore, the large range of Rb/Sr ratios observed in rocks makes this system particularly valuable for geochronological applications, a utility that continues to be proven in studies from terrestrial metamorphic terrains to planetary materials (Borg et al., 2023).

As discussed previously, Rb exhibits characteristics of high solubility and incompatibility within minerals. Similarly, Sr displays moderate solubility and generally behaves incompatibly in mafic and ultramafic igneous systems, but becomes relatively compatible in silica-rich rocks, preferentially partitioning into plagioclase feldspar during crystallization. Consequently, the Earth's mantle possesses a relatively uniform and low initial $^{87}Sr/^{86}Sr$ ratio, whereas the continental

crust exhibits a more variable and, on average, higher initial ratio (Huang et al., 2018; Vukmanovic et al., 2019; Li et al., 2024; Zhang et al., 2024).

The evolution of strontium isotopes within Earth's mantle and continental crust is commonly illustrated using isotope evolution diagrams, where $^{87}Sr/^{86}Sr$ is plotted against time. In a closed system, the trend follows a straight line, with the slope determined by the parent–daughter ratio ($^{87}Rb/^{86}Sr$) (Faure & Mensing, 2005; Dickin, 2005; Vukmanovic et al., 2019; Li et al., 2024). As discussed previously, Rb exhibits high solubility and incompatibility, whereas Sr behaves moderately incompatible in mafic and ultramafic systems but becomes relatively compatible in silica-rich rocks, partitioning strongly into plagioclase. Consequently, the mantle maintains a relatively uniform and low initial $^{87}Sr/^{86}Sr$, while the continental crust shows more variable and generally higher values (Faure & Mensing, 2005; Dickin, 2005; Bell & Blenkinsop, 1987; Hodell et al., 1989; Sun & McDonough, 1989; Rudnick & Fountain, 1995; Taylor & McLennan, 1995; Huang et al., 2018; Vukmanovic et al., 2019; Li et al., 2024; Zhang et al., 2024; Geological Society of London, 2024).

Imagine a scenario where a portion of the mantle undergoes partial melting at 3.8 billion years ago, forming a segment of continental crust. The newly formed crust will have a higher Rb/Sr ratio compared to the mantle due to Rb's greater incompatibility. Consequently, this crust will evolve along a steeper line on the isotope evolution diagram compared to the bulk Earth line. The residual mantle, depleted in Rb relative to the bulk Earth due to this melting event, will evolve along a shallower slope. If this process of mantle melting and crust formation were continuous over time, the mantle would progressively decrease in its Rb/Sr ratio, resulting in an isotope evolution path that curves downward (Faure & Mensing, 2005; Dickin, 2005; Taylor & McLennan, 1995;

Rudnick & Fountain, 1995; Kemp et al., 2010; Vervoort & Kemp, 2016; Hawkesworth et al., 2020; Li et al., 2024).

A potential drawback of the Rb-Sr system for geochronology is the relative mobility of the elements, particularly Rb. This mobility can violate the assumption of a closed system, especially in young rocks that may have been altered by processes like weathering or hydrothermal activity. Movement of Rb or Sr can lead to inaccurate age determinations or incorrect initial ratio assumptions. However, the significant range observed in Rb/Sr ratios of igneous and metamorphic rocks rich in silica makes Rb-Sr ages somewhat less sensitive to variations in the initial $^{87}Sr/^{86}Sr$ ratio (Faure & Mensing, 2005; Dickin, 2005; Villa, 2016; Nebel, 2019; Li et al., 2024).

Due to Rb's volatile nature, the Earth's initial Rb/Sr ratio can only be estimated. Current estimates place the present-day chondritic $^{87}Sr/^{86}Sr$ ratio at around 0.725, whereas the Earth's value is thought to be closer to 0.7035 ± 0.001. An intriguing and valuable aspect of the Rb-Sr system stems from the extended residence time of Sr in seawater and its ease of substitution within calcium carbonate minerals. This long residence time allows for a relatively homogeneous $^{87}Sr/^{86}Sr$ ratio in seawater at any given period. However, this ratio does vary through time (Faure & Mensing, 2005; Dickin, 2005; McArthur et al., 2012; Nebel, 2019; Li et al., 2024).

2.3.3 The Sm-Nd Isotopes system

Accurately determining the provenance of sedimentary rocks is essential in numerous geoscientific disciplines. Understanding the origin of sediments allows researchers to reconstruct past tectonic settings, decipher paleoclimate conditions, and trace the evolution of sedimentary basins. The Sm-Nd isotope system has emerged as a cornerstone technique in sediment provenance studies due to

its unique geochemical properties and ability to record long-term geological history (Goldstein et al., 1984; DePaolo, 1988; McLennan et al., 1990; Anani et al., 2012; Amedjoe et al., 2018; Zobah, 2022). This review delves into the technical aspects of Sm-Nd isotope systematics, explores its application in high-resolution provenance investigations, and critically evaluates the strengths and limitations of this approach.

The Sm-Nd system leverages the radioactive decay of ^{147}Sm to ^{143}Nd, with a half-life of approximately 106 billion years (McDonough & Sun, 1989; Bouvier et al., 2008). This slow decay rate minimizes the influence of geological processes on the isotopic ratios, making it ideal for tracing ancient geological events. The true power of the Nd system lies in the contrasting geochemical behaviors of Sm and Nd. Samarium (Sm) exhibits greater compatibility with certain minerals (e.g., garnet, pyroxene) compared to Nd, which tends to be more incompatible and preferentially resides in the melt phase during mineral crystallization (Taylor & McLennan, 1985; Kemp et al., 2009; Yang et al., 2021; Shao et al., 2023). This differential behavior results in distinct Sm/Nd ratios in various rock types, serving as a robust geochemical fingerprint for their origin.

Sm-Nd isotope data can be employed in high-resolution provenance studies to address a range of critical questions:

- **Discriminating Source Terranes with Subtle Isotopic Variations:** Continental crustal blocks, island arcs, and mid-oceanic ridges possess distinct Sm/Nd signatures due to their unique geological histories and differentiation processes (Armstrong, 1981). By comparing the εNd values and model ages of sediments with potential source rocks, researchers can differentiate between terranes with subtle isotopic variations that may be isotopically indistinguishable using other techniques. For instance, εNd values of Archean cratons are

typically positive and significantly higher than those of Proterozoic terranes, allowing for their clear distinction in the sedimentary record (DePaolo, 1981).

- **Tracing Sediment Dispersal Pathways in Heterogeneous Basins:** Spatial variations in Sm-Nd isotope ratios within a sedimentary basin can be used to map sediment dispersal patterns. Fluvial systems draining source regions with contrasting εNd signatures will deliver sediments with distinct isotopic fingerprints. Analyzing the downstream changes in εNd values can reveal the direction of sediment transport and potentially identify the dominant source areas within a basin (McLennan et al. 1989**)**.
- **Quantifying Mixing of Source Materials:** In many cases, sediments are derived from multiple source regions with overlapping Sm-Nd signatures. Advanced isotope modeling techniques, such as inverse modeling and end-member mixing calculations, can be employed to quantify the relative contributions from various source terranes based on the Sm-Nd isotopic data (Dhuime et al. 2011; Hawkesworth et al. 2013, 2024; Cawood et al. 2013**)**. These quantitative approaches allow for a more nuanced understanding of sediment provenance, particularly in complex settings with multiple potential source areas.

The Sm-Nd isotope system offers several distinct advantages for sediment provenance studies:

- **High Sensitivity:** The significant differences in Sm/Nd ratios between various rock types, particularly between continental crust and mantle reservoirs, enable robust discrimination of source regions (DePaolo and Wasserburg, 1976; Jacobsen and Wasserburg, 1979). This allows researchers to differentiate between sediments derived from geologically distinct terranes, even with subtle variations in isotopic composition (McLennan et al., 1993; Nelson and DePaolo, 1988).

- **Resistance to Alteration:** Sm and Nd are relatively resistant to alteration during weathering and diagenetic processes compared to other elements, ensuring that the Sm-Nd isotopic signature of a sediment reflects its source region more faithfully, even after transport and deposition (McCulloch & Wasserburg, 1978; Goldstein et al., 1984; Taylor & McLennan, 1985; Condie, 1993).
- **Long-Term Geological Record:** The long half-life of ^{147}Sm (approximately 106 billion years) allows researchers to trace sediment provenance over extended geological timescales (McCulloch and Wasserburg, 1978; Dickin, 2018). This is particularly valuable for studying ancient sedimentary basins where other provenance indicators might be less reliable (McLennan et al., 1993).
- **Quantitative Capabilities:** Advanced isotope modeling techniques can be applied to Sm-Nd data to quantify the relative contributions of different source regions to a sedimentary deposit. This allows for a more nuanced understanding of sediment provenance, especially in complex settings with multiple potential source areas (DePaolo, 1988; Nelson & DePaolo, 1988; Grousset & Biscaye, 2005; Chauvel et al., 2014).

The Sm-Nd isotope system remains a powerful tool for high-resolution provenance studies of sediments. Its high sensitivity, resistance to alteration, and ability to track long-term geological processes make it a valuable technique. However, researchers need to be aware of the limitations associated with cost, potential for source mixing, and diagenetic alteration. By carefully considering these factors and integrating Sm-Nd data with other approaches, researchers can gain a deeper understanding of the origin and transport pathways of sediments in various geological settings.

2.3.4 Samarium-Neodymium and Rubidium-Strontium Isotopic studies

Geologists utilize the distinct radiogenic isotope ratios of strontium ($^{87}Sr/^{86}Sr$) and neodymium ($^{143}Nd/^{144}Nd$) in sediments to elucidate their source regions (provenance) and track spatiotemporal variations in sediment delivery to basins (Krom et al., 1999). These ratios act as unique geochemical fingerprints for various rock types, making this technique highly effective. Furthermore, Sr and Nd isotopes offer insights into past environmental conditions (Weldeab et al. 2003; Fu et al. 2012; Baioumy, 2011, 2014).

The isotopic compositions of Nd and Sr, particularly their radiogenic variants, are invaluable tools for deciphering Earth surface processes. Unlike nutrient-based tracers, which can be biased by biological activity or thermodynamic processes (Frank, 2002), these isotopes remain relatively unaffected (Goldstein and Hemming, 2003). Variations in εNd and $^{87}Sr/^{86}Sr$ ratios within continental rocks reflect differences in age and lithology, enabling discrimination between local and regional sources of detrital silicates deposited on the ocean floor (Grousset and Biscaye, 2005). Additionally, the unique Nd isotope signatures of different water masses allow them to be traced using Nd isotopes (Piepgras and Wasserburg, 1980; Lacan and Jeandel, 2005).

Traditionally, the Sm-Nd isotope system has been employed to determine the age of crustal rocks, providing insights into their formation (petrogenesis) and temporal variations in mantle composition (Hamilton et al., 1978; De Paolo, 1981; O'Nions et al., 1983; Nelson and de Paolo, 1984). By analyzing specific Sm and Nd isotope ratios, a "model age" (T_{DM}) can be calculated, reflecting the time elapsed since the rock separated from the mantle (McCulloch and Wasserburg, 1978).

The term "crustal residence age" refers to the age of the continental crust from which sediment originates. The Nd crustal residence age (TCR) is calculated by substituting values for the depleted mantle (DM) with those for the Chondritic Uniform Reservoir (CHUR). Some use "provenance age" interchangeably, but it shouldn't be confused with a specific event like stratigraphic age. Instead, it represents the average crustal residence time of all rock components. Generally, the crustal residence age of a sedimentary rock exceeds its stratigraphic age (McCulloch & Wasserburg, 1978; DePaolo, 1981; Goldstein et al., 1984; Taylor & McLennan, 1985; Condie, 1993).

Model ages obtained from clastic sedimentary rocks provide estimates of their crustal residence time (O'Nions et al., 1983), assuming minimal fractionation of parent-daughter elements relative to the source. However, most continental sediments are a mixture of materials from diverse sources. Consequently, model ages likely represent an average of the detrital input, providing only a minimum estimate or average crustal residence age.

The Sm/Nd ratio in the continental crust is lower than that of the depleted mantle (Jacobsen and Wasserburg, 1979). Consequently, continental crust evolves with lower $^{143}Nd/^{144}Nd$ ratios over time compared to the mantle (DePaolo, 1981). Significantly, Sm and Nd remain relatively immobile during subsequent metamorphic or sedimentary processes after crust formation (McCulloch and Wasserburg, 1978). This characteristic allows Nd isotope ratios in rocks to retain a record of the parent-daughter isotope ratios present in their source region. Additionally, these elements are resistant to alteration under hydrothermal conditions (Pearce et al., 1999). Therefore, Nd isotope ratios accurately reflect the proportions of rock or magma involved in specific

geological processes, although the system may not be sensitive to minor amounts of recycled crust within the mantle (Möller et al. 2002; Zhao et al. 2006; Chauvel et al. 2008).

Epsilon (εNd) Values: Quantifying Depletion Relative to Chondrite

The epsilon value (εNd) for a rock sample formed at a specific time (t) is calculated using the following equation:

$$\varepsilon_{Nd}^{t} = \left[\frac{\left({}^{143}Nd/{}^{144}Nd \right)_{rock,t}}{\left({}^{143}Nd/{}^{144}Nd \right)_{CHUR,t}} - 1 \right] \times 10^{4}$$

The magnitude of the present-day εNd value reflects the degree of time-integrated depletion in Nd relative to the Chondritic Uniform Reservoir (CHUR), as determined by the Sm/Nd ratio.

Over geological time, Earth's mantle and continental crust have differentiated into isotopically distinct reservoirs, identifiable through variations in Sr, Nd, Hf, Pb, and Os isotope ratios. Zindler and Hart (1986) proposed four isotopically distinct mantle domains to explain the observed variations in mid-ocean ridge basalts and ocean island basalts. Similarly, the continental crust can be broadly divided into upper, middle, and lower portions (Rundnick and Gao, 2014), each exhibiting distinct geochemical and isotopic signatures. Generally, the upper and middle crust are more geochemically evolved compared to the more heterogeneous lower crust.

Sedimentary rocks differ from igneous rocks in their formation. They are composed of eroded fragments of older rocks with varying ages. Consequently, the Sm-Nd model age of a sedimentary rock does not represent its actual formation age (stratigraphic age), but rather the average age of the material in its source region. This information is crucial for determining the origin

(provenance) of the sediment. Recognizing this distinction, researchers now widely use the term "$d_{provenance}T$" in provenance studies of sediments across diverse geological settings (McCulloch and Wasserburg, 1978; Goldstein et al., 1984; Nelson and de Paolo, 1988; Mearns et al., 1989; Dalland et al., 1995; Knudsen, 2001).

The Sm-Nd isotope system has traditionally been used to date igneous rocks, providing insights into their formation (petrogenesis) and the evolution of mantle composition. By analyzing the $^{143}Nd/^{144}Nd$ and $^{147}Sm/^{144}Nd$ ratios of a rock, a model age (T_{DM}) can be calculated, reflecting the time elapsed since the rock's precursor separated from the mantle (Faure, 1986). However, for sedimentary rocks formed from the reworking of pre-existing crustal rocks with varying ages, the Sm-Nd model age reflects the weighted average time the material spent in the continental crust (crustal residence time) within the source region (McCulloch and Wasserburg, 1978). Therefore, this value provides valuable information about the provenance, not the stratigraphic age, of the sedimentary material.

The isotopic composition of rocks from the continental crust is extremely variable, and isotope ratios are strictly comparable only if the samples are all of the same age. For this reason, compositional differences are best considered relative to a normalising parameter which takes into account the age of the sample. One such parameter is the composition of CHUR and its evolution through time (Jacobsen and Wasserburg, 1979). For Sr, Nd and Hf isotopes this can be quantified in terms of the epsilon notation, whereas Os isotopes use the gamma notation (Shirey and Walker, 1998).

(a) Upper continental crust. The upper (sialic) continental crust is characterised by high Rb/Sr and consequently has high $^{87}Sr/^{86}Sr$ ratios (Rudnick and Gao, 2014). Neodymium and Hf isotope ratios,

on the other hand, are low relative to mantle values as a consequence of the low Sm/Nd and Lu/Hf ratios which characterise the continental crust (Hawkesworth and Kemp, 2006). U and Th are enriched in the upper continental crust and give rise to high ^{206}Pb, ^{207}Pb and ^{208}Pb isotope ratios (Zartman and Doe, 1981).

(b) Middle continental crust. The mid-continental crust represents extensive areas of exhumed amphibolite facies gneisses found in granite–gneiss terrains. These rocks have retarded $^{143}Nd/^{144}Nd$ and $^{176}Hf/^{177}Hf$ (Vervoort and Patchett, 1996), and $^{87}Sr/^{86}Sr$ is generally lower than in the upper crust (Rudnick and Fountain, 1995). Uranium, however, is depleted, and Th is lower than in the upper crust but not as depleted as U (Rudnick and Gao, 2014). $^{206}Pb/^{204}Pb$ and $^{207}Pb/^{204}Pb$ may be lower than in the mantle (Kramers and Tolstikhin, 1997).

(c) Lower continental crust. The lower continental crust is characterised by mafic rocks and granulite facies metamorphosed rocks and is often strongly Rb-depleted (Rudnick and Fountain, 1995). Thus, it has low $^{87}Sr/^{86}Sr$ ratios which are not greatly different from modern mantle values. This means that a modern granite derived from the lower crust will have an initial $^{87}Sr/^{86}Sr$ ratio very similar to one derived from the mantle. U/Pb and Th/Pb ratios in the lower crust are lower than modern mantle values so that ^{206}Pb, ^{207}Pb and ^{208}Pb isotope ratios are all very low and are therefore sensitive indicators of lower crust and mantle reservoirs (Zartman and Doe, 1981).

(d) Continental lithosphere. The continental lithosphere is the region of mantle that lies beneath and is attached to continental crust. In areas of ancient crust it is extremely thick. It is known as the continental lithospheric mantle (CLM) or the sub-continental lithospheric mantle (SCLM) and is extremely variable in isotopic composition (Pearson, 1999). Isotope data from CLM-derived mantle xenoliths show that the CLM typically has higher $^{87}Sr/^{86}Sr$ (>0.7045), lower εNd (<0) and

higher $^{207}Pb/^{204}Pb$ (at a given $^{206}Pb/^{204}Pb$) when compared with asthenospheric mantle sources (Carlson and Irving, 1994; Pearson, 1999). Nd and Hf isotopes are decoupled during the fractionation of the lithospheric mantle with the result that Nd isotopes are more readily reset than Hf isotopes during mantle metasomatism (Schmidberger et al., 2002). Only very young (0.35 Ga) and small (<5%) depletion events can fractionate Lu from Hf, which results in $^{176}Hf/^{177}Hf$ compositions in the CLM similar to those in the present-day convecting mantle (εHf today ~ +11) (Griffin et al., 2000). Older and more extensive melting generally results in $^{176}Hf/^{177}Hf$ ratios that are more radiogenic than is seen in the convecting mantle and typically exceeds compositions recorded by mantle xenoliths (Griffin et al., 2000). Os isotopic ratios in the CLM are in the range $^{187}Os/^{188}Os$ = 0.1100– 0.1205 and are statistically distinct from peridotites from the convecting mantle ($^{187}Os/^{188}Os$ = 0.1225– 0.1265; Pearson and Wittig, 2014).

2.4 Paleoclimatology

Paleoclimatology, the study of past climates, is fundamental to understanding the Earth's climate system and predicting future climate change. By reconstructing past climate states and their fluctuations, scientists can identify natural climate variability, assess the impacts of anthropogenic forcing, and refine climate models (Petit et al., 1999; Mann et al., 2009).

Some Geological Proxies are enumerated in this paragraph. Oxygen Isotope Analysis which entails the ratio of stable oxygen isotopes ($^{18}O/^{16}O$) in various archives, such as ice cores, marine sediments, and speleothems, serves as a robust proxy for temperature and ice volume variations (Shackleton, 1967; Dansgaard et al., 1982). The lithology, texture, and geochemistry of sedimentary rocks provide crucial information about past depositional environments, including climate-sensitive parameters like sea level, temperature, and precipitation (Reading, 2009).

2.4.1 Paleoclimate Reconstruction Techniques

Geochemical proxies serve as essential tools for reconstructing past climate conditions by preserving the chemical signatures of the environment in which they formed. Stable isotope ratios of oxygen, carbon, and hydrogen, as well as trace elements like aluminum, titanium, and rare earth elements, offer quantitative indicators of temperature, precipitation, ocean chemistry, and atmospheric composition (Shackleton, 1967; Dansgaard et al., 1982; Broecker and van Donk, 1970; Dessert et al., 1993; Henderson, 1984). Additionally, the geochemical composition of sedimentary rocks and the formation of authigenic minerals provide complementary information about redox conditions, weathering intensity, and paleoceanography (Holland, 1978; Berner, 1980). By integrating multiple geochemical proxies and addressing challenges such as diagenesis, researchers can develop robust paleoclimate records, enhancing our understanding of Earth's climate history (Zachos et al., 2001; Petit et al., 1999).

2.5 The Voltaian Supergroup

The Voltaian Supergroup of Ghana, a thick sequence of Neoproterozoic sedimentary rocks, has long attracted attention due to its uncertain depositional setting, provenance, and tectonic significance within the context of West African geology. While numerous petrographic and geochemical studies have contributed to understanding its composition and stratigraphic framework, a deeper connection to broader geological models remains essential. Situating the Voltaian within global frameworks of basin evolution, supercontinent cycles, and geochemical provenance models allows for a more integrative understanding of its significance.

2.5.1 Petrographic Studies and Provenance Models

The Voltaian Supergroup is an extensive, Neoproterozoic to Paleozoic sedimentary basin covering large parts of Ghana, Togo, Benin, and Burkina Faso. It represents one of the largest intracratonic basins in West Africa, formed in a foreland basin setting associated with the Pan-African orogeny (e.g., the collision between the West African Craton and the Benin-Nigerian shield) (Affaton et al., 1991; Kalsbeek et al., 2008). The Supergroup is traditionally subdivided into three major units: the Kwahu-Bombouaka Group, Oti-Pendjari Group and Tamale-Obosum Group in Ghana (Junner, 1940; Bessoles, 1977). This review synthesizes existing literature on the petrography—the mineralogical and textural composition—of the sandstones and other lithologies within the Oti-Pendjari and Tamale-Obosum Groups, highlighting their provenance, depositional environment, and diagenetic history.

The Oti-Pendjari Group forms the basal unit of the Voltaian Supergroup and is characterized by a mix of siliciclastic and carbonate rocks. The group consists of a sequence of conglomerates, sandstones, siltstones, shales, and prominent limestone and dolomite beds (Affaton et al., 1991; Trompette et al., 1980). The presence of carbonates is a key distinguishing feature from the overlying groups.

Sandstones of the Oti-Pendjari Group are typically feldspathic arenites to subarkoses (Carney et al., 2010; Anani, 1999). Petrographic studies reveal a composition dominated by quartz (often >70%), with significant amounts of potassium feldspar (microcline) and plagioclase. Lithic fragments are generally subordinate but can include metaquartzite and fine-grained volcanic rock fragments.

The high feldspar content is a critical petrographic indicator. It suggests a proximal provenance from a crystalline basement source that underwent relatively little chemical weathering or extensive sediment reworking (Dickinson & Suczek, 1979). This points to erosion of the nearby Birimian supercrustal rocks and the granitoids of the West African Craton's basement (Carney et al., 2010). The mineralogical maturity (high quartz) increases upwards in the sequence, indicating more prolonged transport or reworking over time.

The limestones and dolomites are often fine-grained (micritic) to recrystallized. Stromatolitic structures have been identified, suggesting shallow marine depositional conditions within the basin (Affaton et al., 1991).

The Tamale-Obosum Group rocks are predominantly siliciclastic and are composed overwhelmingly of massive, poorly sorted sandstones, with interbeds of siltstone, shale, and rare conglomerates. The sandstones often form spectacular escarpments due to their resistance to erosion. In stark contrast to the Oti Group, the Tamale-Obosum sandstones are overwhelmingly quartz arenites (Anani, 1999; Kalsbeek et al., 2008). Petrographic analysis shows them to be with quartz content frequently exceeding 95%. The quartz grains are predominantly monocrystalline with undulose extinction. Feldspar is a minor component (<5%), and what is present is often highly altered to sericite or clay minerals. Lithic fragments are rare. Despite their high mineralogical maturity, the sandstones are often texturally immature. They are poorly to moderately sorted, and sub-angular to sub-rounded, suggesting a history of short transport or rapid deposition without extensive abrasion (Anani, 1999).

The petrographic evolution from feldspathic sandstones (Oti-Pendjari) to supermature quartz arenites (Tamale-Obosum) records a significant shift in tectonic regime. The supermature

composition indicates a provenance from a stable cratonic interior, likely involving extensive reworking of older sedimentary sequences (Dickinson & Suczek, 1979). This is consistent with the foreland basin model, where the Tamale-Obosum Group represents the molasse-stage deposits derived from the uplifted orogenic belt (the Pan-African terranes to the east), which provided highly weathered and recycled sediment (Kalsbeek et al., 2008).

The Oti-Pendjari feldspathic arenites were deposited in a developing foreland basin with a proximal, crystalline basement source, likely from the West African Craton. The intercalated carbonates confirm periods of marine incursion.

The Tamale-Obosum quartz arenites represent a later, more mature stage of the basin. Their supermature composition reflects a distal, recycled orogenic source (the Pan-African belt) and deposition in a fluvial to shallow marine environment within a well-established foreland basin. The textural immaturity suggests rapid erosion and burial, preventing extensive abrasion.

2.5.2 Geochemical Studies on the Voltaian Supergroup

The Voltaian Supergroup (Neoproterozoic–Early Palaeozoic) is an extensive siliciclastic succession that covers large parts of Ghana and borders in West Africa. It records sedimentation along the eastern margin of the West African Craton during Pan-African to post-Pan-African tectonic events and contains a variety of siliciclastic facies from terrestrial fluvial deposits through distalmarine mudstones and carbonates in places that make it ideal for geochemical and provenance investigations (Carney et al., 2010; Zobah, 2022). Geochemical studies of the Voltaian have aimed to (1) determine sediment provenance, (2) constrain basin evolution and depositional

age, (3) assess paleoenvironments (redox, salinity, productivity), and (4) evaluate diagenetic overprints that affect resource potential and basin interpretation (Amedjoe et al., 2018; Anani et al., 2012).

Published geochemical work on the Voltaian employs a typical suite of modern tools: whole-rock major-element XRF; trace element and REE analyses by ICP-MS; clay mineral and fine fraction analyses; detrital zircon U–Pb geochronology and Lu–Hf isotopes; heavy mineral analysis; and radiogenic isotope systems (Sm–Nd, Rb–Sr, Sr–Nd) applied to whole rocks or specific mineral fractions (Anani et al., 2012; Amedjoe et al., 2018; Kwayisi et al., 2024). Recent studies increasingly apply multi-proxy strategies (trace elements + isotopes + detrital zircon) to reduce ambiguity inherent in single proxies (Elburg et al., 2022; Zobah, 2022).

Whole-rock major element data for Voltaian sandstones and mudrocks commonly indicate compositionally mature to submature siliciclastics with variable feldspar contents and abundant quartz in many units consistent with derivation from evolved continental crust (Amedjoe et al., 2018; Anani et al., 2012). Geochemical discrimination diagrams (e.g., SiO_2 vs. K_2O/Na_2O, A–CN–K trends) used in some works show weathering and recycling signals typical of passive margin/continental interior sedimentary regimes in parts of the basin (Amedjoe et al., 2018).

Trace element and REE patterns have been used to fingerprint sources, identify diagenetic alteration, and infer depositional redox. Voltaian shales and fine sediments typically show light-REE enriched patterns with negative Eu anomalies in many samples supporting derivation from evolved felsic sources (Amedjoe et al., 2018). Trace-element ratios (e.g., V/Cr, Ni/Co, U/Th) have been applied cautiously to assess paleo-redox conditions in organic-rich intervals, but authors stress correcting for detrital dilution and sedimentation rate effects (Tribovillard et al., 2006;

Amedjoe et al., 2018). Where carbonate horizons occur, Sr behavior and REE patterns help separate detrital vs diagenetic signals (Carney et al., 2010; Zobah, 2022).

Detrital zircon U–Pb and Lu–Hf studies in the region (Elburg et al., 2022; regional surveys) complement whole-rock isotopes by providing maximum depositional ages and direct age spectra for source terranes. Heavy-mineral analyses and petrography similarly corroborate a dominantly felsic, recycled crustal signature with episodic volcanic input in parts of the basin (Anani et al., 2012; Amedjoe et al., 2018).

Multiple authors stress diagenetic alteration particularly of clay and fine fractions — as a serious complicating factor for geochemistry and isotopic systems (Clauer & Deynoux cited; Kwayisi et al., 2024). Rb and Sr mobility in clays, authigenic mineral growth, and fluid flow can reset signatures; thus, careful mineral separation, use of robust phases (zircon, certain heavy minerals), and multi-isotope/multi-proxy approaches are recommended (Deynoux et al., 2006; Amedjoe et al., 2018).

Geochemical proxies applied to selected Voltaian intervals provide tentative reconstructions of depositional conditions: many units reflect continental to shallow marine siliciclastic deposition with variable oxygenation and organic preservation potential (Amedjoe et al., 2018). Trace element proxies (e.g., Mo, U, V) and coupled TOC data have been used where organic-rich beds occur, but authors caution about sedimentation rate effects and detrital dilution (Tribovillard et al., 2006; Amedjoe et al., 2018). Paleo-salinity proxies (B/Ga, Sr/Ba) have been suggested for restricted carbonate intervals but data are fragmentary.

Comparisons with adjacent basins and the Birimian basement indicate the Voltaian received most detritus from proximal Birimian terrains; episodic distal input and recycled sedimentation are inferred for certain intervals (Anani et al., 2012; Elburg et al., 2022; Zobah, 2022). These provenance signals are used to interpret passive-margin vs. foreland-type basin behaviour at different times during Voltaian deposition and to relate basin fill to Pan-African tectonic events (Carney et al., 2010; Kwayisi et al., 2024).

Despite steady advances, geochemical research on the Voltaian Supergroup still faces several challenges. Most studies remain geographically or stratigraphically limited, underscoring the need for systematic isotope sampling across complete successions to better resolve temporal provenance trends (Anani et al., 2012; Zobah, 2022). The adoption of modern in-situ techniques, such as laser-ablation Rb–Sr analyses of clays and authigenic phases, offers promising avenues to improve chronological reliability (Kwayisi et al., 2024). Likewise, integrating multi-proxy datasets—combining Sm–Nd isotopes with zircon U–Pb/Lu–Hf, heavy minerals, and trace-element proxies—would reduce interpretive ambiguity (Elburg et al., 2022). Improved understanding of diagenesis and weathering, particularly fluid-driven processes, will also refine Sr-based interpretations (Deynoux et al., 2006). Current evidence indicates a dominantly evolved Birimian crustal provenance with local variability, with Sm–Nd providing robust source-age constraints, Rb–Sr highlighting diagenetic overprints, and trace-element proxies aiding paleoenvironmental reconstruction. Progress hinges on stratigraphically resolved, multi-proxy studies supported by modern analytical innovations.

2.5.3 Sm–Nd and Rb–Sr studies of the Voltaian Supergroup (Ghana)

The Voltaian Supergroup blankets much of Ghana and parts of neighbouring countries. Its stratigraphy (lower to upper Voltaian: Kwahu-Bombouaka, Oti-Pendjari, Tamale-Obosum groups, etc.) and basin evolution have been the subject of sustained study because the succession records sedimentation along the eastern margin of the West African Craton and the influence of Pan-African tectonism (Carney et al., 2010; Kwayisi et al., 2024). Determining sediment provenance and depositional ages is central to reconstructing paleogeography and tectonic setting; Sm–Nd and Rb–Sr isotope systems have played key roles in this effort.

2.5.3.1 Sm–Nd studies: provenance and crustal evolution signals

Sm–Nd whole-rock and detrital studies are especially well suited to provenance studies because Sm and Nd have contrasting compatibilities and long half-lives that preserve deep-time source signatures. Several studies have applied Sm–Nd to Voltaian sandstones and shales with the primary goals of: (1) identifying whether the Birimian basement (adjacent Archean–Palaeoproterozoic rocks) was the dominant source, (2) testing for signals of Pan-African contributions, and (3) estimating model Nd ages for source terranes.

An early targeted study by Anani et al. (2012) analysed Sm–Nd isotopes in sandstones of the Lower Voltaian (Kwahu-Morago Group) and Middle Voltaian (Oti-Pendjari Group). The authors reported εNd values and model ages that were consistent with derivation from old upper-crustal Birimian metasediments and associated granitoids, with some contributions from more juvenile volcanic sources in parts of the basin (Anani et al., 2012). These results supported earlier

petrographic and heavy-mineral provenance indicators that implicated the surrounding Birimian basement as a key sediment source (Anani, 1999; Carney et al., 2010).

Wider geochemical studies that include Nd isotopes (e.g., Amedjoe et al., 2018) strengthen this picture. Amedjoe and colleagues combined major/trace element data and Sr–Nd isotopic compositions of shales and siltstones, concluding that felsic sources (granitoids/granodiorites) were primary contributors, with some recycled sediment and subordinate andesitic-derived material. Their Nd isotopic data support a dominantly evolved crustal source signature for much of the Voltaian succession (Amedjoe et al., 2018).

Recent regional syntheses and reviews (Zobah, 2022; Elburg et al., 2022) place these local Sm–Nd findings into a broader West African Craton framework: while the Birimian basement is the dominant proximate source, detrital zircon (U–Pb/Lu–Hf) and Sm–Nd trends point to variable inputs through time and possible distal contributions during specific intervals (Elburg et al., 2022; Zobah, 2022). In short, Sm–Nd data for the Voltaian generally indicate old continental crustal input with limited juvenile input except in localized sectors or stratigraphic intervals.

2.5.3.2 Rb–Sr studies: age constraints, clay minerals and basin timing

Rb–Sr work in the Voltaian has been applied in two complementary ways: (1) Rb–Sr whole-rock or mineral isochrons to provide depositional/diagenetic age estimates (often on clay fractions), and (2) Sr isotopes as provenance or diagenesis tracers. Earlier Rb–Sr clay mineral isochrons yielded dates that were widely cited in basin age discussions — for example, Rb–Sr ages on clay fractions from parts of the Kwahu-Bombouaka succession were reported in earlier work and used to argue for deposition around ca. 1000 Ma or, in other interpretations, younger Neoproterozoic ages

(Clauer & Deynoux cited in syntheses; Clauer & Deynoux-type data summarized in basin overviews). Clauer & Deynoux (1987) and later compilations reported Rb–Sr isochron ages on shales/clays that have been used to constrain lower-Voltaian deposition (see syntheses by Carney et al., 2010; Kwayisi et al., 2024).

More recent basin reconstructions (Kwayisi et al., 2024) combine Rb–Sr clay dates with detrital zircon geochronology and sedimentary facies constraints to refine age ranges: some Rb–Sr clay ages have been interpreted as indicating deposition near 959 ± 62 Ma for parts of the Kwahu-Bombouaka Group (Kwayisi et al., 2024; see also Deynoux et al. cited in regional overviews). However, authors emphasize the caveats associated with clay Rb–Sr ages (open-system behaviour, diagenetic resetting) and recommend combining Rb–Sr with other absolute dating tools.

In addition to absolute dating, Sr isotopes have been used as provenance and diagenetic tracers. Rb–Sr (and Sr isotopic) data from shales and carbonates provide additional constraints on basin evolution and possible seawater signatures where carbonate horizons are present (regional compilations and reviews: Carney et al., 2010; Zobah, 2022).

2.5.4 Integrated interpretations

Combined Sm–Nd and Rb–Sr lines of evidence converge on some clear conclusions for the Voltaian Supergroup:

The bulk of detritus supplying the Voltaian succession was derived from the adjacent Birimian basement—old, evolved crustal sources dominate Sm–Nd signatures (Anani et al., 2012; Amedjoe et al., 2018).

There are spatial and temporal variations: some formations (or parts of formations) record inputs from more juvenile or volcanic sources, and Nd model ages vary accordingly (Amedjoe et al., 2018; Elburg et al., 2022).

Rb–Sr clay mineral ages and Sr-isotope data provide useful chronological and diagenetic constraints but must be interpreted cautiously because of potential post-depositional mobility and open-system behaviour. Where Rb–Sr ages and detrital zircon ages agree, depositional age constraints are more secure (Carney et al., 2010; Kwayisi et al., 2024).

2.5.5 Geological Evolution of the Voltaian Supergroup

The Voltaian basin's geotectonic evolution is intimately linked to the Pan-African Dahomeyide orogeny. The Bombouaka Group is interpreted as continental and passive margin sediments associated with the opening of a Pan-African Ocean (Carney et al., 2010; Kalsbeek et al., 2008; Trompette, 1994). Subsequent collision and uplift during the orogeny led to the deposition of molasse-type sediments (Oti-Pendjari and Tamale-Obosum Groups) derived from the Dahomeyan terrane (Carney et al., 2010; Kalsbeek et al., 2008; Trompette, 1994). The Voltaian succession correlates with the Togo and Buem units (Carney et al., 2010; Kalsbeek et al., 2008). More recently, isotopic and detrital zircon studies have revived debates about its connection to Gondwana assembly, with implications for the evolution of the West African Craton and its margins (Abu, 2003; Mahamuda et al., 2013; Hirdes et al., 2020).

2.5.6 Tectonic and Paleogeographic Models

The evolution of the Voltaian Basin has been the subject of competing models, each highlighting different tectonic drivers and depositional settings. The cratonic sag basin model views the basin as the product of long-term thermal subsidence following supercontinent breakup, emphasizing its broad, stable geometry and thick sediment accumulation in an intracratonic setting (Kogbe, 1976). In contrast, the foreland basin model links the Voltaian to crustal flexure and subsidence resulting from Pan-African convergence, thereby positioning it as a peripheral depositional system influenced by orogenic loading (Affaton et al., 1991). A third interpretation considers the basin to have originated as a rift associated with Rodinia breakup, stressing extensional tectonics and syn-rift subsidence (Villeneuve & Cornée, 1994). While each of these models captures aspects of the basin's geometry and stratigraphy, recent detrital zircon geochronology (Hirdes et al., 2020; Gehrels et al., 2021) complicates the picture by revealing mixed age spectra indicative of polyphase sediment supply. Such evidence suggests that the Voltaian Basin cannot be adequately explained by a single tectonic model but rather records multiple phases of basin development, including possible transitions from initial rifting to cratonic sag subsidence and subsequent reactivation under Pan-African tectonism. This comparative perspective underscores the basin's significance as a dynamic archive of Neoproterozoic tectonic processes in West Africa.

The debate mirrors wider basin evolution theories, in which single basins often record multiple tectonic processes (Ingersoll & Busby, 1995). The Voltaian provides a key African example of how large intracratonic basins may evolve through multiple cycles of subsidence, sediment recycling, and tectonic overprinting, offering parallels to other Neoproterozoic basins such as the Taoudeni and Congo basins.

2.5.7 Synthesis and Theoretical Framework

The literature reveals that interpretations of the Voltaian Supergroup alternate between models of stability and tectonic dynamism. Petrographic and geochemical evidence suggest a mature cratonic sedimentary system, while isotopic data point to inputs from evolving Pan-African terranes. This tension reflects broader theoretical debates in geology concerning the interplay between cratonic stability and peripheral orogenesis during supercontinent assembly.

The literature on the Voltaian Supergroup highlights both significant advances and persistent uncertainties in understanding its geological history. By explicitly situating petrographic, geochemical, and isotopic findings within global models of provenance, basin evolution, and supercontinent cycles, the Voltaian emerges not merely as a regional sedimentary basin but as a critical archive for testing and refining broader geological theories. This theoretical framework sets the stage for the present study, which aims to integrate petrography and isotopic geochemistry to further constrain the depositional and tectonic evolution of the Voltaian Supergroup.

Table 2.1 Geotectonic Models for the Oti-Pendjari and Tamale-Obosum Groups of the Voltaian Supergroup, Ghana

Group / Formation	Proposed Geotectonic Model	Basis of Interpretation	Key References
Tamale Sandstone (Tamale-Obosum Group)	Passive continental margin	Mature quartz arenites, high CIA values (intense weathering), felsic source derivation, isotopic evidence of upper crustal sources	Affaton et al. (1980); Abu-Mahamuda et al. (2020)
Densubon Sandstone (Tamale-Obosum Group)	Active continental margin / transitional arc	Immature sandstones, mixed felsic and mafic inputs, variable CIA and ICV, Nd isotopic signatures suggesting recycled orogenic sources	Affaton et al. (1980); Bempah et al. (2021)
Undivided Obosum Formation (Tamale-Obosum Group)	Cratonic interior / passive margin	High quartz content, felsic provenance, high CIA (intense chemical weathering), isotopic ties to Birimian crust	Abu-Mahamuda et al. (2020); Kalsbeek et al. (2012)
Sang Conglomerates (Tamale-Obosum Group)	Continental island arc / syn-orogenic basin	Immature clastics, variable CIA, plagioclase-rich contributions, deposition in tectonically active setting	Affaton (1990); Bempah et al. (2021)
Older Oti Formations (Oti-Pendjari Group)	Glaciogenic foreland basin / passive margin	Evidence of glacial diamictites, mature litharenites, low to moderate CIA values, relatively stable tectonic setting	Affaton et al. (1980); Trompette (1994)
Younger Oti Formations (Oti-Pendjari Group)	Rift-related setting / active margin	Compositional variability, arkosic sandstones, volcanic arc detritus, Nd isotopes indicating inputs from Pan-African belts	Affaton et al. (1991); Abu-Mahamuda et al. (2020)
Oti-Pendjari (Upper units)	Volcanic arc / syn-orogenic setting	Presence of volcanic detritus, mixed felsic–mafic sources, tectonic activity linked to Pan-African orogeny	Affaton (1990); Bempah et al. (2021)

CHAPTER 3

3. MATERIALS AND METHODOLOGIES

In this study, the sampling strategy was carefully designed to ensure that the collected materials are representative of the lithological and stratigraphic variations within the Voltaian Supergroup. Sampling locations were selected based on a combination of field mapping, accessibility, and the need to capture both lateral and vertical variations across different formations. Particular attention was given to sites that exhibited well-preserved outcrops with minimal weathering or alteration, thereby maximizing the reliability of petrographic and geochemical analyses. The number of samples collected from each locality was determined by the diversity of lithologies present and the necessity to obtain statistically meaningful datasets, ensuring that both dominant and subordinate rock types were adequately represented. This approach provides a robust foundation for interpreting the provenance, depositional environments, and tectonic evolution of the basin.

A total of sixty (60) samples (consisting of sandstones, siltstones, mudstones, and carbonate rocks) were collected from the Tamale-Obosum and Oti-Pendjari Groups (Table 3.1). The collected samples were subdivided into four aliquots, with each allocated for distinct analytical procedures: heavy mineral assemblage characterization, petrographic examination, bulk-rock major and trace element analysis, and isotopic composition determinations.

Table 3.1 Sampling criteria for the Tamale-Obosum and Oti-Pendjari Groups.

GROUP	FORMATION	FIELD NAMES	NUMBER OF SAMPLES
Tamale-Obosum	Tamale sandstone	Sandstones	6
	Sang conglomerate	Conglomerate	1
	Densubon sandstone	Sandstone	8
	Undivided. Obosum	Sandstone	6
Oti-Pendjari	Bunya Sandstone	Sandstone	8
	Bimbila	Siltstone & sandstones	10
	Ejura sandstone	Sandstone	1
	Afram	Sandstone & shale	2
	Tease sandstone	Sandstone	1

3.1 Heavy mineral studies

The samples were crushed using the jaw crusher at the Geological survey authority after which they were wet sieved to remove the clay content. The sieve sets, stacked in descending order of their sizes, were shaken using mechanical sieve shaker continuously for about 20 minutes. During sieving proper attention was paid to minimize the sand loss from the sieve sets and the fine to medium grained sand sized sediment (63.5 microns to 2 mm in diameter) were collected and oven dried. The samples were subsequently bagged and labelled for separation.

The separation of the heavy minerals was performed by means of high-density liquid bromoform (2.89gm/cc) in fume chamber to extract the toxic fume while carrying out the experiment (Figure 3.1). There is a considerable difference in densities between the lighter and heavier minerals. According to this density variation, the higher density (heavy mineral) will sink, and the lower density (lighter mineral) will float. Thus, the heavy liquid was filled in a separating funnel, the dry and weighed sample of 5 gm was then added to the liquid and later stirred to ensure that the grains were thoroughly wet. Grains adhering to the stirring rod or the side of the funnel were removed

using the heavy liquid. Consequently, the heavy minerals accumulated in the bottom of the funnel above the pinch clip. After three hours, when no more grains sink further, the pinch clip was opened slowly, thus allowing the heavy fraction to pour onto the filter paper in the lower funnel. Then the pinch clip was closed, leaving a layer of clear liquid below the light fraction. A new funnel, with filter paper, was placed under the separating funnel. The fraction was then drained into the new funnel. Subsequently, the wall of the separating funnel was rinsed with acetone and distilled water, and also both fractions are washed thoroughly, and set aside to dry. The used heavy liquid and washings were collected. The heavy liquid was re-used for other sets. Both the fractions were dried and collected in well labelled zip-lock bags. For each sample, three sets of heavy minerals were separated for further morphological, geochemical and petrographic studies (using the SEM, XRD and XRF tools).

Figure 3.1 Set-up for samples for heavy mineral separation via the gravimetric method using Bromoform Liquid.

3.2 Petrographic Studies of Rocks

Samples collected from the field were washed, cut and polished for thin sections. The thin sections were produced at the Department of Earth Science, University of Ghana and the Ghana Geological Survey Authority, and subsequently studied using the Leica DM 2500M optical microscope (Figure 3.2).

Figure 3.2 A) Thin section cutting machine, B) cut sections of rocks for thin section preparation and C) optical microscope for petrographic studies.

3.3 Isotopic measurements

Forty-five (45) samples from the Oti-Pendjari and Tamale-Obosum groups were analyzed for their Rubidium- Strontium and Samarium-Neodymium isotopic compositions at the WIGL of the University of Witwatersrand, Johannesburg. Whole rock analyses using the ICPMS and XRF were carried out prior to this stage, to obtain the elemental compositions of Rb, Sr, Nd and Sm. This was followed by spiking of the samples which entailed measuring the calculated mass of sample and adding the required quantity of Sm-Nd and Rb-Sr. After which, the samples were digested in the following stages:

1. 3 mL conc. HF + 1.5 mL conc. HNO_3 is added to each sample. The samples are placed on a 110 °C hotplate for ~1 week.
2. Samples are left to dry down overnight on the hotplate.
3. Once dry, 3 mL conc. HNO_3 + 1 mL conc. HCl is added to each sample. The samples are placed on a 110 °C hotplate for ~1 week.
4. Samples are left to dry down overnight on the hotplate.
5. Because the samples are sedimentary, an additional H_2O_2 step is done to ensure that there is no organic carbon. 100 µL H_2O_2 is added to each sample and dried down immediately on the hotplate. The reaction can be violent and very hot.
6. Once H_2O_2 has evaporated, 2 mL conc. HNO_3 is added to each sample. The samples are placed on a 110 °C hotplate for 2 days.
7. Samples are left to dry down on the hotplate.
8. Once dry, 3 mL of 6 M HCl is added to each sample. The samples are placed on a 100 °C hotplate for ~2 days.
9. Samples are left to dry down overnight on the hotplate.
10. Once dry, 3 mL of 6 M HCl is added and the samples are left uncapped on the hotplate to dry down immediately.
11. The samples are fully digested and ready for chemistry.

3.3.1 Rb-Sr Chemistry:

Rb and Sr separation: 2 mL BioRad AG50 x8, 200-400 mesh resin

Spiked and digested samples are prepared for chemistry with 1 mL 1.5 M HCl. Samples are centrifuged before loading onto the columns.

condition	2 mL	1.5 M HCl			
	2 mL				
	2 mL				
load	1 mL				
rinse	1 mL				
	1 mL				
matrix	4 mL				
Rb elution	**5 mL**		**Collect**		
Ca	9 mL				
Sr elution	**15 mL**		**Collect**		
HREE	2 mL	6 M HCl			
LREE	**7 mL**		**Collect for Sm-Nd column**		
Wash	10 mL				
	10 mL				
	10 mL				

Samples are left to dry down overnight on a 100 °C hotplate.

Rb and Sr separates: 2-3 drops of concentrated HNO_3 is added to each sample and left to dry down to dissolve any possible resin residue. Once dry, a few drops of 2 % HNO_3 is added to each sample to ensure that dry samples are not lost due to static and handling of the beakers.

Once LREE separates are dry, add 0.3 mL of 0.2 M HCl to each sample. They are ready for the next stage of chemistry.

Columns were re-equilibrated with MQ H_2O before storage.

1. Turn the column upside down and gently add MQ H_2O into the bottom of the column.
2. The resin will start to move down.
3. Let the resin drip into a clean PFA beaker.
4. Once all the resin has dripped into the beaker, flip the column over and fill with H_2O.
5. Ensure that there are no bubbles in the space where the resin bed will be.
6. Swirl the resin in the PFA beaker and pour into the column.
7. The resin will settle to the original level.

8. Place the column in the stand for the water to drip.
9. Once each column is done, store the columns in water in the appropriate box.
10. Repeat for each column.

3.3.2 Sm-Nd Chemistry

Sm and Nd separation: 1 mL Eichrom Ln Spec 100-150 µm resin

Samples should be prepared in 0.3 mL of 0.2 M HCl.

condition	2 mL	0.2 M HCl		
	2 mL			
	2 mL			
load	0.3 mL			
rinse	0.4 mL			
	0.4 mL			
La-Ce	4 mL			
Nd elution	**10 mL**		**Collect**	
rinse	1 mL	0.4 M HCl		
Sm elution	**7 mL**		**Collect**	
Wash	10 mL	6 M HCl		
	10 mL			
	10 mL			

Samples are left to dry down overnight on a 110 °C hotplate.

Once dry, a few drops of 2 % HNO_3 was added to each sample to ensure that dry samples are not lost due to static and handling of the beakers. Nd and Sm isotope measurements were conducted using a low-resolution mode on a Nu Plasma II MC-ICPMS (Nu Instruments, Wrexham) located at the Analytical Facility of the University of Johannesburg. Prior to each measurement session, the instrument underwent optimization to ensure sensitivity and stability. Samples and standards were introduced into a 2% HNO_3 solution using wet plasma, utilizing a self-aspirating 200µl/min Glass Expansion MicroMist U-series nebulizer. This nebulizer was connected to a Peltier cooled quartz Glass Expansion Twister Spray Chamber, maintained at 7°C. Plasma settings included an

RF power of 1300W, coolant gas flow of 13.0 L/min, auxiliary gas flow of 0.80 L/min, and nebulizer setting of approximately 35 psi. Nd and Sr analyses comprised a single block of 50 cycles, each with a 10-second integration time, while Sm and Rb analyses consisted of one block of 20 cycles with a 10-second integration time for each cycle. Background measurements for Sm, Nd, and Rb extracts were conducted at a magnet offset of half a mass unit from the measurement position for 30 seconds prior to each measurement and were subsequently subtracted from the signal. Sr background measurements were performed on peak in a blank solution at the beginning of each measurement session and subtracted from the signal. Automatic peak centering was executed before each measurement, and washout between samples utilized a 2% HNO_3 solution. Data reduction was carried out offline using a customized Microsoft Excel spreadsheet. Mass bias corrections were applied according to the exponential law. Spiked Nd extracts were corrected using a $^{146}Nd/^{145}Nd$ ratio of 2.0719425 (Vance & Thirlwall, 2002), while Sm was corrected using the accepted $^{152}Sm/^{147}Sm$ ratio of 1.78307. For Sr measurements, the accepted $^{88}Sr/^{86}Sr$ ratio of 8.375209 was utilized for mass bias correction calculations, with the $^{85}Rb/^{87}Rb$ ratio of 2.59376 used to correct for ^{87}Rb interference on ^{87}Sr. The JNdi-1 standard was measured after every four samples. Additionally, Sm-Nd isotopic analyses of the USGS reference material BCR-2 produced a $^{143}Nd/^{144}Nd$ ratio of 0.512612 ± 04 (1SD, n=4), which aligned closely with the recommended value of 0.512635 ± 29 from GeoRem (http://georem.mpch-mainz.gwdg.de).

3.4 Whole Rock Geochemistry

3.4.1 XRF major elements

Major elements were determined using the Norrish Fusion 1 technique using in-house correction procedures and using a Panalytical PW2404 X-ray fluorescence spectrometer. Major elements were fused using Johnson Matthey Spectrolflux 105 at 1100°C and raw data corrected using in-

house software. Standard calibrations were made up using synthetic oxide mixtures and international standard rocks as well as in-house controls. Sample weight used was 035 gm and flux weight 2.5 gm. Calibration standards were primary International Reference Materials USGS series (USA) and NIM series (South Africa). Precision is taken as 1% for elements in abundance of greater than 5% by weight, and 5% for elements in abundance less than 5%. The instrument used was the Philips PW2404 x-ray spectrometer. Standard calibrations use BCR2, NIM-P, NIM-D, W-2, NIM-S, GSP-2, NIM-N, NIM-G, PCC1, BHVO2, AGV2, G2 DTS1.

3.4.2 XRF trace elements

Trace elements were determined on pressed pellets using a Moviol solution binder. Standardization was carried out using International Reference Materials USGS series (USA) and NIM series (South Africa). Precision was determined on the basis of counting time and is taken as 5% for elements in abundance greater than 100 ppm, and 10% for elements in abundance between 10 and 100 ppm. The instrument used was the Philips PW2404 x-ray spectrometer.

3.4.3 PGE Analyses

The platinum group elements (Pt, Pd, Rh, Ru, Ir and Os; also to include Au) were determined by standard fire assay methods using S based flux and collected in NiS. Final analysis was by ICP-MS. Detection limits of the PGE and Au are as follows (all in ppb): Pt 2; Pd 2; Rh 1; Ru 2; Ir 2; Os 2; Au 5). Repeated analyses were carried out on 10% of all samples and repeatability was in all cases better than 10%. Instrument used was the Perkin Elmer DRC-e.

3.4.4 ICP-MS Trace Elements

Trace elements were determined using the Perkin Elmer DRC-e and analyzed against certified primary solution standards. International reference materials AGV-2, BCR-1 and BR-1 were

analyzed with every run. The agreement to accepted values of the standards was better than 10% for all elements and in many cases better than 5%. Dissolution of 50 mg of sample was carried out with high purity HF-HNO_3 using a MARS microwave digester.

3.5 Provenance studies of framework grains

Sandstone samples for this study were collected from outcrops in various areas of the Tamale-Obosum and Oti-Pendjari Groups. Fresh rock exposures were scarce due to intense tropical weathering and coverage of the outcrops by water bodies, since the sampling period was met with some unexpected, intensified rains. Twenty (20) of the least weathered samples were selected for petrographic studies. Framework mineral composition was quantified using the point counting method of Gazzi-Dickinson (Ingersoll et al., 1984). For each thin section, 500 counts were made. Matrix-free recalculated data from point counting of the framework grains are listed in Table 4.4. The data was plotted on the QFL diagrams of Folk (1974) for rock classification and Dickinson (1985) for provenance indications, of the sandstones. Polycrystalline quartz, though not as durable as monocrystalline quartz, was placed at Q-pole to obviate the problems of distinction between plutonic polycrystalline quartz and metaquartzite fragments. In the triangular diagram constructed for delineating the provenance, polycrystalline quartz was placed at the rock fragment (RF) pole (in the Lt pole of QmFLt diagram of Dickinson and Suczek (1979)). Also, Chert was placed at the RF pole as its origin can be unequivocally traced to a sedimentary source, though it was plotted at the Q-pole by several earlier workers (Pettijohn et al., 1987; Blatt, 1967). Chert is less stable than quartz during transport and chert fragment placed into the RF-pole (Folk, 1974). The F-pole comprises all types of feldspar grains (Folk, 1974; Pettijohn et al., 1987). For recognition of source rock lithology and tectonic setting of the Tamale and Oti Group rocks, the modal analysis data were plotted on the diamond diagram of Basu et al. (1975) and Tortosa et al. (1991).

3.6 Quality control measures

To ensure the reliability and accuracy of the analytical results, this study incorporated strict quality control measures throughout the laboratory procedures. Internationally certified reference materials, such as USGS standards (e.g., BCR-2, AGV-2, BCR-1 and BR-1), were analyzed alongside the samples to monitor instrument calibration and assess analytical precision. Procedural blanks were run at regular intervals to detect any potential contamination introduced during sample preparation or instrumental analysis. In addition, replicates of selected samples were re-analyzed to evaluate reproducibility and confirm internal consistency across datasets. For isotopic work, standards such as La Jolla Nd and NBS 987 Sr were employed to monitor mass spectrometer stability and ensure data accuracy. Analytical uncertainties are reported at the 2σ level, providing a transparent indication of the precision associated with both elemental and isotopic measurements. These quality control protocols not only enhance confidence in the generated petrographic, geochemical, and isotopic data but also align the study with best practices in sedimentary basin research, thereby ensuring that the interpretations presented are both robust and scientifically defensible.

CHAPTER 4

4. RESULTS

4.1 Petrography

A total of twelve different lithostratigraphic units were identified (Figure 4.11) and collected from the formations as grouped below:

Tamale-Obosum Group - Tamale Sandstone Formation
Sang Conglomerate Formation
Densubon Sandstone Formation
Dunkro Sandstone Formation
Undivided Obosum Formation

Oti-Pendjari Group - Bunya Sandstone Formation
Bimbila Formation
Tease Sandstone Formation
Ejura Sandstone Formation
Afram Formation
Kodjari Formation - Darebe Tuff Member
Buipe Limestone Member

4.1.1 Tamale Sandstone Formation

Outcrops occur in and around Tamale and are chocolate /dark purple/ reddish in colour, medium, angular to sub-rounded grains. Outcrops are hematite stained, mature sediment, micaceous quartz rich arenite. Red, medium-grained, moderately well-sorted quartz rich sandstone with rounded to subangular grains (Figure 4.1). Mineralogical content: Quartz 80, Mica - 10%, Lithics - 5% , Hematite - 5%.

Figure 4.1 Field exposure/ouitcrop of the Tamale sandstones: photomicrographs in plane (PPL) and crossed polarized light (XPL).

4.1.2 Sang Conglomerates Formation

The Sang conglomerates is polymictic and consists of sub-rounded to rounded pebbles and cobbles (clast size range of 3-16cm) of varying lithologies. The cobble and pebble conglomerate is interbedded with lithic and feldspar-rich sandstone bearing pebbly layers and lenticles. Pebbles include quartz and quartzitic sandstone, together with 'basement' lithologies such as green metavolcanic rock, jasper and various types of schist and phyllite. Clasts are locally closely packed, but mostly are supported within a dark grey coarse sand matrix (Figure 4.2).

Figure 4.2 Field exposure/ouitcrop of the Sang conglomerates: photomicrographs in plane (PPL) and crossed polarized light (XPL)

4.1.3 Undivided Obosum Beds

Excavated outcrops of pale green/grey with pink bands, fine to medium grained feldspathic sandstone found along the road to Densubon. Micaceous, poorly sorted, angular grains, immature sediment (Figure 4.3).

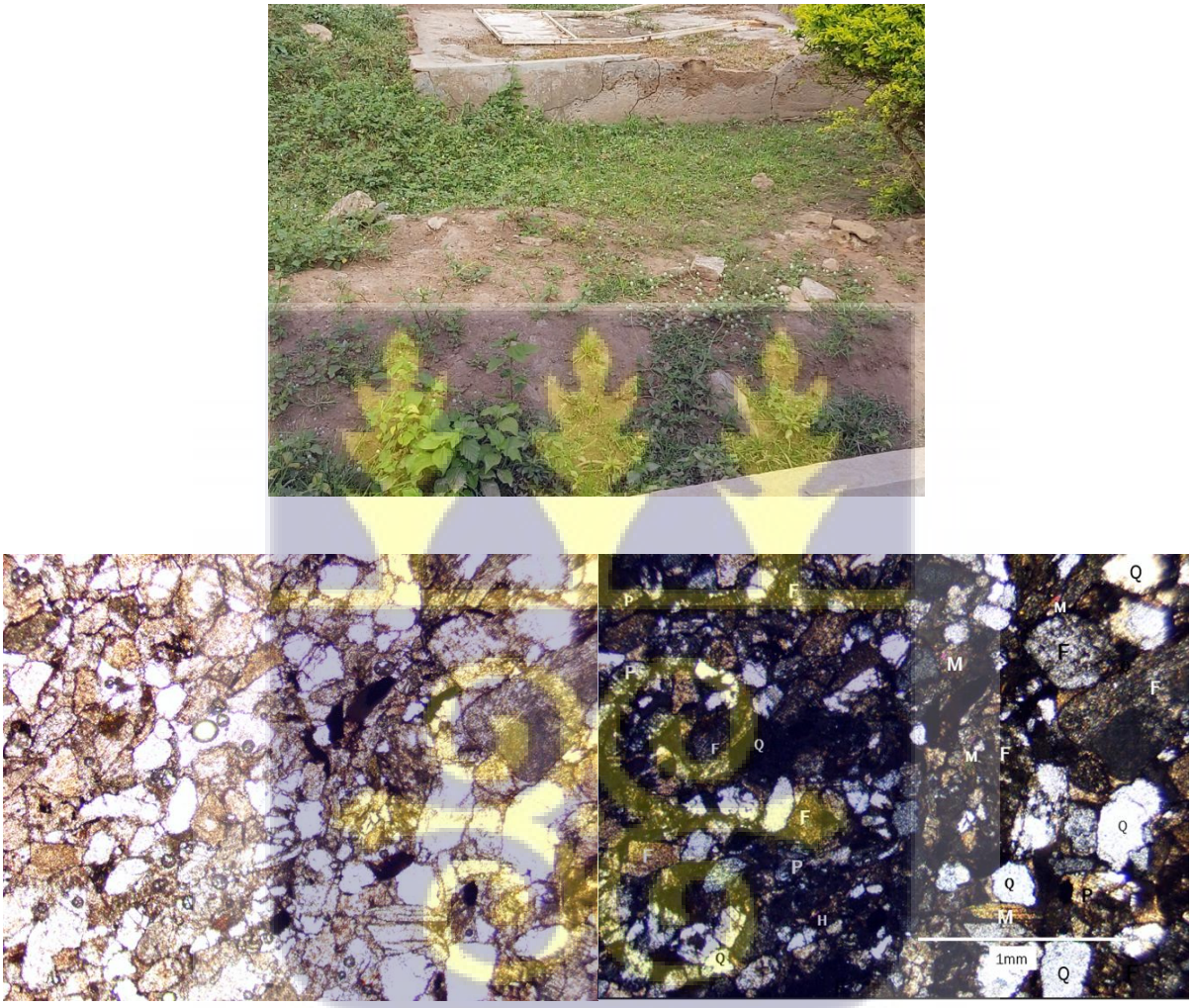

Figure 4.3 Field exposure/outcrop of the Undivided Obosum beds: photomicrographs in plane (PPL) and crossed polarized light (XPL)

4.1.4 Densubon Sandstone Formation

Outcrop exposures were found around the Akroso ferry station. Rock exhibits grey and pink banding, coarse grained, moderately sorted, sub-rounded to rounded grains and feldspathic sandstone. Samples are also characterized by crenulated bedding (Figure 4.4).

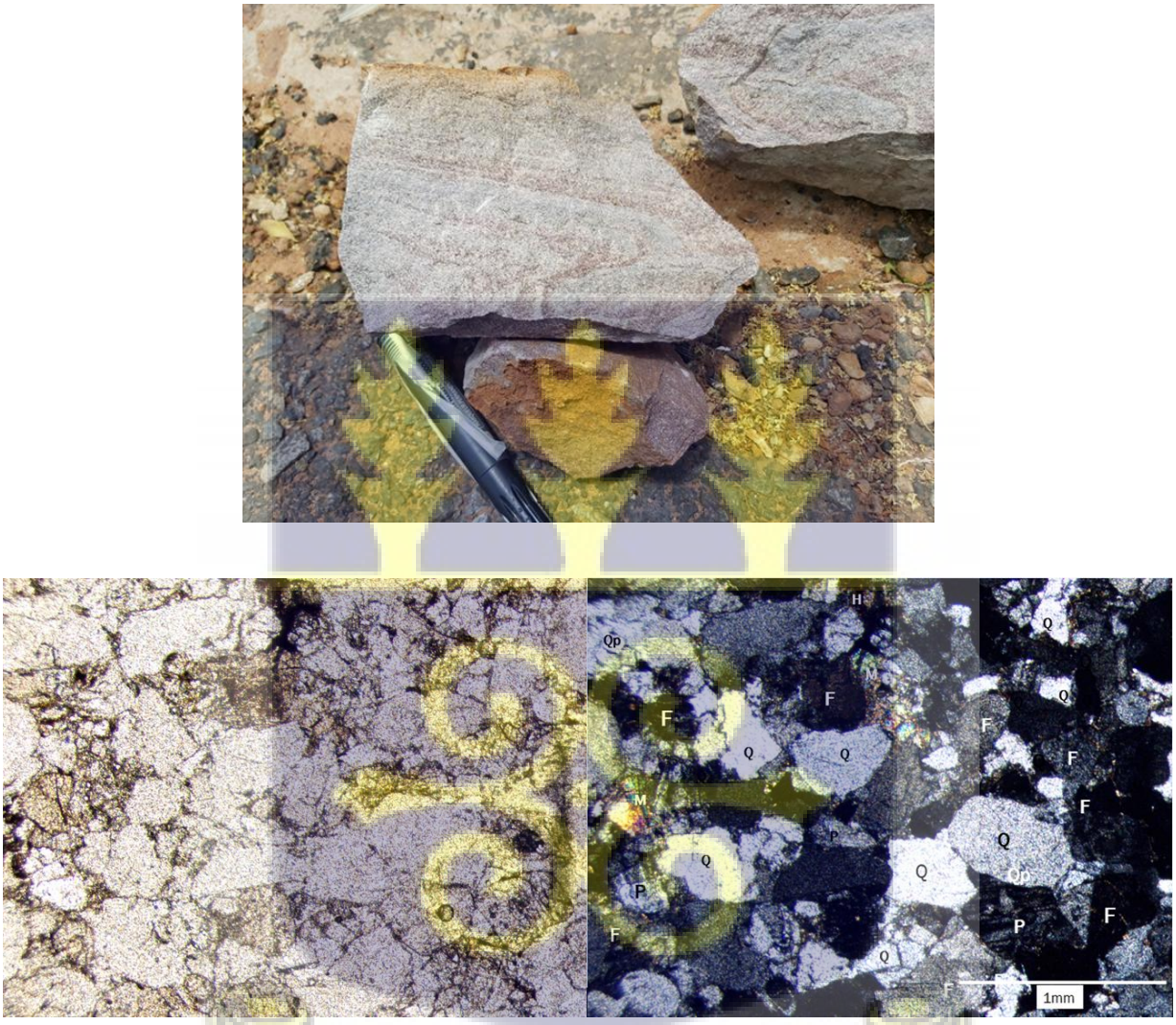

Figure 4.4 Field exposure/outcrop of the Densubon sandstones: photomicrographs in plane (PPL) and crossed polarized light (XPL)

4.1.5 Dunkro Sandstone Formation

Chocolate/maroon, medium to coarse, angular to sub-rounded grained, poorly sorted, immature feldspar-lithic arenites with intercalating beds of polymictic conglomerates (Figure 4.5). Outcrops were located in parts of Somanhyia and its environs. The conglomerate beds contain 'floating' pebbles, cobbles and boulders of basement rocks, including green chert, various granitoid and foliated metamorphic lithologies and dark green-grey porphyritic volcanic rock.

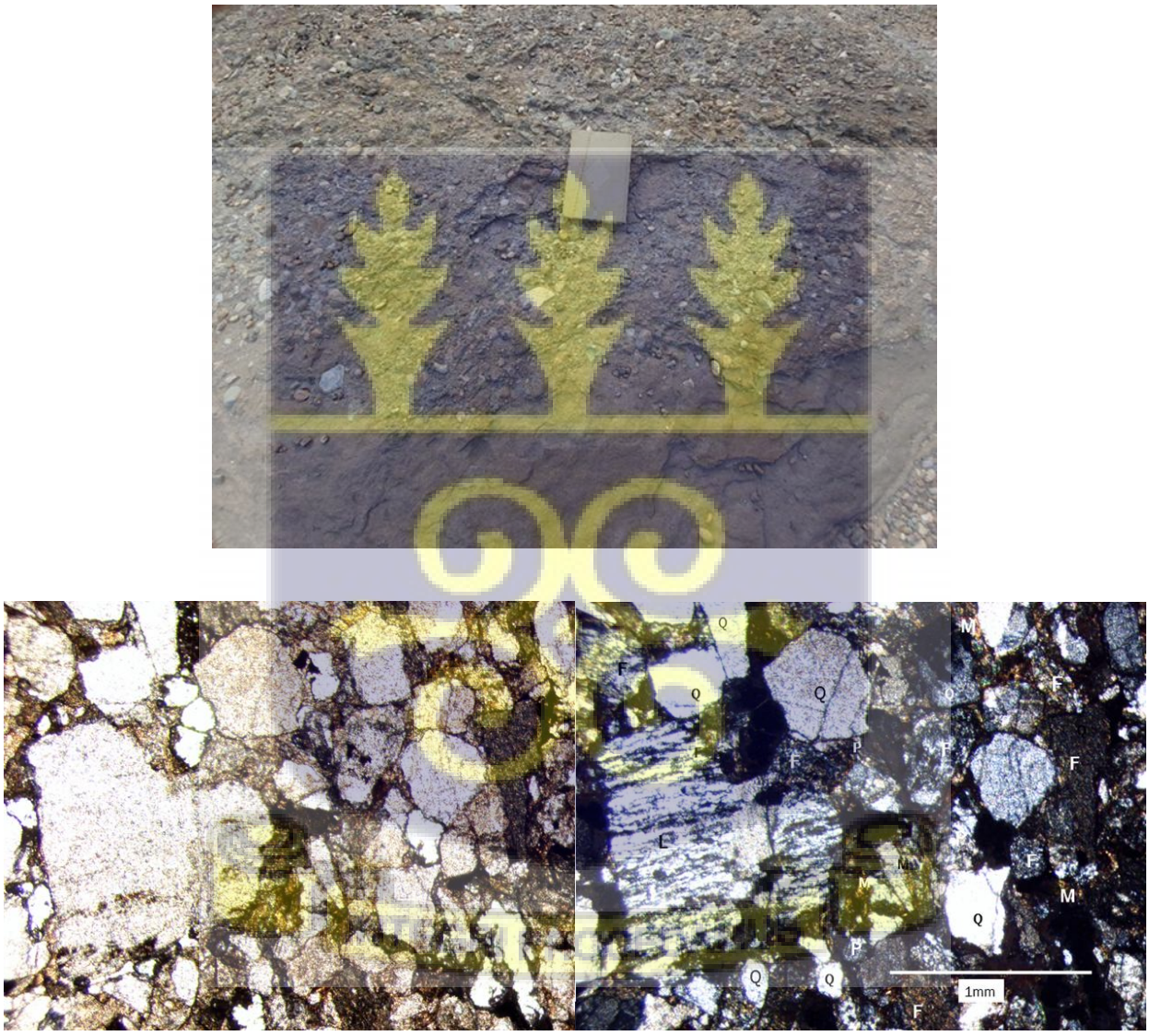

Figure 4.5 Field exposure/outcrop of the Dunkro sandstones: photomicrographs in plane (PPL) and crossed polarized light (XPL).

4.1.6 Bunya Sandstone Formation

Outcrop is medium to coarse grained, thin bedded, cross-stratified, pale yellow/green to tan colour, micaceous, feldspathic, poorly sorted, angular to sub-rounded, immature sandstone (Figure 4.6). Found in locations moving south from Bimbila to Kpandai and Bunya townships.

Figure 4.6 Field exposure/outcrop of the Bunya sandstones: photomicrographs in plane (PPL) and crossed polarized light (XPL).

4.1.7 Bimbila Formation

Yellowish grey medium to coarse grained, angular to sub-rounded, moderately sorted, feldspathic sandstones (Figure 4.7). Located in and around Bimbila township.

Figure 4.7 Field exposure/outcrop of the Bimbila sandstones: photomicrographs in plane (PPL) and crossed polarized light (XPL).

The second lithology is invariably pale grey-green, fine-grained lithic and feldspathic wackes in which angular to subangular grains of plagioclase, K-feldspar and unstable detrital silicates such as clinopyroxene, hornblende and chlorite are abundant (Figure 4.8).

Figure 4.8 Field exposure/outcrop of the Bimbila formation siltstones: photomicrographs in plane (PPL) and crossed polarized light (XPL).

4.1.8 Tease Sandstones

Outcrops are cream to tan in colour, thickly bedded, faulted, coarse grained quartz arenite (Figure 4.9). Outcrops were observed in Tease and its environs.

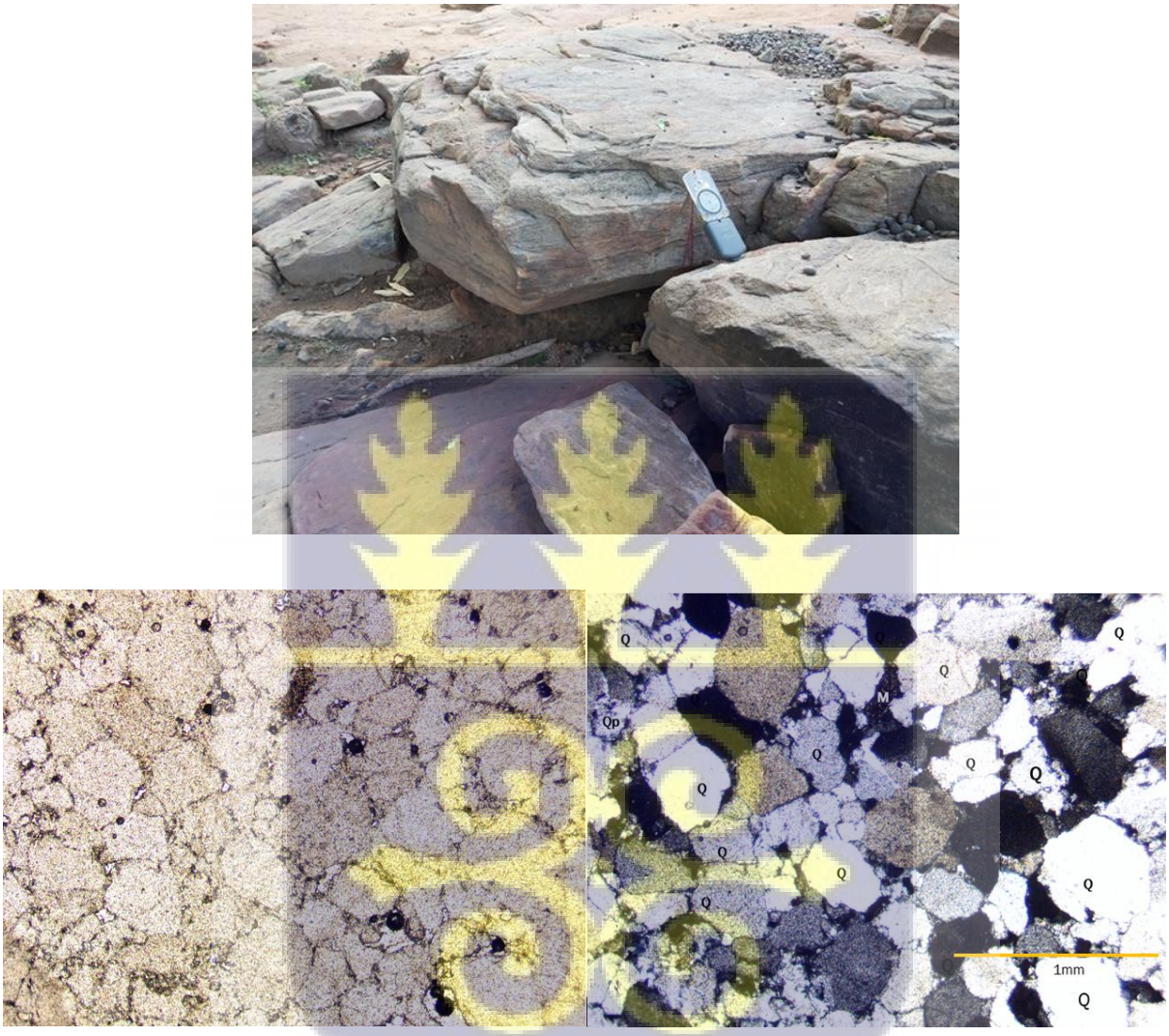

Figure 4.9 Field exposure/outcrop of the Tease sandstones: photomicrographs in plane (PPL) and crossed polarized light (XPL).

4.1.9 Afram Formation

Outcrop exposures of alternating beds of red and grey thin bedded siltstone and sandstone beds, exhibiting almost parallel bedding (Figure 4.10).

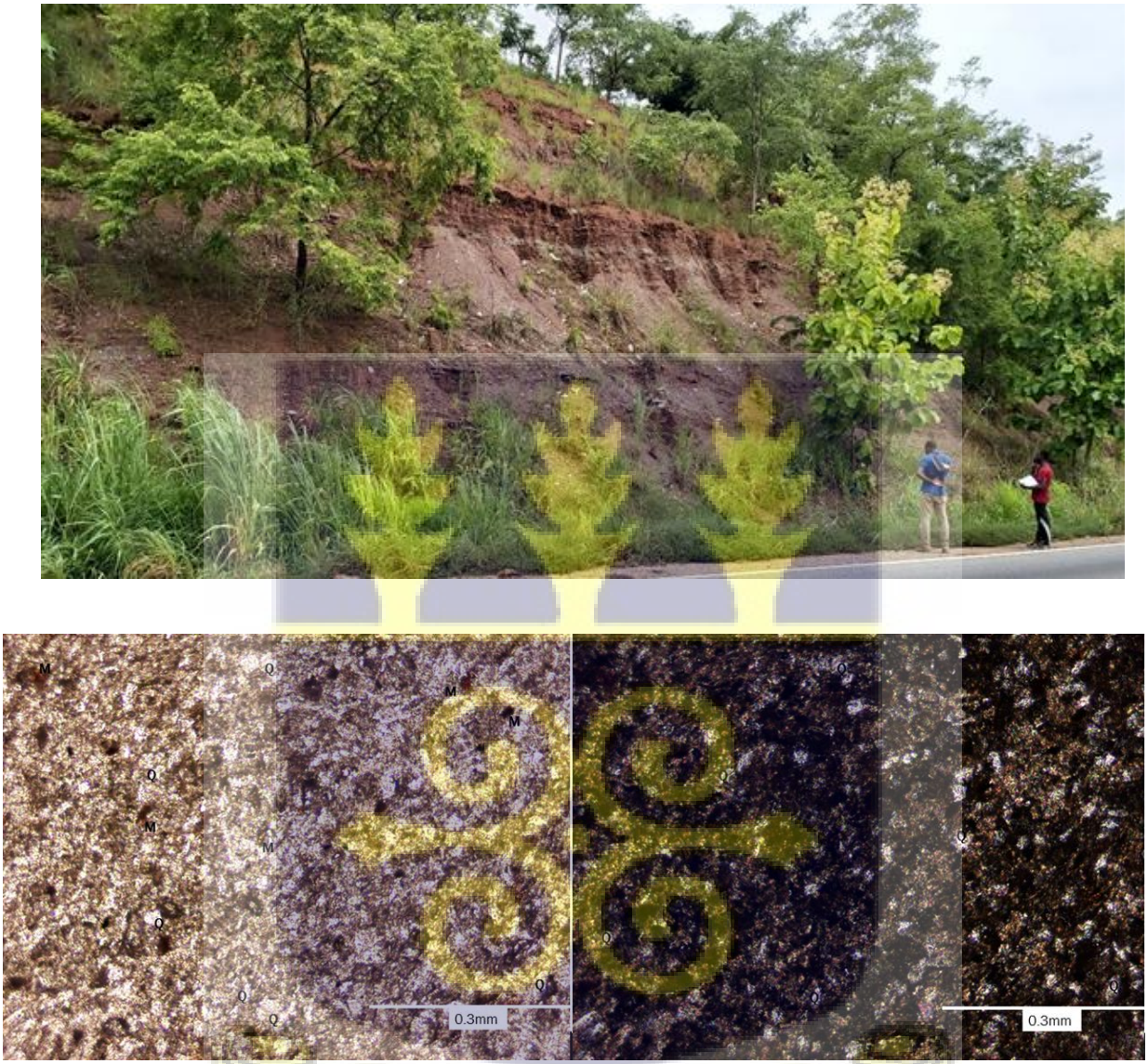

Figure 4.10 Field exposure/outcrop of the Afram formation: photomicrographs in plane (PPL) and crossed polarized light (XPL).

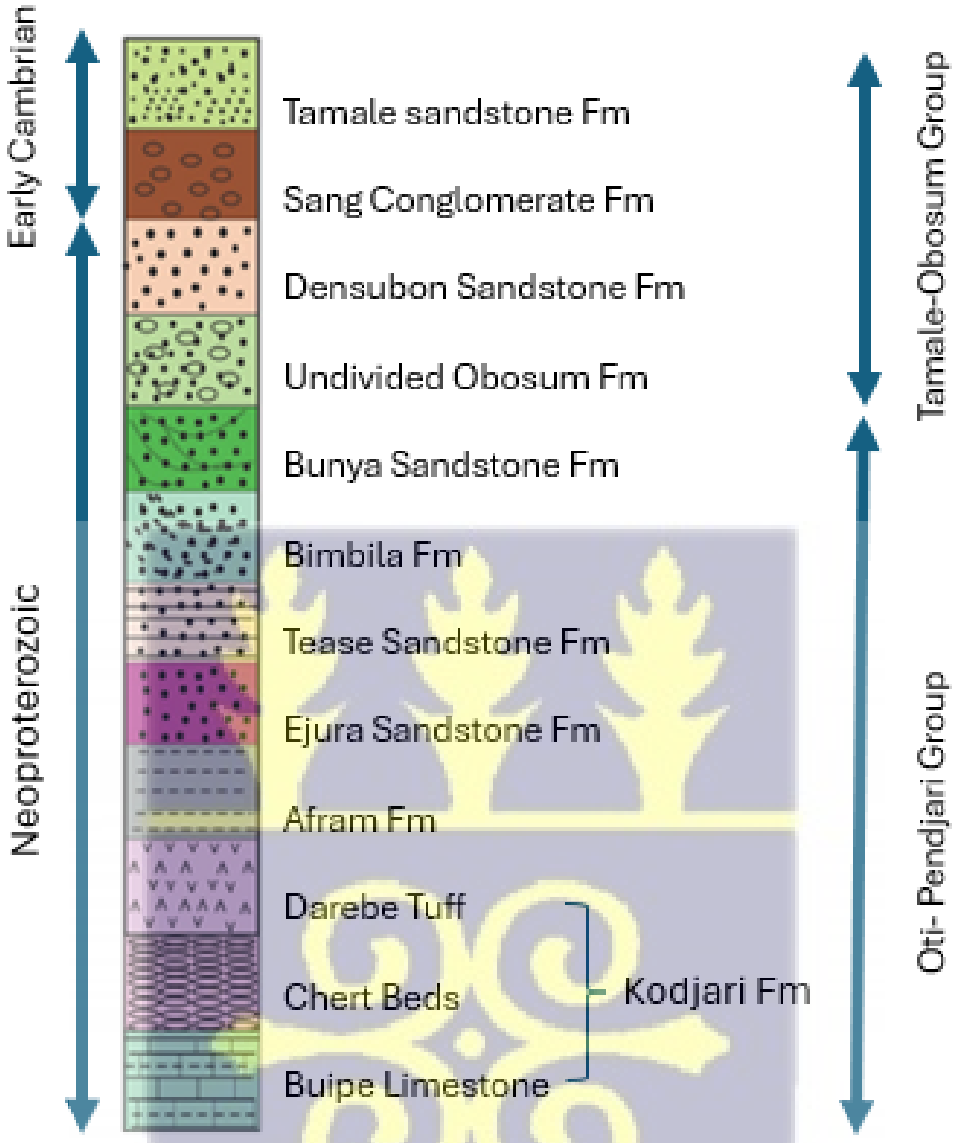

Figure 4.11 Stratigraphy of the Middle and Upper Voltaian Supergroup, Ghana, based on field observations. Age of limestone from Carney et al. 2010.

4.2 Heavy Mineral Composition

The heavy minerals separated from the sandstone samples collected from the field were analyzed using the XRD and the results obtained are represented in Figure 4.12a. The minerals identified in the separates were rutile, zircon, tourmaline, garnet, apatite, spinel, ilmenite, Talc, Dolomite, Chlorite, Wollastonite, Magnesia, Goethite, Carbon, Alumina, Graphite, Cassiterite, Siderite. A portion of the heavy minerals point mounted (Table 4.1) and studied using the optical microscope, showed similar group of minerals as identified by the XRD (Table 4.2), such as tourmalines, rutiles, zircons, biotites, muscovites, garnets, chlorite, amphiboles, epidotes, spinel and others (Figure 4.12b). The samples from the Oti-Pendjari Group (i.e. the Bunya Sandstone Formation) showed two sets of sediment sizes: angular to subrounded fine sized grains and sub-rounded to rounded coarse sized grains. Considering samples from the Tamale-Obosum Group, heavy minerals from the Densubon Formation showed mostly coarse sized grains which were sub-rounded to well rounded, whereas the Tamale Sandstone Formation was constituted by two sets of sediment sizes fractions: angular medium sized grains and sub-rounded to rounded coarse sized grains. The heavy mineral indices for the selected formations of the Tamale and Oti Groups display marked variability, reflecting differences in provenance and sedimentary maturity. In the Tamale Group, the Tamale Sandstone and Undivided Obosum Formation show high ZTR (zircon–tourmaline–rutile) indices. Conversely, the Densubon Sandstone records comparatively lower ZTR values alongside elevated garnet and opaque mineral contents. Within the Oti Group, the Bunya and Bimbila sandstones exhibit moderate ZTR indices with significant variations in garnet–zircon and rutile–zircon ratios. The Afram Formation is distinguished by higher proportions of stable heavy minerals (Table 4.3).

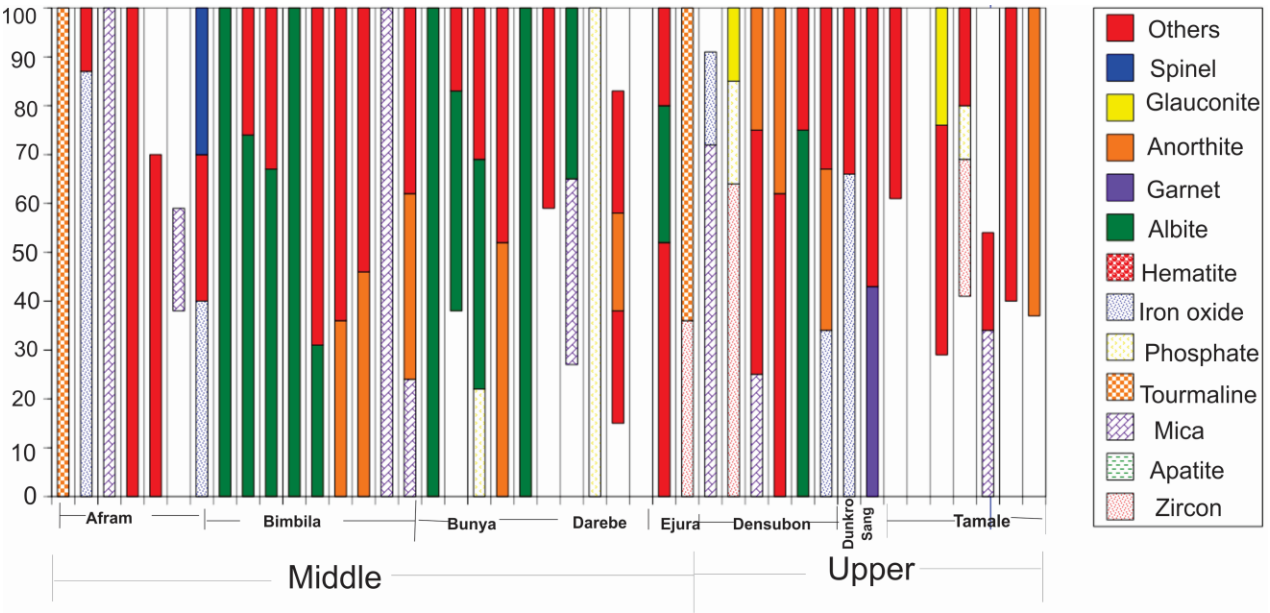

Others = Talc, Dolomite, Chlorite, Wollastonite, Magnesia, Goethite, Carbon, Alumina, Graphite, Cassiterite, Siderite

Figure 4.12a Heavy mineral chart form XRD analyses, normalized to 100% total abundance.

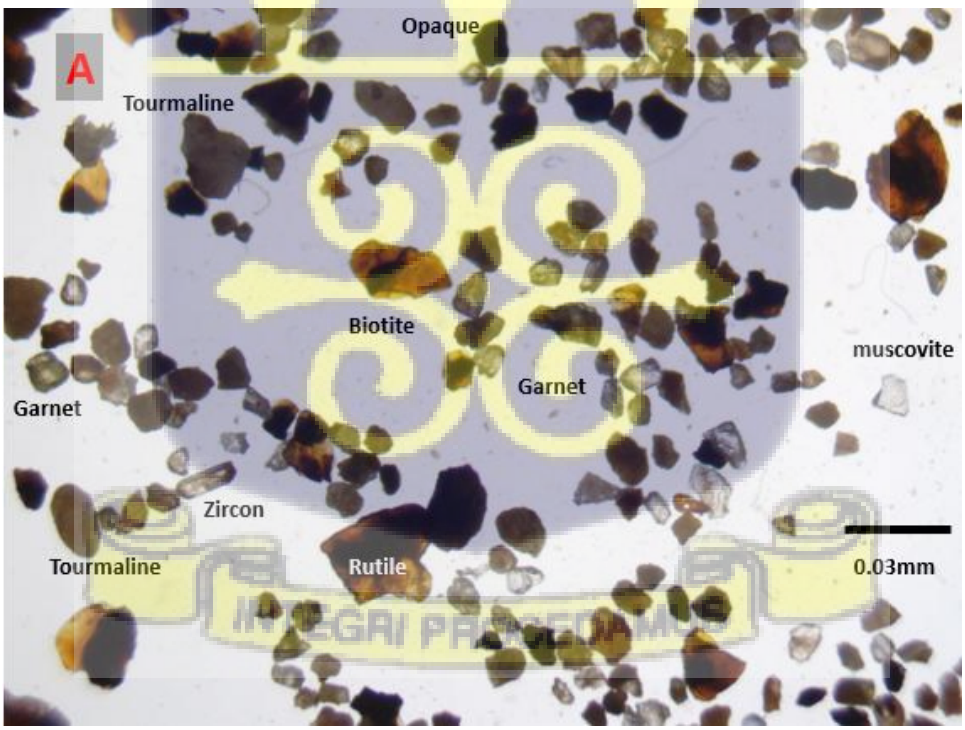

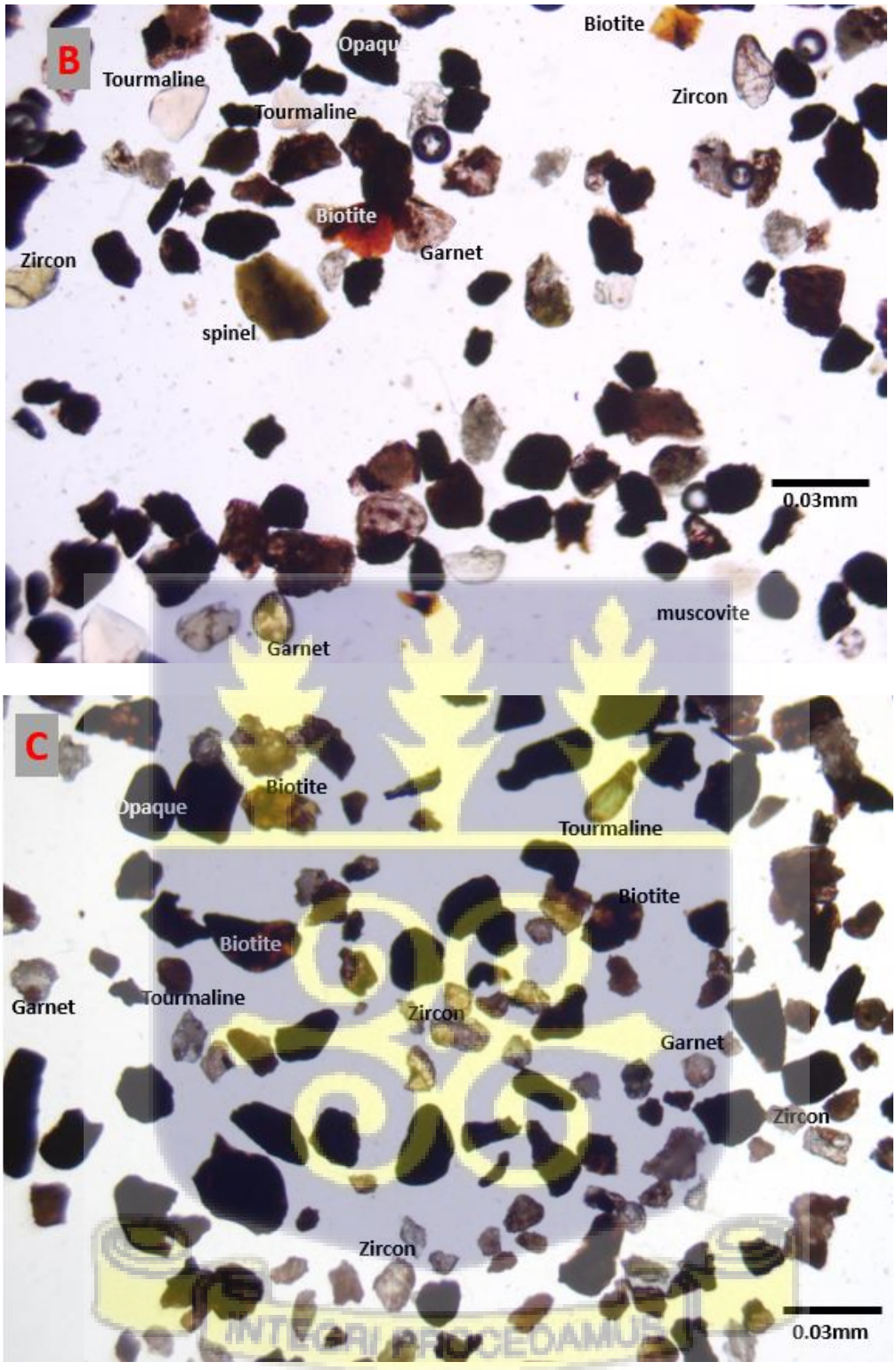

Figure 4.12b Heavy mineral grain mounts, A) Bunya sandstone formation (Oti-Pendjari Group), B) Densubon sandstone formation, C) Tamale sandstone formation (Tamale-Obosum Group)

Table 4.1 Point count of heavy minerals in the formations of the Tamale-Obosum and Oti-Pendjari Groups.

Formation	TUR	ZRN	RT	AP	EP	GRT	BT	MS	ANT	AND	SIL	SP	CST	CHL	KY	SUL	OPA	AMB	PYX
Afram	43.2	15.6	2	1.4	6.2	0	4.8	7	0	5.6	0	0	0.8	2.2	2.6	0.2	0	2.6	0
Densubon	11.6	11	0.4	0.4	0.8	3.8	1.2	1	0	18.4	0	0	1.6	1.2	0.6	0.6	3.4	14.8	22
Bunya	7.8	10.8	0.4	1.8	7.4	0	9.4	1.4	0	9.6	0	8.2	0.6	1.6	3.8	2.2	0.2	2.8	23
Bunya	1.8	4.4	0	0.4	10.8	0	12	1.2	0	0.8	1	0	0	7.6	1.4	0	0.2	38	21
Densubon	30.6	37.4	0	0.2	5.8	0	0	0	0	0	0.6	0	0	0.2	9	0.4	0	0	0
Densubon	7	14.4	1.6	11.4	2.6	0	1.8	1.4	0.6	14	4.4	2	3	1.8	6.8	1.2	0	14.8	11
Densubon	30.6	37.4	0	0.2	5.8	0	0	0	0	15.8	0.6	0	0	0.2	9	0.4	0	0	0
Densubon	5.2	15	2.8	5.4	9.2	14.8	8	11.4	0	0.8	0	0	0	0	6.2	0	0	0	21
Afram	0.8	5	0	3	1.8	0.8	16	5.6	0.2	19.6	23.2	0	0	1	23	0	0	0	0
Dunkro	2.2	5.6	0	0	9.6	2	6.4	7.2	0	5	1.2	5.2	3.2	5.8	1.8	0	0	15	30
Densubon	23	25.2	3	0	0	4.2	4.8	0	0	2.8	2.8	0	6.8	6.8	0.6	0	9.8	1.6	8.6
Tamale	28.8	22.4	3.4	0	3.8	0	3	1.2	0	31.6	0	0.2	0	0	0.8	0	0	0	4.8
Kodjari	7.6	5.6	0.6	0.2	6.6	5.2	7.6	6.4	0	0.6	1.2	0.8	11	2.8	1.4	0	24.4	0	13
Bimbila	5.8	19.8	0.4	7.8	7.2	1	3.6	11	0	7.6	0.8	0.4	0.4	13	6.6	0.2	0.2	4.4	9.6
Tamale	1	67	0.6	0	0.8	0.2	29	0.8	0	0	0	0	0	0	0	0	0	0	0
Undivided Obosum	0	0.2	0	0.2	0.8	2.8	63	4.2	0	13	0	0	1.8	0	5.2	0	0	6	0.2

Table 4.2 XRD Normalized count data for selected formations of the Tamale-Obosum and Oti-Pendjari Groups

			SCORES													
GROUP	FORMATION	ID	RU	ZI	AP	MI	TO	PH	IR	HE	AL	GA	AN	GL	SP	OT
Tamale-Obosum	Tamale Sandstone	MU-26	61													39
	Tamale Sandstone	MU-20	100													
	Tamale Sandstone	MU-25	29							47				24		
	Tamale Sandstone	MU-22	41	28				11								20
	Tamale Sandstone	MU-33				34										20
	Tamale Sandstone	MU-30	40							60						
	Tamale Sandstone	MU-23	37										63			
	Sang	MU-19										43				57
	Densubon Sandstone	MU-38				72			19							
	Densubon Sandstone	MU-49		64				21						15		
	Densubon Sandstone	MU-50				25				50			25			
	Densubon Sandstone	MU-51								62			38			
	Densubon Sandstone	MU-53									75					25
	Densubon Sandstone	MU-52							34				33			82
	Densubon Sandstone	MU-56							40	30					41	30
	Dunkro	MU-61							66							34
Oti-Pendjari	Bunya Sandstone	MU-18									100					
	Bunya Sandstone	MU-43	38								45					17
	Bunya Sandstone	MU-44						22			47					31
	Bunya Sandstone	MU-45											52			48
	Bunya Sandstone	MU-47									100					
	Bunya Sandstone	MU-14	59							41	0					
	Bunya Sandstone	MU-41									95		46			54
	Bimbila	MU-06									100					
	Bimbila	MU-08									74					26

Bimbila	MU-02							67			33
Bimbila	MU-04							100			
Bimbila	MU-05							31			69
Bimbila	MU-07									36	64
Bimbila	MU-12			100							
Bimbila	MU-13			24						38	38
Bimbila	MU-17			100							
Bimbila	MU-57										100
Bimbila	MU-15										70
Ejura Sandstone	MU-35				100						
Ejura Sandstone	MU-39					87	13				
Ejura Sandstone	MU-37						52	28			20
Ejura Sandstone	MU-55		36		64						
Afram	MU-54	38		21							

RU- RUTILE, ZI-ZIRCON, AP-APATITE, MI-MICA, TO- TOURMALINE, PH- PHOSPHATE, IR- IRON OXIDE, HE-HEMATITE, AL-ALUMINIUM, GA- GARNET, AN-ANORTHITE, GL-GLAUCONITE, IL -ILMENITE, SP-SPINEL, OT-OTHERS

Elemental Ratios Indices for Provenance Indications (after Morton and Hallsworth, 1994).

The index ATi is defined as % apatite in total apatite plus tourmaline,

GZi as % garnet in total garnet plus zircon,

RZi as % TiO_2 minerals in total TiO_2 minerals plus zircon,

RuZi as % rutile in total rutile plus zircon,

CZi as % chrome spinel in total chrome spinel plus zircon, and

CGi as % chrome spinel in total garnet plus chrome spinel

Table 4.3 Elemental ratio indices for selected formations of the Tamale-Obosum and Oti-Pendjari Groups

Formation	ID	ATi	GZi	RZi	RuZi	CZi	CGi
Afram Formation	MU-54			100	100		
Densubon Sandstone	MU-56			100		100	100
Bunya Sandstone	MU-43			100	100		
Bunya Sandstone	MU-14			100	100		
Kodjari	MU-31			100	100		
Kodjari	MU-32			100	100		
Kodjari	MU-11			100	100		
Sang Conglomerate	MU-19		100				
Tamale Sandstone	MU-26			100	100		
Tamale Sandstone	MU-20			100	100		

4.3 Framework mineralogy and modal analysis of the Tamale-Obosum Group

Modal analysis and framework mineralogy was performed by observation, descriptions and counting of the framework grains of the sandstone samples with the aid of a standard polarized microscope. The modal compositions of the framework grains are captured in Table 4.4. The modal composition of framework grains across the Voltaian Supergroup sandstones shows significant variability in quartz (Q), feldspar (F), and lithic (L) proportions. The Afram Formation is dominated by monocrystalline quartz (Qm = 73.6%) with minor feldspar (F = 1.2%) and lithics (L = 4%), classifying mainly as quartz arenite. The Bimbila Formation is heterogeneous: some samples are quartz-rich (Qm = 82%) with minor feldspar and lithics (F = 1.0–2.2%; L = 2.2–14.6%), while others contain high feldspar (up to 29.8%) and lithic fragments (up to 34%), plotting as sub-arkose to arkosic arenite. The Bunya Sandstone exhibits intermediate compositions, with quartz contents of 50–64%, feldspar 14–28%, and lithics 6–24%, pointing to sub-arkosic to lithic arkosic character. The Densubon Sandstone displays both quartz-rich samples (Qm = 71–85%, F ≤ 5.8%, L ≤ 10%) and lithic-rich variants (Qm = 51.4%, L = 20.2%), reflecting variable detrital input. The Tamale Sandstone is extremely quartz-rich (Qm 83–99.6%) with negligible feldspar and lithics, classifying predominantly as quartz arenite. The Tease Sandstone is almost monomineralic quartz (Qm = 97.4%), also plotting firmly in the quartz arenite field. The Undivided Obosum Sandstone shows mixed signatures: one sample is sub-arkosic (Qm = 68.2%, F = 22.2%) while others are quartz arenites with minor lithics and feldspar.

Table 4.4 Detrital modes from sandstones of the Tamale-Obosum and Oti-Pendjari Groups (in vol%)

Formations	Qm	Qp	F	Ls	Lm	M	QFL(%)			QmFLt (%)		
							Q	F	L	Qm	F	Lt
Afram	73.6	15.6	1.2	3.4	0.6	5.6	89.2	1.2	4	73.6	1.2	19.6
Bimbila	82	12.4	1	2.2	0	2.4	94.4	1	2.2	82	1	14.6
Bimbila	57.4	6.2	29.8	0	0	6.6	63.6	29.8	0	57.4	29.8	6.2
Bimbila	47.4	17.2	18	9.6	7.2	0.6	64.6	18	16.8	47.4	18	34
Bimbila	76	5	28.4	0	0.6	0	81	28.4	0.6	76	28.4	5.6
Bunya SS	50.8	1.2	24.6	20	0	3.4	52	24.6	20	50.8	24.6	21.2
Bunya SS	64.2	3.6	28.2	3	0	1	67.8	28.2	3	64.2	28.2	6.6
Bunya SS	62.6	8.2	18.4	9.2	0	1.6	70.8	18.4	9.2	62.6	18.4	17.4
Bunya SS	59.8	7.6	14.6	2.6	3.4	12	67.4	14.6	6	59.8	14.6	13.6
Bunya SS	60.4	8.8	19.2	7.4	0.1	4.1	69.2	19.2	7.5	60.4	19.2	16.3
Bunya SS	50.4	10	23.6	14.2	0	1.8	60.4	23.6	14.2	50.4	23.6	24.2
Bunya SS	54	4.6	24.6	9.2	0.4	7.2	58.6	24.6	9.6	54	24.6	14.2
Densubon SS	71.2	6.2	15.8	1.6	2.2	3	77.4	15.8	3.8	71.2	15.8	10
Densubon SS	85.4	5.8	5.8	0	0.2	2.8	91.2	5.8	0.2	85.4	5.8	6
Densubon SS	51.4	11.4	20.2	5.4	2.6	9	62.8	20.2	8	51.4	20.2	19.4
Tamale SS	92.6	2.8	0.5	0	0	4.1	95.4	0.5	0	92.6	0.5	2.8
Tamale SS	83.4	9	1.8	2.8	1	2	92.4	1.8	3.8	83.4	1.8	12.8
Tamale SS	99.6	0.2	0	0.2	0	0	99.8	0	0.2	99.6	0	0.4
Tease SS	97.4	1.8	0	0.4	0	0.4	99.2	0	0.4	97.4	0	2.2
Undivided. Obosum	68.2	5.4	22.2	0.6	0	3.6	73.6	22.2	0.6	68.2	22.2	6
Undivided Obosum	79.2	7.8	0	4	0.4	8.6	87	0	4.4	79.2	0	12.2
Undivided Obosum	75.4	2.2	0.8	0.6	0	21	77.6	0.8	0.6	75.4	0.8	2.8

4.3.1 Major Element Geochemistry of Tamale-Obosum Group

The major oxide compositions of the samples from the Tamale-Obosum Group are presented in Table 4.5. Based on geochemical studies the samples were grouped as Quartz arenites, Wackes and Litharenites. The Tamale Sandstone Formation shows SiO_2 with an average of 91.64 wt.%. The other major oxide averages are: Al_2O_3 – 3.38 wt.%., Fe_2O_3 – 1.45 wt.%., MnO - 0.03 wt.%, MgO - 0.21 wt.%, CaO - 0.17 wt.%, Na_2O - 0.69 wt.%, K_2O - 0.52 wt.%, TiO_2 - 0.17 wt.%, P_2O_5 - 0.03 wt.%, Cr_2O_3 - 0.00 wt.%. Sang Conglomerate Formation has averages as follows: SiO_2 - 70.43 wt.%, Al_2O_3 - 12.01 wt.%, Fe_2O_3 - 5.2 wt.%, MnO - 0.18 wt.%, MgO - 1.62 wt.%, CaO - 1.92 wt.%, Na_2O - 3.26 wt.%, K_2O - 1.95 wt.%, TiO_2 - 0.69 wt.%, P_2O_5 - 0.13 wt.%, Cr_2O_3 - 0.02 wt.%. The Densubon Sandstone Formation range in SiO_2 an average of 74.21 wt.%. The Al_2O_3- 10.53 wt.%, Fe_2O_3 – 3.18 wt.%, MnO – 0.16 wt.%, MgO – 0.98 wt.%, CaO – 2.51 wt.%, Na_2O - 2.90 wt.%, K_2O - 1.77 wt.%, TiO_2 - 0.47 wt.%, P_2O_5 -0.09 wt.%, Cr_2O_3 - 0.01 wt.%. The Undivided Obosum Formation has an SiO_2 average of 93.72 wt.%. The other elements have averages as follows: Al_2O_3 – 2.23 wt.%, Fe_2O_3 -1.45 wt.%, MnO – 0.08 wt.% , MgO - 0.12 wt.%, CaO – 0.05 wt.%, Na_2O – 0.02 wt.%, K_2O – 0.26 wt.%, TiO_2 - 0.12wt.%, P_2O_5 - 0.02 wt.%, Cr_2O_3 - 0.00 wt.%. The Chemical Index of Alteration (CIA) values for sandstones of the Tamale-Obosum Group indicate varying degrees of chemical weathering and compositional maturity. The Tamale Sandstone and Undivided Obosum Formation record relatively high CIA values. In contrast, the Densubon and Dunkro sandstones display moderate CIA values. The Sang Conglomerate exhibits the lowest CIA values within the group (Table 4.6).

Table 4.5 Major oxide (wt. %) concentrations, and elemental ratios for Tamale Sandstone, Sang Conglomerate, Densubon Sandstone and Undivided Obosum formations of the Tamale-Obosum Group

Formations	Tamale Sandstone						Sang	Densubon sandstone								
wt%	MU-23	MU-24	MU-25	MU-26	MU-29	MU-33	MU-19	MU-38	MU-50	MU-51	MU-52	MU-53	MU-54	MU-55	MU-47	MU-56
SiO2	91.67	77.97	96.68	96.32	91.57	95.63	70.43	71.65	68.47	72.64	67.65	69.69	62.46	98.01	71.84	89.22
Al2O3	3.67	10.24	1.17	0.97	3.11	1.09	12.01	13.25	13.41	13.08	13.7	15.19	6.12	0.6	12.68	5.29
Fe2O3	1.52	3.25	0.52	0.68	1.7	1.04	5.2	3.21	4.33	2.91	4.52	3.8	1.55	0.4	4.73	1.19
MnO	0.01	0.08	0.01	0.01	0.02	0.06	0.18	0.1	0.09	0.06	0.08	0.2	0.82	0.01	0.08	0.01
MgO	0.18	0.81	0.05	0.02	0.14	0.04	1.62	1.62	1.53	1.08	1.81	0.39	0.47	0.02	1.2	0.09
CaO	0.13	0.73	0.04	0.03	0.06	0.04	1.92	0.86	2.7	1.69	2.58	0.25	13.73	0.03	1.27	0.04
Na2O	0.39	3.67	0	0	0.1	0	3.26	4.85	3.14	3.34	3.21	6.38	1.34	0	3.43	0.03
K2O	1.03	0.85	0.2	0.03	0.92	0.08	1.95	1.87	1.51	1.94	1.89	1.99	1.15	0.12	2.21	3.1
TiO2	0.2	0.38	0.05	0.05	0.23	0.1	0.69	0.42	0.53	0.34	0.62	0.47	0.61	0.04	0.82	0.13
P2O5	0.02	0.07	0.02	0.02	0.03	0.02	0.13	0.13	0.11	0.08	0.13	0.04	0.08	0.02	0.13	0.03
Cr2O3	0.01	0.01	0	0	0	0	0.02	0.01	0.01	0.01	0.01	0.01	0.01	0	0.01	0
LOI	1.28	1.7	0.65	0.66	1.21	0.8	2.71	1.95	4.45	3.26	4.29	2.04	11.84	0.14	2.08	0.73
Total	100.09	99.74	99.39	98.79	99.08	98.87	100.1	99.91	100.3	100.4	100.5	100.4	100.2	99.36	100.5	99.86

Table 4.5 Major oxide (wt. %) concentrations, and elemental ratios for Tamale Sandstone, Sang Conglomerate, Densubon Sandstone and Undivided Obosum formations of the Tamale-Obosum Group, continued.

Formations	Undivided Obosum					
wt%	MU-34	MU-27	MU-20	MU-22	MU-28	MU-30
SiO2	81.34	96.32	93.21	98.7	97.8	94.95
Al2O3	6.38	0.97	2.44	0.91	0.65	2.05
Fe2O3	5.65	0.68	1.14	0.31	0.21	0.71
MnO	0.41	0.01	0.02	0.01	0.01	0.01
MgO	0.54	0.02	0.07	0.01	0.01	0.08
CaO	0.09	0.03	0.05	0.03	0.04	0.05
Na2O	0.03	0	0	0.11	0	0
K2O	1.06	0.03	0.18	0.03	0.01	0.25
TiO2	0.32	0.05	0.14	0.05	0.04	0.14
P2O5	0.03	0.02	0.02	0.02	0.02	0.02
Cr2O3	0	0	0.01	0	0	0
LOI	3.47	0.66	1.19	0.55	0.39	1.01
Total	99.32	98.79	98.47	100.7	99.18	99.24

Table 4.6 Chemical index values for sandstones from the Tamale-Obosum Group

Formation	IDs	SiO2/Al2O3	Fe2O3/K2O	K2O/Al2O3	MgO/Al2O3	Al2O3/TiO2	ICV	CIA	PIA
Densubon sandstone	MU-47	5.11	2.87	0.11	0.11	25.30	1.02	64.60	67.08
Densubon sandstone	MU-51	5.55	1.50	0.15	0.08	38.47	0.86	65.24	68.89
Densubon sandstone	MU-52	4.94	2.39	0.14	0.13	22.10	1.07	64.08	67.10
Densubon sandstone	MU-53	4.59	1.91	0.13	0.03	32.32	0.87	63.80	66.57
Densubon sandstone	MU-54	10.21	1.35	0.19	0.08	10.03	3.08	27.39	24.80
Densubon sandstone	MU-55	163.35	3.33	0.20	0.03	15.00	1.02	80.00	94.12
Densubon sandstone	MU-56	16.87	0.38	0.59	0.02	40.69	0.87	62.53	96.90
Densubon sandstone	MU-38	5.41	1.72	0.14	0.12	31.55	0.97	63.61	66.59
Sang conglomerate	MU-19	5.86	2.67	0.16	0.13	17.41	1.22	62.75	66.01
Undivided Obosum	MU-20	38.20	6.33	0.07	0.03	17.43	0.65	91.39	97.84
Undivided Obosum	MU-22	108.46	10.33	0.03	0.01	18.20	0.59	84.26	86.27
Undivided Obosum	MU-27	99.30	22.67	0.03	0.02	19.40	0.84	94.17	96.91
Undivided Obosum	MU-28	150.46	21.00	0.02	0.02	16.25	0.48	92.86	94.12
Undivided Obosum	MU-30	46.32	2.84	0.12	0.04	14.64	0.60	87.23	97.30
Undivided Obosum	MU-32	7.94	2.97	0.13	0.13	18.10	1.57	50.06	50.06
Tamale Sandstone	MU-29	29.44	1.85	0.30	0.05	13.52	1.01	74.22	93.19
Tamale Sandstone	MU-33	87.73	13.00	0.07	0.04	10.90	1.19	90.08	96.19
Tamale Sandstone	MU-34	12.75	5.33	0.17	0.08	19.94	1.21	84.39	97.79
Tamale Sandstone	MU-23	24.98	1.48	0.28	0.05	18.35	0.94	70.31	83.54
Tamale Sandstone	MU-25	7.61	3.82	0.08	0.08	26.95	0.95	66.11	68.09
Tamale Sandstone	MU-26	82.63	2.60	0.17	0.04	23.40	0.74	82.98	96.04

4.3.2 Trace and Rare Earth Element Geochemistry of Tamale-Obosum Group

Elemental ratios are powerful tools for discriminating between source rocks with different compositions. Ratios of both incompatible elements (less readily incorporated into the crystal structure of common minerals) and compatible elements (easily incorporated) prove useful in this regard. These ratios can help distinguish between contributions from felsic (silicic-rich) and mafic (iron-magnesium-rich) source rocks.

Compared with UCC, the samples from the Tamale-Obosum Group have relatively low contents of V, Cr, Co, Ni, Nb, Ta, Y, Rb, Zr, Hf and Cs, with high contents of Sr and Ba (Table 4.7). The averages of the elements in the Tamale Sandstone, Sang Conglomerate, Densubon Sandstone and Undivided Obosum formations respectively are as follows:
Sr (43.48ppm, 225.34ppm, 139.91ppm, 29.85ppm), Ba (794.71ppm, 593.98ppm, 578.52ppm, 537.30ppm), Zr (77.01ppm, 62.13ppm, 80.81ppm, 35.60ppm), Hf (2.62ppm, 2.56ppm, 2.47ppm, 1.29ppm), Cs (0.78ppm, 0.79ppm, 1.43ppm, 0.46ppm), V (22.86ppm, 95.77ppm, 39.81ppm, 15.33ppm), Cr (15.39ppm, 46.22ppm, 30.46ppm, 11.22ppm), Co (8.63ppm, 9.99ppm, 7.17ppm, 1.61ppm), Ni (10.83ppm, 45.44ppm, 16.35ppm, 4.07ppm), Nb (3.00ppm, 8.28ppm, 4.93ppm, 1.97ppm), Ta (0.22ppm, 0.55pp, 0.35ppm, 0.15ppm), Y (6.56ppm, 38.47ppm, 16.37ppm, 4.33ppm).

The REE concentrations of the Tamale-Obosum Group sandstones reveal systematic variations in total abundances (ΣREE), fractionation patterns, and europium anomalies. The Tamale Sandstone Formation is marked by relatively low ΣREE values (42–93 ppm) with light rare earth element (LREE) enrichment (LREE/HREE = 5–9) and near-flat heavy rare earth element (HREE) profiles. LaN/YbN ratios are generally below 1.5. The Sang Conglomerate displays higher ΣREE (186

ppm), with moderate LREE enrichment (LREE/HREE ≈ 5–6) and a slight positive Eu anomaly (Eu/Eu* = 1.23. The Densubon Sandstone Formation shows the highest REE concentrations overall (ΣREE = 26–333 ppm), with significant variability in LaN/YbN (0.9–4.7). Some samples exhibit strong LREE enrichment and mild positive Eu anomalies (Eu/Eu* ≈ 1.1–1.3), while others show negative Eu anomalies (<1). The Undivided Obosum Formation is generally REE-poor (ΣREE = 18–137 ppm) but displays variable LaN/YbN ratios (0.7–3.6). Negative Eu anomalies are common (Eu/Eu* = 0.8–0.9), with isolated higher Eu/Eu* values (Table 4.8).

Table 4.7 Trace elements concentrations (ppm) of sandstones from the Tamale-Obosum Group

	Li	P	Sc	Ti	V	Cr	Co	Ni	Cu	Zn	Rb	Sr	Y	Zr	Nb	Sn	Ba	Hf	Ta	Pb	Th	U
TAMALE FORMATION																						
MU-29	9.02	56.77	1.88	862.23	14.61	11.67	2.16	4.72	12	15.3	26.82	24.83	9.76	168.9	3.2	1.54	210.25	5.79	0.24	10.5	3.93	0.96
MU-23	4.56	41.34	1.64	766.78	21.46	13.16	1.52	5.64	11.9	12.98	26.51	27.3	5.08	30.11	2.7	0.79	206.06	1.34	0.21	5.82	2.85	0.84
MU-25	18.2	232.4	6.17	1772.7	46.09	29.36	5.45	15.72	11.8	36.34	25.08	166.7	10.2	49.31	4.45	1.09	3752.1	1.67	0.31	8.05	3.44	0.72
MU-26	2.69	26.44	0.65	191.17	5.86	5.23	1.01	2	3.31	4.91	5.61	9.04	1.87	16.68	0.73	0.4	50.65	0.67	0.07	1.67	1.15	0.29
MU-33	8.69	43.67	0.91	428.4	6.36	6.85	0.89	1.81	5.55	3.82	3.19	11.15	3.84	61.63	1.76	0.43	147.9	2.11	0.12	4.53	1.59	0.49
MU-34	39.5	85.48	3.77	1398.8	42.76	26.07	40.7	35.08	18.1	44.52	38.07	21.86	8.6	135.4	5.16	1.2	401.31	4.16	0.36	32.3	4.35	1.3
SANG CONGLOMERATE FORMATION																						
MU-19	11	453.97	8.62	3348.5	95.77	46.22	9.99	45.44	14.9	55.84	41.26	225.3	38.5	62.13	8.28	1.95	593.98	2.56	0.55	10.3	7.46	1.92
DENSUBON SANDSTONE FORMATION																						
MU-50	11.3	386.13	8.84	2540.8	64.15	36.77	9.89	34.25	17	50.36	42.12	187.2	22.6	51.38	5.35	1.44	488.27	1.78	0.38	9.6	4.81	1.03
MU-51	9.7	260.51	6	1582.5	35.79	22.7	6.8	18.55	10.7	33.19	46.59	197.4	20.7	41.86	5.03	1.45	616.09	1.37	0.36	9.56	3.88	0.75
MU-52	14.7	500.23	10.5	2987.4	66.28	61.06	11.3	28.27	20	50.92	56.5	207.7	24.7	55.65	6.22	1.52	557.48	1.8	0.42	11.5	5.24	1.35
MU-53	4.47	118.17	7.51	2262.1	58.6	26.28	12.8	10.24	13.3	33.15	58.9	134.6	18.5	65.02	6.52	1.59	790.03	2.12	0.44	13.7	5.39	1.65
MU-56	7.31	91.02	1.01	501.39	4.97	5.67	3.08	5.79	6.96	19.97	86.82	38.02	6.18	56.04	2.28	0.93	447.93	2.02	0.2	9.91	3.38	0.69
MU-38	16.5	477.12	7.04	2082.5	51.44	29.35	8.86	22.75	11.8	50.67	45.11	197.2	13.3	56.81	5.75	1.21	540.83	1.74	0.41	9.09	4.14	0.91
MU-55	4.26	17.54	0.23	126.21	3.39	6.15	0.68	2.25	2.14	2.38	3.33	5.61	1.95	18.63	0.45	0.21	10.28	0.67	0.05	1.69	0.73	0.32
MU-54	11.9	294.82	5.66	3048.3	33.82	55.7	3.96	8.71	14.3	27.37	38.58	151.6	23	301.1	7.8	1.75	1177.3	8.28	0.53	6.18	7.85	1.62
UNDIVIDED OBOSUM FORMATION																						
MU-20	5.83	36.84	1.10	548.16	9.17	8.14	1.14	1.90	3.73	5.83	6.07	9.31	2.87	28.90	2.02	0.62	59.94	1.36	0.17	2.82	2.32	0.55
MU-22	3.82	15.47	0.29	159.33	2.61	3.90	0.23	0.93	1.77	4.40	0.96	5.00	1.44	19.21	0.69	0.27	16.21	0.88	0.05	1.27	0.98	0.25
MU-27	3.31	16.46	0.42	202.20	4.80	3.37	0.28	1.21	3.76	4.32	1.04	2.73	1.06	11.44	0.58	0.26	10.99	0.45	0.05	1.13	0.87	0.20
MU-30	9.06	44.73	1.16	551.63	7.60	7.80	0.43	1.38	5.25	13.26	8.38	16.31	3.99	63.30	2.20	0.53	61.87	2.21	0.16	6.68	1.89	0.51
MU-32	23.44	431.05	8.00	2503.39	66.01	42.48	7.20	18.29	14.17	43.42	38.42	142.19	15.53	80.27	5.99	1.41	3052.77	2.43	0.43	8.69	5.07	1.02
MU-28	2.94	10.61	0.24	112.90	1.81	1.63	0.39	0.71	3.50	1.98	0.61	3.54	1.10	10.49	0.33	0.26	22.05	0.41	0.03	1.04	0.78	0.19

Table 4.8 Rare earth elements concentrations (ppm) of sandstones from the Tamale-Obosum Group

	La	Ce	Pr	Nd	Sm	Eu	Gd	Tb	Dy	Ho	Er	Tm	Yb	Lu	ΣREE	LREE	HREE	LaN/YbN	Eu/Eu*
TAMALE SANDSTONE FORMATION																			
MU-29	14.46	34.3	3.12	12.16	2.29	0.5	2.28	0.33	2.06	0.41	1.2	0.19	1.33	0.2	74.86	66.86	8	0.80	1.02
MU-23	11.19	25	2.48	9.67	1.86	0.43	1.81	0.23	1.31	0.25	0.66	0.1	0.67	0.1	55.79	50.66	5.13	0.90	1.06
MU-25	20.09	37	4.44	18.01	3.39	1.14	3.06	0.39	2.25	0.44	1.21	0.18	1.21	0.18	92.96	84.04	8.92	1.31	1.11
MU-26	11.61	21.7	1.52	4.73	0.68	0.13	0.64	0.08	0.44	0.09	0.25	0.04	0.26	0.04	42.24	40.4	1.84	1.26	1.66
MU-33	9.91	19	1.91	6.91	1.03	0.21	0.96	0.13	0.81	0.16	0.47	0.08	0.52	0.08	42.14	38.93	3.21	3.44	0.93
MU-34	13.69	52.8	2.82	10.63	1.95	0.44	1.94	0.28	1.76	0.35	1.04	0.17	1.15	0.17	89.19	82.33	6.86	1.43	0.99
SANG CONGLOMERATE FORMATION																			
MU-19	38.83	62.3	9.52	37.74	7.44	1.94	7.42	1.15	7.51	1.56	4.5	0.7	4.66	0.64	185.9	157.7	28.1	0.68	1.23
DENSUBON SANDSTONE FORMATION																			
MU-50	63.73	163	15.25	55.84	9.96	2.32	8.25	1.1	6.02	1.1	2.91	0.4	2.67	0.36	332.7	309.9	22.8	1.99	1.20
MU-51	106.9	48.7	19.04	65.82	8.91	2.13	7.25	0.9	4.71	0.86	2.25	0.3	1.87	0.26	269.8	251.4	18.4	4.68	1.25
MU-52	36.72	49	7.13	28.15	5.35	1.45	5.24	0.77	4.78	1.01	2.92	0.46	3.11	0.46	146.6	127.8	18.8	0.91	1.29
MU-53	68.22	116	14.32	51.8	7.96	1.83	6.73	0.84	4.44	0.81	2.12	0.28	1.79	0.25	277	259.7	17.3	3.13	1.18
MU-56	15.49	27.7	3.32	12.55	2.12	0.49	1.81	0.25	1.43	0.28	0.78	0.12	0.77	0.12	67.2	61.64	5.56	1.48	1.17
MU-38	24.69	47.6	5.27	20.34	3.69	0.97	3.39	0.46	2.72	0.54	1.51	0.22	1.47	0.22	113.1	102.6	10.5	1.29	1.29
MU-55	5.61	11.7	1.2	4.6	0.85	0.15	0.75	0.09	0.48	0.1	0.27	0.04	0.27	0.04	26.1	24.06	2.04	1.54	0.90
UNDIVIDED OBOSUM FORMATION																			
MU-54	23.26	53	6.7	29.74	6.49	1.5	5.67	0.76	4.38	0.85	2.35	0.35	2.38	0.36	137.8	120.7	17.1	0.72	1.16
MU-20	14.57	17.73	2.15	6.81	1.07	0.22	0.94	0.12	0.72	0.14	0.42	0.07	0.47	0.07	45.48	42.54	2.94	2.38	1.04
MU-22	8.95	15.11	1.15	3.53	0.48	0.09	0.48	0.06	0.32	0.06	0.19	0.03	0.20	0.03	30.67	29.31	1.36	3.60	0.83
MU-27	6.99	7.16	0.64	2.07	0.32	0.06	0.29	0.04	0.24	0.05	0.14	0.02	0.17	0.02	18.19	17.23	0.96	3.42	0.88
MU-30	13.45	21.63	2.57	9.93	1.80	0.36	1.54	0.19	1.02	0.19	0.52	0.08	0.55	0.08	53.92	49.74	4.18	1.85	1.00
MU-32	19.24	39.96	4.64	18.83	3.83	1.19	3.71	0.53	3.16	0.60	1.61	0.23	1.53	0.22	99.28	87.69	11.6	0.98	1.48
MU-28	6.36	14.20	1.07	3.29	0.32	0.06	0.33	0.04	0.23	0.05	0.14	0.02	0.15	0.02	26.28	25.3	0.98	3.25	0.82

4.3.3 Major Element Geochemistry of the Oti-Pendjari Group

The major oxide compositions of the samples from the Oti-Pendjari Group are represented in Table 4.9 below. SiO_2 contents are generally high across all samples, ranging from ~65 wt.% in the Bimbila and Ejura formations (e.g., MU-04: 66.98 wt.%, MU-07: 66.05 wt.%) to very silica-rich values in the Tease formation (MU-17: 96.65 wt.%, MU-58: 97.53 wt.%). Al_2O_3 concentrations are moderate in the Bimbila and Ejura sandstones (13.8–14.7 wt.%) but extremely depleted in the Tease samples (≤1.5 wt). Fe_2O_3 contents range between 4.7–5.8 wt.% in the Bimbila and Ejura sandstones but decline sharply to ≤0.75 wt.% in the Tease samples. Similarly, MgO (2.1–2.8 wt.%) and CaO (1.2–2.3 wt.%) are relatively higher in the less mature Bimbila–Ejura sandstones, while Tease samples record extremely low values (<0.1 wt.% for CaO and MgO). Na_2O (3.9–5.2 wt.%) is relatively enriched in the Bimbila and Ejura formations, but virtually absent in Tease (<0.05 wt.%). By contrast, K_2O values remain moderate (1.9–2.1 wt.%) in Bimbila–Ejura and variable in Tease (0.16–2.42 wt.%). SiO_2 values range from moderately high in the Bunya samples (~66.8 wt.%, MU-09, MU-18) to very silica-rich in the Kodjari (up to 91.25 wt.% in MU-49) and Afram formations (87.38–97 wt.% in MU-10, MU-36). Al_2O_3 contents decrease from ~14.5 wt.% in Bunya to ≤1 wt.% in the most mature Afram sample (MU-36: 0.7 wt.%), Fe_2O_3 and MgO are relatively higher in Bunya (Fe_2O_3 ~4.5–4.6 wt.%, MgO ~1.2–1.8 wt.%), but strongly depleted in Kodjari (<1 wt.% in MU-49) and Afram (<0.5 wt.% in MU-36). Na_2O and CaO follow a similar trend, with Bunya and some Kodjari samples retaining moderate contents (Na_2O ~3.3–4.5 wt.%, CaO ~1.2–1.7 wt.%), while Afram samples show extreme depletion (Na_2O <0.05 wt.%, CaO <0.1 wt.%),. K_2O is relatively stable across all formations (~1.7–2.5 wt.%).

Table 4. 9. Major oxide composition of Oti-Pendjari Group rocks.

Formation	Bimbila										Ejura Ss	Tease
Oxides(wt%)	MU-04	MIU-05	MU-06	MU-07	MU-08	MU-13	MU-14	MU-12	MU-15	MU-17	MU-35	MU-58
SiO2	66.98	68.10	64.88	66.05	66.66	66.69	67.23	70.16	81.89	96.65	95.79	97.53
TiO2	0.70	0.69	0.68	0.75	0.82	0.76	0.77	0.61	0.39	0.08	0.09	0.03
Al2O3	14.37	13.78	14.61	14.66	14.50	14.54	13.87	14.12	7.39	1.50	1.49	0.32
Fe2O3	4.76	4.69	5.81	5.41	5.11	4.92	5.59	3.72	2.79	0.33	0.56	0.75
MnO	0.09	0.10	0.11	0.11	0.10	0.09	0.12	0.06	0.04	0.01	0.02	0.00
MgO	2.12	2.20	2.75	2.36	2.08	1.95	2.43	1.13	0.92	0.04	0.06	0.02
CaO	1.32	1.24	1.47	1.44	1.58	2.30	1.64	1.10	0.58	0.03	0.05	0.02
Na2O	4.90	3.97	4.29	5.00	5.00	4.24	4.07	5.17	0.43	0.00	0.00	0.03
K2O	2.04	1.98	2.16	2.00	1.94	2.04	1.87	1.33	2.42	0.16	0.47	0.03
P2O5	0.18	0.20	0.19	0.20	0.21	0.19	0.22	0.18	0.08	0.03	0.03	0.02
Cr2O3	0.01	0.01	0.01	0.01	0.02	0.02	0.02	0.01	0.01	0.01	0.00	0.00
NiO	0.00	0.00	0.00	0.00	0.00	0.00	0.00	0.00	0.00	0.00	0.00	0.00
LOI	2.64	3.63	3.30	2.51	2.61	2.96	2.81	2.53	2.44	0.53	0.81	0.20
Total	100.11	100.60	100.27	100.50	100.63	100.71	100.65	100.11	99.37	99.37	99.35	98.95
SiO2/Al2O3	4.66	4.94	4.44	4.51	4.60	4.59	4.85	4.97	11.08	64.43	64.29	304.78
Fe2O3/K2O	2.33	2.37	2.69	2.71	2.63	2.41	2.99	2.80	1.15	2.06	1.19	25.00
K2O/Al2O3	0.14	0.14	0.15	0.14	0.13	0.14	0.13	0.09	0.33	0.11	0.32	0.09
Al2O3/TiO2	20.53	19.97	21.49	19.55	17.68	19.13	18.01	23.15	18.95	18.75	16.56	10.67
K2O/Na2O	0.42	0.50	0.50	0.40	0.39	0.48	0.46	0.26	5.63	0	0	1.00
ICV	1.10	1.07	1.17	1.16	1.14	1.11	1.18	0.92	1.02	0.43	0.83	2.75
ICA	63.50	65.71	64.85	63.46	62.99	62.89	64.66	65.01	68.30	88.76	74.13	80.00
PIA	66.47	69.37	68.37	66.28	65.62	65.65	67.76	67.10	83.11	97.81	95.33	85.29

Table 4. 9. Major oxide composition of Oti-Pendjari Group rocks, continued.

	Bunya								Kodjari Fm	Kodjari	Afram Fm	Afram Fm
Oxides(wt%)	MU-09	MU-18	MU-41	MU-43	MU-44	MU-45	MU-46	MU-49	MU-32	MU-10	MU-57	MU-36
SiO2	66.83	66.75	78.42	72.56	77.35	77.37	71.84	91.25	70.42	87.38	89.46	97
TiO2	0.65	0.63	0.25	0.67	0.32	0.50	0.82	0.11	0.49	0.28	0.10	0.04
Al2O3	14.49	14.49	10.97	11.93	10.96	10.81	12.68	4.45	8.87	7.05	4.99	0.7
Fe2O3	4.48	4.55	2.31	4.85	2.78	3.00	4.73	0.58	3.45	0.75	2.09	0.45
MnO	0.07	0.05	0.05	0.09	0.10	0.06	0.08	0.00	0.30	0.00	0.03	0
MgO	1.77	1.23	0.52	1.18	0.89	0.97	1.20	0.15	1.14	0.39	0.07	0.02
CaO	1.66	1.51	0.43	1.26	0.63	0.84	1.27	0.06	5.16	0.08	0.04	0.05
Na2O	4.49	4.34	3.37	3.45	3.42	3.28	3.43	0.05	2.53	0.01	0.02	0
K2O	2.41	2.54	2.52	1.96	2.02	1.75	2.21	2.17	1.16	1.09	2.02	0.04
P2O5	0.15	0.17	0.04	0.11	0.08	0.11	0.13	0.02	0.12	0.08	0.03	0.03
Cr2O3	0.02	0.01	0.00	0.01	0.01	0.01	0.01	0.00	0.01	0.01	0.01	0
NiO	0.00	0.01	0.00	0.00	0.00	0.00	0.00	0.00	0.00	0.00	0.00	0
LOI	3.18	3.44	1.97	2.19	1.83	1.76	2.08	0.92	5.68	3.07	1.09	0.44
Total	100.20	99.71	100.86	100.27	100.39	100.46	100.49	99.76	99.33	100.16	99.94	98.73
SiO2/Al2O3	4.61	4.61	7.15	6.08	7.06	7.16	5.67	20.51	7.94	12.39	17.93	138.57
Fe2O3/K2O	1.86	1.79	0.92	2.47	1.38	1.71	2.14	0.27	2.97	0.69	1.03	11.25
K2O/Al2O3	0.17	0.18	0.23	0.16	0.18	0.16	0.17	0.49	0.13	0.15	0.40	0.06
Al2O3/TiO2	22.29	23.00	43.88	17.81	34.25	21.62	15.46	40.45	18.10	25.18	49.90	17.5
K2O/Na2O	0.54	0.59	0.75	0.57	0.59	0.53	0.64	43.40	0.46	109.00	101.00	0
ICV	1.07	1.02	0.86	1.12	0.92	0.96	1.08	0.70	1.57	0.37	0.87	0.85
CIA	62.86	63.33	63.45	64.14	64.36	64.81	64.73	66.12	50.06	85.66	70.58	88.60
PIA	66.26	67.13	68.98	67.92	68.82	68.74	69.02	95.40	50.06	98.51	98.02	92.95

4.3.4 Trace and rare earth element geochemistry of the Oti-Pendjari Group

The studied samples of the Oti-Pendjari Group rocks are characterized by REE fractionation with high (La/Yb)N ratios ranging from 1.25 to 124.59, mostly greater than that of PAAS (9.15) as shown in Table 4.10. All samples show chondrite-normalized REE patterns similar to that of UCC, with significant LREE enrichment, flat HREE and negative Eu anomalies (Eu/Eu* = 0.0–8.5).

Compared with UCC, the samples from the Bimbila and Bunya Ss Formations have relatively high contents of V, Cr, Co, Ni, Nb, Ta, Y, Rb, and Cs, with low contents of Sr, Ba, Zr, and Hf as seen in Table 4.10. Compared with UCC, samples of the Ejura Sandstone, Afram, Tease Sandstone and Kodjari Formations have relatively low contents of V, Cr, Co, Ni, Nb, Ta, Y, Rb, and Cs, with high contents of Sr, Ba, Zr, and Hf. The contents of ferromagnesian trace elements (Cr, Co, Ni) increase while those of high field strength elements (Zr, Th, Y, Nb, Ta) decrease for Bunya and Bimbila formations which are the upper members of the Group. This trend possibly indicates a higher proportion of mafic minerals in the upper members due to the changes in source rocks and/or sedimentary environment (Table 4.11).

Table 4.10 Rare Earth Element composition of Oti-Pendjari Group rocks

La	Ce	Pr	Nd	Sm	Eu	Gd	Tb	Dy	Ho	Er	Tm	Yb	Lu	ΣREE	ΣLREE	ΣHREE	LaN/YbN	Eu/Eu*
BUNYA SANDSTONE																		
39.40	29.51	25.64	18.81	11.50	8.38	7.28	5.50	4.97	4.30	0.57	0.59	0.59	0.58	157.62	133.24	24.38	66.48	0.03
103.83	60.44	54.42	40.26	21.49	13.10	16.22	10.90	9.58	8.73	4.11	4.27	4.19	3.99	355.54	293.56	61.98	24.78	0.14
970.59	84.48	508.47	404.53	203.63	122.64	158.10	105.97	88.90	72.26	8.17	8.03	7.79	7.59	2751.14	2294.34	456.80	124.59	0.78
69.28	50.76	42.79	31.56	18.45	10.95	12.78	9.43	8.51	7.69	61.98	55.20	46.30	41.02	466.69	223.79	242.90	1.50	0.09
123.76	71.81	66.36	51.01	29.60	19.01	25.42	18.59	17.08	15.96	7.39	7.42	7.00	6.75	467.14	361.55	105.59	17.67	0.29
73.93	53.16	43.42	32.96	19.27	13.93	13.40	9.69	8.74	7.81	14.73	13.23	11.37	10.81	326.47	236.68	89.79	6.50	0.33
644.98	122.42	370.83	277.56	148.80	94.37	105.73	73.79	62.92	50.92	7.54	7.84	7.60	7.22	1982.52	1658.96	323.56	84.86	1.82
47.02	35.66	35.23	26.36	15.83	7.90	9.21	6.66	5.64	4.72	44.67	41.97	37.58	31.31	349.74	168.00	181.74	1.25	0.21
BIMBILA FORMATION																		
118.73	88.78	79.82	61.44	37.48	24.91	28.94	22.10	20.44	18.33	4.54	4.55	4.46	4.36	518.88	411.16	107.72	26.65	0.76
87.75	53.20	55.67	42.73	24.79	17.40	18.40	13.19	11.67	10.65	17.29	17.02	15.03	13.78	398.58	281.54	117.03	5.84	0.61
78.30	62.36	48.86	37.34	22.24	14.86	16.00	11.53	10.48	9.55	9.92	9.44	8.77	8.64	348.31	263.98	84.33	8.93	1.93
112.69	54.54	64.85	48.31	27.14	18.57	20.07	14.41	12.77	11.52	9.15	8.99	8.63	8.32	419.96	326.10	93.86	13.06	2.49
91.96	59.77	57.00	43.00	24.94	17.21	17.94	13.03	11.60	10.46	10.69	10.17	9.38	9.24	386.38	293.87	92.51	9.81	2.26
157.71	63.46	77.35	60.84	33.42	23.93	28.97	20.24	18.39	17.47	15.86	14.16	11.71	11.21	554.72	416.71	138.01	13.47	3.28
105.33	62.63	67.63	50.50	28.05	17.90	19.22	13.43	11.83	10.06	9.41	9.38	8.82	7.87	422.06	332.04	90.02	11.94	2.56
71.10	57.88	47.65	36.76	22.22	15.28	15.41	11.40	10.50	9.21	8.84	9.13	8.87	8.16	332.40	250.89	81.51	8.02	0.00
62.93	46.88	37.04	27.68	16.02	8.87	11.01	8.12	7.43	6.62	6.49	6.91	6.85	6.46	259.30	199.43	59.88	9.19	0.01
18.81	12.72	9.74	7.09	4.18	2.16	2.67	1.83	1.56	1.32	1.33	1.40	1.47	1.42	67.69	54.70	12.98	12.82	0.00
TEASE SANDSTONE																		
11.56	6.38	5.10	3.51	2.04	1.01	1.33	0.90	0.76	0.63	0.60	0.59	0.63	0.60	35.65	29.61	6.05	18.38	0.01
EJURA SANDSTONE																		
16.73	11.91	8.72	6.38	3.54	1.89	2.53	1.93	1.85	1.67	1.70	1.88	1.86	1.81	64.41	49.17	15.24	8.98	0.05
AFRAM FORMATION																		
35.43	26.65	24.15	19.01	11.85	6.14	7.38	4.22	2.91	2.04	1.63	1.43	1.29	1.21	145.35	123.23	22.11	27.45	8.50
37.34	31.31	22.16	16.34	9.28	5.17	6.20	4.79	4.34	3.92	3.80	4.04	3.93	3.78	156.40	121.59	34.81	9.51	0.00
KODJARI FORMATION																		
118.21	79.04	58.09	40.40	21.39	12.70	16.28	9.78	7.46	5.77	4.92	4.52	4.23	3.91	386.71	329.84	56.87	27.97	0.00
231.36	169.73	130.20	89.43	35.06	23.72	19.58	9.62	5.95	3.85	3.09	2.16	1.74	1.50	726.98	679.49	47.49	133.12	0.00

Table. 4.11. Trace element composition of Oti-Pendjari Group Formations

	Bunya		Bimbila										Tease
SAMPLE ID	VO-39	V-MU-9	VO-34	VO-08	VO-09	VO-10	VO-11	VO-12	VO-32	VO-33	VO-35	VO-38	V-MU-18
Li	12.43	2.53	20.40	20.70	20.49	24.49	22.41	18.59	17.50	21.42	11.61	5.60	2.48
P	604.26	46.49	866.11	698.64	726.90	717.18	722.69	833.03	644.48	698.91	202.94	46.28	21.86
Sc	8.74	0.98	11.09	11.87	11.63	11.88	12.32	11.73	9.28	11.15	4.66	0.49	0.22
Ti	2944.67	410.55	3765.38	3482.76	3358.44	3401.08	3761.37	4056.59	2910.12	3574.39	1576.90	238.24	83.52
V	84.38	8.75	102.17	100.09	93.42	101.40	105.85	101.66	69.37	98.25	38.91	2.68	3.04
Cr	44.13	4.21	70.64	69.46	66.16	63.50	72.65	70.93	50.36	65.89	26.43	4.02	5.21
Co	8.81	1.21	14.04	12.24	13.76	14.65	12.88	11.49	9.12	12.63	4.74	0.35	0.47
Ni	48.68	3.29	48.30	34.29	36.22	40.13	37.11	32.23	24.59	31.93	12.51	1.74	2.20
Cu	22.54	2.66	27.19	26.18	27.86	32.66	28.47	24.42	24.27	23.41	17.53	2.72	8.01
Zn	61.53	8.32	69.24	60.17	59.30	72.51	70.97	67.12	54.74	62.57	40.43	3.77	2.13
Ga	24.03	5.57	17.25	16.25	15.80	17.65	17.03	16.50	13.60	15.38	9.48	1.80	0.68
AS	4.02	0.48	2.12	1.80	1.74	1.94	1.80	1.76	1.82	1.24	0.44	0.12	0.24
Rb	68.51	60.94	46.84	44.92	53.37	54.07	44.81	44.54	31.67	49.04	77.10	5.18	0.90
Sr	220.16	26.20	178.32	177.71	159.61	182.84	183.20	189.95	164.14	248.18	56.56	6.47	3.92
Y	108.97	8.68	41.74	25.33	22.19	28.63	23.89	48.81	21.31	18.90	12.58	2.36	1.06
Zr	90.95	127.50	113.90	117.26	124.91	122.32	129.06	113.69	91.09	92.60	104.99	25.02	16.40
Nb	7.67	1.74	9.29	7.56	8.03	8.10	8.53	8.93	6.78	7.75	5.58	1.04	0.31
Sn	1.59	0.96	2.08	1.61	1.76	1.83	1.72	1.89	1.61	1.67	1.75	0.39	0.26
Sb	0.76	0.43	1.06	0.95	1.02	1.01	0.97	1.14	0.95	1.05	0.48	0.16	0.12
Cs	0.98	1.13	1.36	1.00	1.62	1.55	0.96	0.96	0.94	1.48	4.28	0.14	0.04
Ba	822.66	294.65	605.16	802.78	703.29	855.12	762.50	780.73	454.53	593.45	399.82	86.36	13.80
Lu	1.19	0.17	0.53	0.33	0.32	0.35	0.35	0.43	0.30	0.31	0.25	0.05	0.02
Hf	3.46	3.98	4.11	3.46	3.64	3.63	3.79	3.99	3.13	3.37	4.39	1.17	0.61
Ta	0.54	0.14	0.63	0.49	0.53	0.50	0.54	0.60	0.46	0.54	0.36	0.08	0.03
W	2.54	0.49	0.85	0.58	0.60	0.67	0.65	0.75	0.46	0.74	0.44	0.18	0.12

Tl	0.41	0.40	0.30	0.30	0.33	0.35	0.30	0.31	0.20	0.31	0.50	0.03	0.00
Pb	10.87	6.35	12.04	11.50	12.47	12.18	10.87	11.03	12.42	11.67	5.68	4.03	1.48
Th	5.76	2.81	8.08	5.38	5.97	6.22	5.72	6.38	5.95	5.65	6.89	1.24	0.70
U	1.47	0.77	1.99	1.41	1.42	1.43	1.54	1.64	1.50	1.49	1.35	0.34	0.17

Table 4.11 Trace element composition of Oti Group formations, continued.

	Ejura	Afram	Afram	Kodjari	Kodjari
SAMPLE ID	VO-68	VO-69	V-MU-17	VO-22	VO-50
Li	2.46	1.75	3.13	14.22	7.59
P	77.81	71.72	56.92	240.61	1684.80
Sc	0.66	0.80	1.10	4.75	10.91
Ti	290.88	165.51	340.16	1202.42	15399.00
V	3.89	5.63	8.64	34.47	85.97
Cr	2.63	2.06	4.88	48.24	453.86
Co	1.42	0.17	2.04	0.91	29.74
Ni	1.73	1.05	3.93	3.58	243.71
Cu	3.83	3.46	4.79	4.30	11.80
Zn	5.83	4.04	9.08	18.66	94.43
Ga	1.82	2.29	5.67	9.65	12.45
AS	0.19	0.28	0.63	0.90	1.15
Rb	16.26	1.46	54.33	37.11	20.74
Sr	11.73	12.66	20.79	28.61	80.99
Y	3.16	3.45	7.32	10.93	7.86
Zr	34.66	21.19	42.47	36.53	150.83
Nb	1.58	0.61	1.94	4.16	160.55
Sn	0.42	0.31	1.13	1.39	1.71

Sb	0.28	0.16	0.83	0.72	0.51
Cs	0.41	0.07	0.72	1.97	0.52
Ba	98.27	36.85	249.42	584.57	93.86
Hf	1.20	0.80	1.55	1.46	3.94
Ta	0.13	0.05	0.19	0.31	10.64
W	0.13	0.17	0.32	0.55	0.39
Tl	0.09	0.00	0.37	0.20	0.09
Pb	2.93	1.54	13.03	16.44	10.90
Th	1.59	1.07	4.71	3.32	9.28
U	0.35	0.57	0.59	0.87	3.86

4.4 Sm-Nd and Rb-Sr Isotopes of the Tamale-Obosum and Oti-Pendjari Groups

The Sm–Nd isotopic compositions of the Voltaian Supergroup formations show marked variations in Nd concentrations (2.66–312.18 ppm), Sm concentrations (0.49–50.28 ppm), and $^{147}Sm/^{144}Nd$ ratios (0.0806–0.1265). The Bunya Formation yields relatively high Nd values (14.31–312.18 ppm) with $^{147}Sm/^{144}Nd$ ratios between 0.097 and 0.118, producing negative εNd values from –6.98 to –14.70 and corresponding model ages (T_DM) between ~1.28 and 2.02 Ga (Table 4.12). The Bimbila Formation shows a narrower range of Nd contents (5.98–57.60 ppm) and $^{147}Sm/^{144}Nd$ ratios of 0.107–0.117, with consistently negative εNd values (–7.87 to –17.60) and T_DM ages from ~1.41 to 2.20 Ga. The Afram samples are characterized by relatively low Nd (14.61–16.61 ppm) but elevated $^{147}Sm/^{144}Nd$ (0.0955–0.123), yielding strongly negative εNd values (–15.01 to –15.49) and older T_DM ages (~1.66–1.96 Ga). The Tease and Ejura sandstones show low Nd concentrations (<5 ppm) with εNd values between –8.72 and –11.82 and T_DM ages of 1.87–1.94 Ga. Kodjari samples present intermediate Nd (29.79–65.65 ppm) but display contrasting signatures: one with a very low $^{147}Sm/^{144}Nd$ ratio (0.081) and εNd –10.82 (T_DM = 1.11 Ga), while the second is more radiogenic with εNd –14.53 and T_DM = 1.61 Ga. The Sang Conglomerate and Tamale formations exhibit Nd between 7.24 and 37.56 ppm, εNd values of –11.39 to –15.14, and model ages between 1.60 and 1.92 Ga. The Undivided Obosum samples yield εNd values between –8.61 and –8.94 with T_DM ages of ~1.81–1.91 Ga. Finally, the Densubon Formation shows highly variable signatures, with εNd values ranging from –9.61 to –19.92 and T_DM ages spanning 1.31–2.24 Ga.

The analyzed formations of the Voltaian Supergroup display wide variations in Sr and Rb contents, as well as in $^{87}Rb/^{86}Sr$ and $^{87}Sr/^{86}Sr$ ratios (Table 4.13). The Bunya Formation records Sr

concentrations between 34.04 and 257.95 ppm and $^{87}Rb/^{86}Sr$ ratios ranging from 0.71 to 5.81, corresponding to $^{87}Sr/^{86}Sr$ values of 0.71066–0.82003. The Bimbila Formation exhibits moderately high Sr (67.15–232.93 ppm) and variable $^{87}Rb/^{86}Sr$ ratios (0.51–3.55), yielding $^{87}Sr/^{86}Sr$ ratios between 0.70559 and 0.75973. The Afram Formation shows very low Sr contents (5.23–29.22 ppm) with highly elevated $^{87}Rb/^{86}Sr$ ratios (0.29–6.22) and radiogenic $^{87}Sr/^{86}Sr$ values up to 0.80851. The Kodjari and Tamale formations yield intermediate $^{87}Rb/^{86}Sr$ ratios (0.70–4.61) with $^{87}Sr/^{86}Sr$ ranging between 0.71169 and 0.78025. The Ejura and Undivided Obosum formations present variable radiogenic signatures, with $^{87}Sr/^{86}Sr$ values spanning 0.71552–0.76167. The Densubon Formation displays both low and highly elevated $^{87}Rb/^{86}Sr$ ratios (0.63–5.94), corresponding to $^{87}Sr/^{86}Sr$ values of 0.71171–0.80096 (Table 4.13).

Table 4.12. Sm–Nd isotopic compositions of the Tamale-Obosum and Oti-Pendjari Group of rocks.

Formation	Nd (ppm)	Sm (ppm)	$^{147}Sm/^{144}Nd$	$^{143}Nd/^{144}Nd$	Error (2s)	ƐNd	TCHUR	TDM	*f* Sm/Nd
Bunya	14.31	2.77	0.11698	0.51227	0.000005	-6.98	0.69	1.41	-0.4559
Bunya	312.18	50.28	0.09735	0.51217	0.000007	-8.96	0.71	1.28	-0.5472
Bunya	38.38	7.24	0.11409	0.51220	0.000006	-8.29	0.79	1.44	-0.4694
Bunya	19.87	3.90	0.11849	0.51188	0.000005	-14.70	1.48	2.02	-0.4489
Bunya	198.20	33.70	0.10277	0.51210	0.000007	-9.33	0.87	1.44	-0.5220
Bunya	24.03	4.52	0.11363	0.51215	0.000006	-10.38	0.89	1.51	-0.4715
Bimbila	57.60	10.24	0.10752	0.51217	0.000009	-8.00	0.79	1.41	-0.4999
Bimbila	29.16	5.53	0.11472	0.51219	0.000007	-9.74	0.83	1.50	-0.4664
Bimbila	38.08	6.85	0.10881	0.51216	0.000006	-9.58	0.83	1.44	-0.4939
Bimbila	21.12	4.00	0.11445	0.51173	0.000007	-8.01	1.68	2.20	-0.4677
Bimbila	5.98	1.09	0.11059	0.51174	0.000006	-7.87	1.58	2.10	-0.4856
Bimbila	31.32	6.06	0.11690	0.51222	0.000004	-9.25	0.79	1.51	-0.4563
Bimbila	28.56	5.55	0.11741	0.51213	0.000006	-17.60	0.97	1.60	-0.4539
Bimbila	35.24	6.52	0.11181	0.51214	0.000006	-17.31	0.89	1.51	-0.4800
Bimbila	32.02	6.10	0.11519	0.51222	0.000005	-15.05	0.78	1.43	-0.4642
Bimbila	43.87	8.06	0.11112	0.51223	0.000005	-12.87	0.73	1.41	-0.4831
Afram	14.61	2.96	0.12259	0.51197	0.000004	-15.49	1.35	1.96	-0.4298
Afram	16.61	2.62	0.09550	0.51186	0.000005	-15.01	1.21	1.66	-0.5558
Tease	2.66	0.49	0.11127	0.51184	0.000005	-8.72	1.43	1.94	-0.4825
Ejura Ss	4.79	0.86	0.10923	0.51186	0.000005	-11.82	1.35	1.87	-0.4919
Kodjari	65.65	8.75	0.08059	0.51218	0.000004	-10.82	0.59	1.11	-0.6252
Kodjari	29.79	5.16	0.10478	0.51202	0.000006	-14.53	1.01	1.61	-0.5127
Sang Cong.	37.56	7.44	0.11971	0.51208	0.000007	-14.92	1.11	1.73	-0.4432
Tamale	13.57	2.53	0.11286	0.51189	0.000005	-15.14	1.41	1.91	-0.4751
Tamale	7.24	1.07	0.08912	0.51187	0.000007	-13.38	1.10	1.60	-0.5855
Tamale	10.43	1.92	0.11142	0.51185	0.000004	-11.39	1.41	1.92	-0.4818
Undivided Obosum	10.74	1.96	0.11028	0.51194	0.000004	-8.94	1.22	1.81	-0.4871

Undivided Obosum	18.48	3.87	0.12645	0.51205	0.000004	-8.61	1.31	1.91	-0.4119
Densubon	21.61	3.89	0.10881	0.51209	0.000003	-9.61	0.94	1.53	-0.4939
Densubon	52.65	8.38	0.09621	0.51214	0.000004	-19.92	0.75	1.31	-0.5525
Densubon	5.10	0.93	0.10989	0.51161	0.000004	-14.31	1.80	2.24	-0.4889
Densubon	13.46	2.30	0.10328	0.51190	0.000004	-10.49	1.21	1.72	-0.5196

Table 4.13 Rb-Sr isotopic composition and ratios of the Tamale-Obosum and Oti-Pendjari Groups

Formation	Sr (ppm)	Rb(ppm)	$^{87}Rb/^{86}Sr$	$^{87}Sr/^{86}Sr$	**Error**
Bunya	133.33	76.92	1.67027	0.71775	0.000008
Bunya	119.67	55.06	1.33216	0.71895	0.000008
Bunya	143.57	71.32	1.43862	0.71997	0.000009
Bunya	34.04	67.69	5.81497	0.82003	0.000007
Bunya	257.95	69.69	0.78161	0.71066	0.000008
Bunya	219.47	53.94	0.71112	0.71176	0.000006
Bimbila	211.46	45.05	0.61632	0.71050	0.000008
Bimbila	232.93	58.26	0.72377	0.71225	0.000009
Bimbila	188.37	33.38	0.51264	0.71045	0.000006
Bimbila	67.15	81.98	3.54882	0.75973	0.000007
Bimbila	9.60	6.03	1.81584	0.70559	0.000009
Bimbila	195.44	45.71	0.67664	0.71114	0.000007
Bimbila	175.22	54.22	0.89566	0.71413	0.000006
Bimbila	200.86	54.75	0.78875	0.71262	0.000006
Bimbila	204.85	45.93	0.64877	0.71218	0.000010
Bimbila	212.17	45.48	0.62024	0.71061	0.000007
Afram	16.61	1.69	0.29548	0.72038	0.000006
Afram	29.22	62.23	6.22063	0.80851	0.000010
Afram	5.23	1.05	0.57882	0.71598	0.000010

Ejura	14.99	19.05	3.69615	0.76167	0.000006
Kodjari	78.80	19.02	0.69842	0.71169	0.000006
Kodjari	34.62	39.42	3.30565	0.74519	0.000006
Sang Cong.	257.14	47.24	0.53151	0.71042	0.000005
Tamale	30.16	27.31	2.62931	0.74819	0.000006
Tamale	13.67	3.52	0.74614	0.71915	0.000006
Tamale	25.20	39.88	4.60951	0.78025	0.000005
Undivided Obosum	19.33	11.59	1.73822	0.73351	0.000007
Undivided Obosum	153.83	39.01	0.73409	0.71552	0.000007
Densubon	221.56	48.66	0.63542	0.71171	0.000006
Densubon	157.05	59.79	1.10186	0.71338	0.000009
Densubon	7.75	3.96	1.48379	0.74557	0.000013
Densubon	47.79	97.20	5.93660	0.80096	0.000011

CHAPTER 5

5. Discussions

5.1 Provenance of the Tamale - Obosum Group

5.1.1 Petrographic Rock Classification of Tamale-Obosum Group

Modal analysis of framework grains provides a robust basis for classifying sandstones and inferring provenance. When plotted on the QFL (Quartz–Feldspar–Lithic) triangular diagram of Folk (1974), the sandstones of the Tamale-Obosum Group show a dominance of quartz, with subordinate feldspar and very few lithic fragments (Figure 5.1). Specifically, the Dunkro and Densubon Sandstone Formation samples plot within the sub-arkose field, indicating 5–25% feldspar grains with quartz as the dominant framework component. In contrast, the Tamale Sandstone Formation and Undivided Obosum Formation classify as quartz arenites, with quartz exceeding 90% of the framework grains and feldspar plus lithic components making up less than 10%.

This compositional maturity reflects both sediment recycling and prolonged transport, as unstable feldspars and lithic fragments are preferentially destroyed during weathering and transport, leaving behind more resistant quartz grains (Taylor & McLennan, 1985; Pettijohn et al., 1987). The presence of sub-arkosic sandstones (Dunkro, Densubon) suggests derivation from relatively proximal sources where feldspar survived weathering and abrasion, consistent with inputs from granitic to gneissic basement terranes of the Birimian Supergroup and Pan-African granitoids (Kalsbeek et al., 2008; Abu et al., 2019). Conversely, the quartz arenite character of the Tamale Formation indicates either recycling from older sedimentary units or extended transport and reworking under oxidizing, high-energy fluvial–alluvial to shallow-marine systems typical of late-stage intracratonic red-bed basins (Dickinson & Suczek, 1979; Condie, 1993).

The contrasting petrographic character of the Dunkro/Densubon versus Tamale/Undivided Obosum sandstones highlights stratigraphic and temporal variation in sediment supply and transport regime within the upper Voltaian basin fill. These variations are consistent with an overall progradation from feldspathic-rich, proximal sources toward quartzose, mature sandstones in more distal depositional settings, reflecting the progressive evolution of the basin through the late Neoproterozoic (Carney et al., 2010; Zobah, 2022).

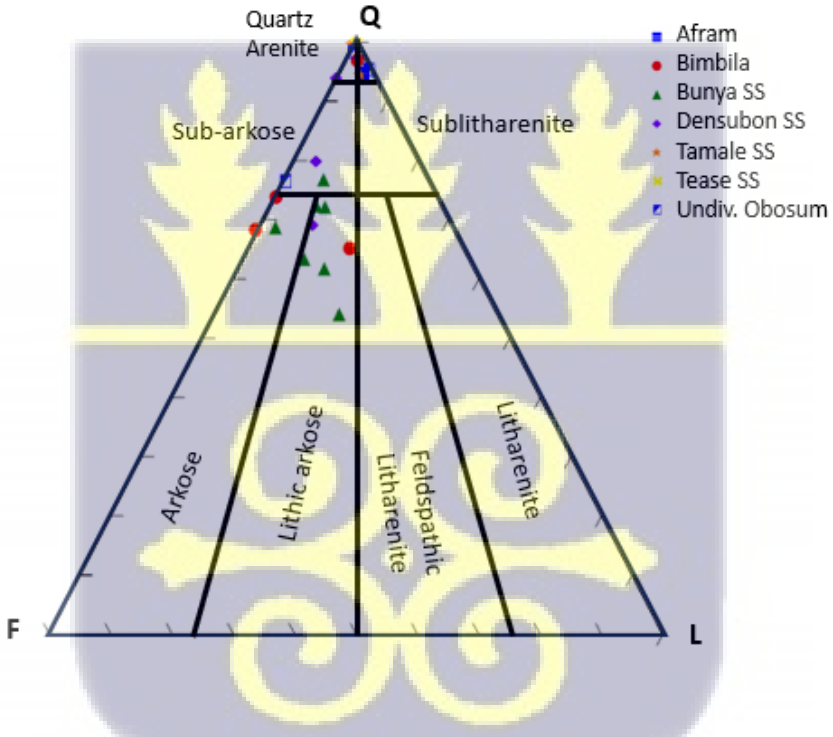

Figure 5.1. A) Detrital composition classification of the sandstones from the Oti-Pendjari and Tamale-Obosum Groups after Folk 1974.

5.1.2 Geochemical Classification of Tamale-Obosum Group

The geochemical classification of clastic sedimentary rocks, an established tool in sedimentary petrology, relies on major-element ratios to infer compositional maturity and provenance. Early frameworks by Pettijohn et al. (1972) applied the log (SiO_2/Al_2O_3) versus log (Na_2O/K_2O) diagram to distinguish quartz-rich from feldspathic sands, reflecting sediment maturity and quaternary compositional trends. This model was refined by Herron (1988), who replaced the Na_2O/K_2O axis with log (Fe_2O_3/K_2O), a modification that better captures the stability of minerals and allows more precise discrimination of arkoses.

When applied to the Tamale-Obosum Group samples, these geochemical diagrams yield robust interpretations: most Tamale Sandstone samples plot within the quartz arenite field, a few as sub-litharenites, while the Densubon Sandstone falls into the wacke field (including sub-arkose and litharenite types). The Sang Conglomerate plots as a wacke, and the Undivided Obosum Formation appears as an Fe-sandstone (Figure 5.2). These geochemical classifications agree with petrographic observations, underscoring their reliability.

Further refinement using the K_2O/Al_2O_3 ratio, which reflects feldspar versus clay dominance (Clay: 0.0–0.3; Feldspar: 0.3–0.9; Cox et al., 1995), confirms the maturity interpretations. Most samples record $K_2O/Al_2O_3 < 0.3$, consistent with clay except for one sample from the Densubon Sandstone, suggesting localized feldspar enrichment.

Collectively, these geochemical results align with broader tectonic and sedimentary paradigms. The quartz- and clay-rich compositions support models of passive-margin or cratonic basin sedimentation, where prolonged weathering and recycling dominate during supercontinent

assembly and breakup cycles. Meanwhile, the feldspar-rich and lithic inputs in Densubon hint at more proximal orogenic sources, resonating with global patterns observed in numerous intracratonic and foreland basins (e.g., Appalachian foreland, Vindhyan Basin, McArthur Basin) undergoing mixing of recycled and juvenile crustal materials during tectonic transitions.

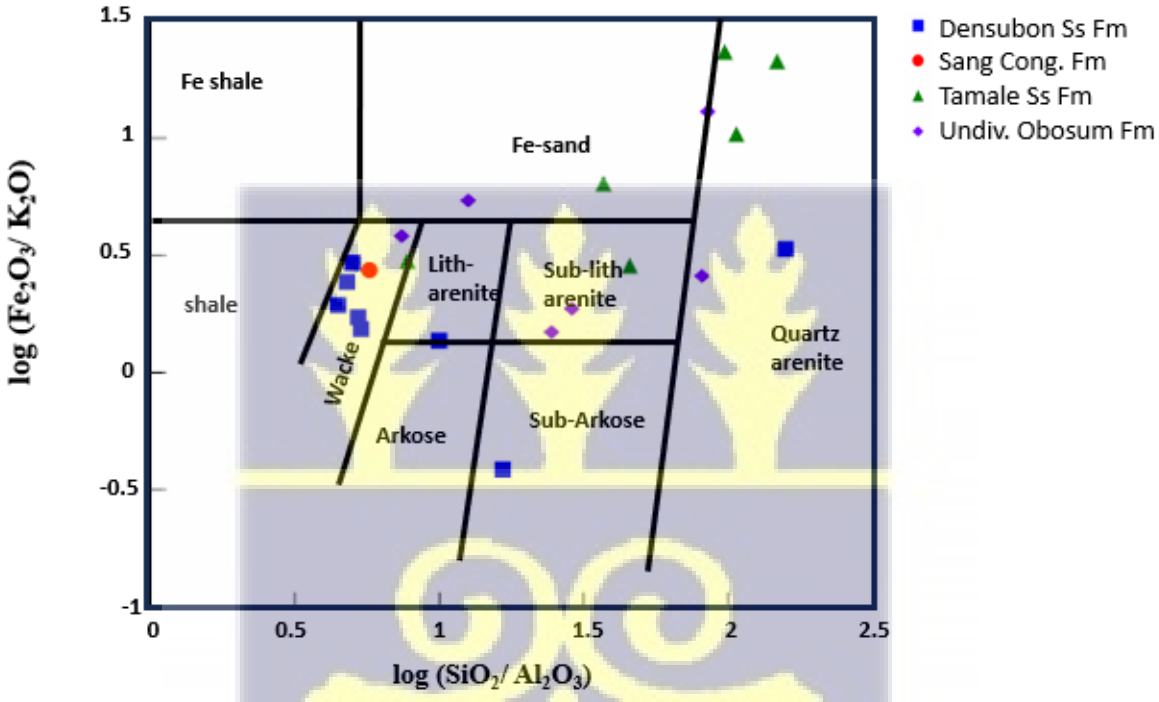

Figure 5.2 Geochemical classification of Tamale-Obosum Group based on log ($SiO_2/Al2O_3$) - log (Fe_2O_3/K_2O) ratio (Herron, 1988).

The major element composition of the Tamale-Obosum Group reflects clear lithological controls and weathering histories. Quartz arenites and wackes are characterized by very low CaO and K_2O contents, coupled with elevated SiO_2 and depleted Al_2O_3, consistent with their mineralogical dominance by quartz and the relative absence of feldspar and lithic fragments. In contrast, litharenites exhibit higher Na_2O, Fe_2O_3, and TiO_2 concentrations, reflecting the greater abundance

of Na-rich plagioclase, alkali feldspar, and phyllosilicate-bearing rock fragments. These geochemical signatures correspond closely with petrographic observations, indicating that feldspars and lithic components were preferentially altered during chemical weathering, leading to quartz enrichment in the arenitic facies (Nesbitt et al., 1996). The strong positive correlations between Al_2O_3 and oxides such as Fe_2O_3, MgO, MnO, TiO_2, and K_2O (McLennan et al., 1983) further confirm the dominant role of clay minerals in controlling major element distribution. Conversely, the negative correlation between SiO_2 and Al_2O_3 reflects the inverse relationship between quartz and aluminosilicate phases during weathering and sediment recycling (Figure 5.3).

Formation-specific variations are also apparent: the Densubon Sandstone and Sang Conglomerate exhibit the highest proportions of Na_2O, CaO, MgO, and Fe_2O_3, indicating relatively immature compositions and weaker weathering compared to the Tamale Sandstone, which shows extreme SiO_2 enrichment and strong feldspar depletion. These trends are reinforced by K_2O/Al_2O_3 ratios (<0.2 in most samples), which suggest clay mineral dominance across the majority of formations. UCC-normalized diagrams with the formations grouped based on their lithological differences, highlight further contrasts: litharenites are depleted in most oxides except Na_2O and CaO, while wackes display enrichment in SiO_2, MnO, and Na_2O (Figure 5.4).

When compared with other African sedimentary basins, these patterns reveal broader tectonosedimentary parallels. The high SiO_2 and clay-controlled chemistry of the quartz arenites are similar to those of the Kalahari and Karoo basins of southern Africa, where prolonged chemical weathering under stable cratonic settings led to quartz enrichment and feldspar depletion (Catuneanu et al., 2005). Conversely, the immature compositions of the Densubon and Sang formations, marked by higher feldspar and lithic contents, closely resemble sandstones from the Taoudeni Basin (Mauritania-Mali), which record variable inputs from both cratonic interiors and

Pan-African orogenic belts (Villeneuve & Dallmeyer, 1987; Ennih & Liégeois, 2008). The enrichment in Na_2O and CaO in these units may also be compared with the Congo Basin, where feldspathic sandstones reflect rapid erosion of uplifted basement terrains during Neoproterozoic–Cambrian tectonism (Kadima et al., 2011). Thus, the Tamale-Obosum Group major element geochemistry not only reflects local mineralogical controls but also situates the Voltaian Supergroup within a broader African context of Proterozoic basin evolution, balancing stable cratonic sedimentation with episodic inputs from adjacent orogenic sources.

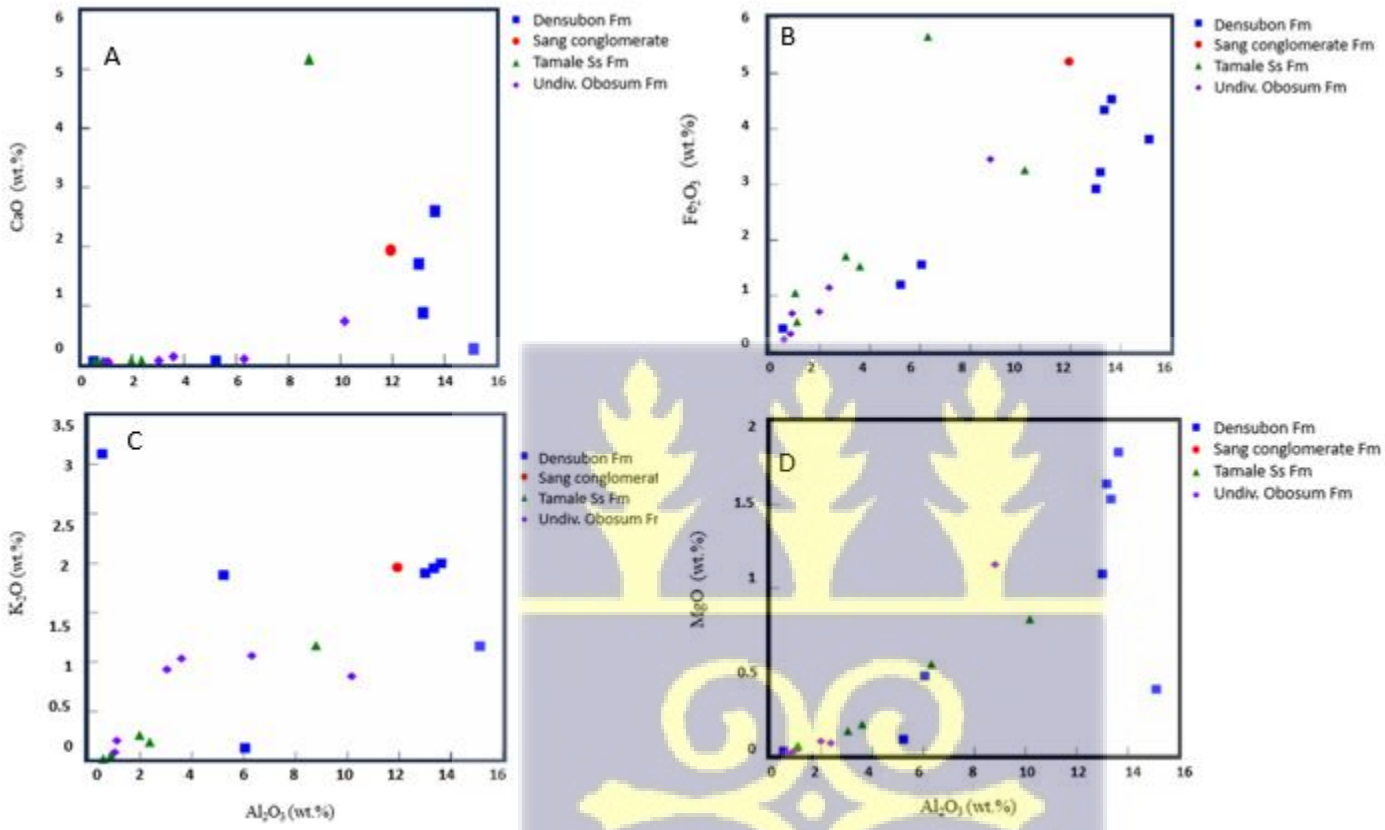

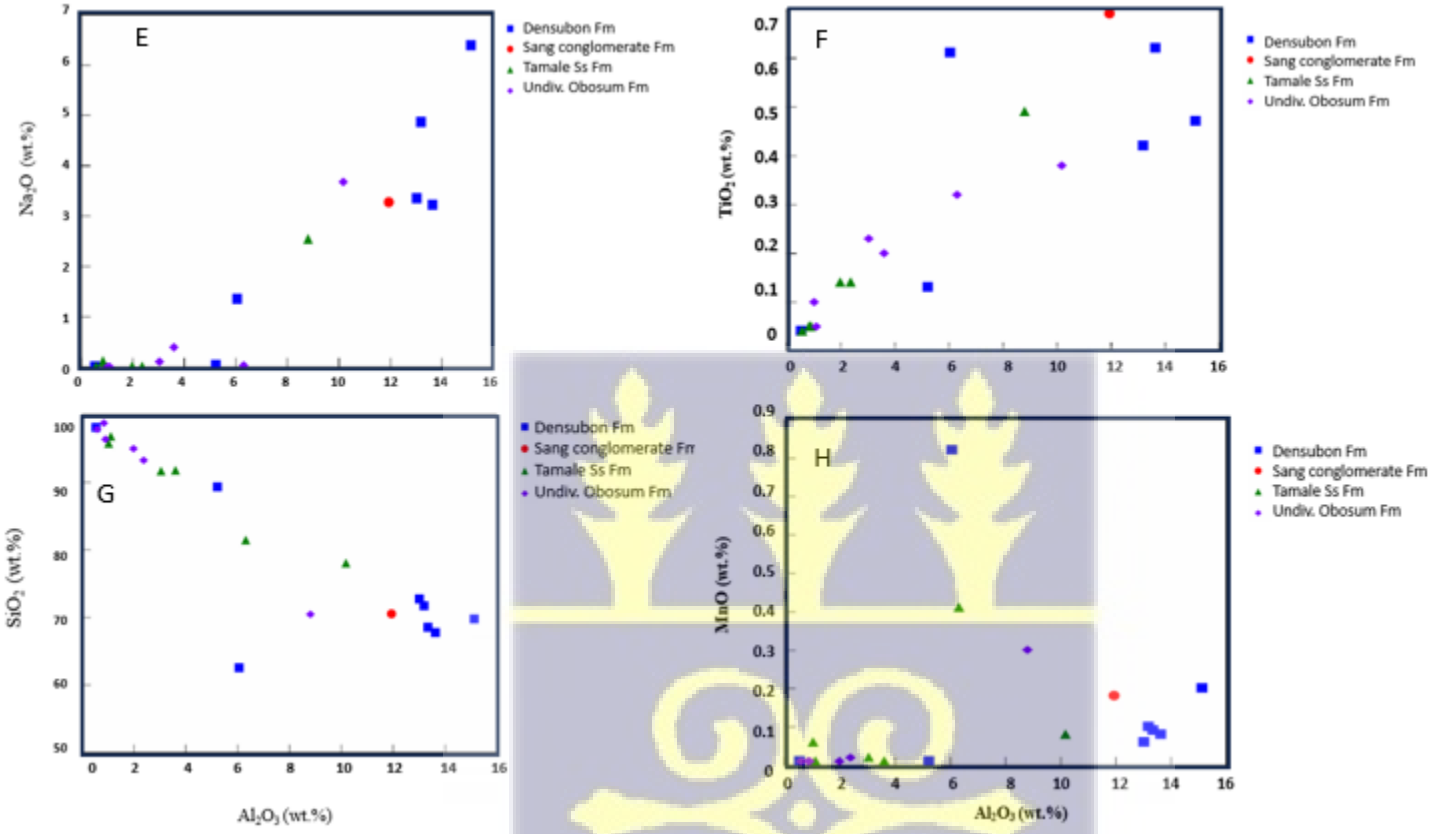

Figure 5.3 Selected major element-Al_2O_3 variation diagram for the Tamale-Obosum Group formations.

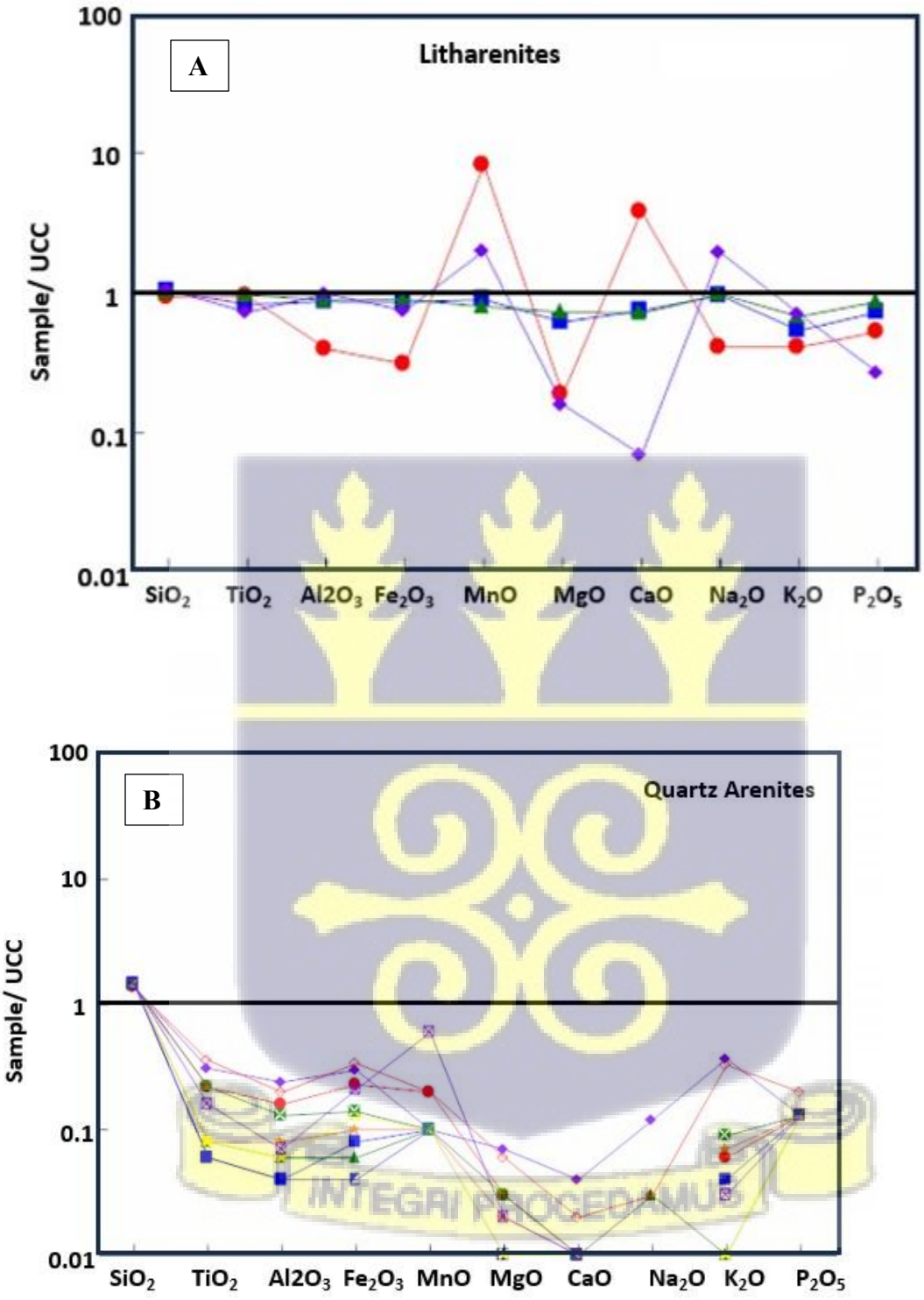

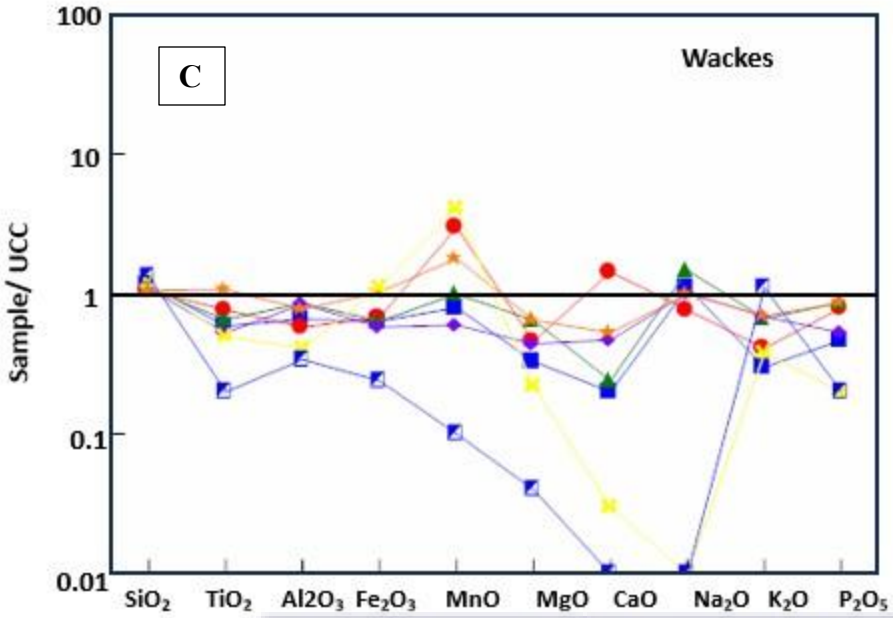

Figure 5.4 Multi-element normalized diagrams for the Tamale-Obosum Group formations, grouped as (A) litharenites, (B) Quartz arenites and (C) Wackes; normalized against average Upper Continental Crust (Taylor and McLennan, 1985).

5.1.3 Paleo-Weathering Conditions of The Tamale Group

The degree and duration of chemical weathering exert a primary control on the alteration of primary minerals, particularly feldspars, in upper crustal rocks. During weathering, feldspars are progressively altered to clay minerals, accompanied by the systematic depletion of mobile cations such as K, Na, and Ca (Nesbitt et al., 1980). The residual concentration of these elements in derived sediments therefore provides a useful proxy for quantifying weathering intensity, most commonly expressed through the Chemical Index of Alteration (CIA) (Nesbitt & Young, 1982). CIA values effectively capture the transition from feldspar-dominated mineralogy to clay-rich assemblages and thus provide insights into paleo-weathering regimes (Fedo et al., 1995; Armstrong-Altrin et al., 2004). High CIA values (76–100) typically reflect intense chemical weathering in tectonically

stable, humid tropical conditions, whereas low values (<50) are associated with immature, unweathered source terranes.

In the present study, very low CaO concentrations were recorded in most samples, precluding distinction between silicate- and carbonate-bound CaO; hence, total CaO was used in CIA calculations. Results indicate that Tamale Sandstone and Undivided Obosum Formation samples display significant depletion in K, Na, and Ca relative to both the Upper Continental Crust (UCC) and Post-Archean Average Shale (PAAS), trending toward the Al_2O_3 (A) apex on the A–CN–K ternary diagram (Figure 5.5). This trend is diagnostic of advanced feldspar alteration and strong chemical weathering, consistent with derivation from mature cratonic sources. By contrast, the Densubon Sandstone and Sang Conglomerate show CIA values lower than PAAS but higher than UCC, reflecting relatively higher proportions of plagioclase and lower contributions of K-feldspar. These samples also follow the Ideal Weathering Trend (IWT) from UCC, suggesting moderate weathering intensity and preservation of less stable feldspathic phases.

When placed in a broader geological framework, these weathering signatures provide insights into sediment provenance. The high CIA values and strong feldspar depletion in the Tamale Sandstone and Undivided Obosum Formation point to derivation from the Birimian granitoid–greenstone terranes of the West African Craton, which are dominated by felsic granitoids highly susceptible to deep weathering (Taylor et al., 1980; Sylvester, 1998). In contrast, the lower CIA values and feldspar-rich character of the Densubon and Sang formations are consistent with inputs from less weathered, tectonically rejuvenated Pan-African orogenic belts, where granitic and volcanic arc rocks contributed fresher plagioclase and lithic material (Affaton et al., 1991; Kalsbeek et al., 2008). Thus, the geochemical weathering trends recorded in the Voltaian Supergroup sediments capture the interplay between stable cratonic granitoid sources and active Pan-African orogenic

sources, reflecting both long-term chemical weathering of basement granitoids and episodic supply from uplifted arc-related terranes during Gondwana assembly.

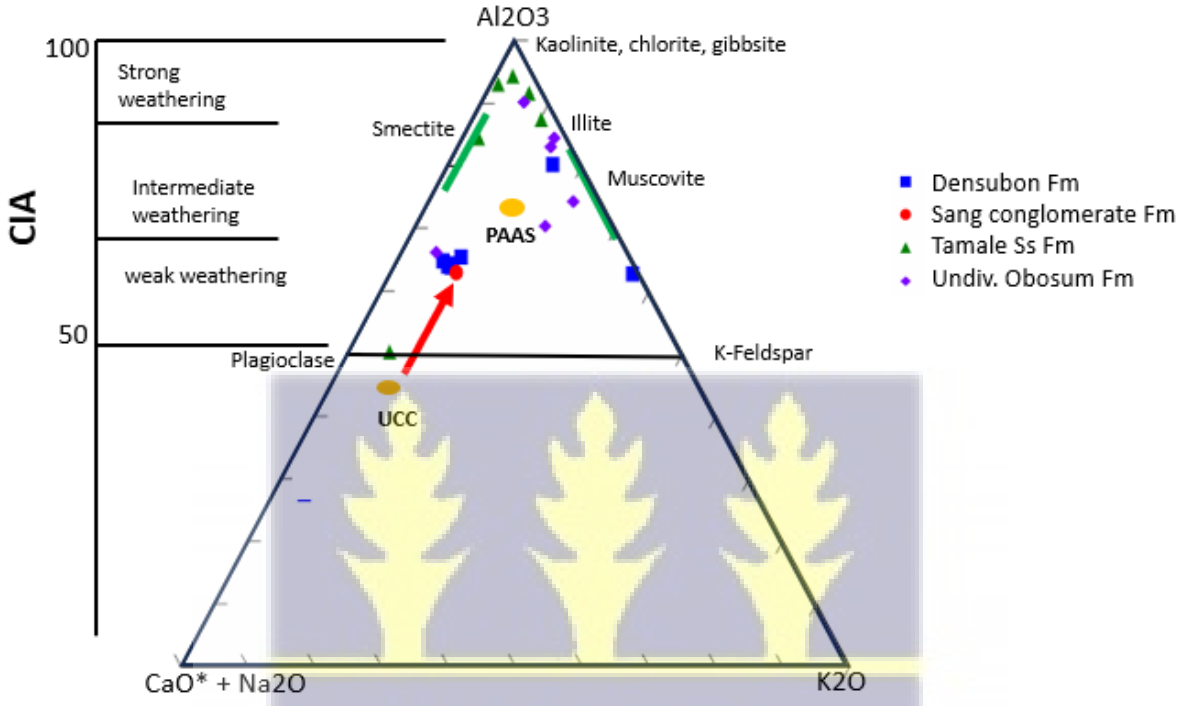

Figure 5.5 A-CN-K diagram (*after* Nesbitt and Young, 1982) showing samples of the Tamale-Obosum Group and average composition of upper continental crust (UCC; Taylor and McLennan, 1985). A = Al_2O_3; CN = CaO* + Na_2O; K = K_2O (molecular proportion; CaO* = CaO in silicate fraction only); CIA = Chemical Index of Alteration (Nesbitt and Young, 1982).

Potassium (K) enrichment is a key diagenetic process that can significantly modify the primary geochemical signature of sediments and sedimentary rocks, potentially obscuring their original provenance (Glazner, 1988; Nesbitt & Young, 1989; Sutton & Maynard, 1992; Condie, 1993; Fedo et al., 1995, 1997a, 1997b). This process, known as K-metasomatism, commonly occurs through the interaction of sediments with K-rich pore fluids, driving mineralogical transformations such as (i) conversion of kaolinite to illite in the clay matrix, or (ii) replacement of plagioclase feldspar by

K-feldspar. While the former pathway lowers the Chemical Index of Alteration (CIA) due to K-addition, the latter often leaves CIA values unchanged since it represents an isochemical substitution of Ca or Na by K (Glazner, 1988; Fedo et al., 1995).

In this study, the Tamale Sandstone Formation (quartz arenites) generally shows high CIA values, consistent with advanced chemical weathering and negligible influence of K-metasomatism. However, certain arenites and wackes, particularly from the Densubon Sandstone Formation, trend toward the K-apex on A–CN–K plots, indicating localized K-metasomatic overprint. Petrographic observations support this geochemical signal: plagioclase grains are frequently altered, and illite constitutes a major component of the matrix. These features suggest that diagenetic K-enrichment partly modified the original mineralogy, lowering CIA values in some samples and shifting their geochemical trends toward feldspathic compositions (cf. Fedo et al., 1997a). In contrast, the Sang Conglomerate and parts of the Densubon Formation retain low CIA values and significant proportions of unaltered plagioclase, pointing to limited diagenetic alteration.

When coupled with the Index of Compositional Variability (ICV), a more nuanced interpretation of provenance and weathering emerges. CIA primarily tracks the intensity of chemical weathering, while ICV reflects mineralogical diversity inherited from the source. High ICV values generally denote sediment derivation from lithologically heterogeneous, weakly weathered sources, whereas low ICV values indicate mineralogically uniform and strongly weathered inputs (Cox et al., 1995; Cullers, 2000). In the Voltaian Supergroup, the Tamale Sandstone Formation displays low ICV and high CIA values, suggesting derivation from a relatively uniform felsic source that experienced intense chemical weathering prior to deposition (Figure 5.6). This geochemical signature is consistent with derivation from Birimian granitoids, whose felsic to intermediate

composition and prolonged exposure on the West African Craton subjected them to deep weathering under tropical conditions (Taylor et al., 1980; Sylvester, 1998).

By contrast, most Densubon Sandstone samples exhibit low CIA and low-to-variable ICV values, implying derivation from sources with less intense weathering and greater lithological diversity. The relatively fresher feldspathic signatures and the preservation of plagioclase grains in these sediments point toward contributions from Pan-African orogenic sources, particularly the Dahomeyide belt to the east, where Neoproterozoic granitic and arc-related rocks were uplifted and eroded during Gondwana amalgamation (Affaton et al., 1991; Kalsbeek et al., 2008). The Sang Conglomerates, with their mixed weathering indices and coarse lithic fragments, likely represent proximal deposition of material derived from rejuvenated Pan-African terranes with minimal chemical alteration.

Taken together, the combined CIA–ICV dataset suggests a dual provenance: (i) quartz-rich, highly weathered sediments supplied from the stable Birimian granitoid terranes of the West African Craton, and (ii) feldspar-bearing, variably weathered inputs sourced from Pan-African belts, particularly the Dahomeyide orogen. These contrasting weathering and compositional signatures reflect the tectono-sedimentary evolution of the Voltaian Basin during the late Neoproterozoic, recording both cratonic stability and peripheral orogenic activity during West Gondwana assembly.

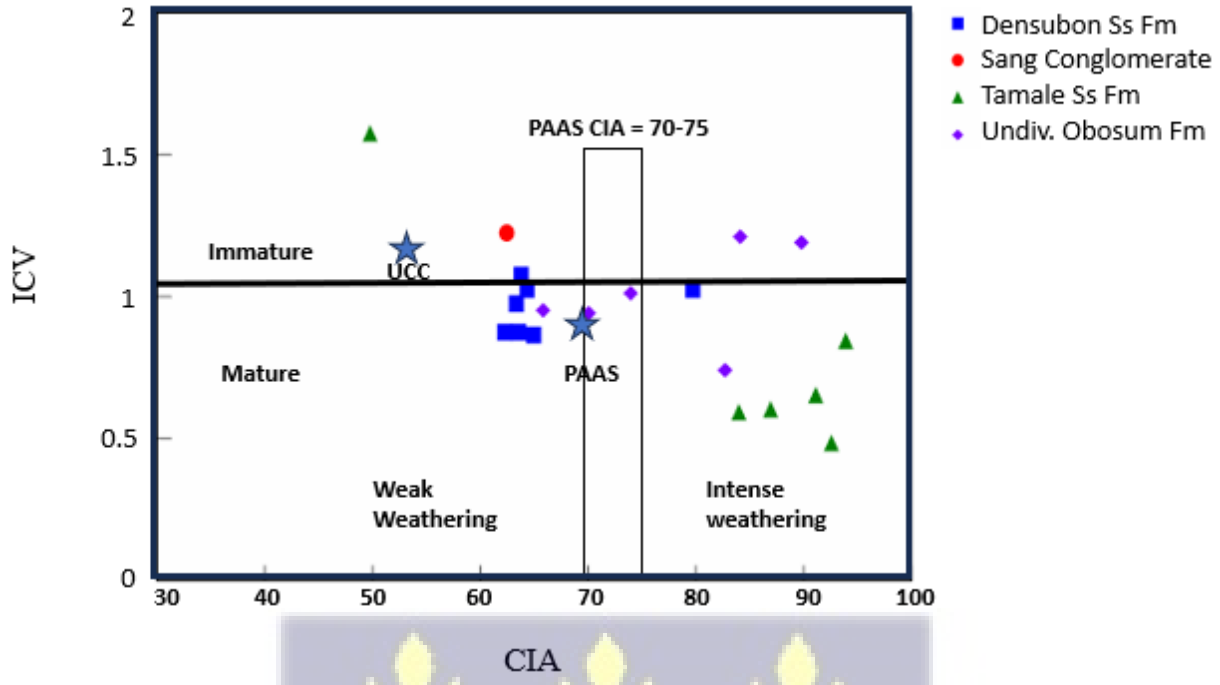

Figure 5.6 ICV (Index of Compositional Variability) versus CIA (Chemical Index of Alteration) plot (after Long et al., 2012) for the Tamale-Obosum Group. UCC (Upper Continental Crust) and PAAS (Post-Archean Australian Shale) values from Taylor and McLennan (1985).

5.1.4 Source rock lithology of the Tamale-Obosum Group, from heavy mineral analyses

Heavy mineral assemblages provide valuable constraints on sediment provenance because minerals such as zircon, rutile, garnet, and chrome spinel retain distinct signatures of their source rocks (Morton & Hallsworth, 1999; Mange & Wright, 2007). In the Tamale–Obosum Group, most samples contain a restricted heavy mineral suite, dominated by one or two stable minerals rather than the full association of zircon, rutile, tourmaline, garnet, and apatite typically linked to felsic magmatic or high-grade metamorphic sources of continental affinity (Morton & Hallsworth, 1994). This limited diversity suggests derivation from selective sources and/or post-depositional processes that reduced mineral variability.

The Densubon Sandstone Formation is distinctive, with one sample yielding ilmenite and spinel, minerals diagnostic of a mafic to ultramafic provenance (including chrome spinel–ilmenite–leucoxene associations; Garzanti & Andò, 2007). Elevated chrome spinel:zircon (CZi) and chrome spinel:garnet (CGi) ratios in the Densubon samples reinforce this interpretation, indicating contributions from mafic-ultramafic source rocks. While pyroxenes would also be expected from ultramafic terrains, their absence can be attributed to their instability during burial diagenesis (Morton & Hallsworth, 1999). This signature suggests that the Densubon sediments may have incorporated detritus derived from Pan-African ophiolitic fragments within the Dahomeyide belt (Affaton et al., 1991; Kalsbeek et al., 2008), where mafic-ultramafic complexes are known to occur as tectonic slivers accreted during Neoproterozoic collision.

By contrast, the Tamale Sandstone Formation and Sang Conglomerate Formation exhibit high rutile:zircon (RuZi) and zircon:rutile (RZi) indices, indicating derivation from metasedimentary terranes rich in rutile and zircon (Mange et al., 2002; Hallsworth et al., 2008). These assemblages are consistent with sources in the Birimian granitoid-greenstone terranes of the West African Craton, where felsic granitoids and metasedimentary belts (particularly mica schists and quartzites) provide abundant rutile and zircon.

The Sang Conglomerate Formation also shows relatively high garnet:zircon (GZi) values compared to the other units. Elevated GZi ratios are typical of metamorphic and metasedimentary source rocks where garnet is stable and abundant (Morton & Hallsworth, 1999; Morton et al., 2005). This suggests a significant input from medium- to high-grade metamorphic terranes, likely derived from the reworked Birimian basement to the west or from metamorphic units within the Pan-African Dahomeyide belt to the east.

Taken together, the heavy mineral indices suggest a dual provenance. Quartzose, zircon- and rutile-rich assemblages in the Tamale Sandstone and Sang Conglomerate reflect contributions from Birimian granitoids and metasedimentary rocks on the stable West African Craton. Chrome spinel- and ilmenite-bearing assemblages in the Densubon Formation point to input from Pan-African mafic-ultramafic terranes, particularly the Dahomeyide belt, where fragments of ophiolitic complexes and arc-related basalts are preserved. This mixed provenance signature aligns with the regional tectonostratigraphic framework of the Voltaian Basin, which records sediment influx from both the cratonic interior and the Pan-African mobile belt during Neoproterozoic basin development (Affaton et al., 1991; Kalsbeek et al., 2008; Anani et al., 1999).

5.1.5 Source rock lithology of the Tamale-Obosum Group from framework mineralogy and modal analyses

The Tamale–Obosum Group largely reflects this global pattern. Petrographic and geochemical analyses indicate that the Tamale Sandstone, Densubon Sandstone, and Dunkro Sandstone formations are dominated by detritus from plutonic sources (granites) (Figure 5.7), pointing to derivation from the widespread Birimian granitoid terranes of the West African Craton (Leube et al., 1990; Taylor et al., 1992). The presence of feldspar- and quartz-rich arenites, coupled with minor contributions from high-grade metamorphic lithics, further suggests input from Pan-African gneissic terranes of the Dahomeyide Belt to the east (Affaton et al., 1991; Kalsbeek et al., 2008). This dual provenance underscores the transitional tectonic setting of the Voltaian Basin during the late Neoproterozoic, where sediments were sourced from both the stable cratonic interior and the actively deforming Pan-African orogen.

The stratigraphic architecture of the group also records spatial variations in depositional environments. During the later stages of Pan-African mountain building, flexural downwarping at

the foreland of the Dahomeyide orogen created accommodation space within the Voltaian Basin. Proximal coarse-grained deposits, such as those of the Densubon and Dunkro Sandstone formations, were deposited in the Obosum Syncline, representing foredeep accumulation adjacent to the orogenic front (Anani et al., 1999). These formations are characterized by abundant feldspar and lithic fragments, reflecting short transport distances and derivation from newly uplifted Pan-African basement rocks.

Farther to the north, the Tamale Sandstone Formation represents a more distal depositional system, consisting of reddish fluvial sandstones with higher quartz contents. These sediments likely incorporate significant reworked detritus from the Birimian granitoids to the north and northwest, transported into the basin by river systems draining the stable cratonic hinterland (Kalsbeek et al., 2008; Villeneuve, 2005). The dominance of quartzose arenites in the Tamale Formation thus reflects both longer transport distances and greater sedimentary reworking compared to the more feldspathic proximal deposits.

In summary, the Tamale–Obosum Group records a mixed provenance signature: (1) proximal feldspathic and lithic-rich deposits (Densubon, Dunkro) linked to Pan-African metamorphic and granitoid sources, and (2) distal quartz-rich fluvial deposits (Tamale Sandstone) reflecting contributions from Birimian granitoid terranes. This dual sediment routing system highlights the interaction between cratonic stability and Pan-African orogenesis, consistent with the basin's position at the interface of the West African Craton and the Dahomeyide Belt during the late Neoproterozoic.

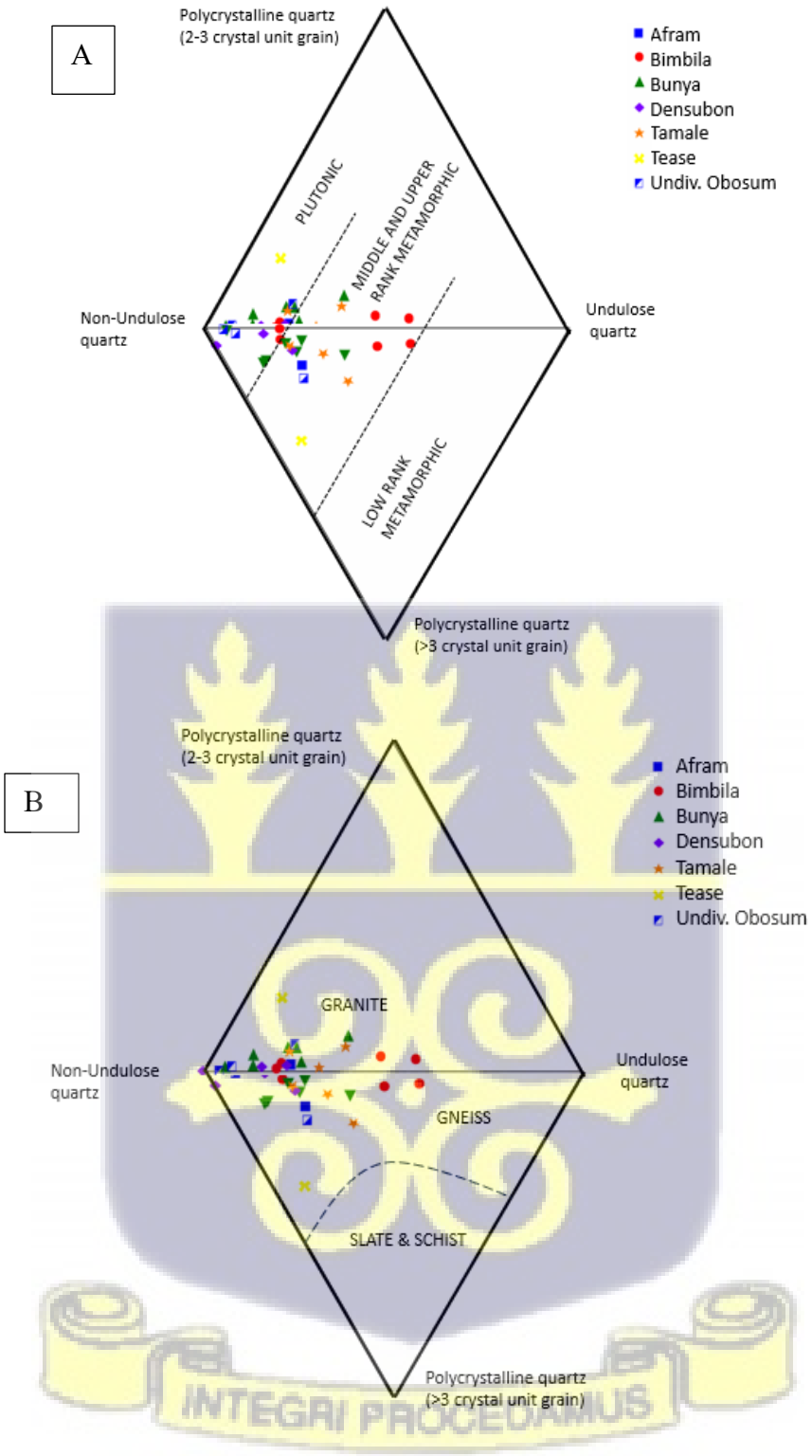

Figure 5.7 (A) Diamond diagram plot, after Tortosa (1991) showing the source of quartz grains (B) Diamond diagram showing the provenance of quartz grains in the Tamale-Obosum Group sandstones (Basu et al., 1975).

5.1.6 Source rock lithology of the Tamale-Obosum Group from Trace and Rare Earth Elements

The chemical composition of fine-grained sedimentary rocks is a well-established proxy for inferring tectonic setting and sediment provenance (Condie et al., 1991). Fine-grained rocks act as natural geochemical integrators of mixed detritus, preserving signals that reflect the average composition of their source terranes. To interpret these signals, compositions are commonly normalized against global reference standards such as the Upper Continental Crust (UCC; Rudnick & Gao, 2014), the Post-Archaean Australian Shale (PAAS; Pourmand et al., 2012), or the North American Shale Composite (NASC; McLennan, 1989). This approach highlights subtle deviations from the average crustal composition and constrains both provenance and depositional setting. For instance, Totten et al. (2000) demonstrated how NASC-normalized multi-element patterns of the Stanley Shale could distinguish passive margin from arc-related sources.

In the Tamale–Obosum Group, UCC-normalized multi-element plots (Figure 5.8) reveal distinct patterns across formations. The Tamale Sandstone is enriched in Sr, Ba, Ni, and Yb but depleted in P, Ta, Nb, Hf, Zr, Y, and Sc. The Sang Conglomerate displays significant enrichment in Sr, Ba, V, Cr, Ni, Yb, Ti, Y, and La, while depleted in Cs, Ta, Nb, Hf, Zr, U, and P. Similarly, the Densubon Sandstone is enriched in Sr, Ba, Cr, Ni, Yb, La, and Ce but depleted in P, Ta, Nb, Hf, Zr, Ti, Sc, and Th. The Undivided Obosum Formation shows enrichment in Sr, Ba, V, Cr, and Ni but depletion in Nb, Ta, Hf, and Zr. Collectively, these trends show relative depletion in high-field strength elements (HFSE: Zr, Nb, Ta, Hf, Th, Y) and ferromagnesian trace elements (Cr, Ni, Co) compared to UCC, consistent with derivation from predominantly felsic crustal sources.

The low abundance of Cr, Co, and Ni, typically concentrated in olivine, pyroxene, and amphibole, suggests limited input from mafic or ultramafic terranes, which are characteristic of the Birimian

volcanic belts but less of the granitoid complexes (Leube et al., 1990; Taylor et al., 1992). Instead, the geochemistry points to erosion of felsic plutonic and high-grade metamorphic rocks, likely sourced from the Birimian granitoids to the north and northwest of the basin and the gneissic complexes of the Pan-African Dahomeyide Belt to the east (Affaton et al., 1991; Kalsbeek et al., 2008).

The depletion in HFSEs (Zr, Nb, Ta, Hf, Y, Th) is particularly diagnostic. These elements, generally immobile during weathering and diagenesis, tend to concentrate in zircon, monazite, and other heavy minerals (McLennan, 1989). Their low concentrations in the Tamale–Obosum Group suggest either (1) source terranes poor in zircon and HFSE-bearing phases, or (2) hydraulic sorting that preferentially winnowed heavy minerals during fluvial transport (Mange & Wright, 2007). This supports derivation from weathered granitoid and gneissic rocks, where zircon and monazite may be retained in residual soils or selectively removed during transport.

The Th/U ratios (average 4.04) fall between UCC (3.8) and PAAS (4.7), consistent with a dominantly felsic source with limited mafic contribution (Rudnick & Gao, 2014). This ratio further rules out significant juvenile volcanic input from contemporaneous Pan-African magmatism, reinforcing the dominance of older Birimian granitoid and metamorphic contributions.

The systematic enrichment in Sr and Ba across all formations requires special attention. Elevated Sr and Ba can be inherited from detritus derived from carbonates or clay-rich sediments (Veizer, 1986; Weaver, 1989), or from igneous rocks associated with subduction-related magmatism that are often enriched in these elements (Davidson et al., 2007). In this context, the Sang Conglomerate and Densubon Sandstone formations, which show the highest Sr and Ba, likely record contributions from Pan-African suture-zone lithologies, including metasedimentary and metavolcanic units enriched in these elements. Their higher Ca, Mg, Fe, Na, and K contents

relative to the Tamale and Undivided Obosum sandstones further suggest a more proximal derivation from active orogenic terranes. By contrast, the Tamale and Undivided Obosum sandstones, with lower Sr and Ba, may reflect input from Birimian granitoid and cratonic sources, overprinted by post-depositional fluid-rock interaction (Milliken, 2000).

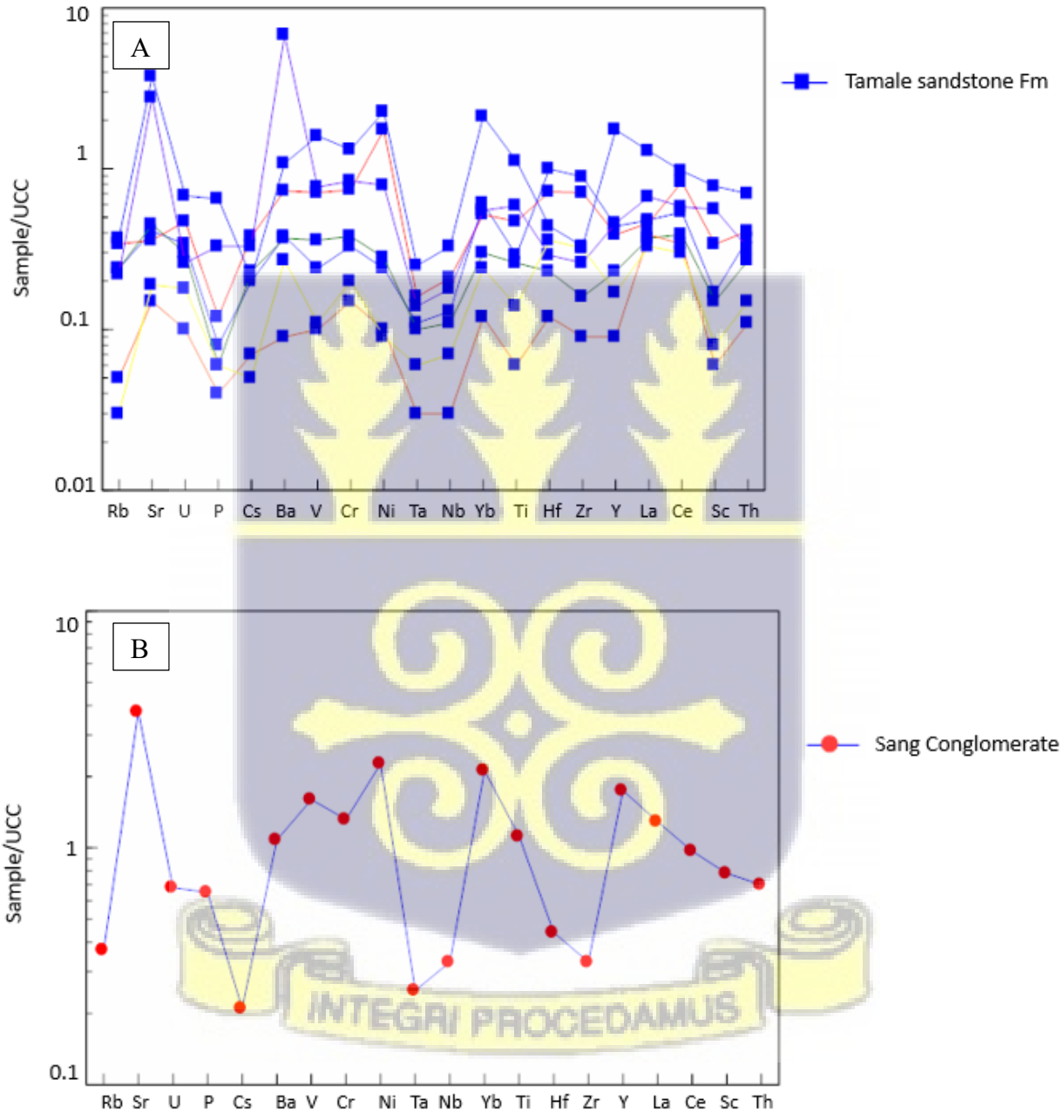

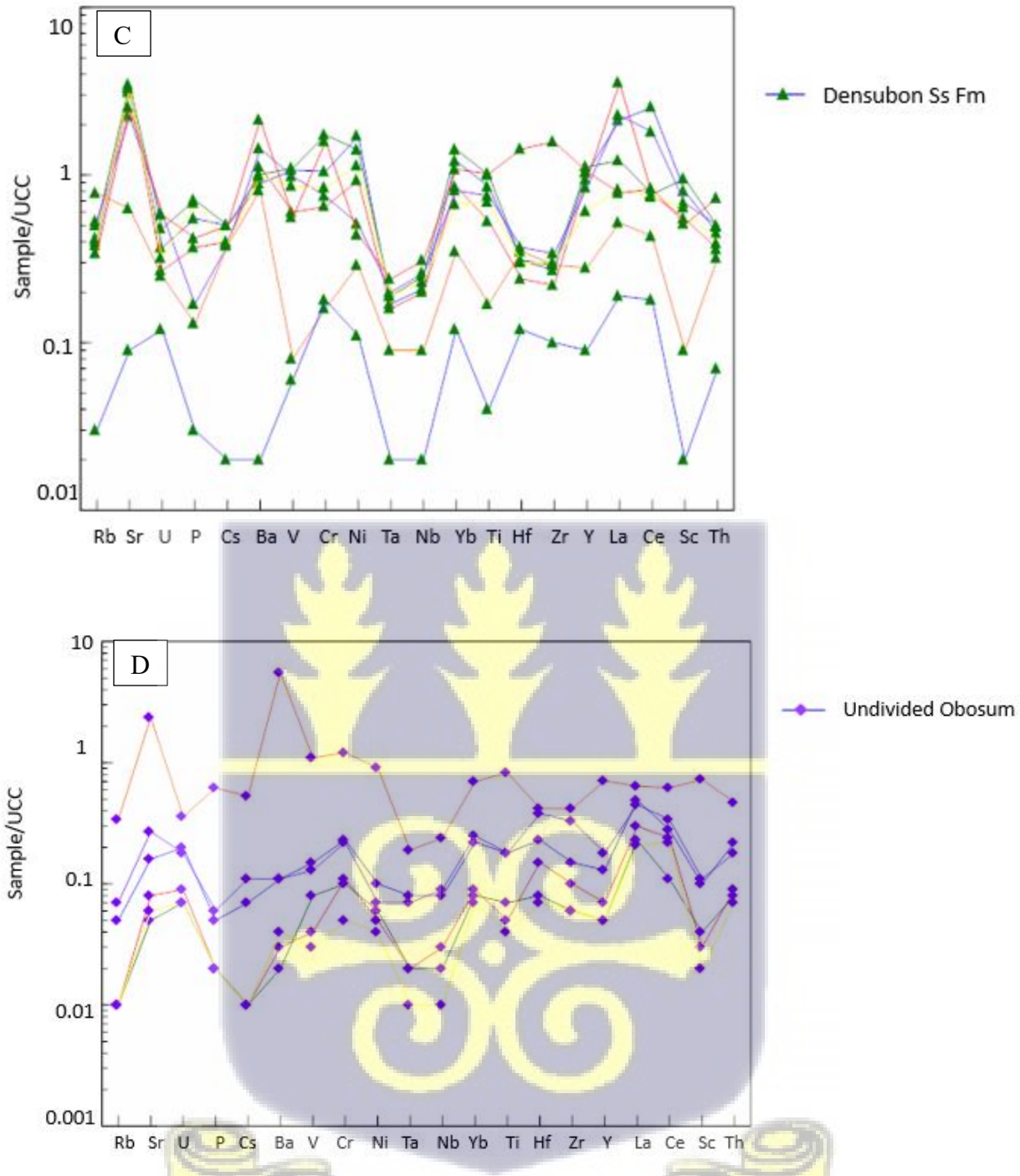

Figure 5.8 Multi-element discrimination diagram for A) Tamale sandstone B) Sang Conglomerate C) Densubon Sandstone and D) Undivided Obosum formations (after Floyd et al., 1991) normalized to the upper continental crust values of Taylor and McLennan (1985).

Trace element geochemistry has long been applied in provenance studies of fine-grained sediments, as certain immobile elements retain robust signatures of their source lithologies despite weathering and diagenesis (Cullers et al., 1988; Condie & Wronkiewicz, 1990; McLennan & Taylor, 1991; Totten et al., 2000). The contrasting behavior of elements such as Th, La, Sc, Cr, Ni, Co, and Zn provide a reliable means of distinguishing between felsic and mafic source contributions. Thorium (Th) and lanthanum (La), for instance, are enriched in felsic igneous rocks, whereas scandium (Sc) and chromium (Cr) are preferentially concentrated in mafic and ultramafic rocks.

Provenance discrimination diagrams based on these ratios, such as Th/Sc versus Sc and Cr/Th versus Sc/Th (Langmuir et al., 1978; Floyd et al., 1989), quantify the extent of mixing between felsic and mafic sources. More recent approaches (Tang et al., 2016) utilize Ni/Co and Cr/Zn ratios, capitalizing on the partitioning of Ni and Cr into early-crystallizing mafic minerals (e.g., olivine, pyroxene) versus the relative mobility of Co and Zn during weathering. Since these ratios remain largely unaffected by diagenesis, they provide an effective measure of the mafic contribution in clastic sediments.

Applying this framework to the Tamale–Obosum Group, clear compositional distinctions emerge (Figure 5.9). The Tamale Sandstone Formation and Undivided Obosum Formation exhibit elevated Th/Sc ratios, indicating a predominantly felsic provenance. Such values are consistent with derivation from granitoid and high-grade metamorphic sources, likely the Birimian granitoids of the West African Craton and the adjacent Pan-African gneissic complexes (Leube et al., 1990; Kalsbeek et al., 2008). By contrast, the Densubon Sandstone and Sang Conglomerate formations show lower Th/Sc ratios and higher Cr/Th values, reflecting a stronger mafic contribution. These

signatures are consistent with input from mafic to ultramafic units within the Birimian volcanic belts, and possibly from Pan-African mafic intrusives along the Dahomeyide suture.

A positive Zr–Cr correlation in sandstones from the Oti–Pendjari and Tamale–Obosum Groups is best explained by the coupled delivery and/or hydraulic concentration of two provenance-diagnostic heavy minerals—zircon (host for Zr) and chromian spinel or chromite (primary host for Cr). Zircon abundance tracks input from felsic, granitoid to high-grade metamorphic sources and is strongly resistant to weathering and diagenesis (Taylor & McLennan, 1985; McLennan, 1989), whereas Cr is elevated where detritus includes mafic–ultramafic lithologies or arc/ophiolitic fragments that supply Cr-spinel (Garver & Brandon, 1994; Arai, 1992). Their co-variation therefore indicates (i) sediment mixing between cratonic granitoid–gneiss terranes (zircon-rich) and mafic/ultramafic or arc-derived sources (Cr-spinel-rich), and/or (ii) hydraulic sorting that co-enriches dense, mechanically robust heavy minerals into the same grain-size fractions and bedforms (e.g., bars, shoreface lags), producing placer-like concentration trends independent of bulk matrix composition (Morton & Hallsworth, 1999; Garzanti & Andò, 2007). Because both zircon and Cr-spinel are among the most diagenetically stable detrital phases, such correlations are commonly preserved through burial (Morton, 1991; Weltje & von Eynatten, 2004).

Regionally, this pattern is consistent with mixing of detritus from the zircon-fertile Birimian granitoid–greenstone crust of the West African Craton to the west (Leube et al., 1990; Kalsbeek et al., 2008) and Cr-spinel–bearing Pan-African Dahomeyide arc–ophiolitic rocks along the eastern basin margin (Caby, 1989; Affaton et al., 1991). The stronger Zr–Cr coupling expected in upper Oti-Pendjari units (Bunya, Bimbila) aligns with independent arc/active-margin signals in trace-element diagrams and ~600 Ma zircon inputs (Kalsbeek et al., 2008), whereas more distal Tamale–Obosum units show cratonic signatures with intermittent mafic pulses. Globally, analogous Zr–Cr

(zircon–spinel) co-enrichment has been documented where foreland or rift basins integrate cratonic and arc/ophiolitic sources and where high-energy transport focuses dense minerals (e.g., Alpine–Apennine systems: Garzanti et al., 2002; Cordilleran forearc/foreland: Garver & Brandon, 1994; Indo-Gangetic sands: Garzanti & Andò, 2007). In sum, the positive Zr–Cr trend in the Voltaian sandstones records (1) dual felsic–mafic provenance, (2) heavy-mineral hydraulic concentration, and (3) limited post-depositional overprint—thereby reinforcing a tectono-sedimentary model of Pan-African arc unroofing delivering Cr-spinel–rich detritus into a basin otherwise dominated by zircon-rich cratonic flux.

This dual geochemical signal suggests that the Tamale Sandstone and Undivided Obosum formations represent relatively mature sediments, dominated by felsic detritus derived from the craton interior, whereas the Densubon and Sang formations capture a more mixed provenance, with significant mafic input likely linked to proximal orogenic belts. Such variability aligns with the stratigraphic and sedimentological evidence for shifting depositional environments during basin evolution—from more stable cratonic sources to orogen-proximal contributions during the Pan-African collision.

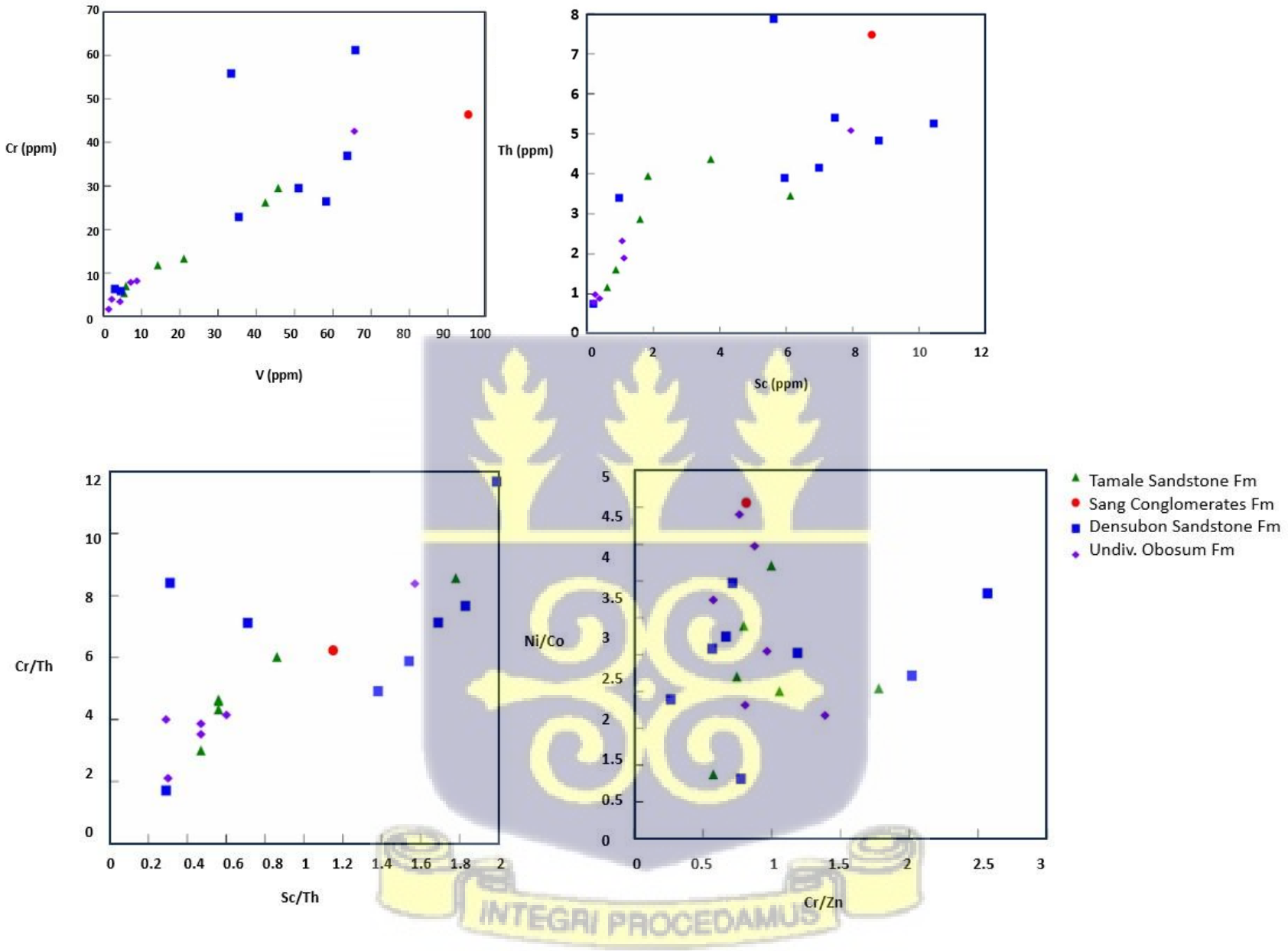

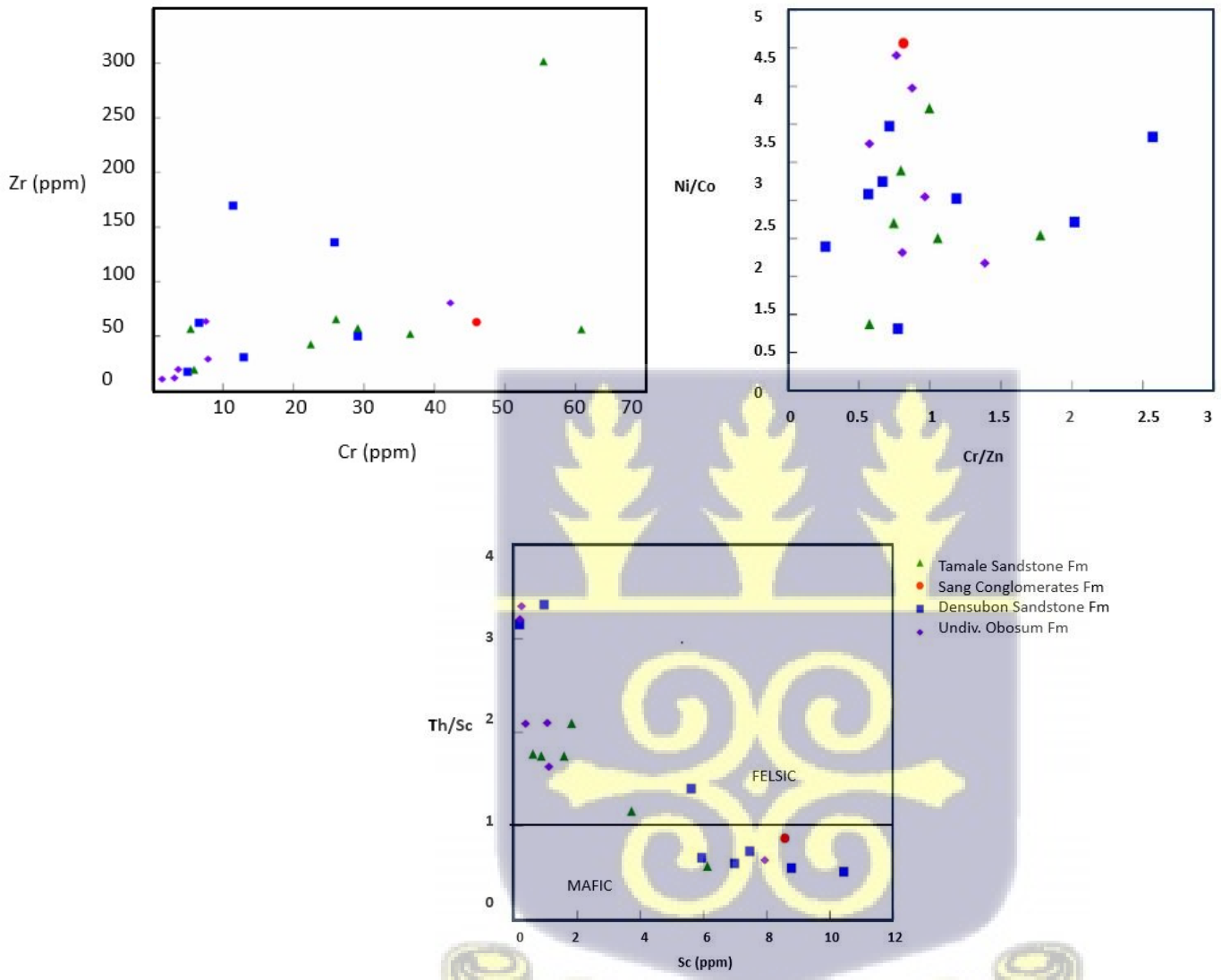

Figure 5.9 Immobile trace element discrimination diagrams for Tamale-Obosum Group formations.

The trace element geochemistry of the Tamale–Obosum Group indicates a predominantly felsic provenance with subordinate mafic input restricted to certain formations. Discrimination diagrams such as Cr/V versus Y/Ni, La–Th–Sc, and Th–Hf–Co (Figure. 5.10) consistently point to derivation from granitic to high-grade metamorphic source rocks, reflecting sediment input from the Birimian granitoid complexes of the West African Craton (Leube et al., 1990; Taylor & McLennan, 1985). However, the Densubon Sandstone and Sang Conglomerate formations display subtle but significant trace element anomalies, including shifts in Hf versus La/Th plots after the criteria of Floyd & Leveridge (1987) (Figure 5.11). These signatures suggest contributions from mafic to intermediate terranes, possibly linked to the Birimian volcanic belts or reworked material from Pan-African Dahomeyide units along the cratonic margin (Kalsbeek et al., 2008; Affaton et al., 1991).

This dual geochemical signal reflects the tectonosedimentary evolution of the Voltaian Basin during the late Neoproterozoic to early Paleozoic. While the majority of sediments record stable cratonic input from the Archean–Paleoproterozoic West African Craton, the localized mafic influence in the Densubon and Sang units likely records pulses of sediment supply during syn- to post-orogenic activity associated with the Pan-African collision and subsequent basin reorganization (Caby, 1989; Trompette, 1994). Thus, the geochemical evidence underscores a provenance shift from stable intracratonic felsic sources toward mixed felsic–mafic inputs as basin subsidence migrated toward the active Dahomeyide–Voltaian foreland system.

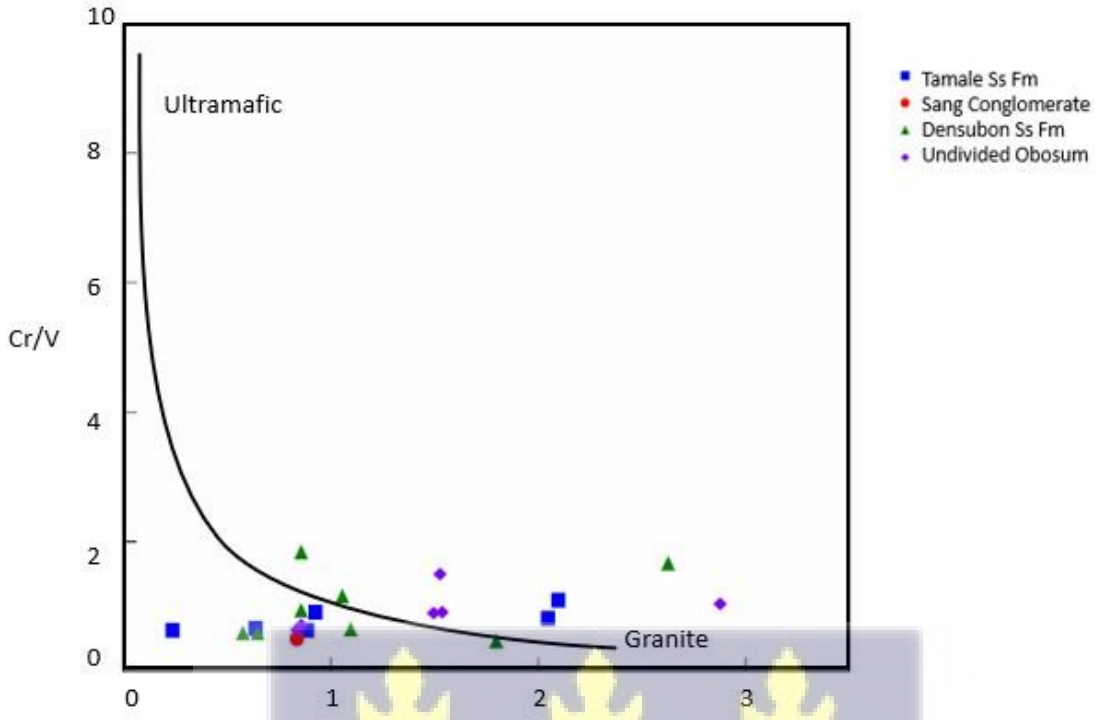

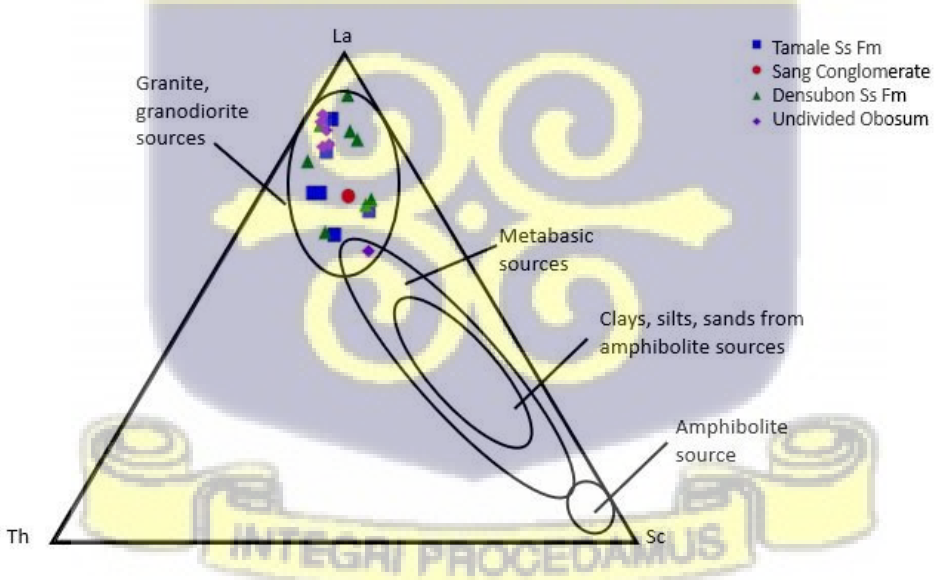

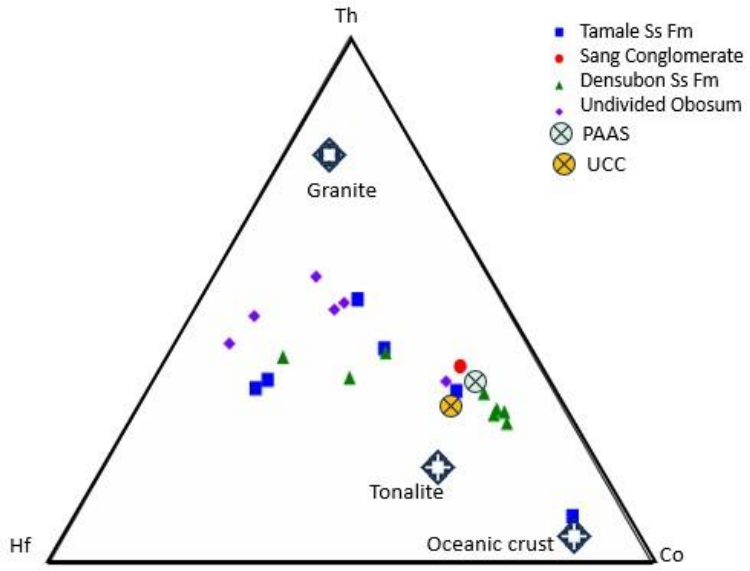

Figure 5.10. Plots of Cr/V vs Y/Ni, La-Th-Sc, Th-Hf-Co for provenance indications of the Tamale Group formations.

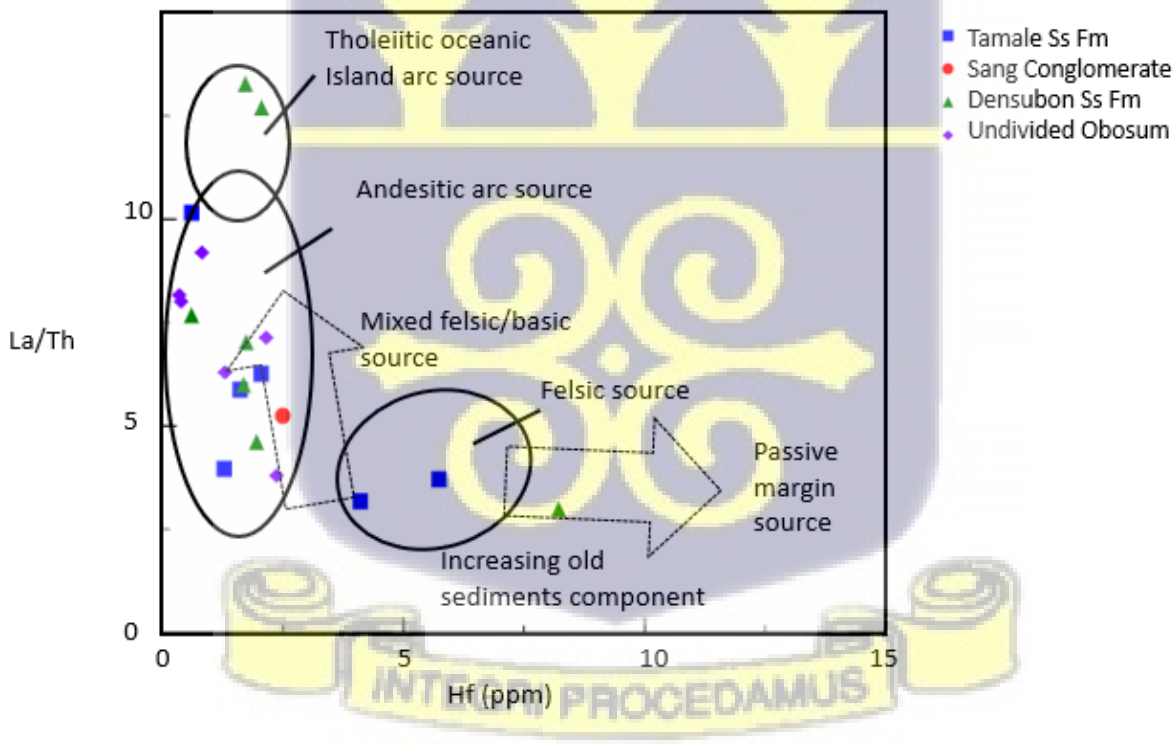

Figure 5.11. Discrimination diagram Hf vs. La/Th diagram after Floyd and Leveridge (1987).

The Rare Earth Element (REE) distribution patterns of the Tamale–Obosum Group provide important insights into their provenance and tectonic evolution. As established in earlier works (Taylor & McLennan, 1985; Wronkiewicz & Condie, 1987, 1989; Cullers & Graf, 1983; Bauluz et al., 2000), REE patterns can distinguish between felsic and mafic sources: mafic rocks typically display low Light to Heavy REE (LREE/HREE) ratios with little or no Eu anomaly, whereas felsic rocks are characterized by higher LREE/HREE ratios and commonly exhibit negative Eu anomalies due to feldspar fractionation. These geochemical signatures, once established in the source, are generally preserved in derivative sedimentary successions.

In the Tamale-Obosum Group, normalization to Upper Continental Crust (UCC) highlights LREE enrichment and HREE depletion, consistent with derivation from felsic continental crust. (Figure. 5.12). This anomaly can be interpreted in several ways. First, it reflects the dominant felsic provenance of the Voltaian Basin sediments, most plausibly sourced from the Birimian granitoid–gneiss terranes of the West African Craton (Leube et al., 1990; Taylor & McLennan, 1985). In felsic systems, accessory minerals such as allanite, monazite, and zircon tend to sequester HREEs. Their relative resistance to mechanical breakdown and chemical weathering means that much of the HREE budget may be retained in the source area, leaving the derived sandstones depleted. Second, localized contributions from mafic–intermediate sources (e.g., volcanic belts within the Birimian or reworked Pan-African Dahomeyide rocks to the east) could also explain the subdued HREE content in the Densubon and Sang units (Floyd & Leveridge, 1987; Kalsbeek et al., 2008). Mafic rocks are inherently HREE-poor and their input would further lower HREE abundances.

Weathering and diagenesis may also have played a role. In tropical weathering regimes, typical of West Africa since the late Neoproterozoic (Trompette, 1994), preferential dissolution of REE-bearing accessory phases during chemical breakdown could mobilize HREEs. During diagenesis,

fluid–rock interaction in porous sandstones may have selectively leached HREE-enriched minerals (Milliken, 2000), contributing to the observed depletion.

Taken together, the REE patterns of the Tamale–Obosum Group record a provenance dominated by felsic granitoid–gneissic crust of the West African Craton, punctuated by episodic inputs of mafic–intermediate detritus, likely linked to reworking of Pan-African Dahomeyide terranes along the eastern basin margin (Caby, 1989; Affaton et al., 1991). The stronger HREE depletion in the Densubon and Sang formations reflects their position within more proximal depositional settings, where coarse-grained inputs from active orogenic fronts were mixed with typical cratonic detritus. In contrast, the Tamale Sandstone and Undivided Obosum formations preserve the signature of more distal, craton-derived sediment fluxes.

Thus, the REE geochemistry corroborates a dual provenance model for the Tamale Group: a stable felsic cratonic hinterland to the west, and a more tectonically active Pan-African orogenic zone to the east, with sediment dispersal reflecting the transition from intracratonic to foreland basin conditions during late Neoproterozoic basin development.

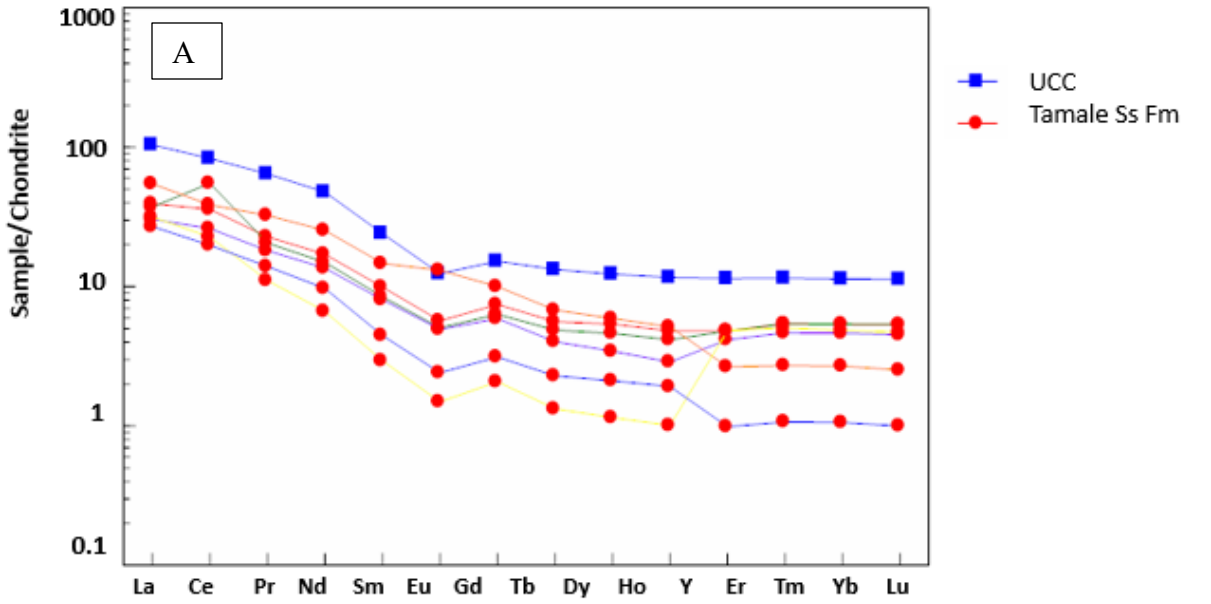

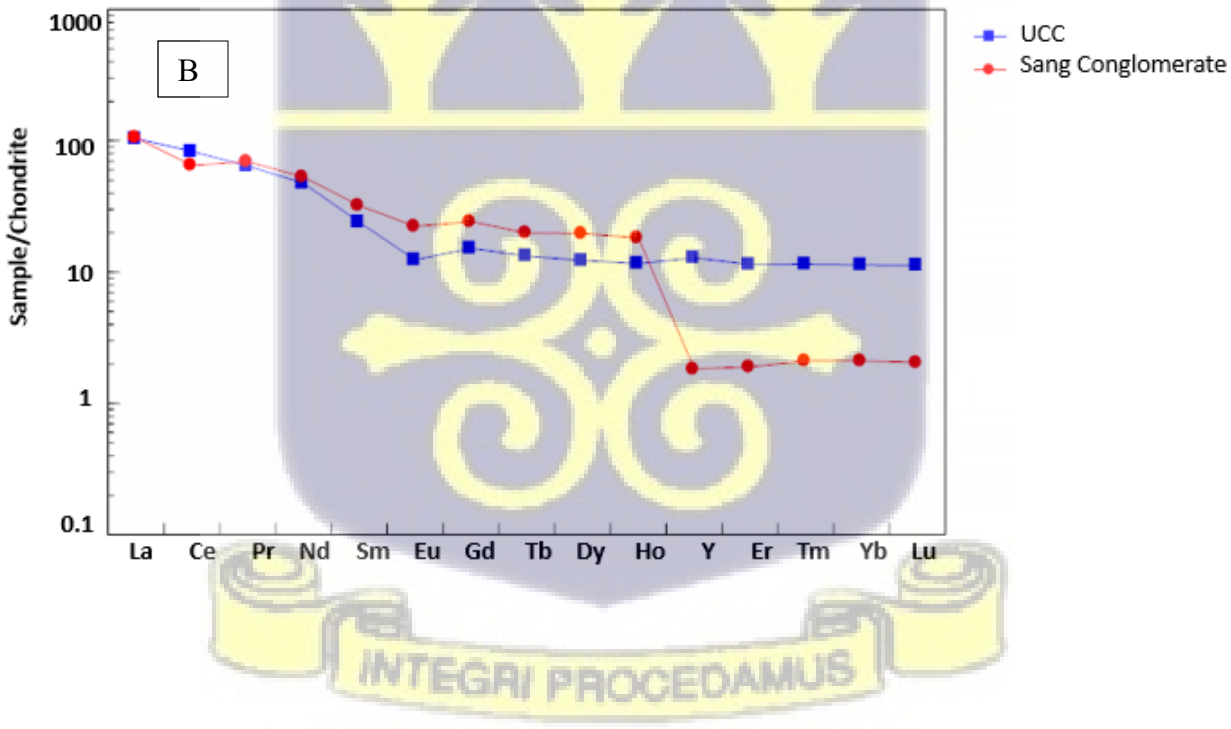

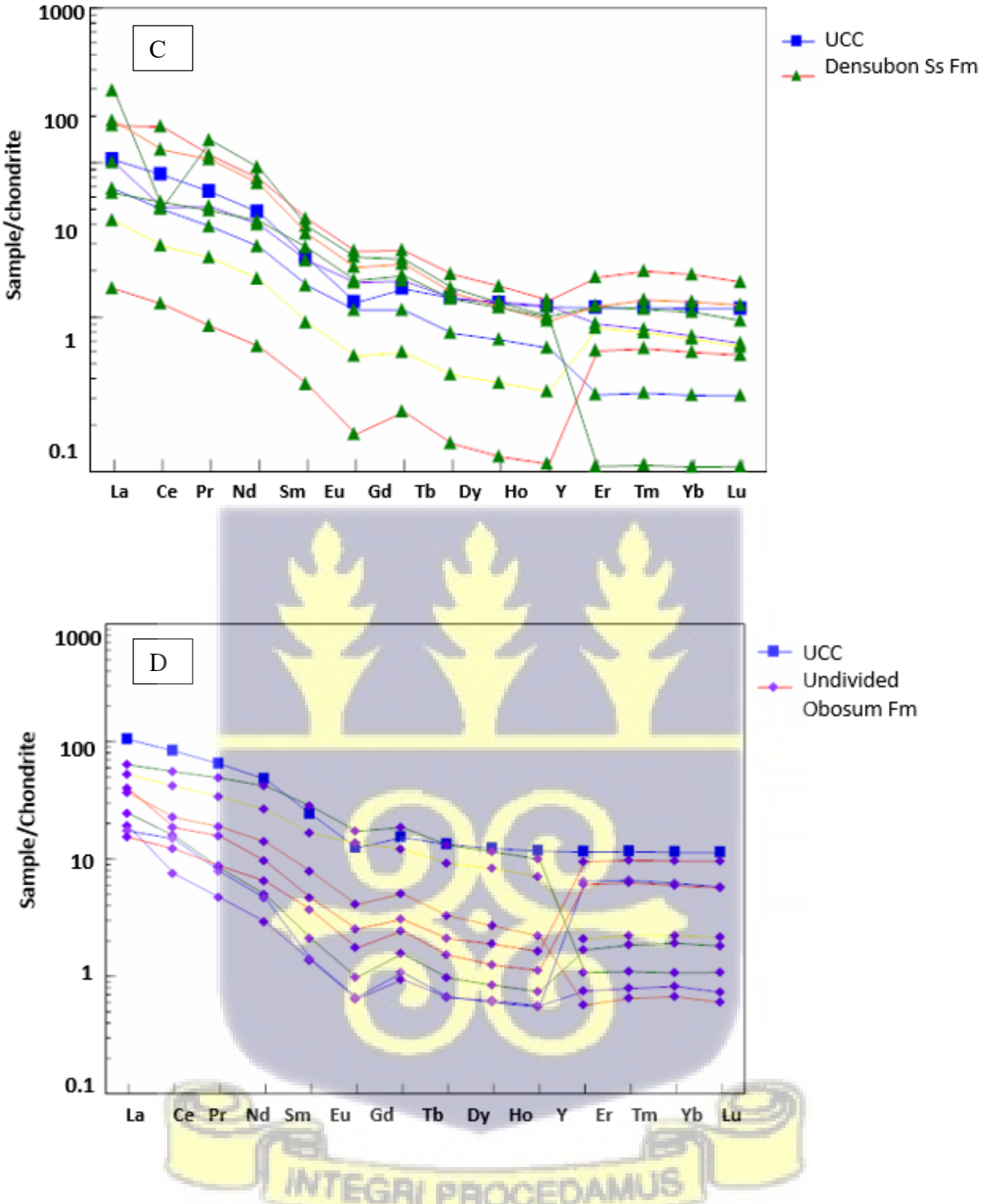

Figure 5.12. Chondrite-normalized REE patterns of the (A)Tamale Sandstone, (B)Sang Conglomerate, (C)Densubon Sandstone and (D)Undivided Obosum formations of the Tamale-Obosum Group.

5.1.7 Tectonic settings of the Tamale-Obosum Group, from petrography

To better constrain the plate tectonic setting of the source terranes of the Tamale–Obosum Group, sandstone framework compositions were evaluated using QFL (Quartz–Feldspar–Lithic) and QtFL (Total Quartz–Feldspar–Lithic) ternary discrimination diagrams (Figure 5.13) of Dickinson & Suczek (1979) and Dickinson (1985). These diagrams have proven effective in distinguishing between sandstones derived from craton interiors, recycled orogens, magmatic arcs, and transitional settings based on detrital framework modes.

The Dunkro and Densubon Sandstone formations plot dominantly within the transitional arc and mixed orogenic fields of both QFL and QtFL diagrams. Their higher lithic content and moderate feldspar abundance suggest derivation from active arc-related sources with contributions from recycled sediments. This petrographic signature is consistent with input from the Pan-African Dahomeyide Belt, which comprises arc-related complexes, high-grade metamorphic rocks, and reworked sedimentary successions (Caby, 1989; Affaton et al., 1991). The relatively immature framework composition of these units implies proximity to uplifted arc terranes and limited transport distance, typical of syn-orogenic foreland basin settings.

In contrast, the Undivided Obosum Formation sandstones plot firmly within the craton interior field, characterized by quartz-rich, mineralogically mature sandstones with negligible lithic input. This points to derivation from the stable granitoid–gneiss terranes of the West African Craton (Leube et al., 1990; Taylor & McLennan, 1985). The dominance of monocrystalline quartz and the scarcity of feldspars and lithic fragments indicate prolonged chemical weathering and recycling, hallmarks of a stable intracratonic environment.

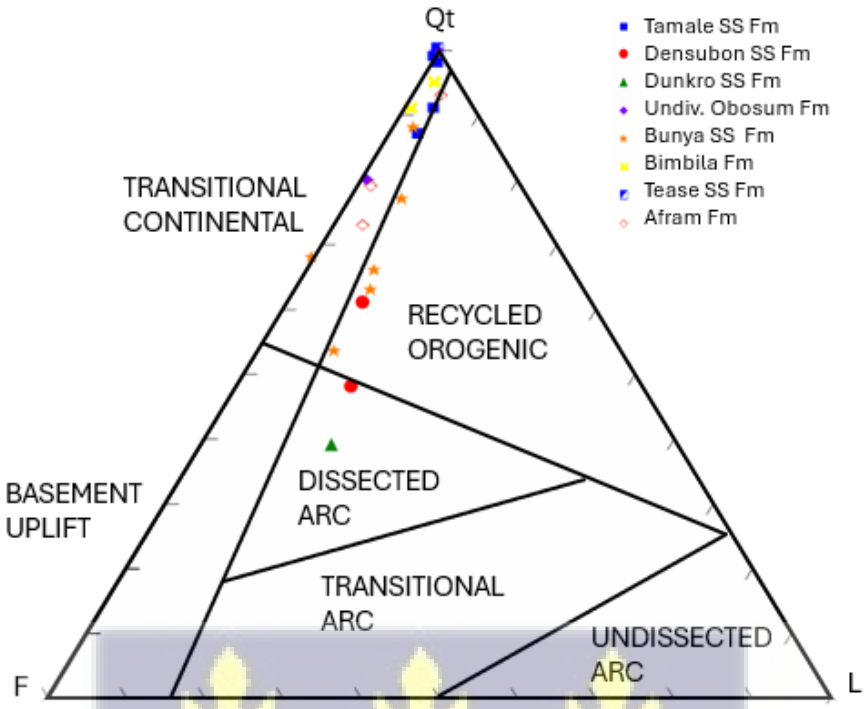

Figure 5.13 QtFL (Total Quartz–Feldspar–Lithic) ternary discrimination diagram for the Tamale-Obosum and Oti-Pendjari groups.

The Tamale Sandstone Formation, however, falls within the recycled orogen field on the QtFL diagram. Its high quartz content, coupled with evidence of sedimentary recycling, suggests derivation from uplifted sedimentary and metasedimentary rocks within the Pan-African Dahomeyide Belt. Such recycled quartz-rich detritus reflects the unroofing of fold–thrust belts and the reworking of pre-existing Birimian and Proterozoic sedimentary successions during Pan-African convergence (Hallsworth & Morton, 1999; Dickinson, 1985).

Together, these tectonic settings highlight a provenance duality within the Tamale–Obosum Group. The Dunkro and Densubon formations record arc- and mixed-orogen inputs from the Dahomeyide suture to the east. The Undivided Obosum Formation reflects craton-derived detritus sourced from the granitoid–gneiss complexes of the West African Craton. The Tamale Sandstone

Formation represents recycled orogenic detritus, marking the reworking of older sedimentary successions during Pan-African basin inversion. This provenance pattern aligns with the late Neoproterozoic evolution of the Voltaian Basin, where initial intracratonic sedimentation progressively gave way to foreland-style deposition under the influence of the Pan-African Dahomeyide orogeny (Trompette, 1994; Affaton et al., 1991).

5.1.8 Tectonic Settings of the Tamale-Obosum Group from Major Oxide Compositions

The application of major element geochemistry to discriminate tectonic settings of sedimentary basins has largely relied on bivariate plots proposed by Bhatia (1983) and Roser and Korsch (1986). These diagrams, centred on elemental ratios such as SiO_2/Al_2O_3, K_2O/Na_2O, and CaO/Al_2O_3, have been widely employed to differentiate between oceanic island arcs, continental island arcs, active continental margins, and passive continental margins. However, the efficacy of these diagrams in accurately classifying sedimentary basins has been subject to considerable debate.

A primary criticism of the Bhatia and Roser-Korsch diagrams is their inability to distinguish between tectonically similar environments. For instance, the differentiation between continental island arcs and active continental margins remains ambiguous within these frameworks (Armstrong-Altrin and Verma, 2005). Furthermore, the exclusion of collisional and rift settings from these classifications limits their applicability to a broad spectrum of tectonic environments.

A more fundamental issue lies in the statistical underpinnings of these diagrams. Compositional data, such as major element concentrations in rocks, do not adhere to Euclidean geometry, necessitating specialized statistical treatments (Aitchison, 1986, 1999; Egozcue et al., 2003;

Aitchison and Egozcue, 2005; Thomas and Aitchison, 2005). The failure to account for these compositional characteristics undermines the reliability of traditional discrimination diagrams.

Recognizing these limitations, recent studies have sought to develop more robust and statistically sound approaches to tectonic discrimination. Verma et al. (2012) introduced a multivariate discriminant function analysis based on natural logarithms of major element ratios, with SiO_2 as the common denominator. By focusing on siliciclastic sediments and subdividing the dataset into high- and low-silica groups, the influence of provenance-related factors was minimized, allowing for a more direct assessment of tectonic control on geochemical composition. This approach offers a statistically rigorous and effective means of discriminating between arc, rift, and collisional tectonic settings. The development of these new discrimination diagrams represents a significant advancement in the field of provenance and tectonic studies, offering a more reliable and informative approach to characterizing sedimentary basins.

The tectonic setting of the Tamale–Obosum Group siliciclastics was evaluated using the discriminant function (DF) diagrams of Verma and Armstrong-Altrin (2013), which distinguish depositional environments based on immobile trace-element geochemistry. The majority of samples from the Tamale Sandstone and Undivided Obosum Formation cluster within the continental rift field, whereas the Densubon Sandstone and Sang Conglomerate plot in a transitional position between continental rift and active continental margin/volcanic arc fields (Figure 5.14). This geochemical distribution indicates that while most of the sedimentary supply was derived from an extensional intracontinental regime, there was also a notable arc-related input, particularly within the Densubon and Sang successions.

A continental rift environment implies deposition linked to lithospheric extension and subsidence, consistent with passive margin evolution or intracratonic rift development (Verma & Armstrong-

Altrin, 2013). Regionally, this interpretation resonates with the tectonostratigraphic reconstructions of Carney et al. (2010), who documented significant erosional sculpting during the Tonian–Cryogenian. This event truncated the older Kwahu and Bombouaka Groups, leaving behind prominent massifs separated by wide palaeovalleys. These depressions became filled by the Oti–Pendjari Group, which reflects a distinct shift in sedimentation patterns and subsidence style within the Voltaian Supergroup.

By the late Neoproterozoic–early Cambrian, the tectonic regime shifted once again under the influence of the Pan-African Dahomeyide orogeny. During the waning stages of orogenesis, the foreland basin system of the Voltaian Supergroup was flexurally deformed, driving westward migration of sedimentation. Within this framework, the Tamale–Obosum Group represents the terminal molasse stage of basin infill. The Dunkro and Densubon Sandstone formations in the Obosum Syncline comprise coarse, bouldery, proximal alluvial fan and fluvial deposits, recording sedimentation in fault-bounded depocentres adjacent to uplifted orogenic blocks. To the north, the Tamale Sandstone Formation records distal red-bed fluvial systems, characterized by mineralogically mature sandstones with significant input from the Palaeoproterozoic Birimian granitoid–gneiss terranes of the West African Craton.

The geochemical evidence for dual provenance, continental rift signatures in the Tamale and Obosum formations, and mixed rift–arc signatures in the Densubon and Sang units, underscores the transitional geodynamic setting of the Volta Basin at this time. The eastern margin of the basin, adjacent to the Pan-African Dahomeyide Belt, supplied recycled arc-related and syn-orogenic detritus, while the western hinterland (the West African Craton) delivered craton-derived quartzose sediments. This tectono-sedimentary duality is consistent with a basin that evolved from intracratonic extension and passive-margin sedimentation (Oti–Pendjari deposition) to foreland-

style molasse accumulation during the final stages of Pan-African convergence (Tamale–Obosum deposition) (Caby, 1989; Affaton et al., 1991; Trompette, 1994).

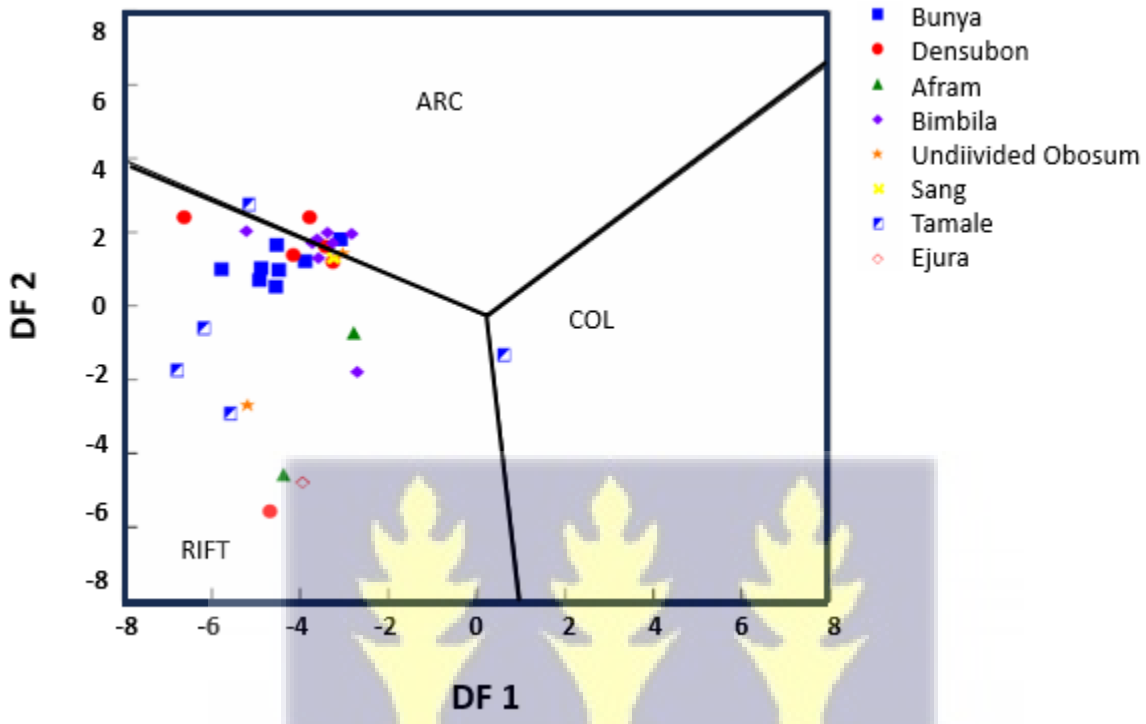

Figure 5.14 Discriminant-function multi-dimensional diagram for high-silica clastic sediments of the Tamale-Obosum Group, after Verma and Armstrong-Altrin (2013).

5.1.9 Tectonic settings of the Tamale-Obosum Group from Trace and Rare Earth Element composition

Geochemical proxies, particularly trace element ratios plotted on ternary and binary discrimination diagrams (Figure 5.15), provide important insights into the tectonic setting and provenance of the Tamale–Obosum Group formations. The Tamale Sandstone and Undivided Obosum formations display geochemical signatures consistent with a passive continental margin setting. Elevated Th/Sc ratios in these formations indicate a dominance of felsic source rocks, as Th is preferentially enriched in felsic continental crust relative to Sc, which is more abundant in mafic lithologies (McLennan et al., 1990). This felsic provenance is further supported by relatively low La/Yb ratios

and flat REE patterns, suggesting limited fractionation between light and heavy REEs during weathering and sediment transport—features typical of detritus eroded from stable cratonic interiors and deposited along passive continental margins (Taylor & McLennan, 1985)

In contrast, the Densubon Sandstone and Sang Conglomerate formations record more complex tectonic signatures. Their trace element ratios, particularly the relative enrichment of large ion lithophile elements (LILE; e.g., Ba, Sr) over high field strength elements (HFSE; e.g., Nb, Ta), are characteristic of sedimentation in active continental margin or continental island arc settings. This pattern is often associated with subduction-related processes, where slab-derived fluids enrich sediments in LILEs relative to immobile HFSEs (Pearce et al., 1984). Similar geochemical signals have been documented in Pan-African suture-related terranes of West Africa (Affaton, 1990; Kalsbeek et al., 2010), suggesting that the Densubon and Sang units may reflect input from proximal Pan-African Dahomeyide sources, where arc–continent collision and subsequent uplift supplied volcanogenic and arc-derived detritus into the developing Voltaian foreland basin.

Regionally, these geochemical patterns align with the tectonostratigraphic evolution of the Volta Basin. Following the Tonian–Cryogenian erosional sculpting and valley incision (Carney et al., 2010), the Oti–Pendjari Group reflects syn-rift sedimentation in an intracratonic extensional setting. In the late Neoproterozoic, however, the onset of the Pan-African Dahomeyide orogeny led to the closure of the Trans-Saharan Ocean (Caby, 1989; Affaton et al., 1991) and the development of a flexural foreland basin along the craton margin. Within this context, the Tamale and Undivided Obosum formations capture the distal flux of sediment derived from the West African Craton interior, whereas the Densubon and Sang formations represent more proximal molasse deposits with an additional signature of arc-related material shed from the adjacent Dahomeyide orogenic front.

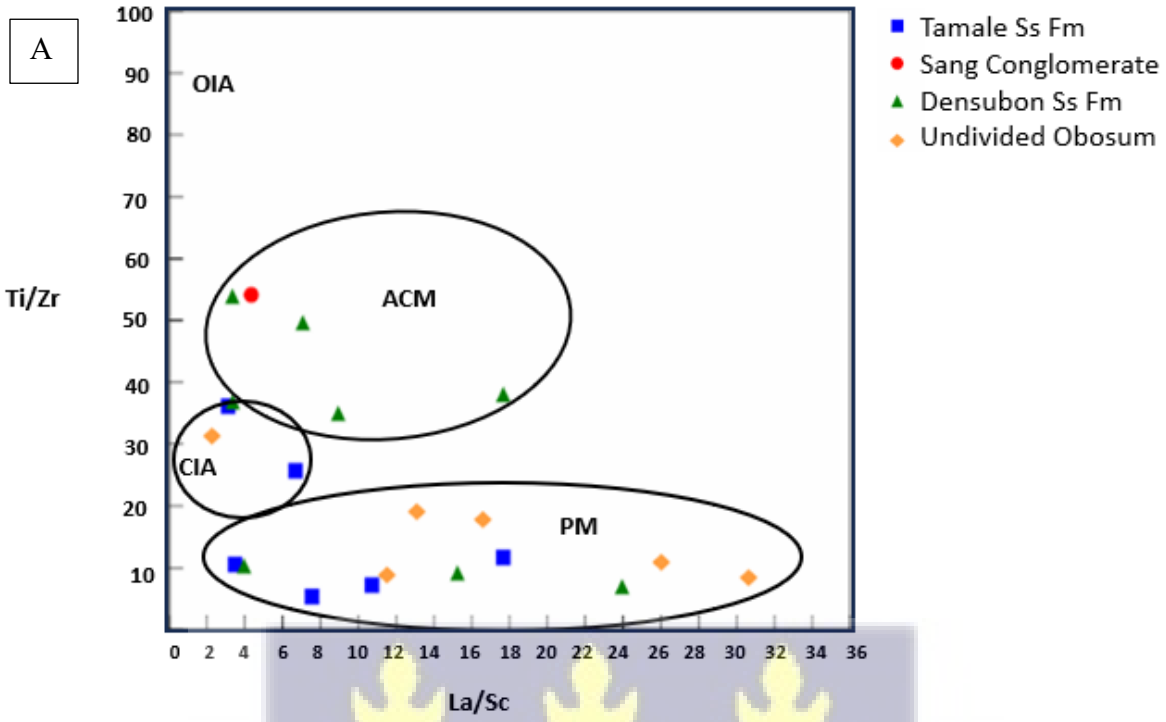

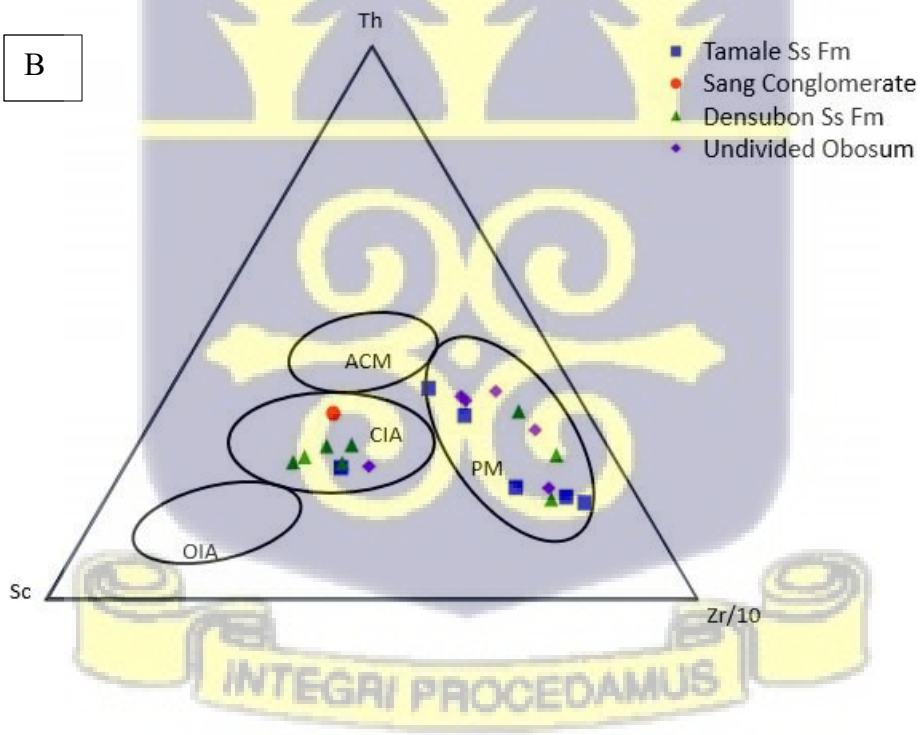

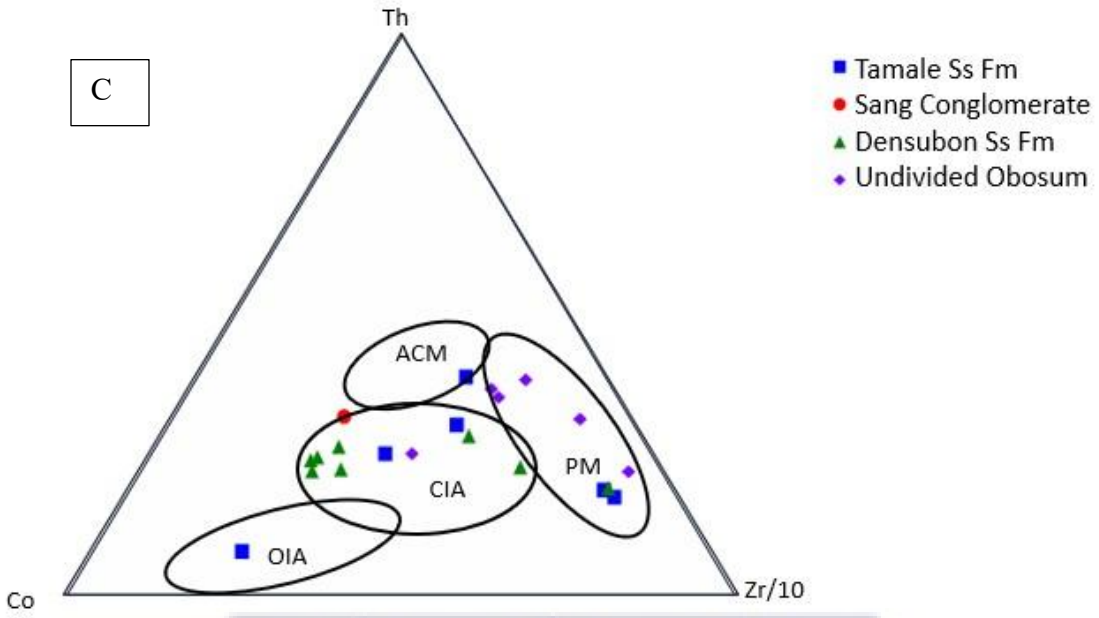

Figure 5.15. Binary and ternary plots (A) Ti/Zr vs La/Sc, (B) Th-Sc-Zr/10 and (C) Th-Co-Zr/10 for tectonic environments of the Tamale-Obosum Group formations.

5.2 Provenance of the Oti-Pendjari Group

5.2.1 Petrographic Rock Classification of Oti-Pendjari Group rocks

Petrographic classification indicates that the Oti-Pendjari Group sandstones span a spectrum from quartz arenites to arkosic and lithic arkosic sandstones, reflecting variability in source terranes and depositional maturity (Figure 5.1). The Afram and Tease formations, dominated by quartz arenites, record extensive chemical weathering, multi-cycle sedimentary recycling, and derivation from stable cratonic interiors of the West African Craton. In contrast, the Bimbila Formation, dominated by arkoses and lithic arkoses, points to relatively short transport distances from granitoid and gneissic sources, with a strong imprint of basement-derived detritus from the Birimian terranes and possibly Pan-African granitoids. The Bunya Formation, with its mixed petrographic character

(lithic arkose, subarkose, and arkose), suggests input from both stable cratonic sources and active orogenic belts, consistent with its position within a more dynamic foreland setting.

When projected onto Dickinson's (1985) QFL ternary diagrams, the Afram and Tease formations plot within the craton interior and recycled orogen fields, characteristic of mature passive margin assemblages with high quartz content. Conversely, the Bimbila and Bunya formations plot closer to the transitional continental arc and recycled orogen fields, indicating sediment derivation from uplifted orogenic belts and granitoid batholiths exposed during the Pan-African orogeny (ca. 600 Ma).

Regionally, these petrographic and tectonic signatures reflect the dual influence on the Voltaian basin during the Neoproterozoic. The quartz-rich Afram and Tease sandstones represent intracratonic stability and recycling of older sedimentary successions, whereas the arkosic Bimbila and Bunya formations capture the influx of first-cycle detritus from the Dahomeyide Belt, formed during the collision between the West African and Congo cratons (Affaton et al., 1991; Caby, 1989; Kalsbeek et al., 2010). This transition documents the basin's evolution from a passive-margin intracratonic setting into a foreland basin system associated with Pan-African orogenesis.

Thus, the petrographic variability of the Oti-Pendjari Group sandstones directly mirrors the tectonosedimentary evolution of the Voltaian basin: from stable craton-derived quartz arenites (Afram, Tease) to orogen-influenced arkosic and lithic arkosic sandstones (Bimbila, Bunya), reflecting the progressive encroachment of Pan-African tectonism into the depositional system.

5.2.2 Geochemical Classification of the Oti-Pendjari Group

Classification of the Oti-Pendjari Group sandstones reveals distinct compositional variability that reflects both source terrane characteristics and post-depositional processes. The Afram Formation and the Tease Sandstone Formation plot within the quartz arenite field, consistent with their high compositional maturity and extensive sediment recycling. By contrast, sandstones of the Bimbila and Bunya formations predominantly fall within the wacke field, with subordinate samples plotting in the arkosic and sub-litharenite fields. This petrographic signature indicates a less mature assemblage, likely reflecting short transport distances and contributions from mixed granitoid, gneissic, and metasedimentary sources. The Ejura Sandstone Formation and an additional Afram sample plot in the sub-arkose field, pointing to intermediate compositional maturity and a feldspar-rich detrital suite (Figure 5.16).

Geochemical proxies further refine these interpretations. The K_2O/Al_2O_3 ratios of most Oti Group samples fall below 0.3, suggesting an abundance of clay minerals relative to feldspar in the Bimbila and Bunya formations. In contrast, higher K_2O/Al_2O_3 ratios in samples from the Ejura Sandstone and Afram Formation point to a stronger feldspathic component, consistent with derivation from nearby granitoid and gneissic terranes of the Birimian basement or Pan-African granitoids exposed in the Dahomeyide Belt.

These combined petrographic and geochemical observations align closely with thin-section petrography, strengthening the interpretation of variable sediment maturity across the Oti-Pendjari Group. The quartz arenites of the Afram and Tease formations represent recycling from stable cratonic interiors of the West African Craton, whereas the feldspathic Ejura and Afram sandstones record direct first-cycle input from granitoid-gneissic uplifts. The clay-rich Bimbila and Bunya wackes, on the other hand, reflect deposition in more proximal foreland settings, where rapid

weathering and short sediment transport preserved immature, fine-grained, matrix-rich assemblages.

Placed in a regional context, this petrographic and geochemical diversity underscores the dual provenance of the Oti Group. Cratonic sources from the stable Birimian granitoid-gneiss terranes to the west supplied mature quartz-rich sands (Afram, Tease). Orogenic sources from the Pan-African Dahomeyide Belt to the east provided immature feldspathic and matrix-rich detritus (Ejura, Bimbila, Bunya). This variability mirrors the tectonosedimentary evolution of the Voltaian basin during the Neoproterozoic, when sediment supply alternated between stable intracratonic conditions and active foreland basin deposition driven by the Pan-African orogeny (Affaton, 1990; Caby, 1989; Kalsbeek et al., 2010).

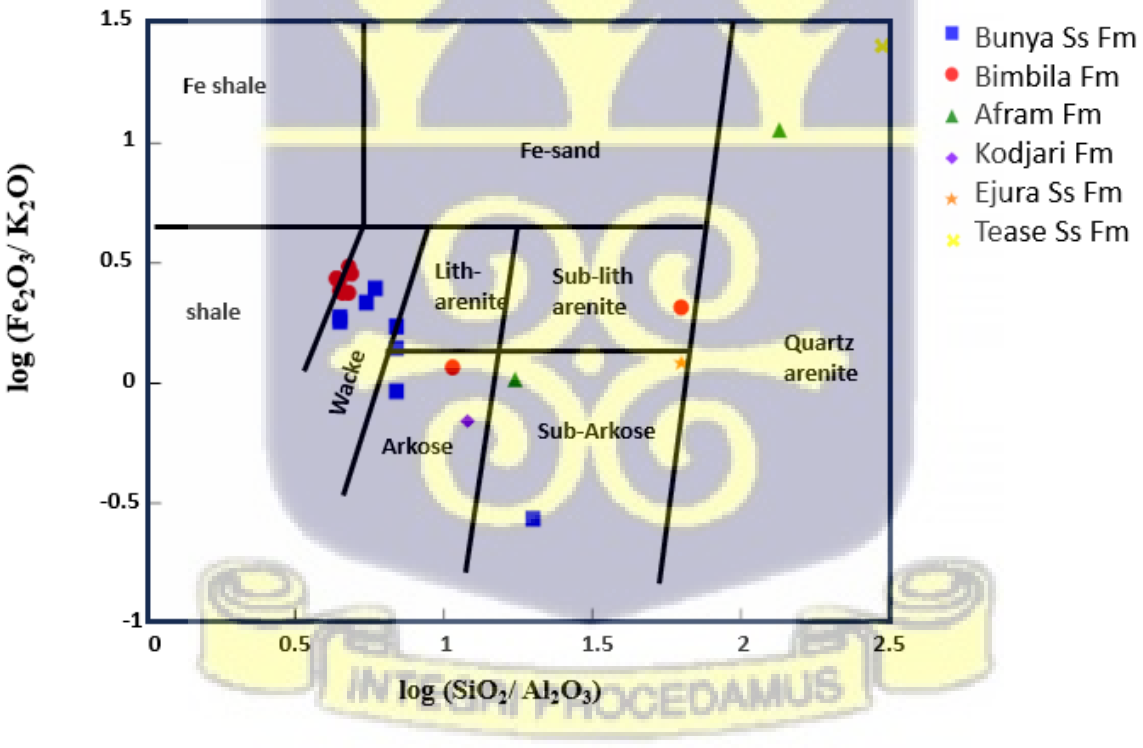

Figure 5.16 Geochemical classification of Oti-Pendjari Group samples based on log (SiO_2/Al_2O_3) - log (Fe_2O_3/K_2O) ratio (Herron, 1988).

The major element geochemistry of the Oti-Pendjari Group sandstones exhibits systematic compositional variations that provide insights into their sedimentary maturity and provenance signatures. A strong negative correlation is observed between SiO_2 and most major oxides, whereas a strong positive correlation exists between Al_2O_3 and the other oxides, except for SiO_2 (Figure 5.17). This geochemical trend is consistent with mineralogical variations, where increased quartz content is associated with the depletion of feldspars and lithic fragments.

Within the stratigraphy, the younger formations—notably the Bunya and Bimbila sandstones, show relatively lower and more variable SiO_2 contents, reflecting a higher proportion of feldspathic and lithic components, and thus reduced mineralogical maturity. By contrast, the older units—including the Tease Sandstone, Ejura Sandstone, and Afram Formation—are characterized by higher SiO_2 concentrations (up to ~90%), indicative of greater mineralogical maturity, with quartz dominating the detrital assemblage. This compositional differentiation likely reflects the mixing of distinct sediment sources. Similar relationships between increasing SiO_2 and decreasing feldspar/lithic content have been reported by Bhatia (1983) in turbidite sandstones from eastern Australia, highlighting the universal control of sediment recycling and weathering on sandstone geochemistry.

When compared with global standards such as the Post-Archean Australian Shale (PAAS, SiO_2 = 64.8%) and the Upper Continental Crust (UCC, SiO_2 = 66.0%) (Taylor and McLennan, 1985), the quartz arenites of the Oti-Pendjari Group are notably enriched in SiO_2, pointing to extensive recycling and sediment derivation from stable cratonic sources within the West African Craton. In contrast, the litharenites and wackes show significant chemical heterogeneity: Litharenites are occasionally enriched in MnO, CaO, TiO_2, and Na_2O, suggesting contributions from feldspathic and mafic lithologies. Wackes tend to be depleted in CaO, K_2O, MnO, and MgO, but enriched in

Na_2O, TiO_2, and P_2O_5, consistent with derivation from less mature, fine-grained, matrix-rich sediment supplies (Figure 5.18).

Regionally, these trends can be linked to the tectonosedimentary evolution of the Volta Basin during the Neoproterozoic. The older, quartz-rich Afram, Ejura, and Tease formations likely record recycling of sediments from the stable cratonic interior of the West African Craton, where prolonged weathering and reworking produced mineralogically mature quartz arenites. In contrast, the younger Bimbila and Bunya formations, characterized by feldspathic and lithic-rich compositions, reflect an increased contribution from active orogenic belts, particularly the Pan-African Dahomeyide Belt, where rapid uplift and erosion supplied less mature detritus into the basin.

Thus, the geochemical variations within the Oti-Pendjari Group reflect a temporal shift from stable cratonic sediment supply in the early basin history toward orogenic input during the Pan-African collision and uplift, recording the progressive tectonic reorganization of the Volta Basin in response to Gondwana amalgamation (Affaton, 1990; Kalsbeek et al., 2010; Caby, 1989).

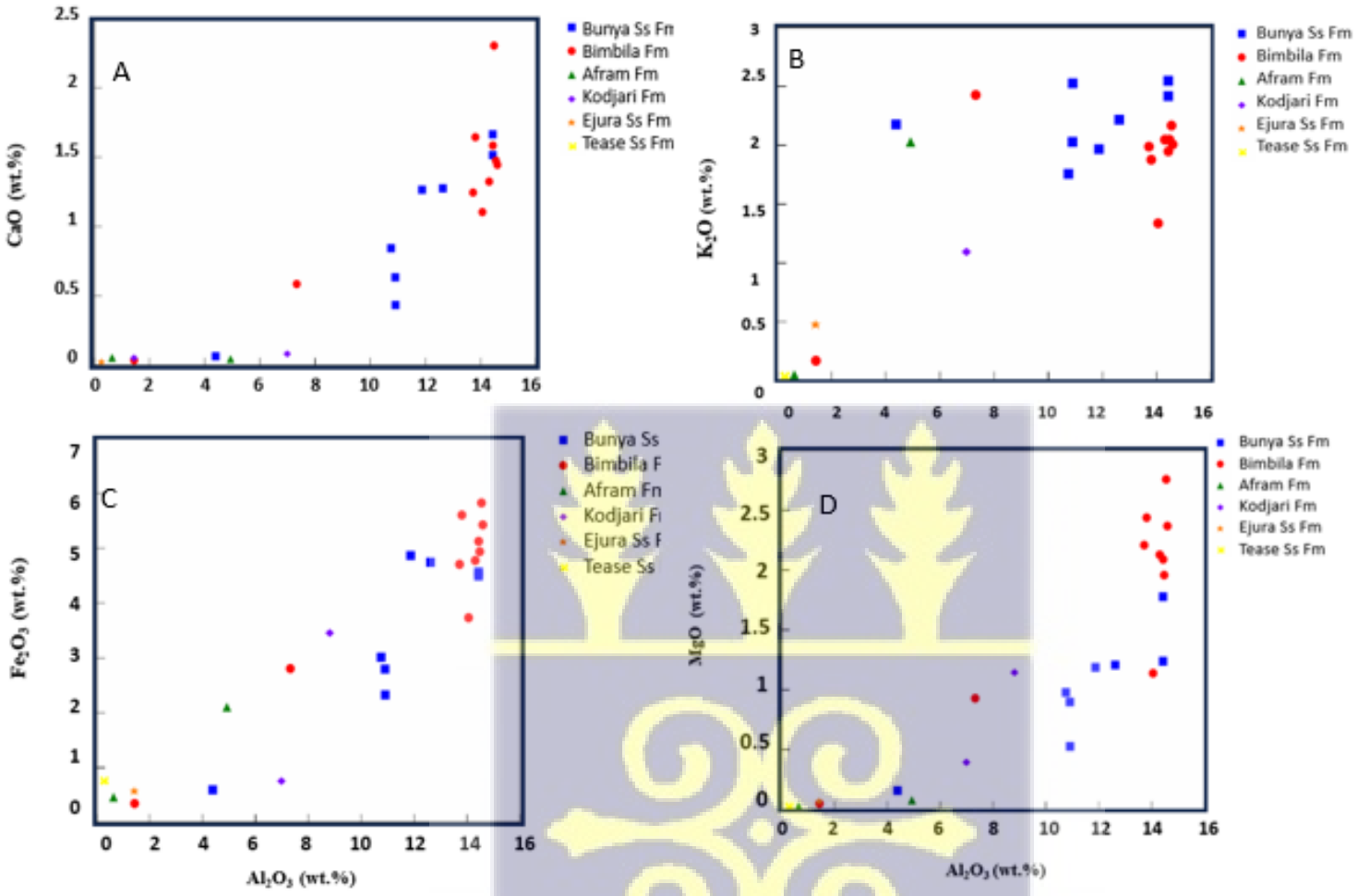

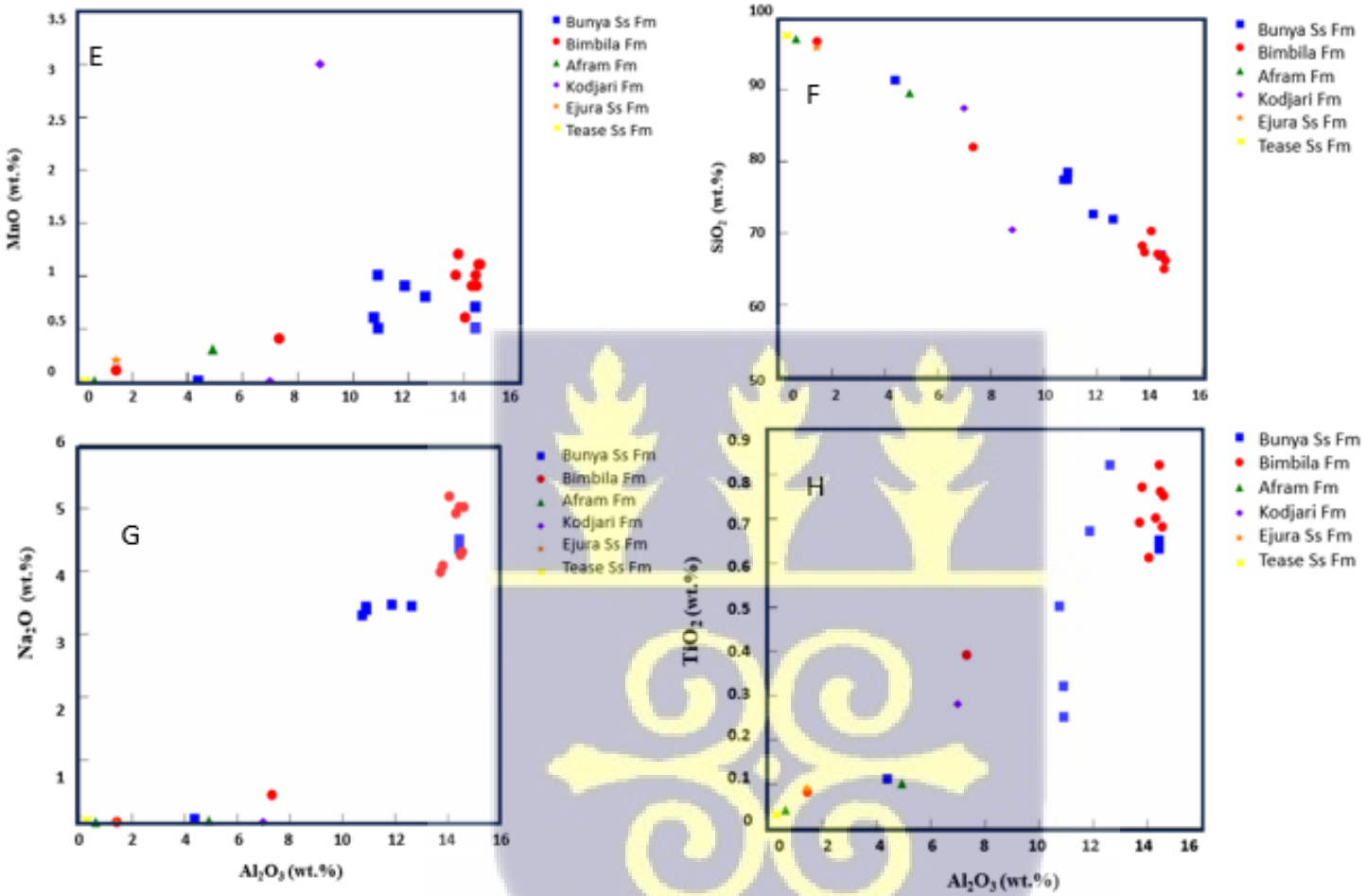

Figure 5.17 Selected major element-Al_2O_3 variation diagram for the Oti-Pendjari Group formations

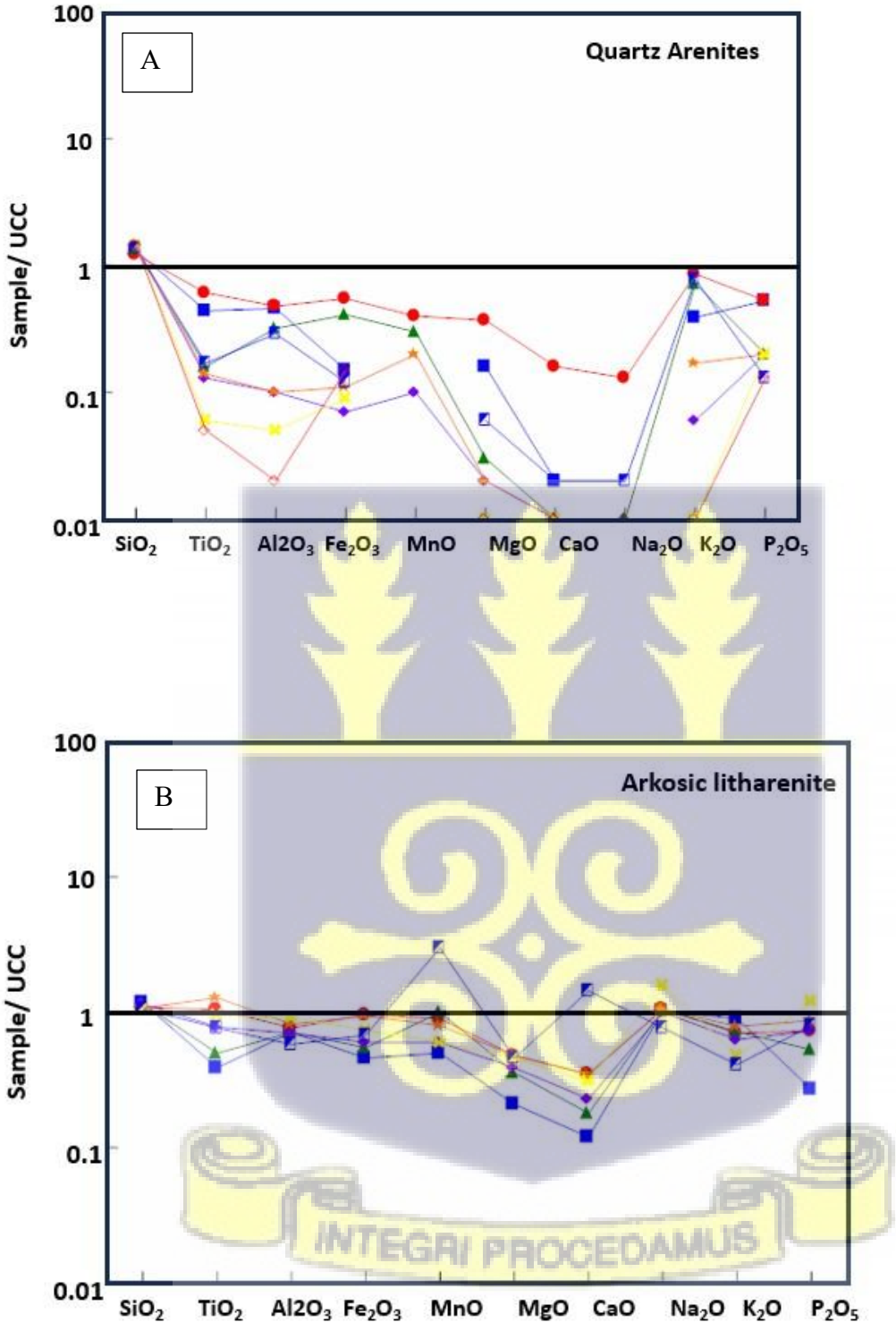

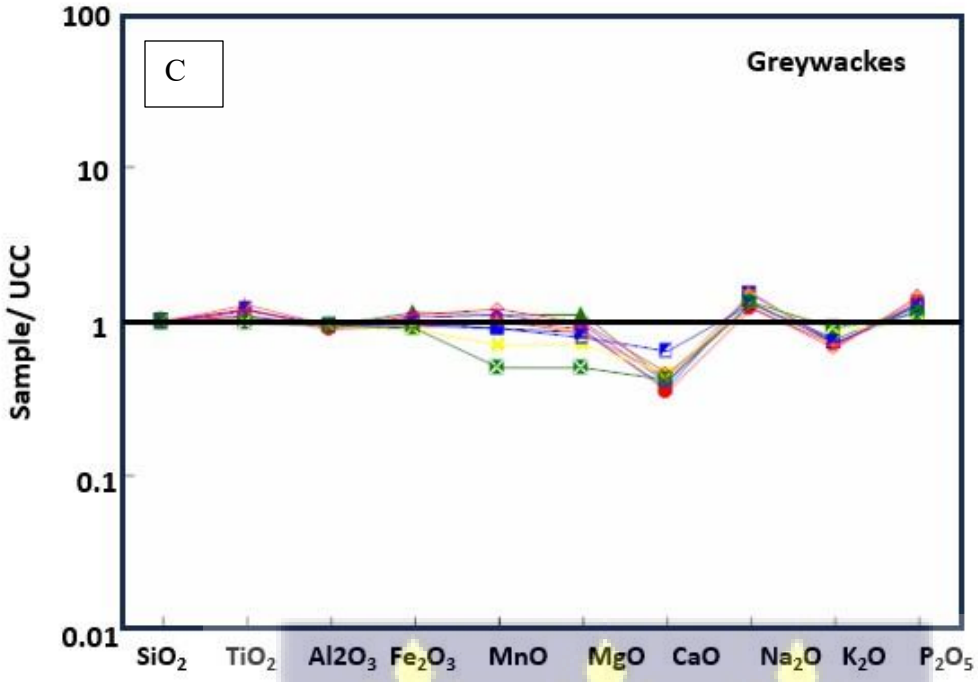

Figure 5.18 Multi-element normalized diagrams for the Oti-Pendjari Group formations, grouped as (A) Quartz arenites, (B) Arkosic Litharenites and (C) Greywackes; normalized against average Upper Continental Crust (Taylor and McLennan, 1985).

5.2.3 Paleo-Weathering Conditions of The Oti-Pendjari Group

The Chemical Index of Alteration (CIA) values of the Oti-Pendjari Group sandstones range between 60 and 90, with an average of 66.8. These values are slightly lower than those of the Post-Archaean Australian Shale (PAAS; 69; Taylor and McLennan, 1985), indicating that chemical weathering in these sediments has generally not advanced to the stage where alkali (Na, K) and alkaline earth (Ca) elements are completely leached. This is particularly evident in the Bunya and Bimbila formations, which record CIA values toward the lower end of the spectrum. Their relatively low CIA values are consistent with petrographic evidence of abundant feldspars,

suggesting that weathering was moderate and did not result in extensive feldspar breakdown (Figure 5.19).

In contrast, the older formations, including the Afram, Ejura Sandstone, Tease Sandstone, and Kodjari Formation show distinctly higher CIA values, reflecting more intense feldspar depletion and enhanced chemical alteration. These results indicate that earlier depositional stages of the Oti-Pendjari Group received sediment that had been subjected to stronger chemical weathering, leading to a greater enrichment of quartz at the expense of feldspar.

Regionally, this temporal variation in CIA values can be linked to changes in tectonic setting, sediment routing, and palaeoclimate across the Volta Basin during the late Neoproterozoic. The relatively higher CIA values in the older units point to sediment derivation from a stable cratonic hinterland of the West African Craton, where prolonged subaerial exposure and intense tropical–subtropical weathering promoted feldspar breakdown. By contrast, the younger Bunya and Bimbila formations, with their lower CIA values, were likely deposited during more active tectonic phases, when rapid uplift and erosion of the adjacent Dahomeyide Belt supplied fresh, feldspar-rich detritus into the basin. The reduced chemical alteration reflects shorter residence times of sediments in weathering profiles and quicker transfer into the depositional system.

These findings are consistent with broader Pan-African tectonosedimentary models. During the orogenic climax and subsequent foreland basin development, sediment supply to the Oti basin shifted from mature cratonic quartz-rich inputs to feldspar- and lithic-rich material sourced from newly uplifted orogenic terranes (Caby, 1989; Affaton, 1990; Kalsbeek et al., 2010). The CIA trends therefore record the progressive tectonic reorganization of West Gondwana, in which the Volta Basin captured both long-weathered cratonic sediments and freshly eroded Pan-African orogenic detritus.

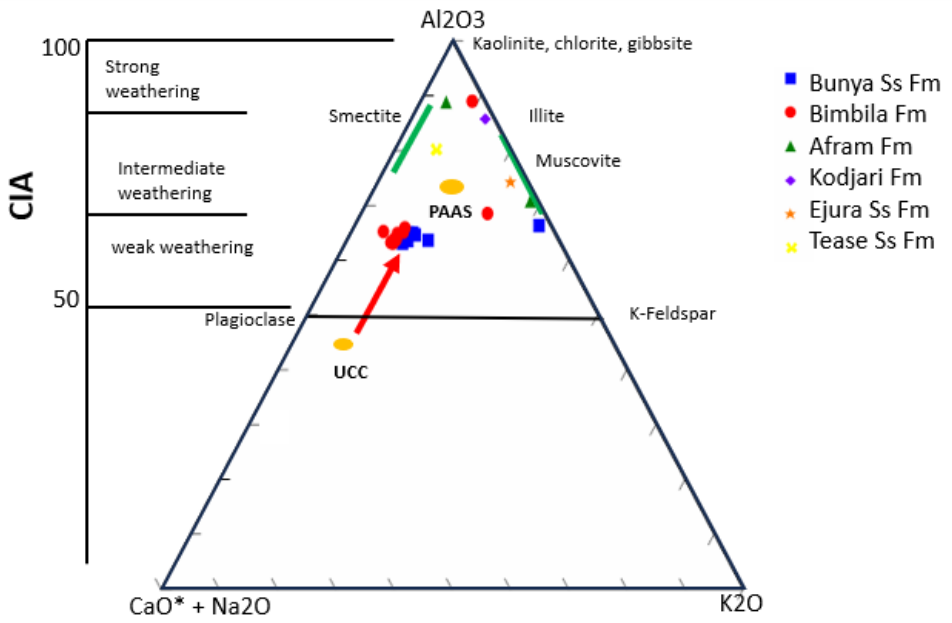

Figure 5.19 A-CN-K diagram (*after* Nesbitt and Young, 1982) showing samples of the Oti-Pendjari Group and average composition of upper continental crust (UCC; Taylor and McLennan, 1985). A = Al_2O_3; CN = CaO* + Na_2O; K = K_2O (molecular proportion; CaO* = CaO in silicate fraction only); CIA = Chemical Index of Alteration (Nesbitt and Young, 1982).

The Index of Compositional Variability (ICV), when considered alongside the Chemical Index of Alteration (CIA), provides an important framework for evaluating sediment provenance, weathering intensity, and the degree of sediment recycling (Cox et al., 1995; Cullers, 2000). Generally, high ICV values (>1.0) indicate immature sediments derived from recycled sources or tectonically active settings, where detrital inputs include abundant unstable minerals such as feldspars and lithic fragments. In contrast, low ICV values (<0.7) reflect compositionally mature sediments dominated by quartz and clay minerals, often sourced from primary igneous or metamorphic rocks that have undergone intense chemical weathering.

The Chemical Index of Alteration (CIA) and the Index of Compositional Variability (ICV) together offer valuable insights into sedimentary processes and provenance characteristics. A high CIA coupled with a low ICV typically indicates intense chemical weathering of primary igneous

or metamorphic sources, suggesting prolonged exposure to weathering agents in stable tectonic settings. Conversely, low CIA values paired with high ICV reflect weak chemical weathering but significant sediment recycling, often derived from older sedimentary successions. When both CIA and ICV are high, it implies a dynamic environment where intense weathering and active recycling occur simultaneously—conditions commonly associated with tectonically active regions. In contrast, low values for both indices suggest minimal weathering and limited recycling, often indicative of short transport distances and rapid deposition. This interplay between CIA and ICV thus serves as a diagnostic framework for interpreting sedimentary histories and tectonic regimes.

Within the Oti-Pendjari Group, the younger formations (Bunya and Bimbila) yield ICV values between 0.7 and 1.2, suggesting derivation from recycled orogenic sources with relatively immature mineralogical compositions (Figure 5.20). This interpretation aligns with their lower CIA values and petrographic evidence of feldspar and lithic fragment abundance, pointing to inputs from uplifted Pan-African Dahomeyide terranes along the eastern margin of the Volta Basin (Affaton, 1990; Kalsbeek et al., 2010). The combination of moderate weathering and high compositional variability indicates rapid erosion and deposition during the late stages of basin infill, consistent with a foreland basin setting influenced by active tectonism.

By contrast, the older formations (Afram, Ejura Sandstone, Tease Sandstone, and Kodjari) record lower ICV values (0.3–0.8) (Figure 5.20). These values, coupled with higher CIA indices, reflect more compositionally homogeneous sediments derived largely from felsic cratonic sources of the West African Craton (Leube et al., 1990; Taylor & McLennan, 1985). Their greater chemical maturity suggests prolonged weathering under stable tectonic and climatic conditions, where feldspar was extensively leached, and quartz became the dominant detrital phase.

In a regional context, these geochemical trends highlight a temporal evolution in sediment supply to the Voltaian basin. The older units reflect input from a stable cratonic hinterland, heavily weathered under tropical climatic regimes, consistent with intracratonic rift-related subsidence during the early Neoproterozoic. The younger Bimbila and Bunya units, however, reflect a shift toward tectonically rejuvenated sources, incorporating recycled material from uplifted Pan-African orogens during foreland basin development. This progression documents the transition of the Voltaian basin from a relatively quiescent intracratonic depocenter to a tectonically active foreland system during the Pan-African collisional assembly of Gondwana (Caby, 1989; Trompette, 1994).

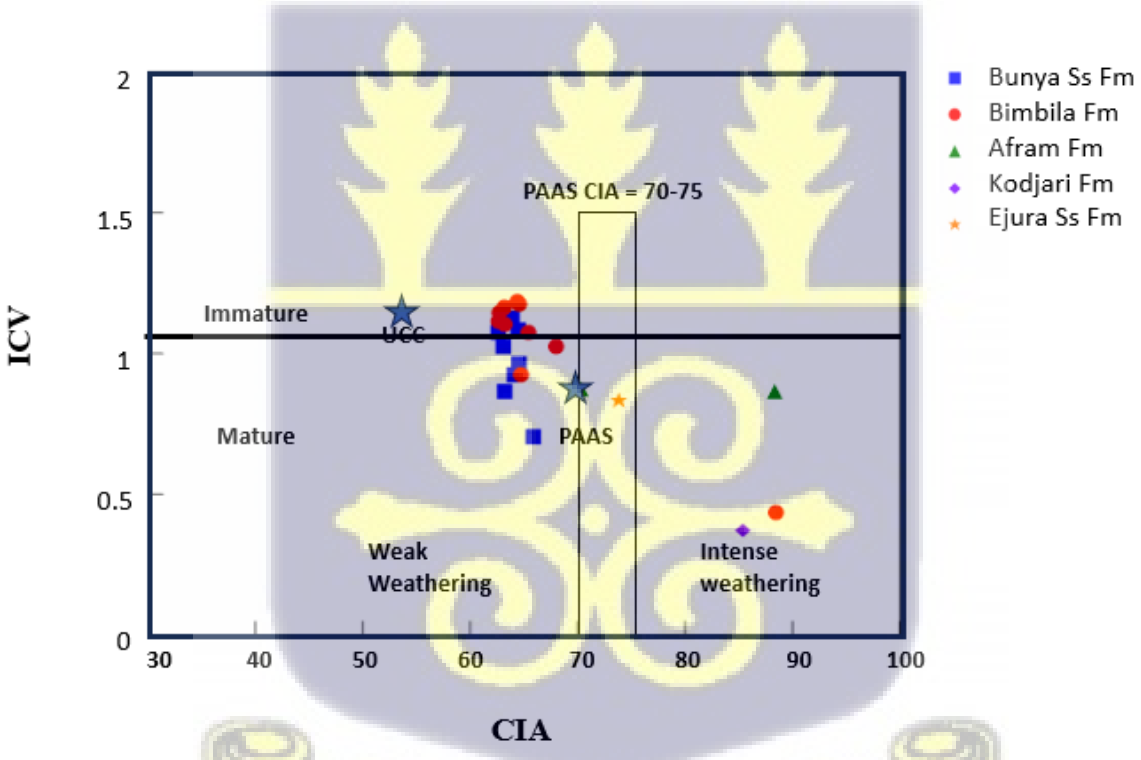

Figure 5.20 ICV (Index of Compositional Variability) versus CIA (Chemical Index of Alteration) plot (after Long et al., 2012) for the Oti-Pendjari Group samples. UCC (Upper Continental Crust) and PAAS (Post-Archean Australian Shale) values from Taylor and McLennan (1985).

5.2.4 Source rock lithology of the Oti-Pendjari Group from heavy mineral studies

The Bunya Sandstone Formation and Kodjari Formation exhibit relatively high ZTR-derived indices, particularly the RZi (Rutile–Zircon index) and RuZi (Rutile/Zircon index). Elevated values of these parameters typically reflect contributions from metasedimentary source terranes, since rutile and zircon are highly resistant heavy minerals that accumulate preferentially during the erosion of medium- to high-grade metamorphic rocks (Mange et al., 2002; Morton & Hallsworth, 1999). Their concentration in these formations suggests derivation from mature source regions enriched in accessory phases, such as the metasedimentary belts of the Birimian Supergroup or recycled Pan-African Dahomeyide units along the eastern margin of the Volta Basin.

By contrast, low GZi (Garnet–Zircon index) and RuZi ratios in other Oti Group sandstones reflect a relative depletion in garnet and rutile compared to zircon, implying a provenance signal dominated by felsic igneous and stable cratonic sources rather than high-grade metamorphic terranes (Mange et al., 2002; Hallsworth et al., 2008). Since zircon is the most mechanically and chemically stable heavy mineral, its dominance in these units points toward recycling of older cratonic sedimentary successions, in which garnet and rutile may have already been winnowed out during multiple sedimentary cycles.

Placed in a regional geological framework, these heavy mineral assemblages provide evidence for a dual provenance model in the Oti Group. The high RZi and RuZi signatures in the Bunya and Kodjari formations record contributions from Pan-African orogenic sources, particularly the Dahomeyide belt, where amphibolite- to granulite-facies metamorphism produced rutile- and garnet-bearing lithologies (Caby, 1989; Affaton, 1990). This input is consistent with the late

Neoproterozoic collisional assembly of Gondwana, when the eastern Volta Basin acted as a foreland depocenter receiving detritus from the uplifting Dahomeyides.

In contrast, the lower indices in other Oti units reflect a stronger influence from the West African Craton hinterland, where granitoid–gneiss terranes provided abundant zircon but only limited rutile or garnet. Such contrasts underscore the tectonosedimentary evolution of the Voltaian Supergroup, from deposition in a relatively stable intracratonic rift setting to the later foreland basin stage, where Pan-African collisional processes supplied metamorphic detritus to the basin fill.

5.2.5 Source rock lithology of the Oti-Pendjari Group from framework mineralogy and modal analyses

Provenance signals from the Bimbila Formation indicate derivation from a mixed source terrain, comprising both plutonic granitoids and medium- to high-grade metamorphic rocks (gneisses) (Figure 5.7). This suggests erosion of the Birimian granitoid–gneiss terranes of the West African Craton, which provided a dual contribution of fresh felsic detritus and recycled metamorphic components.

By contrast, sandstones of the Bunya Formation and Tease Sandstone Formation display a stronger plutonic affinity, with compositional signatures dominated by granitic sources, though still incorporating a minor but discernible contribution from upper-rank metamorphic rocks. The dominance of granitoid-derived detritus in these formations is consistent with sediment input from the extensive Paleoproterozoic granitoid batholiths of the craton, which formed a major sediment reservoir during late Neoproterozoic basin development.

Regionally, these provenance trends reflect the broader tectonosedimentary evolution of the Oti–Pendjari Group within the Voltaian Supergroup. The basal units, including the Kodjari Formation, preserve a record of Cryogenian global glaciation (~635 Ma), expressed as a glacial diamictite overlain by a cap carbonate succession. This sequence is widely interpreted as a stratigraphic marker of the Sturtian–Marinoan icehouse–greenhouse transition (Trompette, 1994; Carney et al., 2010). Following deglaciation, sedimentation transitioned into a shallow-marine environment, with basin development strongly influenced by a fault-controlled volcanic arc system along the eastern margin. U–Pb zircon ages from the Darebe Tuff Member (~600 Ma; Carney et al., 2010) confirm that volcanic activity persisted until the latest Cryogenian, supplying juvenile volcanic detritus to the eastern basin margin.

By approximately 590 Ma, compressional tectonics associated with the Pan-African Dahomeyide orogeny reactivated earlier fault systems, transforming the basin into a foreland setting. This orogenic activity generated subsidence along the orogenic front, creating accommodation space for thick siliciclastic successions of the Oti–Pendjari Group. The Bimbila, Bunya, and Tease sandstones, with their lithic- and feldspar-rich wacke compositions, thus represent detritus derived from uplifted orogenic highlands to the east, mixed with contributions from the stable cratonic hinterland to the west.

This dual sediment supply underscores the transitional tectonic regime of the Volta Basin during the Cryogenian–Ediacaran: initially an intracratonic depocenter influenced by global climatic perturbations, later evolving into a flexural foreland basin recording the advance of Pan-African collisional processes along the Dahomeyide suture zone (Caby, 1989; Affaton et al., 1991; Carney et al., 2010).

5.2.6 Source rock lithology for Oti-Pendjari Group from Trace and Rare Earth Elements

When compared with the Upper Continental Crust (UCC), the Bunya Sandstone and Bimbila Formation, representing the younger members of the Oti-Pendjari Group, show enrichment in ferromagnesian trace elements (Cr, Co, Ni) and concomitant depletion in high field strength elements (HFSEs: Zr, Th, Y, Nb, Ta) (Figure. 5.21 & 5.22). This geochemical pattern suggests an increased influx of mafic detritus into the basin, likely reflecting shifts in provenance and/or sedimentary environments during the late Neoproterozoic. Such patterns are diagnostic of tectonically active basins where sediment input is derived from a mixture of felsic cratonic and mafic orogenic sources (Bhatia, 1983; McLennan et al., 1993).

The enrichment in Large Ion Lithophile Elements (LILEs) such as Sr and Ba in the younger units is consistent with input from felsic to intermediate sources, while their simultaneous depletion in HFSEs indicates limited sediment recycling and relatively rapid burial. This implies a tectonically dynamic setting, where active uplift and erosion of both Pan-African Dahomeyide orogens to the east and cratonic granitoid terranes to the west supplied detritus into the Voltaian Basin (Affaton et al., 1991; Caby, 1989). Comparable signatures are observed in Pan-African foreland basins across North Africa (e.g., Tuareg Shield basins; Kalsbeek et al., 2008) and in Neoproterozoic foreland successions of Brazil, where rapid deposition during orogenesis also preserved mafic detrital signatures (Almeida et al., 2000).

The Kodjari Formation, forming the basal succession of the Oti–Pendjari Group, shows a more complex geochemical fingerprint (Fig. 5.23). UCC-normalized patterns reveal enrichment in Sr, U, P, Cr, Ni, Ta, Nb, Ti, La, and Ce, together with depletion in Cs, Ba, Yb, Hf, Zr, Sc, and Th. This duality suggests multi-sourced detritus with a stronger contribution from mafic and ultramafic lithologies, possibly linked to Pan-African arc terranes along the Dahomeyide belt. The enrichment

in U and V further points to fluctuating redox conditions during deposition, consistent with sedimentation in a tectonically active foreland basin with restricted circulation (Veizer, 1983; Milliken, 2000). The lack of pronounced Eu anomalies indicates minimal plagioclase fractionation, suggesting derivation from relatively unweathered parent rocks.

By contrast, the Afram, Ejura, and Tease Sandstone formations, representing older members of the Oti Group, display a more felsic-dominated provenance. Their enrichment in elements such as Sr, U, Ba, V, Yb, La, Ce, Th, Hf, and Zr is consistent with detrital input from granitic and gneissic terranes of the West African Craton (Figure 5.23). Simultaneously, their depletion in Cs, Ta, Nb, Ti, and Sc suggests efficient weathering and sorting, indicative of higher mineralogical maturity relative to the younger members. The presence of U and V also reflects depositional redox variability, possibly linked to fluvial–deltaic depositional systems at the craton margin (Trompette, 1994).

In a global context, these geochemical patterns place the Oti-Pendjari Group within the spectrum of Neoproterozoic basins that record Pan-African orogenic cycles. Similar trends of felsic-to-mafic provenance mixing and LILE–HFSE fractionation are reported from the Araçuaí–Ribeira belts of Brazil (Pedrosa-Soares et al., 2001), the Damara Belt of Namibia (Miller, 2008), and the Tuareg Shield basins in Niger and Mali (Kalsbeek et al., 2008). In all cases, sediment composition reflects the interplay between stable cratonic sources and adjacent collisional orogens, with foreland flexure and syn-orogenic molasse deposition marking the transition from intracratonic to collisional basin regimes. Thus, the Oti-Pendjari Group geochemistry not only documents a dual provenance system (felsic cratonic + mafic orogenic input) but also situates the Voltaian Basin within the broader Pan-African geodynamic framework, where late Neoproterozoic foreland basins across West Gondwana recorded the assembly of the Gondwanan supercontinent.

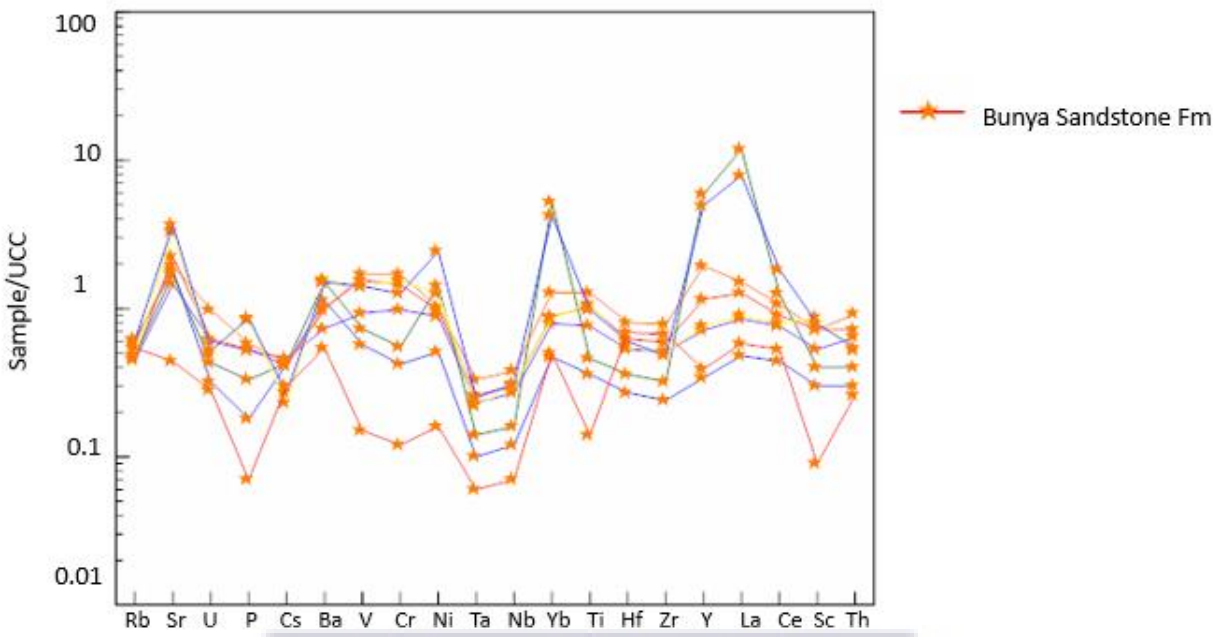

Figure 5.21 Multi-element discrimination diagram for Bunya sandstone formation (after Floyd et al., 1991) normalized to the upper continental crust values of Taylor and McLennan (1985).

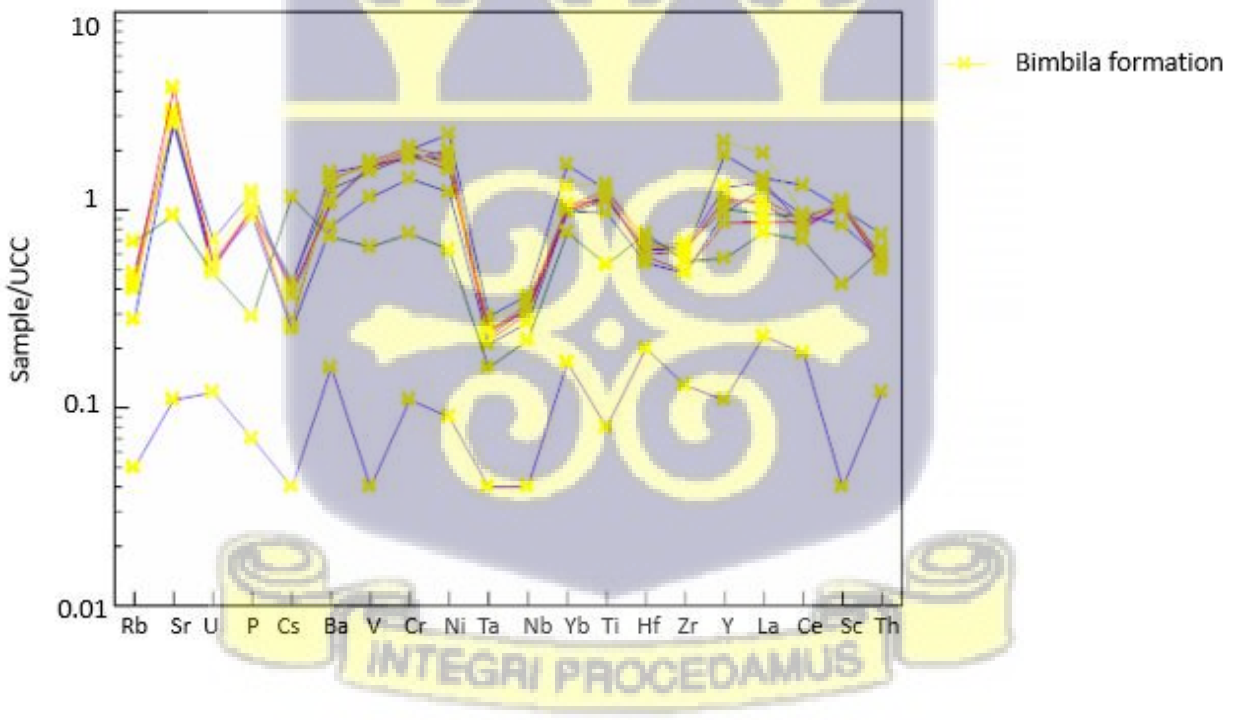

Figure 5.22. Multi-element discrimination diagram for Bimbila formation (after Floyd et al., 1991) normalized to the upper continental crust values of Taylor and McLennan (1985).

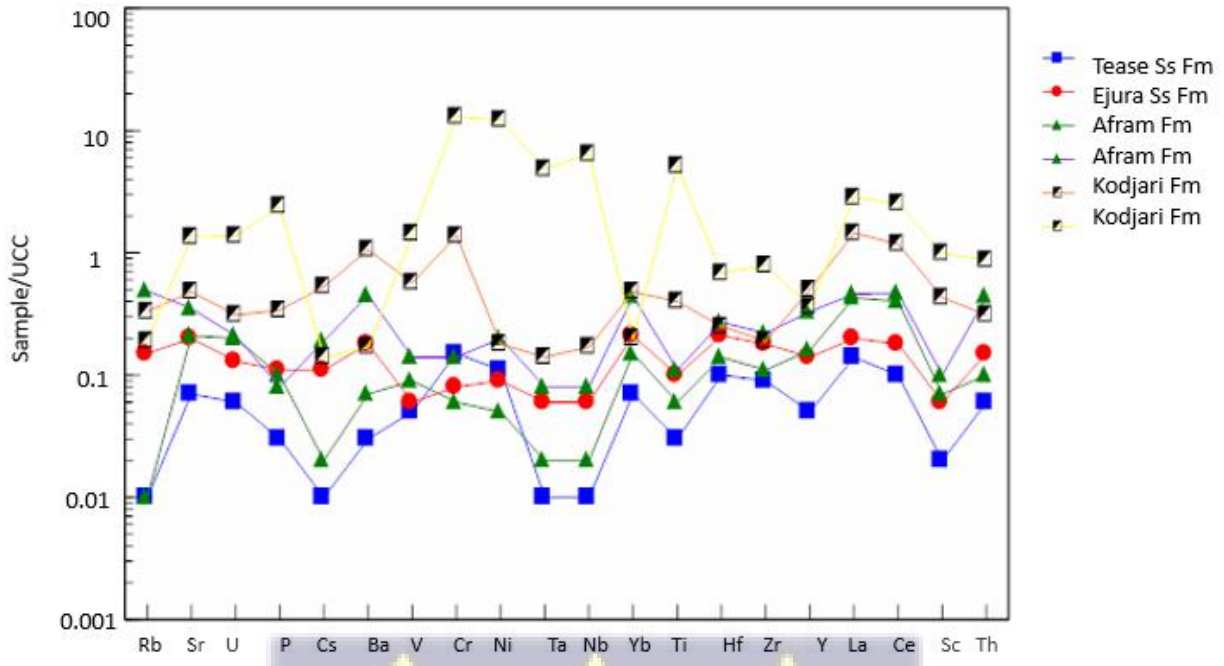

Figure 5.23. Multi-element discrimination diagram for Ejura Sandstone, Tease Sandstone, Afram, Kodjari formation (after Floyd et al., 1991) normalized to the upper continental crust values of Taylor and McLennan (1985).

Trace element discrimination diagrams such as Th–La–Sc and Th–Hf–Co are widely employed to constrain the provenance of sedimentary rocks because they utilize the differential behavior of incompatible and compatible elements during magmatic differentiation and weathering (Bhatia & Crook, 1986; Taylor & McLennan, 1985). In the Th–La–Sc diagram, high Th/Sc and La/Sc ratios typically indicate input from felsic sources, whereas lower ratios reflect a stronger mafic contribution. Similarly, the Th–Hf–Co diagram provides additional resolution, since Hf is sensitive to zircon input and chemical weathering, while Co remains relatively immobile, offering a stable reference for mafic signatures (Pearce et al., 1984; Condie, 1993).

Application of these diagrams to the Oti-Pendjari Group rocks (Figure. 5.24) reveals a dominant felsic provenance, consistent with derivation from granitic terranes of the West African Craton.

This interpretation is supported by the clustering of most samples in the felsic field of both diagrams, reflecting sustained input from cratonic granitoids and gneisses. However, subtle deviations are observed in the Hf versus La/Th plot (Figure. 5.25), where certain samples exhibit a slight mafic or intermediate influence. These signatures suggest episodic contributions from Pan-African Dahomeyide arc-related sources, providing evidence for a mixed but felsic-dominated provenance. Comparable results have been documented in Neoproterozoic basins worldwide, where felsic cratonic input dominates but is locally overprinted by syn-orogenic mafic detritus (Griffin et al., 1998; McLennan et al., 1993).

In a global context, the Oti Group provenance patterns parallel those reported from Neoproterozoic foreland and intracratonic basins such as the Damara Belt in Namibia (Miller, 2008), the Araçuaí–Ribeira belts of Brazil (Pedrosa-Soares et al., 2001), and the Tuareg Shield basins in Niger and Mali (Kalsbeek et al., 2008). In each case, trace element discrimination diagrams reveal felsic-dominated detrital sources with minor mafic input, reflecting the dual influence of stable cratonic blocks and Pan-African collisional orogens. This provenance duality is characteristic of late Neoproterozoic basins formed during the assembly of Gondwana, where sediment supply reflected both the erosion of ancient continental nuclei and contemporaneous orogenic belts (Trompette, 1994; Caby, 1989).

Thus, the trace element geochemistry of the Oti-Pendjari Group not only corroborates petrographic evidence of a dominantly granitic source with minor mafic contributions but also situates the Voltaian Basin within the broader framework of Pan-African tectonosedimentary systems, comparable to other foreland basins that recorded the interplay of cratonic stability and orogenic activity during Gondwana amalgamation.

A

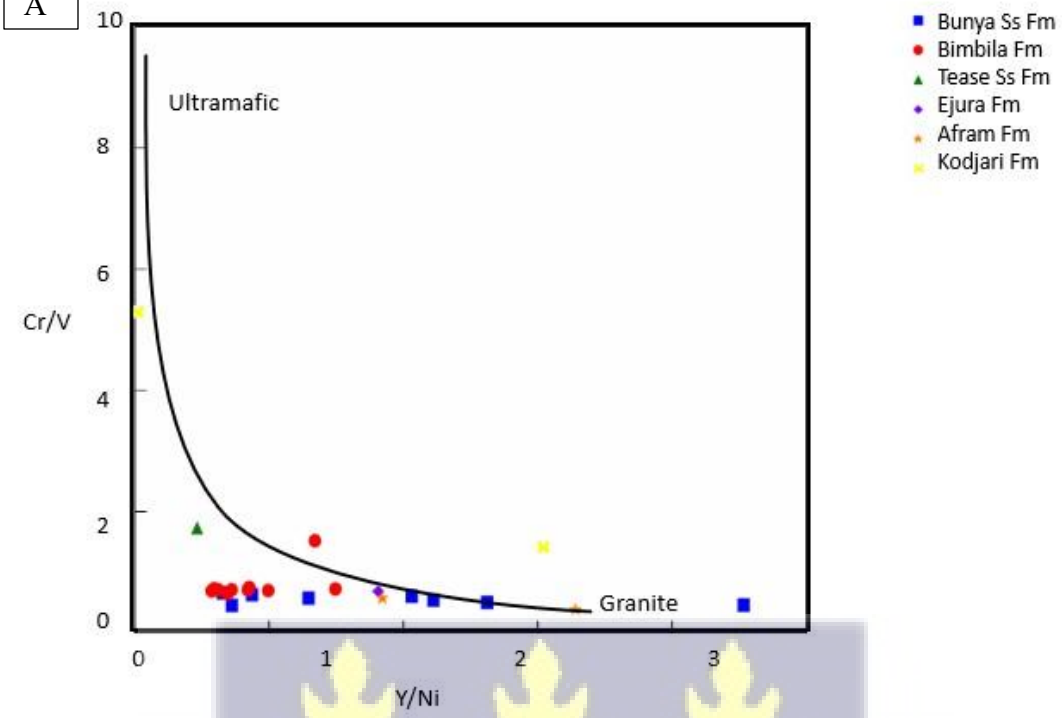

B

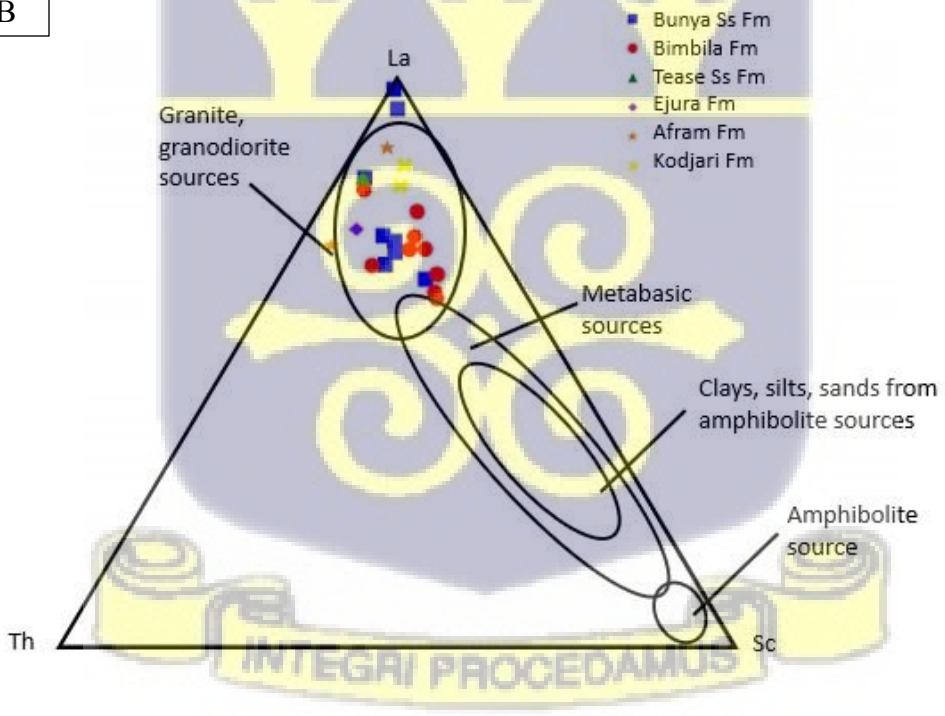

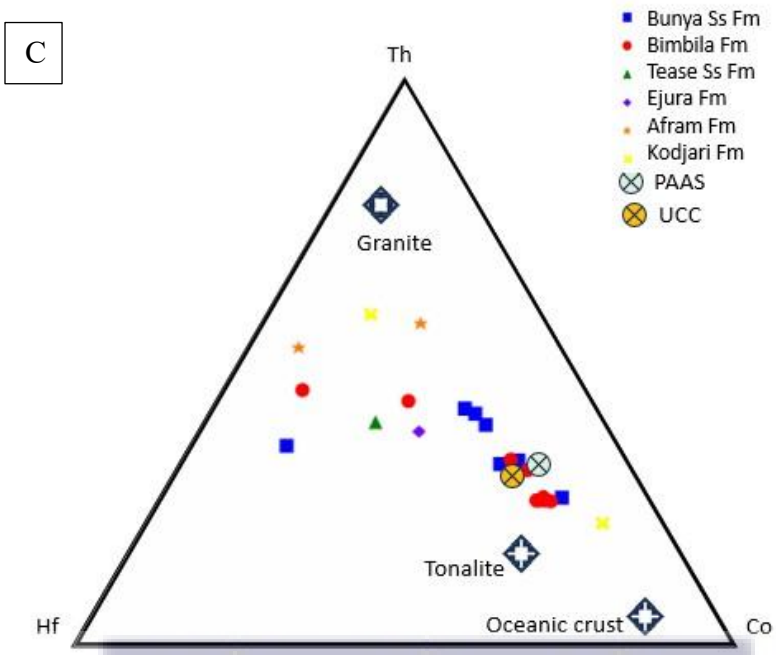

Figure 5.24. Binary and ternary plots of selected trace element compositions of the Oti-Pendjari Group as (A) Cr/V vs Y/Ni (B) Th-La-Sc and (C) Th-Hf-Co

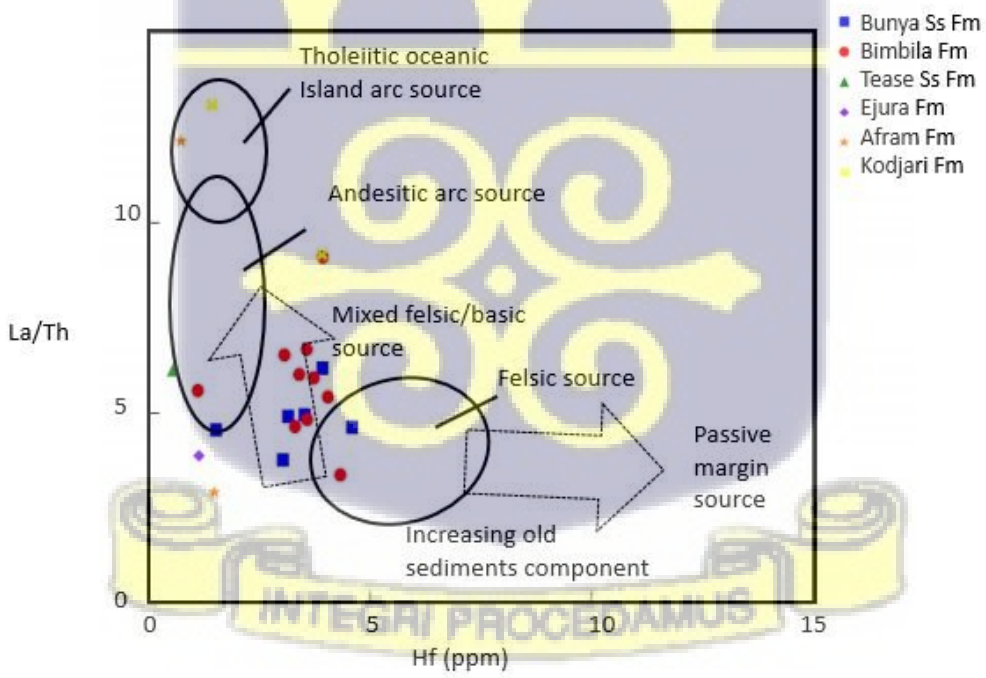

Figure 5.25 Sedimentary provenance discrimination diagrams of Hf versus La/Th (Floyd and Leveridge, 1987) for the Oti-Pendjari Group.

The Oti-Pendjari Group sandstones display distinct REE fractionation patterns, with chondrite-normalized (La/Yb)N ratios ranging from 1.25 to 124.59, significantly higher than the Post-Archean Australian Shale (PAAS) reference value of 9.15 (Taylor & McLennan, 1985). This indicates a strong enrichment in light rare earth elements (LREEs) relative to heavy rare earth elements (HREEs). The upper members of the succession (Bunya Sandstone and Bimbila Formation) exhibit slight positive Eu anomalies relative to PAAS, coupled with minor negative Ce anomalies (Figure. 5.26–5.27). In contrast, the older members (Tease Sandstone, Ejura Sandstone, Afram, and Kodjari formations) show more pronounced negative Eu anomalies and subdued Ce anomalies, consistent with sediment derivation from felsic continental sources (Figure. 5.28).

When normalized to chondrite, the upper members generally mimic the Upper Continental Crust (UCC) pattern, with LREE enrichment, relatively flat HREE distributions, and negative Eu anomalies, although a few Bunya Sandstone samples show noticeable HREE variability (Figs. 5.24–5.26). Such heterogeneity likely reflects a combination of provenance diversity and sedimentary processes. Source rocks containing accessory phases such as zircon and monazite exert strong control on HREE budgets, as these minerals preferentially host Y, Hf, and HREEs (Frey & Green, 1969; McLennan, 1989). The variations observed within the Bunya Sandstone suggest episodic sediment input from granitic terranes of the West African Craton as well as minor contributions from Pan-African arc-related volcanic sources in the Dahomeyide orogen (Carney et al., 2010).

Sedimentary processes, including hydraulic sorting during fluvial transport, may also have enhanced HREE variability by concentrating heavy mineral fractions (zircon, rutile, monazite) in certain sandstone beds (McLennan, 1989). Furthermore, post-depositional processes such as burial

diagenesis or hydrothermal alteration could have subtly modified REE distributions, though the preservation of coherent patterns argues against extensive remobilization (Rollinson, 1993).

Regionally, the REE patterns of the Oti-Pendjari Group are consistent with those documented in other Neoproterozoic basins across West Africa, such as the Gourma and Taoudéni basins in Mali (Bertrand-Sarfati & Moussine-Pouchkine, 1988; Kalsbeek et al., 2008), where strong LREE enrichment and negative Eu anomalies point to dominant felsic cratonic sources with minor arc contributions. The persistence of negative Eu anomalies in the older Oti-Pendjari Group formations reflects the erosion of Palaeoproterozoic granites and gneisses of the Birimian terranes, while the subtle positive Eu anomalies in the younger members likely record inputs from Pan-African arc volcanics and syn-orogenic granitoids.

Thus, the REE geochemistry of the Oti-Pendjari Group rocks not only highlights source heterogeneity and evolving sediment supply through time but also situates the Voltaian Basin within the broader framework of Neoproterozoic Pan-African foreland systems, where felsic cratonic detritus was progressively mixed with arc-related inputs during Gondwana amalgamation.

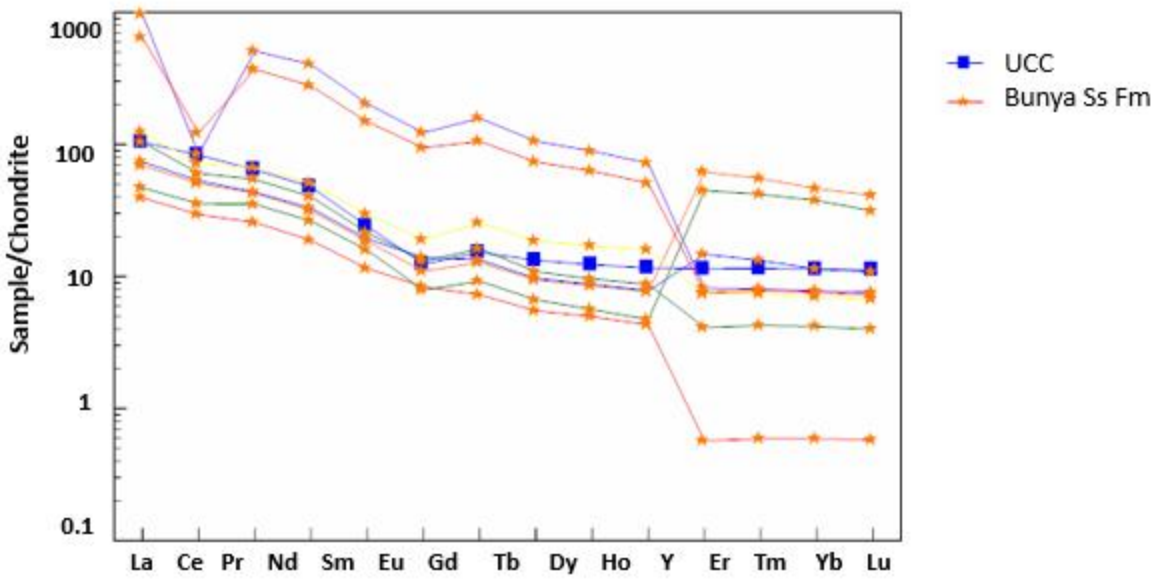

Figure 5.26. Chondrite-normalized (UCC) REE patterns of the Bunya Sandstone Formation

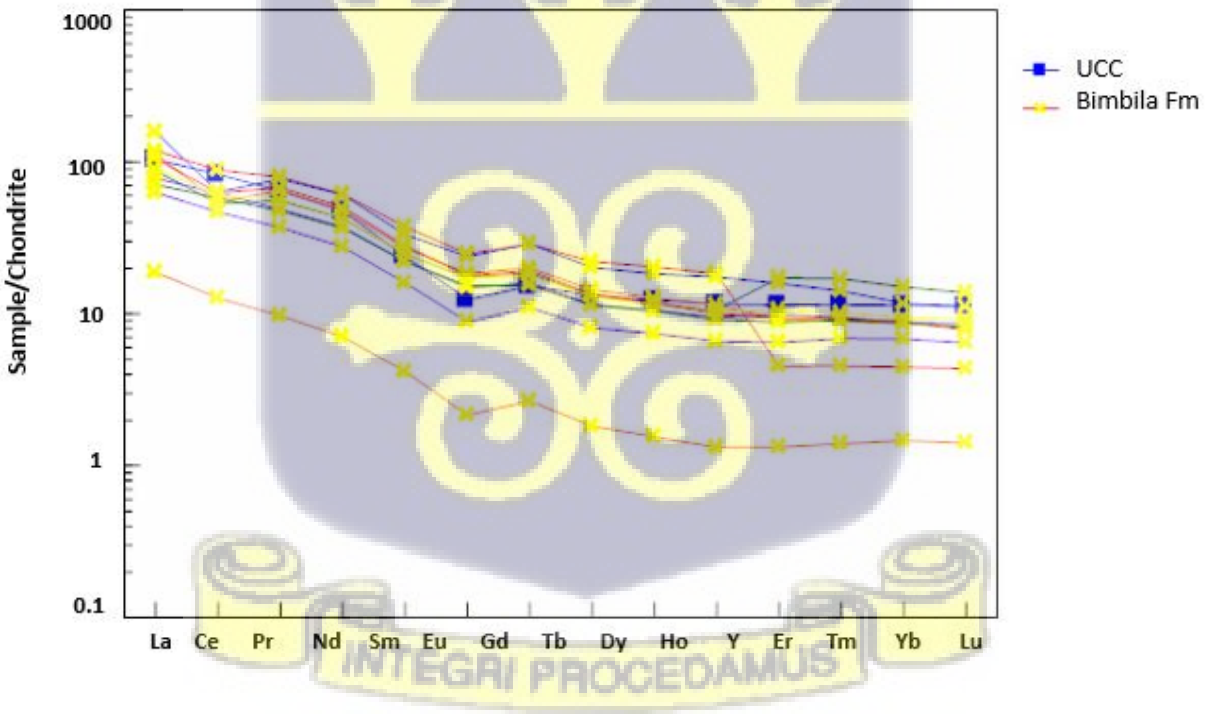

Figure 5.27. Chondrite-normalized REE patterns of the Bimbila Sandstone Formation

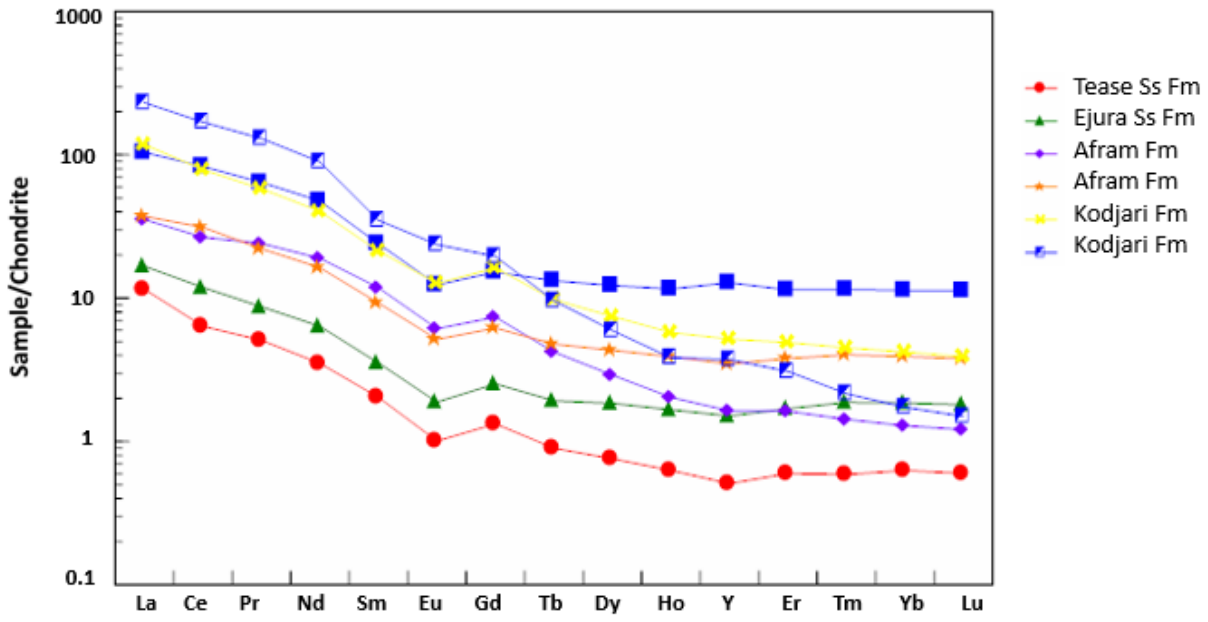

Figure 5.28. Chondrite-normalized REE patterns of the Tease Sandstone, Ejura Sandstone, Afram and Kodjari formations of the Oti-Pendjari Group.

5.3 Tectonic settings from petrography and major oxide compositions of the Oti-Pendjari Group

Provenance and tectonic discrimination diagrams highlight the complex tectonic setting recorded by the Oti-Pendjari Group. Samples from the Afram Formation predominantly plot within the recycled orogenic field, reflecting derivation from uplifted older sedimentary successions and recycled felsic crust. By contrast, the Tease Sandstone Formation plots within the craton interior field, consistent with a quartzose, stable continental provenance (Figure 5.13). This observation aligns with Anani et al. (2013), who proposed that parts of the Oti-Pendjari Group were derived from felsic sources, specifically quartzose recycled provenances within plate interiors or stable continental terranes. Within the Bimbila Formation, contrasting signatures emerge: while one sample records derivation from recycled orogens, another reflects an arc-related provenance,

suggesting heterogeneous source terrains. The Bunya Sandstone Formation shows the greatest variability, with samples straddling the transitional continental, mixed, and recycled orogenic fields, indicating contributions from both stable cratonic and orogenic sources.

Major oxide–based tectonic discrimination further supports this heterogeneity. Most Oti-Pendjari Group samples plot near the boundary between rift and arc fields (Figure 5.14). The older members (Afram, Ejura Sandstone, Tease Sandstone, Kodjari Formation) display stronger rift signatures, whereas the younger members (Bimbila and Bunya formations) show arc-related geochemical affinities, occasionally mixed with rift characteristics. Such dual arc–rift signatures complicate paleotectonic reconstructions but are best explained by the erosion of Pan-African arc terranes and redeposition of volcaniclastic detritus within a syn-rift to post-rift basin. This process reflects the interplay between arc erosion and rift-basin subsidence, where volcanic arc material was reworked into the evolving Volta Basin depocenter.

Regional stratigraphic and tectonic reconstructions support this interpretation. Carney et al. (2010) proposed that during the Tonian–Cryogenian, erosion sculpted the Kwahu and Bombouaka Groups into massifs separated by wide paleovalleys, which were subsequently infilled by the Oti-Pendjari succession. The Kodjari Formation preserves evidence of glacigenic sedimentation and Marinoan cap carbonates (~635 Ma), recording the influence of global Neoproterozoic glaciation. Following glaciation, an epeiric sea developed, flanked by rift-related volcanic centers to the east. U-Pb zircon ages from the Darebe Tuff Member (~600 Ma) confirm active volcanism during this stage. By ~590 Ma, progressive compression associated with the Dahomeyide orogeny inverted earlier rift systems and initiated foreland basin development. Within this foreland setting, proximal molasse deposits such as conglomerates of the Afram Formation (Akroso Member) accumulated

along the basin margin, while more distal feldspathic–lithic wackes of the Bimbila and Bunya Formations were deposited farther into the basin.

The Oti-Pendjari Group thus records a tectonic transition from syn-rift sedimentation influenced by arc volcanism to foreland basin deposition during Pan-African orogenesis, a pattern consistent with other Neoproterozoic successions across the West African Craton and its peripheries (Affaton, 1990; Kalsbeek et al., 2010).

5.3.1 Tectonic settings of the Oti-Pendjari Group from Trace and Rare Earth Element composition

Trace element discrimination diagrams reveal a diachronous tectonic evolution within the Oti Group. The younger Bunya and Bimbila formations display geochemical signatures typical of continental island arc (CIA) and active continental margin (ACM) settings (Figure 5.29). These units are enriched in large-ion lithophile elements (LILEs) and light rare earth elements (LREEs), both of which are diagnostic of subduction-related magmatic environments (Pearce et al., 1984). Such signatures point to sediment derivation from arc terranes linked to Pan-African tectonism along the Dahomeyide orogenic belt.

By contrast, the older formations (Ejura, Tease, Afram) exhibit geochemical affinities consistent with a passive continental margin (PM) setting, characterized by enrichment in elements derived from the prolonged weathering of stable continental crust. This interpretation agrees with earlier reconstructions by Affaton (1990) and Kalsbeek et al. (2010), who argued that much of the Oti-Pendjari Group represents passive margin deposits associated with the rifting and opening of a Pan-African oceanic domain to the east. Supporting this, tholeiitic pillow lavas with MORB-like

affinities, interbedded with Oti strata in the Buem tectonic unit, provide direct evidence of contemporaneous oceanic crust generation (Affaton et al., 1997).

However, provenance constraints from detrital zircon geochronology refine this interpretation. The presence of abundant ~600 Ma zircons in Oti-Pendjari Group sandstones (Kalsbeek et al., 2008) demonstrates input from syn-orogenic Pan-African magmatism, suggesting that at least portions of the Oti Group accumulated within a foreland basin setting rather than a purely passive margin. From the present geochemical evidence, this foreland affinity can be assigned to the younger Bimbila and Bunya formations, which record arc-related inputs and sediment fluxes from the actively deforming Dahomeyide front.

In regional context, this dual tectonic signal highlights the transitional nature of the Voltaian basin during the late Neoproterozoic. The older formations (Ejura, Tease, Afram) preserve the legacy of early rifted passive margins, while the younger formations (Bimbila, Bunya) reflect the onset of foreland basin deposition linked to the Pan-African collisional system. This tectonostratigraphic evolution parallels other West African Neoproterozoic successions, such as the Taoudéni and Gourma basins, where initial passive margin sedimentation gave way to syn-orogenic foreland deposition during the Pan-African orogeny (Trompette, 1994; Villeneuve & Cornée, 1994).

A

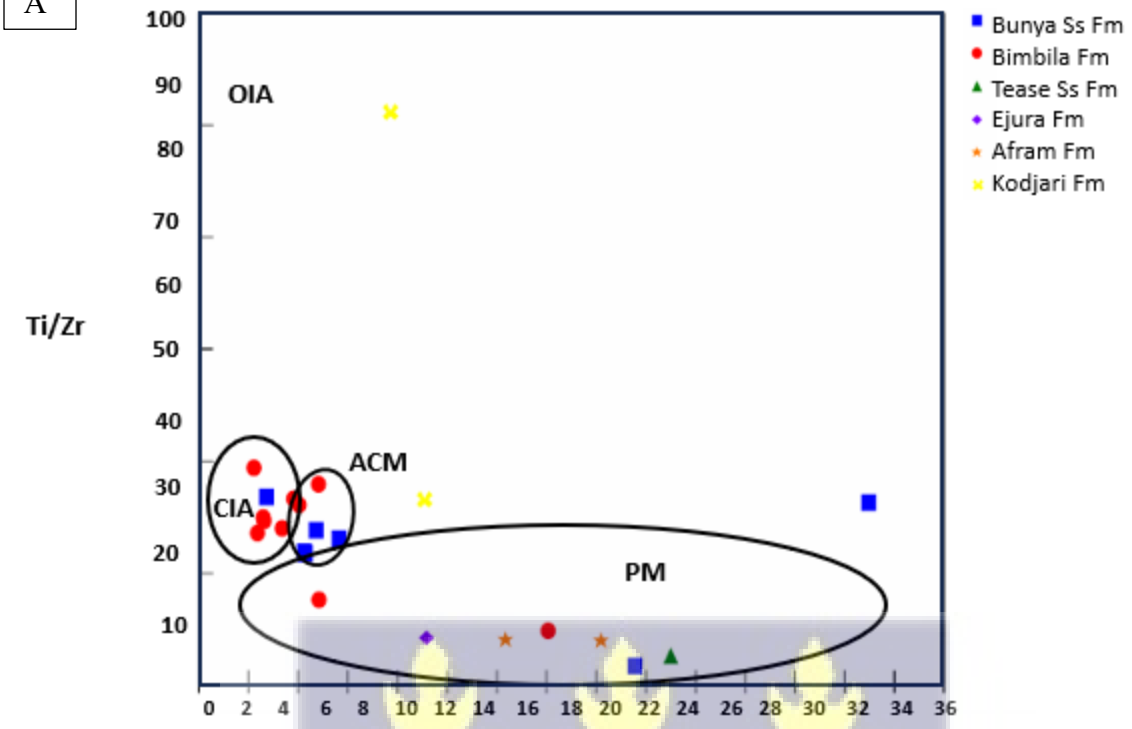

B

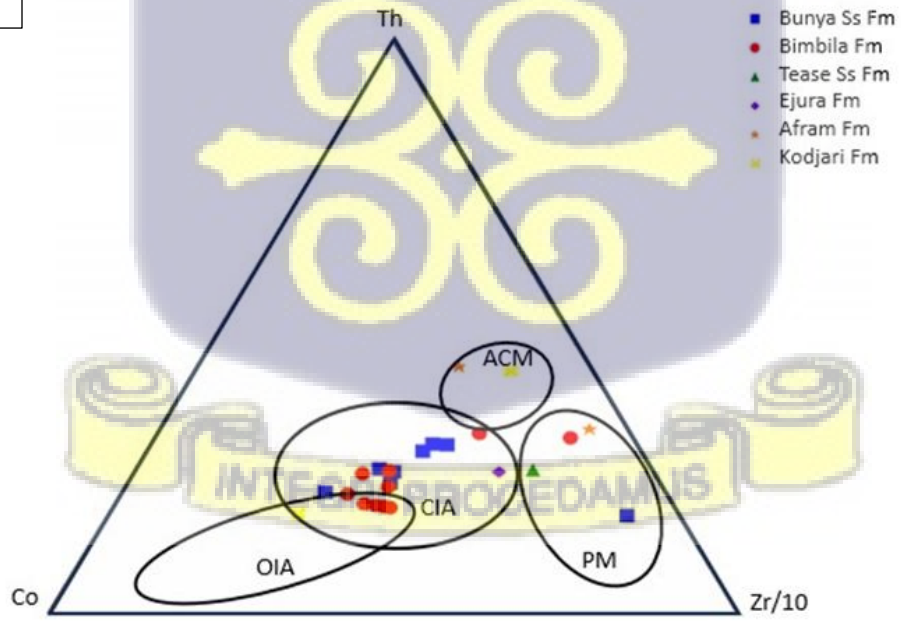

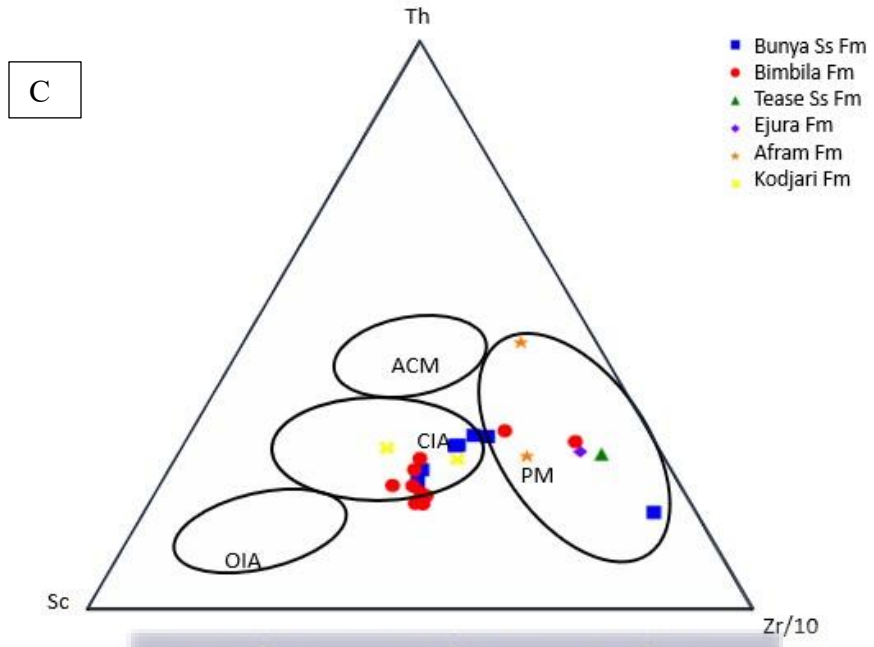

Figure 5.29. Tectonic discrimination diagrams of (A) Ti/Zr-La/Sc, (B) Th-Co-Zr/10 and (C) Th-Sc-Zr/10 (after Bhatia, 1986) for the clastic rocks from the Oti-Pendjari Group Formations. OIA - oceanic island arc, CIA-continental island arc, ACM-active continental margin, PM-passive margin

5.3.2 Provenance from Sm-Nd and Rb-Sr isotopic compositions

CHUR model ages were calculated from the present-day $^{147}Sm/^{144}Nd$ and $^{143}Nd/^{144}Nd$ of the Tamale and Oti Group samples using the equation:

$$T_{CHUR}^{Nd} = \frac{1}{\lambda} \ln \left[\frac{\left(^{143}Nd/^{144}Nd\right)_{sample\ today} - \left(^{143}Nd/^{144}Nd\right)_{CHUR\ today}}{\left(^{147}Sm/^{144}Nd\right)_{sample\ today} - \left(^{147}Sm/^{144}Nd\right)_{CHUR\ today}} + 1 \right]$$

where λ is the decay constant for ^{147}Sm to ^{143}Nd.

In using $^{143}Nd/^{144}Nd_{CHUR} = 0.51263$, $\lambda = 6.54E\text{-}12$, $^{147}Sm/^{144}Nd_{CHUR} = 0.196$ from Bouvier et al. (2008).

T_{DM}(depleted mantle) model ages were also calculated by substituting the appropriate DM (depleted mantle) values in place of ($^{143}Nd/^{144}Nd$)CHUR and ($^{147}Sm/^{144}Nd$)CHUR in the above equation. Parameters used in calculating T_{DM} are those of Goldstein et al.(1984); $(^{143}Nd/^{144}Nd)_{DM}$ today = 0.51316, $(^{147}Sm/^{144}Nd)_{DM}$ today = 0.215 and the decay constant l = 6.54 × 10−12yr−1.

Epsilon Nd (εNd) quantifies the isotopic deviation of neodymium (Nd) in a sample relative to the chondritic uniform reservoir (CHUR) (DePaolo and Wasserburg, 1976). This parameter, derived from the Sm-Nd isotopic system, is a valuable tracer of geological materials' origins and evolutionary histories. Positive εNd values signify mantle-derived, depleted Nd isotopic compositions, while negative values indicate crustal, enriched compositions (McCulloch and Wasserburg, 1978). The fractionation factor (fSm/Nd), analogous to εNd, measures Sm/Nd enrichment relative to CHUR (DePaolo, 1988). The fractionation factor (fSm/Nd), analogous to εNd, measures Sm/Nd enrichment relative to CHUR.

It is often written as $f_{Sm/Nd}$ and is calculated from the expression:

$$f = [(^{147}Sm/^{144}Nd_{today} / ^{147}Sm/^{144}Nd_{CHUR}) - 1]$$

A positive f Sm/Nd value, such as the +0.09 adopted for some depleted mantle models, implies a 9% higher Sm/Nd ratio compared to CHUR, resulting in progressively positive εNd values over time.

Continental crust exhibits lower Sm/Nd ratios compared to the depleted mantle, resulting in the production of comparatively lower $^{143}Nd/^{144}Nd$ ratios over time (McCulloch and Wasserburg, 1978). Due to the resistance of Sm and Nd to significant fractionation during metamorphism and sedimentation, Nd isotope compositions effectively record the isotopic characteristics of their source materials (DePaolo, 1988). The immobility of these elements under hydrothermal

conditions ensures that Nd isotope ratios accurately reflect the proportions of source rocks or magmas involved in petrogenetic processes (Pearce, 2008). However, the Sm-Nd system exhibits limited sensitivity to minor amounts of recycled crustal material within the mantle (Chauvel et al., 2008).

A plot of $^{143}Nd/^{144}Nd$ against $^{87}Sr/^{86}Sr$ ratios of the Tamale-Obosum and Oti-Pendjari Groups reveals that the formations from both groups have sediment sources of continental crustal material. (Figure 4.30) The Oti-Pendjari Group sediments exhibit middle continental crustal source signatures and align with seawater signatures suggesting the presence of an ocean interaction at the time of formation of the source material. On the other hand, the Tamale-Obosum samples exhibit higher Sr signatures typical of upper continental crustal material. A plot of the fractionation factor fSm/Nd against εNd indicates an old upper crust source for both groups.

The Sm–Nd isotopic systematics indicate that the Voltaian Supergroup sediments were derived predominantly from evolved continental crustal sources with limited input from juvenile material. The consistently negative εNd values (–6.9 to –19.9) across all formations point to derivation from Proterozoic to Archean basement terranes rather than juvenile Neoproterozoic sources (DePaolo, 1981; Taylor & McLennan, 1985). The Bunya and Bimbila formations, with T_DM ages clustering between 1.3 and 2.2 Ga, suggest significant input from the Paleoproterozoic Birimian terranes and Eburnean-aged granitoids of the West African Craton (Feybesse et al., 2006; Kalsbeek et al., 2012). The Afram, Tamale, and Sang Conglomerate formations, with their older T_DM ages (up to ~1.9–2.0 Ga) and more negative εNd values, imply recycling of older crustal material, possibly from the Archean Man Shield or reworked Paleoproterozoic granitoid–gneiss complexes. Kodjari samples, with mixed isotopic signals, may represent contributions from both relatively younger Pan-African granitoids (εNd closer to –10, T_DM ~1.1 Ga) and older Proterozoic crust (εNd –

14.53, T_DM ~1.6 Ga), reflecting heterogeneous provenance. The Undivided Obosum formation shows relatively less negative εNd values (–8.6 to –8.9) compared to other units, suggesting a greater contribution from younger Proterozoic sources. The large isotopic spread in the Densubon Formation points to multiple sediment supply domains, including old cratonic sources and potentially reworked Pan-African granitoid material.

Overall, the Sm–Nd isotopic evidence supports a provenance dominated by the West African Craton and reworked Paleoproterozoic basement, with episodic contributions from Pan-African belts. This interpretation is consistent with previous isotopic and detrital zircon studies that emphasize recycling of Birimian–Eburnean sources during Neoproterozoic basin filling in Ghana and adjoining West African basins (Anani et al., 2012; Toteu et al., 2006; Zobah, 2022).

The wide spread of $^{87}Rb/^{86}Sr$ and $^{87}Sr/^{86}Sr$ values indicates heterogeneous sediment sources and complex post-depositional histories within the Voltaian Supergroup. The relatively radiogenic signatures of the Bunya and Afram formations suggest strong input from old continental crustal material and/or recycling of evolved sediments, consistent with provenance from the Paleoproterozoic Birimian terranes and Eburnean-aged granitoids (Taylor et al., 1980; Feybesse et al., 2006). In contrast, the less radiogenic compositions of the Bimbila and Sang Conglomerate reflect derivation from comparatively juvenile or mixed felsic sources, with limited isotopic resetting, comparable to Nd–Sr signatures reported from detrital sediments of the Pan-African Dahomeyide and Trans-Saharan orogenic belts (Kalsbeek et al., 2012; Nehlig et al., 2016). The intermediate isotopic values in the Kodjari, Tamale, Ejura, and Undivided Obosum formations highlight contributions from both radiogenic and juvenile sources, consistent with sediment supply from adjacent Pan-African orogenic belts combined with reworking of cratonic sources (Anani et

al., 2012; Zobah, 2022). The Densubon Formation, with its extreme variability, points to multiple provenance domains and possible diagenetic modification, a trend that has also been observed in other intracratonic basins such as the Taoudeni and Iullemmeden basins (Deynoux et al., 2006; Toteu et al., 2006). Overall, the Sr–Rb isotopic data support a provenance dominated by evolved continental crust with episodic juvenile input, reflecting the tectono-sedimentary evolution of the Voltaian basin during Neoproterozoic to early Paleozoic times.

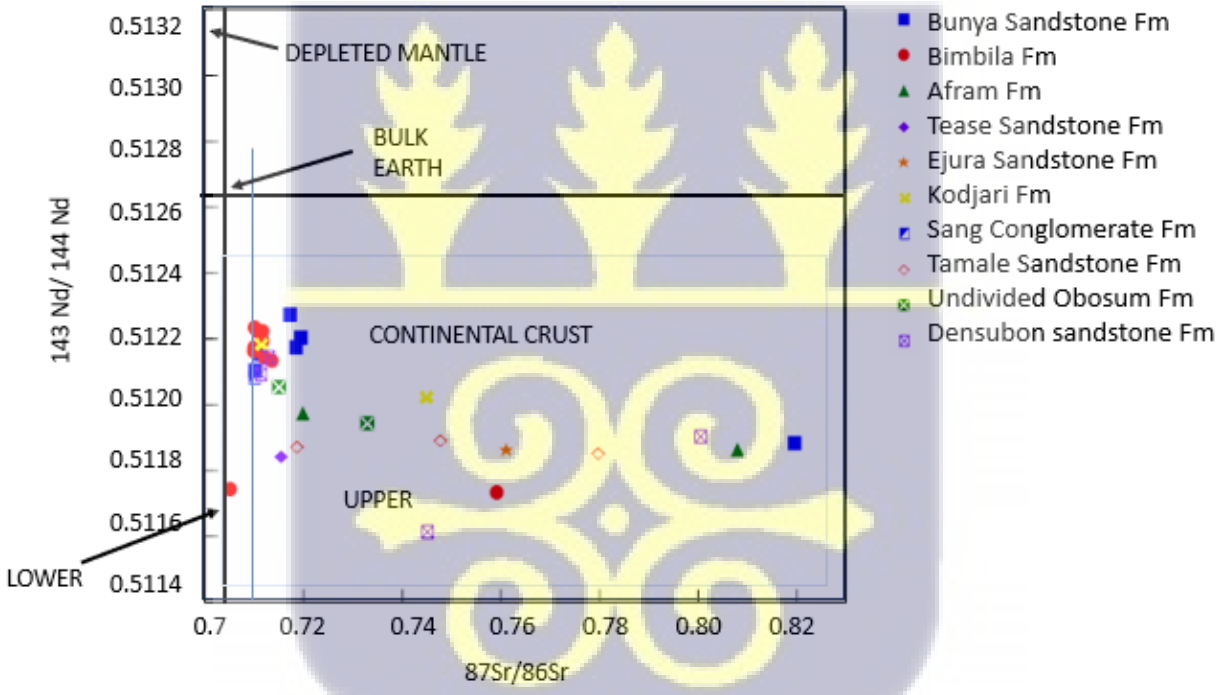

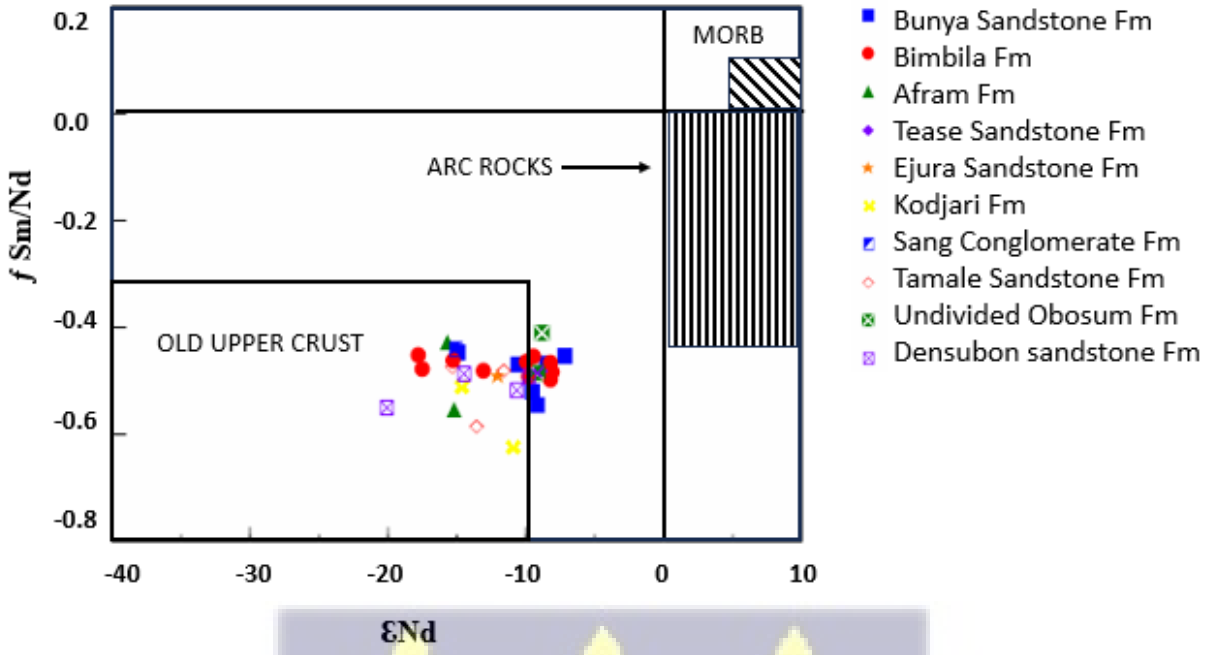

Figure 5.30 Diagrams illustrating the Sm-Nd and Rb-Sr isotopic compositions of the Tamale-Obosum and Oti-Pendjari Group rocks.

CHAPTER 6

6. Conclusions and Recommendations

6.1 Conclusions

Petrographic and geochemical analyses of the Voltaian Supergroup provide insight into its mineralogy, provenance, and tectonic history. The study identified twelve lithostratigraphic units, including formations of the Tamale-Obosum Group (Tamale Sandstone, Sang Conglomerate, Densubon Sandstone, Dunkro Sandstone, and Undivided Obosum) and the Oti-Pendjari Group (Bunya, Bimbila, Tease, Ejura, Afram, and Kodjari). Modal data, whole-rock chemistry, trace elements, and isotopes collectively demonstrate a complex depositional system recording both stable cratonic input and tectonically active sources linked to Pan-African convergence.

Sandstones of the Tamale-Obosum Group are dominated by quartz with minor feldspar and lithic grains, classifying mainly as quartz arenites and sub-arkoses. Their high quartz content, coupled with elevated Chemical Index of Alteration (CIA) values and low Index of Compositional Variability (ICV), indicates derivation from felsic, chemically weathered sources within stable cratonic and recycled orogenic terranes.

In contrast, Oti-Pendjari Group sandstones are compositionally diverse, ranging from litharenites to arkoses. Their higher feldspar and lithic content, moderate CIA values, and higher ICV reflect less intense weathering and more immature sediment supply from igneous and metamorphic sources. This variability points to provenance from tectonically active belts alongside contributions from stable cratonic interiors.

Petrography and heavy mineral assemblages highlight distinct source terrains. The Densubon Formation records mafic–ultramafic input with high Cr-spinel, while the Tamale, Kodjari, Bunya, and Sang Conglomerate formations are enriched in zircon and rutile, indicating felsic–metasedimentary sources. High garnet–zircon ratios in the Sang Conglomerate point to a metamorphic contribution.

Formations within the Tamale-Obosum Group show varied signatures: Dunkro and Densubon reflect transitional arc input, while Tamale Sandstone and Obosum samples indicate cratonic and recycled orogenic derivation. Within the Oti-Pendjari Group, the Afram Formation is dominated by metamorphic sources, the Bimbila Formation reflects mixed igneous–metamorphic input, and the Bunya and Tease sandstones are linked primarily to plutonic sources. These patterns confirm the role of multiple terranes, including Pan-African orogens, in shaping sediment composition.

Major element ratios distinguish lithologies ranging from quartz arenites to litharenites. High SiO_2 contents in quartz arenites reflect feldspar depletion and chemical maturity, while litharenites show higher Al_2O_3, Fe_2O_3, and alkalis, consistent with feldspathic and mafic detritus. Al_2O_3 correlations suggest a dominant clay control on element distributions, whereas negative SiO_2 correlations mark quartz–clay trade-offs. CIA and ICV values reinforce stronger weathering in quartzose formations and weaker alteration in feldspathic and mafic-rich units.

Trace element data support a predominantly felsic source for most units. Low Cr, Ni, and HFSE (Zr, Nb, Ta, Y) concentrations are consistent with granitic sources, although the Densubon and Sang Conglomerate formations show minor mafic input. Enrichment of Sr and Ba relative to upper continental crust (UCC) suggests sedimentary or arc-related igneous contributions, with diagenesis partly controlling concentrations. REE data normalized to PAAS reveal flat to slightly fractionated patterns, with LREE enrichment and HREE depletion typical of continental crust. Pronounced

negative HREE anomalies in Densubon and Sang Conglomerate indicate mafic or hydrothermal sources.

Geochemical discriminant functions indicate varied tectonic regimes. The Tamale Sandstone and Undivided Obosum formations reflect passive continental margin or rift deposition, while the Densubon and Sang Conglomerate formations show transitional signatures consistent with active margins. This highlights a polyphase tectonic evolution of the basin during Neoproterozoic cycles and Pan-African orogenesis.

Within the Oti-Pendjari Group, older formations (Tease, Ejura, Afram) are quartz-rich, mineralogically mature, and linked to passive margin sedimentation. Younger formations (Bunya, Bimbila) contain more feldspars and lithics, recording deposition in tectonically active rift–arc environments. This progression reflects the shift from stable cratonic sedimentation to tectonic reworking during basin evolution.

Nd and Sr isotopic compositions confirm continental crustal sources for the Oti-Pendjari Group, reflecting derivation from middle crustal rocks with possible oceanic influences. Sm-Nd model ages (1.3–2.2 Ga) point to Mesoproterozoic to Paleoproterozoic crustal sources, including the Birimian and Bombouaka terranes, with younger inputs from Pan-African belts. These results are consistent with previous interpretations that Oti-Pendjari sandstones were sourced from Pan-African arcs following the closure of pre-Pan-African oceans (Anani et al., 1999; Kalsbeek et al., 2008).

6.1.1 Major findings of the research

Petrographic and modal analyses identified significant differences in sandstone composition between the two groups. The Tamale-Obosum Group is dominated by quartz arenites and sub-arkoses, indicating high textural and mineralogical maturity consistent with derivation from stable cratonic interiors and recycled orogenic sources. The Oti-Pendjari Group, in contrast, contains litharenites and arkoses with higher proportions of feldspar and lithic fragments, reflecting more heterogeneous sediment sources and deposition in tectonically active settings. Heavy mineral assemblages revealed contrasting signatures: the Densubon Sandstone showed a strong mafic/ultramafic affinity (Cr-spinel-rich), while formations such as Sang Conglomerate and Bunya Sandstone contained rutile, zircon, and garnet, pointing to metasedimentary and plutonic sources.

Provenance interpretations indicate a diverse range of source regions, including cratonic interiors, recycled orogens, and transitional to active volcanic arcs. The Tamale and Undivided Obosum formations are mainly linked to cratonic and recycled orogenic sources. The Dunkro and Densubon formations exhibit transitional arc and mixed provenance signatures, with contributions from both felsic and mafic terranes. Within the Oti-Pendjari Group, the Afram Formation reflects predominantly metamorphic sources, while the Bimbila Formation records a mixed igneous–metamorphic provenance. The Bunya and Tease formations show plutonic dominance with minor metamorphic input. Collectively, the data demonstrate that the Voltaian Supergroup sediments were sourced from both stable Birimian and Bombouaka terranes and tectonically rejuvenated Pan-African belts, reflecting polyphase sediment supply.

Geochemical indices, particularly the Chemical Index of Alteration (CIA) and Index of Compositional Variability (ICV), revealed varying intensities of chemical weathering among formations. The Tamale Sandstone and Undivided Obosum formations display high CIA values

and low ICV, suggesting intense chemical weathering from uniform felsic sources. Conversely, the Densubon and Sang Conglomerate formations exhibit moderate CIA values and higher ICV, reflecting less weathered, compositionally diverse sources with greater plagioclase input. Evidence of K-metasomatism in the Densubon Sandstone highlights the role of diagenetic alteration in modifying primary geochemical signatures. These results underscore the interplay between provenance, weathering, and diagenesis in shaping the mineralogical and geochemical characteristics of the sediments.

Major and trace element geochemistry distinguished compositional variations across formations, ranging from quartz arenites (high SiO_2, strongly weathered) to litharenites and wackes (Al_2O_3, Fe_2O_3, and alkali-rich, less weathered). Discriminant function diagrams and trace element ratios place the Tamale and Undivided Obosum formations within continental rift/passive margin settings, while the Densubon Sandstone and Sang Conglomerate show transitional signatures between rift and volcanic arc environments. Within the Oti-Pendjari Group, the older formations (Ejura, Tease, Afram, Kodjari) exhibit felsic sources and passive margin affinities, whereas younger formations (Bimbila, Bunya) record greater mafic input and signatures transitional between rift and active continental margin settings. REE patterns across both groups generally reflect continental crustal provenance, with LREE enrichment, flat HREE, and negative Eu anomalies, but anomalies in the Densubon and Sang Conglomerate suggest localized mafic or hydrothermal inputs.

Nd and Sr isotopic analyses support a dominantly Proterozoic crustal source for both groups, with TDM model ages (1.3–2.2 Ga) linking the Tamale-Obosum Group largely to the Birimian and Bombouaka terranes, and the Oti-Pendjari Group to a mix of Birimian sources and Pan-African orogenic belts. This isotopic evidence supports deposition of Oti-Obosum sediments during or

after Pan-African ocean closure, consistent with regional tectonic reconstructions. The integrated dataset demonstrates that the Voltaian basin records multiple tectonic phases, including initial rift-related subsidence, cratonic sag development, and later foreland influence during Pan-African convergence. Comparisons with other basins, such as the Taoudeni Basin (Mauritania-Mali), Congo Basin (Central Africa), and Bambui Group (Brazil), show striking parallels in quartz-rich sediment dominance, isotopic signatures of mixed crustal sources, and tectonic transitions from stable cratonic to orogen-influenced depositional systems. Thus, the Voltaian Supergroup contributes valuable insights into Neoproterozoic basin evolution and sediment dispersal during the assembly of Gondwana, serving as a key analogue for intracratonic basins in other continents.

6.2 Limitations and recommendations

The primary constraint encountered during this research was a limited research budget, which necessitated a sequential approach to fieldwork and sample collection. This resulted in discrepancies between sample labels and field descriptions. The preparation of thin sections was outsourced due to time constraints, leading to labeling errors and suboptimal section quality. These factors hindered microscopic mineral identification and limited the availability of petrographic data for all samples analyzed geochemically. Consequently, there may be discrepancies between the formations studied for petrography and those analyzed for geochemical composition. Despite these challenges, the research endeavored to include a representative sample of formations from each group to ensure comprehensive analysis.

To address the challenges encountered in this research, future studies should prioritize adequate funding and resource allocation, implement robust fieldwork and data management practices,

establish partnerships with experienced laboratories, and foster collaboration among researchers. By addressing these recommendations, future research can mitigate the limitations faced in this study and produce more comprehensive and reliable results.

The following recommendations have been suggested to improve the quality of the research.

A comprehensive understanding of the Voltaian Basin's depositional history hinges on robust sedimentological and paleocurrent analyses, which remain conspicuously absent in current literature. Facies analysis offers critical insights into the basin's paleoenvironmental conditions, enabling reconstruction of fluvial, lacustrine, or deltaic systems that shaped sediment accumulation. By classifying sedimentary structures, grain size distributions, and lithofacies associations, researchers can delineate depositional environments and stratigraphic architecture with greater precision. Paleocurrent measurements, derived from directional sedimentary structures such as cross-bedding and ripple marks, further enhance provenance interpretations by revealing sediment transport pathways and source terrane orientations. These studies not only refine basin evolution models but also provide foundational data for hydrocarbon and groundwater exploration. Prioritizing these methodologies in future field campaigns will significantly elevate the basin's geological resolution and unlock new avenues for resource assessment and academic inquiry.

The mineralogical and geochronological characterization of Voltaian Basin sediments is essential for unraveling diagenetic histories, provenance evolution, and tectonic affiliations. Advanced techniques such as Scanning Electron Microscopy (SEM), X-ray Diffraction (XRD), and cathodoluminescence imaging can illuminate mineral stability, cementation patterns, and post-depositional alterations that influence reservoir quality. Coupling these with detrital zircon U-Pb geochronology enables precise dating of sediment deposition and identification of contributing

source terranes, such as the Birimian or Pan-African domains. This dual approach not only strengthens stratigraphic correlations but also supports tectono-sedimentary reconstructions across West Africa. Expanding these datasets will provide a more nuanced understanding of sediment pathways, crustal recycling, and basin maturation. Moreover, such data are invaluable for cross-disciplinary applications, including materials informatics and sustainable mineral targeting, making this expansion a strategic imperative for future research.

The creation of an open-access, geospatially integrated database for the Voltaian Basin would revolutionize data accessibility, collaboration, and stakeholder engagement. Currently, geological data are fragmented across institutions and publications, limiting interdisciplinary synthesis and regional planning. A centralized digital repository—housing stratigraphic logs, petrographic images, geochemical profiles, paleocurrent maps, and geochronological datasets—would empower researchers, policymakers, and industry actors alike. Such a platform should be designed with user-friendly interfaces, metadata standards, and visualization tools to facilitate comparative studies and predictive modeling. Open data fosters transparency, accelerates innovation, and democratizes scientific knowledge, particularly for emerging researchers and institutions in Ghana and across Africa. By investing in this digital infrastructure, the basin's research community can transition from isolated efforts to a dynamic, collaborative ecosystem that supports sustainable development and global scientific integration.

The Voltaian Basin's potential for energy minerals, groundwater, and construction materials necessitates a coordinated, multi-stakeholder approach to resource development. Establishing collaborative platforms that bring together geoscientists, environmental experts, local communities, government agencies, and private sector actors can ensure that exploration and extraction are both scientifically sound and socially responsible. These platforms should facilitate

knowledge exchange, joint fieldwork, and co-authored publications, while also integrating traditional ecological knowledge and community priorities. By aligning geological insights with sustainability goals, such collaborations can mitigate environmental risks, enhance local capacity, and attract ethical investment. Moreover, these networks can serve as incubators for interdisciplinary innovation—bridging geoscience with AI, materials science, and policy. As Ghana positions itself as a leader in sustainable resource governance, the Voltaian Basin can become a model for inclusive, data-driven development rooted in scientific excellence and regional empowerment.

Geoscientific research in the Voltaian Basin must increasingly inform policy decisions related to land use, mineral licensing, and environmental stewardship. Provenance studies, sedimentological mapping, and mineralogical assessments offer critical data for zoning, conservation planning, and infrastructure development. Integrating these insights into national and regional policy frameworks can enhance transparency, reduce land-use conflicts, and optimize resource allocation. For instance, identifying formations with aquifer potential or energy mineral concentrations can guide strategic investment and regulatory oversight. Researchers should engage with policymakers through policy briefs, stakeholder workshops, and advisory roles to translate scientific findings into actionable governance tools. This science-policy interface is particularly vital in contexts where resource extraction intersects with community livelihoods and ecological resilience. By embedding geological expertise into decision-making processes, future work in the Voltaian Basin can contribute meaningfully to sustainable development, equitable resource distribution, and long-term environmental security.

REFERENCES

Abu, M., Adeleye, M., Ehinola, O., & Asiedu, D. (2020). The hydrocarbon prospectivity of the Mesoproterozoic-Paleozoic intracratonic Voltaian basin, West African craton, Ghana. Journal of Petroleum Exploration and Production Technology, 11(2), 617-625.

Abu, M., Sunkari, E. D., & Anani, C. (2019). Petrography and geochemistry of Voltaian sandstones, Ghana: Implications for provenance and tectonic setting. *Journal of African Earth Sciences, 156*, 94–108.

Affaton, P., 1990. Le bassin des Volta (Afrique de l'Ouest): une marge passive, d'âgeprotérozoiquesupérieur,tectoniséeau Pan africain (600±50Ma).Editions ORSTOM, Collection Etudes et Thèses. Paris, 500 pp.

Affaton, P., 2008. LithostratigraphyoftheVoltaBasinandrelatedstructuralunits.In: Kalsbeek, F. (Ed.), The Voltaian Basin, Ghana. Workshop and Excursion, March 10-17, 2008, Abstract Volume. Geological Survey of Denmark and Greenland (GEUS), Copenhagen, pp. 13-17.

Affaton, P., Kröner, A., & Seddoh, K. F. (2000). Pan-African granulite formation in the Kabye Massif of northern Togo (West Africa): Pb? Pb zircon ages. International Journal of Earth Sciences, 88, 778-790.

Affaton, P., Rahaman, M. A., Trompette, R., & Sougy, J. (1991). The Dahomeyide orogen: Tectonothermal evolution and relationships with the Volta Basin. In R. D. Dallmeyer & J. P. Lecorché (Eds.), *The West African orogens and circum-Atlantic correlatives* (pp. 89–118). Springer.

Affaton, P., Sougy, J., Trompette, R., 1980. The tectono-stratigraphic relationships between the Upper Precambrian and Lower Paleozoic Volta basin and the Pan African Dahomeyide orogenic belt (West Africa). American Journal of Science 280, 224-248.

Agbossoumondé, Y., Guillot, S., & Ménot, R. P. (2004). Pan-African subduction-collision event evidenced by high-P coronas in metanorites from the Agou massif (southern Togo). Precambrian Research, 135(1-2), 1-21.

Agbossoumondé, Y., Guillot, S., & Ménot, R. P. (2004). Pan-African subduction-collision event evidenced by high-P coronas in metanorites from the Agou massif (southern Togo). Precambrian Research, 135(1-2), 1-21.

Agbossoumondé, Y., Ménot, R. P., & Guillot, S. (2001). Metamorphic evolution of Neoproterozoic eclogites from south Togo (West Africa). Journal of African Earth Sciences, 33(2), 227-244.

Algeo, T. and Lyons, T. (2006). Mo-total organic carbon covariation in modern anoxic marine environments: implications for analysis of paleoredox and paleohydrographic conditions. Paleoceanography, 21(1).

Algeo, T.J., Kuwahara, K., Sano, H., Bates, S., Lyons, T., Elswick, E., Hinnov, L., Ellwood, B., Moser, J. and Maynard, J.B., (2011). Spatial variation in sediment fluxes, redox conditions, and productivity in the Permian–Triassic Panthalassic Ocean. Palaeogeography, Palaeoclimatology, Palaeoecology, 308(1-2), pp.65-83.

Allen , P. A. 2007. The Huqf Supergroup of Oman: basin development and context for Neoproterozoic glacia-tion. Earth Science Reviews, 84, 139-185.

Allen, P. A., & Etienne, J. L. (2008). Sedimentary challenge to snowball Earth. Nature Geoscience, 1(12), 817-825.

Amedjoe, C. G., Gawu, S. K. Y., Ali, B., Asiedu, D. K., & Nude, P. M. (2018). Geochemical compositions of Neoproterozoic to Lower Palaeozoic shales and siltstones in the Volta Basin, Ghana: Constraints on provenance and tectonic setting. *Sedimentary Geology, 368*, 114–131. https://doi.org/10.1016/j.sedgeo.2018.03.002

Anani, C. Y., [additional authors not listed]. (1999). Provenance of Voltaian sediments in Ghana: Implications for basin evolution. *Journal of African Earth Sciences, 28*, 175–190.

Anani, C., Asiedu, D., Manu, J., Nude, P., Kutu, J., & Asamoah-Sakyi, P. (2012). Preserved Sm–Nd isotopic composition as useful provenance indicators in Neoproterozoic sandstones in the Voltaian Basin, Ghana. *International Journal of Geosciences, 3*(3), 463–468.

Annan-Yorke, R., 1971 (edited by J.E. Cudjoe). Geology of the Voltaian Basin (Summary of Current Ideas). Special Bulletin for oil exploration. Geological Survey Department, Accra, Ghana. 29 pp.

Arai, S. (1992). Chemistry of chromian spinel in volcanic rocks as a potential guide to magma chemistry. *Mineralogical Magazine, 56*(383), 173–184.

Armstrong, R. L. (1981). Radiogenic isotopes: the case for crustal recycling on a near-steady-state no-continental-growth Earth. Philosophical Transactions of the Royal Society of London. Series A, Mathematical and Physical Sciences, 301(1461), 443-472.

Armstrong-Altrin, J. S., Lee, Y. I., Verma, S. P., & Ramasamy, S. (2004). Geochemistry of sandstones from the Upper Miocene Kudankulam Formation, southern India: Implications for

provenance, weathering, and tectonic setting. *Journal of Sedimentary Research, 74*(2), 285–297.

Asmerom, Y., DuFrane, S., Mukasa, S., Cheng, H., & Edwards, R. (2005). Time scale of magma differentiation in arcs from protactinium-radium isotopic data. Geology, 33(8), 633-636.

Attoh, K. 1998a. High-pressure granulite facies meta-morphism in the Pan-African Dahomeyide orogen,West Africa. Journal of Geology, 106, 236- 246.

Attoh, K. 1998b. Models for orthopyroxene- plagioclase eand other corona reactions in metanorites, Dahomeyide orogen, West Africa. Journal of Metamorphic Geology, 16, 345-362

Attoh, K., 1990. Dahomeyides of southeastern Ghana: evidence for oceanic closure and crustal imbrication in a Pan African orogen. 15th Colloquium on African Geology (Nancy, France), CIFEG Occasional Publications, vol. 22, pp. 159-164.

Attoh, K., Dallmeyer, R.D., Affaton, P., 1997. Chronology of nappe assembly in the Pan-African Dahomeyide orogen, West Africa: evidence from 40Ar/39Ar mineral ages. Precambrian Research 82, 153-171.

Augustsson, C. (2021). Influencing factors on petrography interpretations in provenance research-a case-study review. Geosciences, 11(5), 205.

Baioumy, H. (2011). Rare earth elements and sulfur and strontium isotopes of upper Cretaceous phosphorites in Egypt. Cretaceous Research, 32(3), 368-377.

Baioumy, H. (2014). Provenance of sedimentary kaolin deposits in Egypt: Evidences from the Pb, Sr and Nd isotopes. Journal of African Earth Sciences, 100, 532-540.

Baiyegunhi, T. L., Liu, K., Gwavava, O., & Baiyegunhi, C. (2020). Textural characteristics, mode of transportation and depositional environment of the Cretaceous sandstone in the Bredasdorp Basin, off the south coast of South Africa: Evidence from grain size analysis. Open Geosciences, 12(1), 1512-1532.

Barfod, G.H., Vervoort, J.D., Montanez, I.P., Riebold, S., 2004. Lu-Hf geochronology of phosphates in ancient sediments. 13th Goldschmith Conference, Copenhagen. Geochimica et Cosmochimica Acta, Abstract Volume, vol. 68, p. A336.

Basu, A., Young, S. W., Suttner, L. J., James, W. C., & Mack, G. H. (1975). Re-evaluation of the use of undulatory extinction and polycrystallinity in detrital quartz for provenance interpretation. *Journal of Sedimentary Petrology, 45*(4), 873–882.

Bekker, A., Kaufman, A. J., Karhu, J. A., & Eriksson, K. A. (2005). Evidence for Paleoproterozoic cap carbonates in North America. Precambrian Research, 137(3-4), 167-206.

Bell, K., & Blenkinsop, J. (1987). Archean depleted mantle: Evidence from Nd and Sr isotopes in the Lac de Gras area, N.W.T., Canada. *Geochimica et Cosmochimica Acta, 51*(11), 2915–2924.

Bempah, C., Abu-Mahamuda, M., & Anani, C. Y. (2021). Provenance and tectonic implications of the Voltaian Supergroup sediments, Ghana: Petrographic and geochemical perspectives. *Journal of African Earth Sciences, 181,* 104247.

Benshati , H., K Hoja , A. & S Ola , M. 2009. Infracam-brian sediments in Libyan sedimentary basins. In:Craig , J., T Hurow , J., T Husu , B., W Hitham , A.& A Butarruma , Y. (eds) Global NeoproterozoicPetroleum Systems: The Emerging Potential in NorthAfrica. Geological Society, London, Special Publi-cations, 326, 181-191.

Berner, R. A. (1980). Early diagenesis: a theoretical approach (Vol. 241). Princeton University Press.

Bertrand-Sarfati, J., & Moussine-Pouchkine, A. (1988). Is cratonal sedimentation consistent with available models? An example from the Upper Proterozoic of the West African craton. *Sedimentary Geology, 58*(3–4), 255–276.

Bertrand-Sarfati, J., & Moussine-Pouchkine, A. (1988). The Proterozoic of West Africa. In M. J. McElhinny & R. T. Daly (Eds.), *The Proterozoic Earth* (pp. 65–87). Cambridge University Press.

Bessoles, B. (1977). *Géologie de l'Afrique: Le craton Ouest-Africain.* BRGM.

Blatt, H. (1967). *Petrology: Igneous, sedimentary, and metamorphic*. W. H. Freeman.

Blatt, H., & Pettijohn, F. J. (1972). *Petrology of sedimentary rocks.* Freeman.

Blatt, H., Middleton, G., & Murray, R. (1980). *Origin of sedimentary rocks* (2nd ed.). Prentice-Hall.

Boggs, S. (2009). *Petrology of sedimentary rocks* (2nd ed.). Cambridge University Press.

Bonhomme, M., 1962. Contribution a letude geochronologique de la platforme de louest africaine. Annales Faculte Science Universite Clermont-Ferrand 5, Geologie et Mineralogie, Clermont-Ferrand.

Borg, L. E., Carlson, R. W., & Gaffney, A. M. (2023). Rb–Sr geochronology of lunar and planetary materials. *Geochimica et Cosmochimica Acta, 338,* 22–40.

Bosch, D., Bruguier, O., Pidgeon, R. T., & Fialin, M. (2022). Advances in Rb–Sr geochronology: Implications for magmatic and metamorphic processes. *Chemical Geology, 594,* 120788.

Boulter, C. A., Petford, N., & Harvey, P. K. (2004). Sediment provenance studies: A case study from the Scottish Highlands. *Sedimentary Geology, 170*(3–4), 161–178.

Bouvier, A., Vervoort, J. D., & Patchett, P. J. (2008). The Lu–Hf and Sm–Nd isotopic composition of CHUR: Constraints from unequilibrated chondrites and implications for the bulk composition of terrestrial planets. *Earth and Planetary Science Letters, 273*(1–2), 48–57.

Bozhko, N.A., 1972. On the possible oil and gas potential of Upper Precambrian formations in West Africa. Publication of the Higher Institute of Oil and Gas 11, 3-5.

Bozhko, N.A., 2008. Stratigraphy of the Volta Basin on evidence derived from borehole drillings. In: Kalsbeek, F. (Ed.), The Voltaian Basin, Ghana. Workshop and Excursion, March 10-17, 2008, Abstract Volume. Geological Survey of Denmark and Greenland (GEUS), Copenhagen, pp. 7-12.

Brems, D., Ganio, M., Latruwe, K., Balcaen, L., Carremans, M., Gimeno, D., Silvestri, A., Vanhaecke, F., Muchez, P. and Degryse, P., 2013. Isotopes on the beach, part 2: neodymium isotopic analysis for the provenancing of Roman glass-making. Archaeometry, 55(3), pp.449-464.

Brems, D., Muchez, P., Petrus, J. A., Schneider, J., & Boyce, A. (2013). Nd isotopic constraints on sediment sources in foreland basins. *Sedimentary Geology, 294,* 122–134.

Broecker, W. S., & van Donk, J. (1970). Insolation changes, ice volumes, and the O18 record in deep-sea cores. *Reviews of Geophysics, 8*(1), 169–198.

Caby, R. (1989). Precambrian terranes of Benin, Nigeria and northeast Brazil and the late Proterozoic South Atlantic fit. In *Precambrian terranes of the Benin–Nigeria–Brazil region*

(Geological Society of America Special Paper 230, pp. 145–158). Geological Society of America.

Calver, C. R., Black, L. P., Everard, J. L., & Seymour, D. B. (2004). U-Pb zircon age constraints on late Neoproterozoic glaciation in Tasmania. Geology, 32(10), 893-896.

Carlson, R. W., & Irving, A. J. (1994). Depletion and enrichment history of subcontinental lithospheric mantle: An Os, Sr, Nd and Pb isotopic study of ultramafic xenoliths from the northwestern Wyoming Craton. *Earth and Planetary Science Letters, 126*(4), 457–472.

Carney J, Jordan C, Thomas C, McDonnel P (2008): A revised lithostratigraphy and geological map of the Voltaian basin derived from image interpretation and field mapping. In: Kalsbeek F (ed), The Voltaian Basin, Ghana. Workshop and Excursion, March 10-17, 2008, Abstract Volume. Geological Survey of Denmark and Greenland (GEUS),Copenhagen, pp 107-132

Carney, J. N., Allott, S., & Thomas, R. J. (2010). *Geology of Ghana.* British Geological Survey.

Carney, J. N., Bates, M. P., Wightman, W. G., & Addy, J. S. (2008). *Geology of the Volta Basin.* Ghana Geological Survey Report.

Carney, J. N., Bates, M. P., Wightman, W. G., & Addy, J. S. (2010). Stratigraphy, sedimentology, and basin evolution of the Neoproterozoic Volta Basin, Ghana. *Precambrian Research, 183*(1), 1–22.

Carney, J., Jordan, C., Thomas, C., Condon, D., Kemp, S., & Duodo, J. (2010). Lithostratigraphy, sedimentation and evolution of the Volta basin in Ghana. Precambrian Research, 183(4), 701-724.

Cascalho, J. (2019). Provenance analysis using heavy minerals: Principles and case studies. *Geosciences, 9*(3), 117.

Castro, A., Corretgé, L., Rosa, J., Fernández, C., López, S., Moreno, O., … & Chacón, H. (2003). The appinite-migmatite complex of sanabria, nw iberian massif, spain. Journal of Petrology, 44(7), 1309-1344.

Castro, A., Gerya, T. V., & Garcia-Casco, A. (2003). Whole-rock geochemistry of granitic magmatism: Petrogenetic implications. *Lithos, 70*(3–4), 283–310.

Catuneanu, O. (2005). A stratigraphic framework for the Karoo basins of southern Africa. *Journal of African Earth Sciences, 43*(1–3), 211–253.

Catuneanu, O., Wopfner, H., Eriksson, P. G., Cairncross, B., Rubidge, B. S., Smith, R. M. H., & Hancox, P. J. (2005). The Karoo basins of south-central Africa. *Journal of African Earth Sciences, 43*(1–3), 211–253.

Cawood, P. A., Hawkesworth, C. J., & Dhuime, B. (2012). Detrital zircon record and tectonic setting. *Earth-Science Reviews, 111*(1–2), 62–76.

Cawood, P. A., Hawkesworth, C. J., & Dhuime, B. (2013). The continental record and the generation of continental crust. *Geological Society of America Bulletin, 125*(1–2), 14–32.

Chauvel, C., Garçon, M., Bureau, S., & Droop, G. (2014). High-precision Sm–Nd isotopic data and quantitative provenance studies. *Chemical Geology, 387,* 63–75.

Chauvel, C., Lewin, E., Carpentier, M., Arndt, N. T., & Marini, J. C. (2008). Role of recycled oceanic basalt and sediment in generating the Hf–Nd mantle array. *Nature Geoscience, 1*(1), 64–67.

Chen, J., & Yang, J. (2000). Nd isotopic constraints on sedimentary provenance in East Asian basins. *Chemical Geology, 168*(1–2), 63–82.

Chen, Y., & Yang, Z. (2000). Nd model ages of sedimentary profile from the northwest Yangtze Craton, Guangyuan, Sichuan province, China and their geological implication. Geochemical Journal, 34(4), 263-270.

Chiglino, L., Gaucher, C., Sial, A. N., Bossi, J., Ferreira, V. P., & Pimentel, M. M. (2010). Chemostratigraphy of mesoproterozoic and neoproterozoic carbonates of the Nico Pérez terrane, Río de la Plata craton, Uruguay. Precambrian Research, 182(4), 313-336.

Chmielowska, D., Woronko, B., & Dorocki, S. (2021). Applicability of automatic image analysis in quartz-grain shape discrimination for sedimentary setting reconstruction. Catena, 207, 105602.

Chmielowska, E., Środoń, J., & Kotarba, M. J. (2021). Provenance analysis of sandstones using grain size, roundness, and mineralogical indices. *Sedimentary Geology, 415,* 105841.

Clauer, N. (1976). Géochimie isotopique du strontium des milieux sédimentaires. Application à la géochronologie de la couverture du craton ouest-africain (Vol. 45, No. 1, pp. 0-0). Persée-Portail des revues scientifiques en SHS.

Clauer, N., & Deynoux, M. (1987). Rb–Sr and K–Ar dating of diagenetic illites in late Proterozoic sediments of the Taoudeni Basin, West Africa. *Precambrian Research, 37*(2), 133–151.

Collins, A. S. & Pisarevsky , S. A. 2005. Amalga-mating eastern Gondwana. The evolution of the Circum-Indian Orogens. Earth Science Reviews, 71,229- 270.

Condie, K. C. (1993). Chemical composition and evolution of the upper continental crust: Contrasting results from surface samples and shales. *Chemical Geology, 104*, 1–37.

Condie, K. C., & Wronkiewicz, D. J. (1990). The chemical composition of Archean shales from the Pilbara Block, Western Australia: Implications for provenance and metamorphic studies. *Geochimica et Cosmochimica Acta, 54*(6), 1689–1705.

Condie, K. C., Wronkiewicz, D. J., Boryta, M. D., & Bickford, M. E. (1991). The geochemistry of shales from the Archean to the Phanerozoic: Implications for the composition and evolution of the continental crust. The Journal of Geology, *99*(2), 289–303.

Corsetti, F. A., & Kaufman, A. J. (2003). Stratigraphic investigations of carbon isotope anomalies and Neoproterozoic ice ages in Death Valley, California. Geological Society of America Bulletin, 115(8), 916-932.

Cox, R., & Lowe, D. R. (1995). A conceptual review of regional scale controls on the composition of clastic sediment and the provenance value of mudrock geochemistry. *Journal of Sedimentary Research, 65*(1), 1–12.

Cox, R., Lowe, D. R., & Cullers, R. L. (1995). The influence of sediment recycling and basement composition on evolution of mudrock chemistry in the southwestern United States. *Geochimica et Cosmochimica Acta, 59*(14), 2919–2940.

Crick, I. H., Boreham , C. J., Cook , A. C. & Powell ,T. G. 1988. Petroleum geology and geochemistry ofMiddle Proterozoic McArthur Basin, northern Australia II: Assessment of source rock potential.AAPG Bulletin, 72, 1495-1514.

Cullers, R. L. (1995). The controls on major and trace element variation of shales, siltstones, and sandstones of Pennsylvanian–Permian age from uplifted continental blocks in Colorado to platform sediments in Kansas, USA. *Geochimica et Cosmochimica Acta, 59*(22), 4955–4972.

Cullers, R. L. (2000). The geochemistry of shales, siltstones and sandstones of Pennsylvanian–Permian age, Colorado, USA: Implications for provenance and metamorphic studies. *Lithos, 51*(3), 181–203.

Cullers, R. L., Basu, A., & Suttner, L. J. (1988). Geochemical signature of provenance in sand-size material in soils and stream sediments near the Tobacco Root batholith, Montana, USA. *Chemical Geology, 70*(4), 335–348.

Dalland, A., Mearns, E. W., & McBride, J. J. (1995). The application of samarium-neodymium (Sm-Nd) provenance ages to correlation of biostratigraphically barren strata: A case study of the Statfjord Formation in the Gullfaks Oilfield, Norwegian North Sea. Geological Society, London, Special Publications, 89(1), 201-222.

Dansgaard, W., Clausen, H. B., Gundestrup, N., Hammer, C. U., Johnsen, S. F., Kristinsdottir, P. M., & Reeh, N. (1982). A new Greenland deep ice core. *Science, 218*(4579), 1273–1277.

Davidson, J. P., Turner, S., Handley, H., Macpherson, C., & Dosseto, A. (2007). The subduction zone filter and the impact of recycled materials on mantle chemistry and magma genesis. *Nature, 448*, 837–840.

Davidson, J. P., Turner, S., Handley, H., Macpherson, C., & Dosseto, A. (2007). Amphibole “sponge” in arc crust? *Geology, 35*(9), 787–790.

De Corte, F. (1987). The k0-standardization method: A move to the optimization of neutron activation analysis. *Journal of Radioanalytical and Nuclear Chemistry, 113*(1), 145–161.

Deer, W. A., Howie, R. A., & Zussman, J. (1992). *An introduction to the rock-forming minerals* (2nd ed.). Longman.

DePaolo, D. J. (1981). Neodymium isotopes in the Colorado Front Range and crust–mantle evolution in the Proterozoic. *Nature, 291*(5812), 193–196.

DePaolo, D. J. (1981a). Nd isotopic studies: Some new perspectives on Earth evolution. *Eos, Transactions American Geophysical Union, 62*(17), 305–312.

DePaolo, D. J. (1988). Neodymium isotope geochemistry: An introduction. Springer-Verlag.

DePaolo, D. J. (2012). Neodymium isotope geochemistry: an introduction (Vol. 20). Springer Science & Business Media.

DePaolo, D. J., & Wasserburg, G. J. (1976). Nd isotopic variations and petrogenetic models. *Geophysical Research Letters, 3*(5), 249–252.

Dessert, C., Dupré, B., François, L. M., Schott, J., Gaillardet, J., Chakrapani, G., & Bajpai, S. (2001). Erosion of Deccan Traps determined by river geochemistry: impact on the global climate and the 87Sr/86Sr ratio of seawater. Earth and Planetary Science Letters, 188(3-4), 459-474.

Dessert, C., Dupré, B., Gaillardet, J., François, L. M., & Allègre, C. J. (1993). Basalt weathering laws and the impact of basalt weathering on the global carbon cycle. *Chemical Geology*, 107(3-4), 205–219

Deynoux, M., Affaton, P., Trompette, R., & Villeneuve, M. (2006). Pan-African tectonic evolution and glacial events registered in Neoproterozoic to Cambrian cratonic and foreland basins of West Africa. Journal of African Earth Sciences, 46(5), 397-426.

Deynoux, M., Trompette, R., & Affaton, P. (2006). Neoproterozoic glacial deposits in West Africa and Brazil. *Palaeogeography, Palaeoclimatology, Palaeoecology*, 146 (1-4), 1–28.

Dhuime, B., Hawkesworth, C. J., Cawood, P. A., & Storey, C. D. (2011). A change in the geodynamics of continental growth 3 billion years ago. *Science*, 331(6014), 154–157.

Dhuime, B., Hawkesworth, C. J., Storey, C. D., & Cawood, P. A. (2011). From sediments to their source rocks: Hf and Nd isotopes in recent river sediments. Geology, 39(4), 407-410.

Dickin, A. P. (2005). *Radiogenic isotope geology* (2nd ed.). Cambridge University Press.

Dickin, A. P. (2018). *Radiogenic isotope geology* (3rd ed.). Cambridge University Press.

Dickinson, W. R. & Suczek, C. 1979. Plate tectonics and sandstone compositions. American Association of Petroleum Geologists Bulletin, 63, 2164-2182.

Dickinson, W. R. (1985). Interpreting provenance relations from detrital modes of sandstones. In G. G. Zuffa (Ed.), *Provenance of arenites* (pp. 333–361). Springer.

Dickinson, W. R. (1988). Provenance and sediment dispersal in relation to paleotectonics and paleogeography of sedimentary basins. In New perspectives in basin analysis (pp. 3-25). New York, NY: Springer New York.

Dickinson, W. R. (1974). Plate tectonics and sedimentation. In *Society of Economic Paleontologists and Mineralogists Special Publication*, 22, 1–27.

Dickinson, W. R. (1988). Provenance and sediment dispersal in relation to paleotectonics and paleogeography of sedimentary basins. In K. Kleinspehn & C. Paola (Eds.), *New perspectives in basin analysis* (pp. 3–25). Springer-Verlag.

Dickinson, W. R., & Suczek, C. A. (1979). Plate tectonics and sandstone compositions. *AAPG Bulletin, 63*(12), 2164–2182.

Dickinson, W. R., Beard, L. S., Brakenridge, G. R., Erjavec, J. L., Ferguson, R. C., Inman, K. F., Knepp, R. A., Lindberg, F. A., & Ryberg, P. T. (1983). Provenance of North American Phanerozoic sandstones in relation to tectonic setting. *Geological Society of America Bulletin*, 94(2), 222–235.

Dzigbodi-Adjimah, K., & Boamah, D. (1993). A Rb-Sr geochronological study of rocks from the southern Voltaian Basin, Ghana. *Journal of African Earth Sciences*, 17(2), 243 249.

Eggins, S. M. (2003). Laser ablation ICP-MS analysis of geological materials prepared as lithium borate glasses. *Geostandards Newsletter, 27*(2), 147–162.

Elburg, M. A., & Kuiper, Y. D. (2022). Detrital zircon U–Pb ages and Lu–Hf isotopes for sandstones of the Buem structural unit: Implications for provenance and Gondwana connections. *Gondwana Research*, 105, 67–83.

Elburg, M. A., Frei, D., & Gerdes, A. (2022). Provenance of sediments in West African basins: Insights from zircon geochronology and isotope geochemistry. *Precambrian Research*, 372, 106617.

Ennih, N., & Liégeois, J. P. (2008). The boundaries of the West African craton, with special reference to the basement of the Moroccan metacratonic Anti-Atlas belt. *Geological Society, London, Special Publications, 297*(1), 1–17.

Ershova, V. B., Prokopiev, A. V., Khudoley, A. K., & Sobolev, N. N. (2016). Provenance of detrital zircons from Neoproterozoic sandstones of the northeastern Siberian Craton. *Precambrian Research*, 285, 191–206.

Ershova, V.B., Khudoley, A.K., Prokopiev, A.V., Tuchkova, M.I., Fedorov, P.V., Kazakova, G.G., Shishlov, S.B. and O'Sullivan, P., 2016. Trans-Siberian Permian rivers: A key to understanding Arctic sedimentary provenance. Tectonophysics, 691, pp.220-233

Ershova, V.B., Khudoley, A.K., Prokopiev, A.V., Tuchkova, M.I., Fedorov, P.V., Kazakova, G.G., Shishlov, S.B. and O'Sullivan, P., 2016. Trans-Siberian Permian rivers: A key to understanding Arctic sedimentary provenance. Tectonophysics, 691, pp.220-233

Faure, G., & Mensing, T. M. (2005). *Isotopes: Principles and applications* (3rd ed.). John Wiley & Sons.

Fedo, C. M., Eriksson, K. A., & Krogstad, E. J. (1996). Geochemistry of Paleoproterozoic metasedimentary rocks from the Birimian of Ghana, West Africa: Provenance and tectonic setting. *Precambrian Research, 82*(1–2), 77–113.

Fedo, C. M., Nesbitt, H. W., & Young, G. M. (1995). Unraveling the effects of potassium metasomatism in sedimentary rocks and paleosols, with implications for paleoweathering conditions and provenance. *Geology, 23*(10), 921–924.

Fedo, C. M., Nesbitt, H. W., & Young, G. M. (2002). Detrital sedimentary geochemistry and provenance: Requirements and applications. *Journal of Sedimentary Research*, 65(4), 725–735.

Fedo, C. M., Sircombe, K. N., & Rainbird, R. H. (2003). Detrital zircon analysis of the sedimentary record. *Reviews in Mineralogy and Geochemistry*, 53 (1), 277–303.

Fedo, C. M., Young, G. M., & Nesbitt, H. W. (1997). Paleoclimatic control on the composition of Paleoproterozoic paleosols, South Africa. *Journal of Geology, 105*(6), 675–691.

Floyd, P. A., & Leveridge, B. E. (1987). Tectonic environment of the Devonian Gramscatho basin, south Cornwall: Framework mode and geochemical evidence from turbiditic sandstones. *Journal of the Geological Society, 144*(4), 531–542.

Floyd, P. A., Leveridge, B. E., & Franke, W. (1989). Geochemistry of clastic sediments and provenance of the Hercynian Rhenohercynian Flysch. *Geological Society, London, Special Publications, 43*(1), 291–311.

Folk, R. L. (1974). *Petrology of sedimentary rocks*. Hemphill Publishing.

Folk, R. L. (1980). *Petrology of sedimentary rocks* (2nd ed.). Hemphill Publishing.

Frank, M. (2002). Radiogenic isotopes: Tracers of past ocean circulation and erosional input. *Reviews of Geophysics*, 40(1), 1-1–1-38.

Frey, F. A., & Green, D. H. (1969). The mineralogy, geochemistry and origin of peridotite inclusions in basalts from Victoria, Australia. *Geochimica et Cosmochimica Acta, 33*(11), 1423–1449.

Frey, F. A., & Green, D. H. (1969). Trace element geochemistry: Applications to the igneous petrogenesis of terrestrial rocks. *Nature*, 221(5178), 518–520.

Fu, X., Wang, J., Zeng, Y., Tan, F., & FEN, X. (2012). Source regions and the sedimentary paleoenvironment of marine oil shale from the bilong co area, northern tibet, china: an Sr-Nd isotopic study. Oil Shale, 29(4).

Galehouse, J. S. (1971). Counting grain mounts: A laboratory procedure. *Journal of Sedimentary Petrology*, 41(2), 468–470.

Gallastegui, G., Pulgar, J. A., & Gallastegui, J. (2014). Provenance of conglomerates in foreland basins: Tectonic implications. *Tectonophysics*, 633, 165–180.

Garver, J. I., & Brandon, M. T. (1994). Fission-track ages of detrital zircons from Cretaceous strata, southern British Columbia: Implications for the tectonic evolution of the Insular Superterrane. *Tectonics, 13*(2), 401–420.

Garzanti, E. (2000). Provenance of sedimentary rocks: A review. Earth-Science Reviews, 51(1), 153-196.

Garzanti, E. (2019). Petrographic and compositional classification of sandstones: A review. *Sedimentary Geology*, 377, 1–15.

Garzanti, E., & Andò, S. (2007). Heavy mineral concentration in modern sands: Implications for provenance interpretation. *Sedimentary Geology, 202*, 111–125.

Garzanti, E., & Andò, S. (2007). Plate tectonics and heavy mineral suites of modern sands. Developments in Sedimentology, 58, 741-763.

Garzanti, E., Andò, S., & Vezzoli, G. (2002). Actualistic ophiolite provenance: The Cyprus case. *Journal of Sedimentary Research, 72*(6), 869–888.

Garzanti, E., Andò, S., & Vezzoli, G. (2009). Grain-size dependence of sediment composition and environmental bias in provenance studies. *Earth and Planetary Science Letters, 277*(3–4), 422–432.

Garzanti, E., Doglioni, C., Vezzoli, G., & Andò, S. (2007). Orogenic belts and orogenic sediment provenance. *The Journal of Geology, 115*(3), 315–334.

Garzanti, E., Vezzoli, G., Andò, S., France-Lanord, C., Singh, S. K., & Foster, G. (2007). Sand petrology and focused erosion in collision orogens: The Brahmaputra case. *Earth and Planetary Science Letters, 258*(3–4), 478–502.

Garzanti, E., Vezzoli, G., Andò, S., Paparella, P., & Clift, P. D. (2009). Petrology of Indus River sands: A key to interpret erosion history of the Western Himalaya. *Earth and Planetary Science Letters*, *276*(3–4), 163–174.

Gehrels, G. E. (2014). Detrital zircon U-Pb geochronology applied to tectonics. *Annual Review of Earth and Planetary Sciences*, 42, 127–149.

Gehrels, G. E., Pecha, M. A., & Foster, D. A. (2021). Detrital zircon U–Pb geochronology of West African basins: Implications for Neoproterozoic tectonics. *Geosphere*, 17(6), 1751–1773.

GeoRem Database. (n.d.). Geological and environmental reference materials. Max Planck Institute for Chemistry.

George, A. D., Wyrwoll, K. H., & Ghori, K. A. R. (1995). Provenance of sandstones from the Carnarvon Basin, Western Australia. *Sedimentary Geology*, 98(1–4), 263–277.

Glascock, M. D. (1992). Characterization of archaeological ceramics at MURR by neutron activation analysis and multivariate statistics. *Archaeometry*, 34(2), 213–229.

Glazner, A. F. (1988a). Potassium metasomatism of Mesozoic granitic rocks, Sierra Nevada, California. *Geological Society of America Bulletin, 100*(3), 350–357.

Glazner, A. F. (1988b). Stratigraphy, structure, and potassic alteration of Miocene volcanic rocks in the central Sierra Nevada, California. *Geological Society of America Bulletin, 100*(4), 564–581.

Göçmengil, G., Akçay, M., & Göncüoğlu, M. C. (2021). Whole-rock geochemistry of Neoproterozoic–Paleozoic magmatic suites in Turkey: Petrogenesis and tectonic implications. *International Journal of Earth Sciences*, 110(5), 1699–1719.

Goldstein, S. L., & Hemming, S. R. (2003). Long-lived isotopic tracers in oceanography, paleoceanography, and ice-sheet dynamics. In H. Elderfield (Ed.), *Treatise on geochemistry* (Vol. 6, pp. 453–489). Elsevier.

Goldstein, S. L., O'Nions, R. K., & Hamilton, P. J. (1984). A Sm–Nd isotopic study of atmospheric dusts and particulates from major river systems. *Earth and Planetary Science Letters, 70*, 221–236.

Gregory, D. (2020). Trace element proxies in sedimentary geochemistry: Applications for paleoenvironmental reconstruction. *Sedimentary Geology*, 401, 105649.

Griffin, W. L., Pearson, N. J., Belousova, E., Jackson, S. E., van Achterbergh, E., O'Reilly, S. Y., & Shee, S. R. (2000). The Hf isotope composition of cratonic mantle: LAM-MC-ICPMS analysis of zircon megacrysts in kimberlites. *Geochimica et Cosmochimica Acta*, *64*(1), 133–147.

Grousset, F. E., & Biscaye, P. E. (2005). Tracing dust sources and transport patterns using Sr, Nd and Pb isotopes. *Chemical Geology*, 222(3–4), 149–167.

Hallsworth, C., Morton, A. C., & Claoué-Long, J. (2008). Provenance: Heavy minerals and geochronology. *Geological Society, London, Special Publications, 296*, 1–14.

Halverson, G. P., Hoffman, P. F., Schrag, D. P., Maloof, A. C., & Rice, A. H. N. (2005). Toward a Neoproterozoic composite carbon-isotope record. Geological Society of America Bulletin, 117(9-10), 1181-1207.

Hamann, C., Luther, R., Ebert, M., Hecht, L., Deutsch, A., Wünnemann, K., Schäffer, S., Osterholz, J. and Lexow, B., (2016). Correlating laser-generated melts with impact-generated melts: An integrated thermodynamic-petrologic approach. Geophysical Research Letters, 43(20), pp.10-602

Hamann, Y., Ehrlich, S., & van den Boorn, S. H. J. M. (2016). Geochemical constraints on the genesis of siliciclastic sediments. *Chemical Geology*, 420, 98–114.

Hamilton, P. J., O'nions, R. K., Evensen, N. M., Bridgwater, D., & Allaart, J. H. (1978). Sm-Nd isotopic investigations of Isua supracrustals and implications for mantle evolution. Nature, 272(5648), 41-43.

Han, S., Li, M., Zhang, Q., & Li, H. (2019). A mathematical model based on bayesian theory and gaussian copula for the discrimination of gabbroic rocks from three tectonic settings. The Journal of Geology, 127(6), 611-626

Han, Y., Wang, Y., & Zhang, X. (2019). Geochemical discrimination of tectonic settings for granitoids. *Lithos*, 334–335, 170–185.

Hart, N. R., Stockli, D. F., & Hayman, N. W. (2016). Provenance evolution of syntectonic sediments in an extensional basin: Insights from detrital zircon U-Pb geochronology. *Basin Research*, 28(3), 283–307.

Hartono, U., Santosa, S., & Sudrajat, A. (2008). Geochemistry of volcanic rocks from Java: Implications for magma genesis. *Indonesian Journal of Geoscience*, 3(2), 75–89.

Hartono, U., Syafri, I., & Ardiansyah, R. (2008). The origin of cihara granodiorite from south banten. Indonesian Journal on Geoscience, 3(2), 107-116.

Haughton, P. D. W., Bluck, B. J., & Halliday, A. N. (1991). Sediment provenance studies. *Geological Society, London, Special Publications*, 57(1), 1–14.

Hawkesworth, C. J., & Kemp, A. I. S. (2006). The differentiation and rates of generation of the continental crust. *Chemical Geology*, 229(1–3), 1–2.

Hawkesworth, C. J., Cawood, P. A., & Dhuime, B. (2013). The continental record and the generation of continental crust. *Journal of the Geological Society*, 170(2), 229–248.

Hawkesworth, C. J., Cawood, P. A., Kemp, A. I. S., Storey, C. D., & Dhuime, B. (2020). Earth's continental lithosphere through time. *Nature Reviews Earth & Environment*, 1, 149–161.

Hawkesworth, C., Cawood, P. A., Dhuime, B., & Kemp, T. (2024). Tectonic processes and the evolution of the continental crust. Journal of the Geological Society, 181(4), jgs2024-027.

Hawkesworth, C., Cawood, P., & Dhuime, B. (2013). Continental growth and the crustal record. Tectonophysics, 609, 651-660.

Henderson, G. M. (1984). Seawater (234U/238U) during the last 800 kyr. *Earth and Planetary Science Letters*, 128, 635–647.

Henderson, P. A. U. L. (1984). General geochemical properties and abundances of the rare earth elements. In Developments in geochemistry (Vol. 2, pp. 1-32). Elsevier.

Hirdes, W., & Davis, D. W. (2002). U-Pb zircon and rutile metamorphic ages of Dahomeyan garnet-hornblende gneiss in southeastern Ghana, West Africa. Journal of African Earth Sciences, 35(3), 445-449.

Hirdes, W., Davis, D. W., & Loh, G. (2020). Detrital zircon ages and the tectonic evolution of the Voltaian Supergroup, Ghana. *Precambrian Research*, 344, 105768.

Hlebszevitsch , J. C., Gebhard , I., Cruz , C. E. &Consoli , V. 2009. The 'Infracambrian System in the southwestern margin of Gondwana, southern South America. In: Craig , J., Thurow , J., Thusu , B.,Whitham , A. & Abutarruma , Y. (eds) Global Neoproterozoic Petroleum Systems: The Emerging Potential in North Africa. Geological Society, London, Special Publications, 326, 289-302

Hodell, D. A., Mueller, P. A., & Garrido, J. R. (1989). Variations in the strontium isotopic composition of seawater during the Neogene. *Geology*, 17(6), 439–442.

Hoffman, P. F., Kaufman, A. J., Halverson, G. P., & Schrag, D. P. (1998). A Neoproterozoic snowball earth. science, 281(5381), 1342-1346.

Holland, H. D. (1978). *The chemistry of the atmosphere and oceans*. John Wiley & Sons.

Holland, W. R. (1978). The role of mesoscale eddies in the general circulation of the ocean-Numerical experiments using a wind-driven quasi-geostrophic model. Journal of Physical Oceanography, 8(3), 363-392.

Holser, W. T. (1997). Geochemical events documented in inorganic carbon isotopes. Palaeogeography, Palaeoclimatology, Palaeoecology, 132(1-4), 173-182.

Hoskin, P. W. O., & Schaltegger, U. (2003). The composition of zircon and igneous and metamorphic petrogenesis. *Reviews in Mineralogy and Geochemistry*, 53(1), 27–62.

Houk, R. S. (1986). Mass spectrometry of inductively coupled plasmas. *Analytical Chemistry*, 58(1), 97A–105A.

Howard, J. L. (1992). Conglomerate clast populations and sources: Implications for basin analysis. *Journal of Sedimentary Petrology*, 62(6), 857–865.

Hu, X., Li, Y., & Wang, Z. (2024). Detrital zircon constraints on sedimentary provenance in East Asia. *Journal of Asian Earth Sciences*, 250, 105702.

Huang, X., Gao, S., Liu, X., & Hu, Z. (2018). Crustal evolution and differentiation: Insights from Sr–Nd isotopes. *Earth-Science Reviews*, 182, 251–276.

Hubert, J. F. (1962). A zircon-tourmaline-rutile maturity index and the interdependence of the composition of heavy mineral assemblages with the gross composition and texture of sandstones. *Journal of Sedimentary Petrology*, 32(3), 440–450.

Hussain, M., Akhter, S., & Khan, T. (2004). Provenance of Neogene sandstones from Pakistan: Evidence from heavy minerals. *Sedimentary Geology*, 166(1–2), 109–120.

Hussain, M., Al-Ramadan, K., Imam, B., & Saner, S. (2004). Lithologic characteristics and diagenesis of the Devonian Jauf Sandstone at Ghawar Field, Eastern Saudi Arabia. *Marine and Petroleum Geology*, 21(11), 1221–1234.

Ikhane, P. R., Alagbe, O. A., & Fatoba, J. O. (2014). Geochemical signatures of sedimentary rocks in southwestern Nigeria: Paleoenvironmental implications. *Journal of African Earth Sciences*, 95, 65–75.

Ikhane, P., Akintola, A., Bankole, S., Ajibade, O., & Edward, O. (2014). Chemostratigraphic characterization of siliciclastic rocks in parts of the eastern dahomey basin, southwestern nigeria. Journal of Geography and Geology, 6(4).

Ingersoll, R. V. (1987). Provenance of sedimentary rocks: A review. Journal of Sedimentary Petrology, 57(2), 339-344.

Ingersoll, R. V. (1987). Petrofacies and provenance of late Mesozoic forearc basin sandstones, northern and central California. *Geological Society of America Bulletin*, 98(4), 459–472.

Ingersoll, R. V. (1990). Actualistic sandstone petrofacies: Discriminating modern and ancient depositional systems. *Journal of Sedimentary Petrology*, 60(2), 239–252

Ingersoll, R. V. (1993). Sandstone petrofacies and tectonic provenance. In *Geological Society of America Memoirs*, 284, 333–348.

Ingersoll, R. V., Bullard, T. F., Ford, R. L., Grimm, J. P., Pickle, J. D., & Sares, S. W. (1984). The effect of grain size on detrital modes: A test of the Gazzi–Dickinson point-counting method. *Journal of Sedimentary Petrology, 54*(1), 103–116.

Jackson, M. J., Powell, T. G., Summons, R. E. &S Weet, I. P. (1986). Hydrocarbons show petroleum source rocks in sediments as old as 1.7 109 years. Nature, 322, 727- 729

Jacobs , J. & Thomas , R. J. (2002). The Mozambique Belt from an East Antarctic perspective. Bulletin of the Royal Society of New Zealand, 35, 3 -18

Jacobsen, S. B., & Wasserburg, G. J. (1979). The mean age of mantle and crustal reservoirs. *Journal of Geophysical Research: Solid Earth, 84*(B13), 7411–7427.

Jacobsen, S. B., & Wasserburg, G. J. (1979). Nd and Sr isotopic study of the Bay of Islands ophiolite complex and the evolution of the mantle. *Journal of Geophysical Research: Solid Earth*, 84(B11), 7429–7445.

Jarvis, I. (1988). Application of inductively coupled plasma mass spectrometry to the determination of rare earth elements in sediments. *Chemical Geology*, 68(1), 31–39.

Jarvis, K. E. (1988). Inductively coupled plasma mass spectrometry: A new technique for the rapid or ultra-trace analysis of geological materials. *Applied Geochemistry, 3*(5), 549–564.

Jenkins, R. (1999). *X-ray fluorescence spectrometry* (2nd ed.). John Wiley & Sons.

Jenner, G. A. (1996). Trace element geochemistry of igneous rocks: Geochemical indicators of magma genesis. *Geochimica et Cosmochimica Acta*, 60(15), 3101–3111.

Jiang, T., & Yang, S. (2019). Provenance and weathering of Yangtze River sediments: Implications for tectonic and climatic controls. *Sedimentary Geology*, 382, 72–85.

Joshi, R., Bhat, G. M., & Ahmad, S. M. (2021). Geochemistry and provenance of Neoproterozoic sediments from the Lesser Himalaya, India. *Journal of Asian Earth Sciences*, 201, 104514.

Junner NR, Hirst J (1946) The geology and hydrogeology of the Voltaian basin. Gold Coast Geological Survey, Memoir No. 8

Junner, N. R. (1940). *Geology of the Gold Coast and Western Togoland* (Gold Coast Geological Survey Bulletin No. 11). Government Printing Department.

Kadima, E., Delvaux, D., Sebagenzi, S. N., Tack, L., & Kabeya, S. M. (2011). Structure and geological history of the Congo Basin: An integrated interpretation of gravity, magnetic and reflection seismic data. *Basin Research, 23*(5), 499–527.

Kalsbeek, F., Affaton, P., Ekwueme, B. N., Frei, R., & Thrane, K. (2008). Geochronology of granitoid and metasedimentary rocks from Togo and Benin, West Africa: Comparisons with NE Brazil. *Precambrian Research, 159*(3–4), 272–288.

Kalsbeek, F., Affaton, P., Ekwueme, B. N., Frei, R., Thrane, K., & Frei, D. (2008). Geochronology of granitoid and metasedimentary rocks from the Pan-African fold belt in NE Ghana, West Africa. *Precambrian Research, 164*(3–4), 356–370.

Kalsbeek, F., Affaton, P., Ekwueme, B. N., Frei, R., Thrane, K., & Zwedna, A. (2008). Geochronology of granitoid and metasedimentary rocks from the Pan-African Dahomeyide belt, West Africa: Significance for the evolution of the Benin-Nigerian shield. *Journal of the Geological Society*, 165(2), 393–404.

Kalsbeek, F., Frei, D., & Affaton, P. (2008). Constraints on provenance, stratigraphic correlation and structural context of the Volta basin, Ghana, from detrital zircon geochronology: an Amazonian connection? Sedimentary Geology, 212(1-4), 86-95.

Kalsbeek, F., Frei, D., & Affaton, P. (2012). The geochemistry and Sm–Nd isotopic composition of sediments from the Voltaian Supergroup, Ghana. *Precambrian Research*, 200, 1–16.

Kalsbeek, F., Frei, D., Affaton, P., & Frei, R. (2008). Geochemistry and provenance of the Voltaian Supergroup, Ghana. *Precambrian Research*, 162(1–2), 123–140.

Kalsbeek, F., Frei, R., & Thrane, K. (2008). Source components and tectono-thermal evolution of the Birimian (Paleoproterozoic) rocks in southern Ghana: Insights from Nd and Pb isotope studies. *Precambrian Research*, 164(1–2), 94–110.

Karhu, K., Fritze, H., Hämäläinen, K., Vanhala, P., Jungner, H., Oinonen, M., Sonninen, E., Tuomi, M., Spetz, P., Kitunen, V. and Liski, J., (2010). Temperature sensitivity of soil carbon fractions in boreal forest soil. Ecology, 91(2), pp.370-376.

Kaufman, A. J., Knoll, A. H., & Narbonne, G. M. (1997). Isotopes, ice ages, and terminal Proterozoic earth history. Proceedings of the National Academy of Sciences, 94(13), 6600-6605.

Kaufman, A.J., Johnston, D.T., Farquhar, J., Masterson, A.L., Lyons, T.W., Bates, S., Anbar, A.D., Arnold, G.L., Garvin, J. and Buick, R., (2007). Late Archean biospheric oxygenation and atmospheric evolution. Science, 317(5846), pp.1900-1903.

Kaur, P., Chaudhri, N., Raczek, I., Kröner, A., & Hofmann, A. W. (2009). Record of 1.82 Ga Andean-type continental arc magmatism in NE Rajasthan, India: insights from zircon and Sm-Nd ages, combined with Nd-Sr isotope geochemistry. Gondwana Research, 16(1), 56-71.

Kaur, P., Chaudhuri, A. K., & Choudhuri, B. (2009). Nd isotopic constraints on sedimentary recycling in Proterozoic basins of India. *Precambrian Research*, 168(3–4), 163–176.

Kemp, A. I. S., Hawkesworth, C. J., Foster, G. L., Paterson, B. A., Woodhead, J. D., Hergt, J. M., Gray, C. M., & Whitehouse, M. J. (2010). Magmatic and crustal differentiation processes. *Geochimica et Cosmochimica Acta*, 74(12), 3430–3448.

Kendall, B., Creaser , R. A. & Selby , D. (2009).187Re- 187 Os geochronology of Precambrian organic-rich sedimentary rocks. In: Craig , J., Thurow , J.,Thusu , B., Whitham , A. & Abutarruma , Y.(eds) Global Neoproterozoic Petroleum Systems: The Emerging Potential in North Africa. Geological Society, London, Special Publications, 326, 85- 107.

Kennedy, M. J., Runnegar, B., Prave, A. R., Hoffmann, K. H., & Arthur, M. A. (1998). Two or four Neoproterozoic glaciations? Geology, 26(12), 1059-1063.

Kesse, G. O. (1985). *The mineral and rock resources of Ghana*. A.A. Balkema.

Khassen, A., El-Barkooky, A., & Khalil, K. I. (2020). Geochemistry of granitic rocks in the Arabian–Nubian Shield: Tectonic discrimination and petrogenesis. *Precambrian Research*, 341, 105617.

Khassen, B.P., Safonova, I.Y., Yermolov, P.V., Antonyuk, R.M., Gurova, A.V., Obut, O.T., Perfilova, A.A., Savinskiy, I.A. and Tsujimori, T., 2020. The Tekturmas ophiolite belt of central Kazakhstan: Geology, magmatism, and tectonics. Geological Journal, 55(3), pp.2363-2382.

Kirschvink, J. L. (1992). Late Proterozoic low-latitude global glaciation: the snowball Earth. The proterozoic biosphere, 52, 51-52.

Klitsch, M., Bussert, R., & Pazzi, C. (2008). Main results of geological fieldwork in Jabal Arknu, Jabal Babein and Jabal Asbah Areas (SE Al Kufrah Basin) as a base for interpretation of new 2D seismic data in Concession 201, Al Kufrah Basin.(Abstract.) In: Sedimentary Basins of Libya. In Fourth Symposium: Geology of Southern Libya, Tripoli, Libya (pp. 17-20).

Knoll, A. H., Hayes, J. M., Kaufman, A. J., Swett, K., & Lambert, I. B. (1986). Secular variation in carbon isotope ratios from Upper Proterozoic successions of Svalbard and East Greenland. Nature, 321(6073), 832-838.

Knoll, A., Walter, M., Narbonne, G., & Christie, Blick, N. (2006). The Ediacaran Period: a new addition to the geologic time scale. Lethaia, 39(1), 13-30.

Knoll, A.H. & Walter, M.R. 1992: Latest Proterozoic stratigraphy and earth history. Nature 356 , 673 - 678.

Knudsen, T. L. (2001). Contrasting provenance of Triassic/Jurassic sediments in North Sea Rift: a single zircon (SIMS), Sm-Nd and trace element study. Chemical Geology, 171(3-4), 273-293.

Kogbe, C. A. (1976). The Volta Basin: A cratonic sag basin in West Africa. *Geological Magazine*, 113(1), 77–84.

Kramers, J. D., & Tolstikhin, I. N. (1997). Two terrestrial lead isotope paradoxes, forward transport modelling, core formation and the history of the continental crust. *Chemical Geology*, 139(1–4), 75–110.

Krom, M. D., Cliff, R. A., Eijsink, L. M., Herut, B., & Chester, R. (1999). The use of Sr isotopes in detecting desert dust inputs to the eastern Mediterranean. *Marine Chemistry*, 68(1–2), 71–88.

Krom, M. D., Michard, A., Cliff, R. A., & Strohle, K. (1999). Sources of sediment to the Ionian Sea and western Levantine basin of the Eastern Mediterranean during S-1 sapropel times. Marine Geology, 160(1-2), 45-61.

Kuchenbecker, M., Babinski, M., Pedrosa-Soares, A. C., Lopes-Silva, L., & Pimenta, F. (2016). Chemostratigraphy of the lower Bambuí group, southwestern São Francisco craton, Brazil: insights on Gondwana paleoenvironments. Brazilian Journal of Geology, 46, 145-162.

Kuchenbecker, M., Meinhold, G., & Morton, A. C. (2016). Heavy mineral constraints on the provenance of sandstones in West Africa. *Journal of African Earth Sciences*, 120, 12–28.

Kumar, P., Singh, R., & Tandon, S. K. (2021). Application of heavy mineral analysis in fluvial sediment provenance studies. *Sedimentary Geology*, 418, 105934.

Kwayisi, D., Amponsah, P. O., Agra, N. A., Nunoo, S., Thompson, J., Kazapoe, R. W., ... & Nude, P. M. (2024). Neoproterozoic passive margin formation and evolution during the Rodinia–Gondwana supercontinent cycle at the eastern margin of the West African Craton. *Geological Magazine*, *161*, e14.

Kwayisi, D., Lehmann, J., & Elburg, M. (2022). Provenance and depositional setting of the Buem structural unit (Ghana): Implications for the paleogeographic reconstruction of the West African and Amazonian cratons in Rodinia. Gondwana Research, 109, 183-204.

Lacan, F., & Jeandel, C. (2005). Neodymium isotopes as a new tool for quantifying exchange fluxes at the continent–ocean interface. *Earth and Planetary Science Letters*, 232(3–4), 245–257.

Langmuir, C. H., Vocke, R. D., Hanson, G. N., & Hart, S. R. (1978). A general mixing equation with applications to Icelandic basalts. *Earth and Planetary Science Letters, 37*(3), 380–392.

Leube, A., Hirdes, W., Mauer, R., & Kesse, G. O. (1990). The early Proterozoic Birimian Supergroup of Ghana and some aspects of its associated gold mineralization. *Precambrian Research, 46*(1–2), 139–165.

Li , X.-H., Li, Z.-X., Sinclair , J. A., Li, W.-X. & Carter , G. 2006. Revisiting the 'Yanbian Terrane': implications for Neoproterozoic tectonic evolution of the western Yangtze Block, South China. Precambrian Research, 151, 14-30

Li, D., Chen, Y., Zhong, W., Yang, L., & Zhou, J. (2011). Paleozoic sedimentary record of the xing-meng orogenic belt, inner mongolia: implications for the provenances and tectonic evolution of the central asian orogenic belt. Chinese Science Bulletin, 57(7), 776-785.

Li, X. H., Liu, Y., Li, Q. L., & Tang, G. Q. (2020). Advances in Rb–Sr geochronology of igneous and metamorphic rocks. *Gondwana Research*, 80, 282–298.

Li, X., Yang, S., & Li, C. (2011). Geochemistry of river sediments and provenance implications: A case study from China. *Chemical Geology*, 285(1–2), 64–76.

Li, Z. X., Bogdanova, S. V., Collins, A. S., Davidson, A., De Waele, B., Ernst, R. E., Fitzsimons, I. C. W., Fuck, R. A., Gladkochub, D. P., Jacobs, J., Karlstrom, K. E., Lu, S., Natapov, L. M., Pease, V., Pisarevsky, S. A., Thrane, K., & Vernikovsky, V. (2008). Assembly, configuration, and break-up history of Rodinia: A synthesis. *Precambrian Research*, 160(1–2), 179–210.

Luning , S., Kolonic , S., Geiger , M., Thusu , B., Bell , J. S. & Craig , J. 2009. Infracambrian hydro-carbon source rock potential and petroleum prospectivity of NW Africa. In: Craig , J., Thurow , J., Thusu ,B., Whitham , A. & Abutarruma , Y. (eds) Global Neoproterozoic Petroleum Systems: The Emerging Potential in North Africa. Geological Society, London, Special Publications, 326, 157-180.

Luo, M., Chen, J., & Wang, Q. (2007). Sediment provenance and tectonic implications of sandstones in central Asia. *Sedimentary Geology*, 201(3–4), 393–411.

Lupin, D., & Hampson, G. J. (2020). Provenance and depositional processes from petrographic analysis of fluvial sandstones. *Sedimentology*, 67(3), 1183–1204.

Lupin, J. H., & Hampson, G. J. (2020). Sediment-routing controls on sandstone bulk petrographic composition and texture across an ancient shelf: Example from Cretaceous Western Interior Basin, Utah and Colorado, USA. Journal of Sedimentary Research, 90(10), 1389-1409.

Magaritz, M., Holser, W. T., & Kirschvink, J. L. (1986). Carbon-isotope events across the Precambrian/Cambrian boundary on the Siberian Platform. Nature, 320(6059), 258-259.

Magyari, E. K., Szákáll, S., & Záray, G. (1994). Instrumental neutron activation analysis of geological and environmental samples. *Journal of Radioanalytical and Nuclear Chemistry, 183*(2), 297–307.

Mahamuda, M. A., Anani, C. Y., & Abu, A. (2013). Provenance of the Voltaian Supergroup: Insights from petrography and geochemistry. *Journal of African Earth Sciences*, 86, 1–12.

Mahanta, B. N., Sarmah, R. K., & Goswami, T. K. (2019). Elucidation of provenance, palaeoclimate and tectonic setting of the Gondwana sandstones of Arunachal Himalayas: A petrographic approach. *Journal of the Geological Society of India*, 94 (3), 260–266.

Mange, M. A. (2002). Provenance of heavy minerals: A review of methods and applications. *Sedimentary Geology, 152*, 239–268.

Mange, M. A., & Maurer, H. (2012). Heavy minerals in colour. Springer Science & Business Media.

Mange, M. A., & Maurer, H. F. W. (1992). *Heavy minerals in colour*. Chapman & Hall.

Mange, M. A., & Morton, A. C. (2007). Geochemistry of heavy minerals. Developments in sedimentology, 58, 345-391.

Mange, M. A., & Morton, A. C. (2007). Geochemistry of heavy minerals for provenance analysis. In M. A. Mange & D. T. Wright (Eds.), *Heavy minerals in use* (pp. 345–391). Elsevier.

Mange, M. A., & Wright, D. T. (2007). *Heavy minerals in use* (Developments in Sedimentology, Vol. 58). Elsevier.

Mange, M. A., & Wright, D. T. (2007). Heavy minerals in provenance studies. In M. A. Mange & D. T. Wright (Eds.), *Heavy minerals in use* (pp. 1–26). Elsevier.

Mange, M. A., & Wright, D. T. (Eds.). (2007). Heavy minerals in use. Elsevier.

Mann, M. E., Zhang, Z., Hughes, M. K., Bradley, R. S., Miller, S. K., Rutherford, S., & Ni, F. (2009). Global signatures and dynamical origins of the Little Ice Age and Medieval Climate Anomaly. *Science, 326*(5957), 1256–1260.

Marsaglia, K. M., Tazaki, K., & Ingersoll, R. V. (1995). Provenance of sandstones: Framework mineralogy and tectonic setting. *Sedimentary Geology, 100*(1–4), 1–18.

Marsaglia, K., Rimkus, K., & Behl, R. (1995). Provenance of sand deposited in the Santa Barbara basin at site 893 during the last 155,000 years.

McArthur, J. M., Howarth, R. J., & Bailey, T. R. (2012). Strontium isotope stratigraphy: LOWESS version 5 (9 Ma–0 Ma). *Geology, 40*(9), 775–778.

McClellan, E. A.; Steltenpohl, M. G.; Thomas, C.; and Miller, C. F. 2005. Isotopic age constraints and metamorphic history of the Talladega belt: new evidence for timing of arc magmatism

and terrane emplacement along the southern Laurentian margin. In Steltenpohl, M. G., ed. Southernmost Appalachian terranes, Alabama and Georgia. Southeastern section field trip guidebook. Boulder, CO, Geol. Soc. Am., p. 19-50.

McCulloch, M. T., & Wasserburg, G. J. (1978). Sm-Nd and Rb-Sr Chronology of Continental Crust Formation: Times of addition to continents of chemically fractionated mantle-derived materials are determined. Science, 200(4345), 1003-1011.

McDougall, I. A. N., & Watkins, R. T. (2006). Geochronology of the Nabwal Hills: a record of earliest magmatism in the northern Kenyan Rift Valley. Geological Magazine, 143(1), 25-39.

McDougall, I., & Watkins, R. T. (2006). Rb-Sr isotope systematics in weathered sedimentary rocks. *Chemical Geology, 231*(1–2), 1–14.

McLellan, E. L., Spear, F. S., & Pyle, J. M. (2005). Geochemical constraints on metamorphic processes from whole-rock geochemistry. *Journal of Metamorphic Geology, 23*(6), 541–558.

McLellan, M., Schaeffer, A. J., & Audet, P. (2018). Structure and fabric of the crust and uppermost mantle in the northern Canadian Cordillera from Rayleigh-wave tomography. Tectonophysics, 724, 28-41.

McLennan, S. M. (1989). Rare earth elements in sedimentary rocks: Influence of provenance and sedimentary processes. *Reviews in Mineralogy, 21*, 169–200.

McLennan, S. M. (2001). Relationships between the trace element composition of sedimentary rocks and upper continental crust. Geochemistry, Geophysics, Geosystems, 2(4).

McLennan, S. M., & Taylor, S. R. (1991). Sedimentary rocks and crustal evolution: Tectonic setting and secular trends. *Journal of Geology, 99*(1), 1–21.

McLennan, S. M., Hemming, S., McDaniel, D. K., & Hanson, G. N. (1993). Geochemical approaches to sedimentation, provenance, and tectonics. In M. J. Johnson & A. Basu (Eds.), *Processes controlling the composition of clastic sediments* (Vol. 284, pp. 21–40). Geological Society of America.

McLennan, S. M., McCulloch, M. T., Taylor, S. R., & Maynard, J. B. (1989). Effects of sedimentary sorting on neodymium isotopes in deep-sea turbidites. Nature, 337(6207), 547-549.

Mearns, E. W., Knarud, R., Raestad, N., STANLEY, K. T., & Stockbridge, C. P. (1989). Samarium-neodymium isotope stratigraphy of the Lunde and Statfjord formations of Snorre oil field, northern North Sea. Journal of the Geological Society, 146(2), 217-228.

Meert, J. G. (2003). A synopsis of events related to the assembly of eastern Gondwana. *Tectonophysics, 362*(1–4), 1–40.

Melezhik, V. A., Roberts, D., Fallick, A. E., Gorokhov, I. M., & Kusnetzov, A. B. (2005). Geochemical preservation potential of high-grade calcite marble versus dolomite marble: implication for isotope chemostratigraphy. Chemical Geology, 216(3-4), 203-224.

Milliken, K. L. (2000). Diagenetic controls on sequestering of Sr and Ba in sandstones. *Chemical Geology, 168*, 193–209.

Möller, A., Post, N., & Hensen, B. (2002). Crustal residence history and garnet sm-nd ages of high-grade metamorphic rocks from the windmill islands area, east antarctica. International Journal of Earth Sciences, 91(6), 993-1004.

Morad, S., Al-Ruwaih, F. M., & Ketzer, J. M. (2000). Diagenesis of siliciclastic sediments: A brief overview. *Sedimentary Geology, 143*(1–2), 1–7.

Moradi, S., Hosseini-Barzi, M., Armstrong-Altrin, J. S., & Sadeghi, M. (2016). Petrography and geochemistry of the Upper Jurassic sandstones in the Central Alborz Basin, Northern Iran: Implications for provenance and tectonic setting. *Journal of African Earth Sciences, 114*, 166–185.

Morley, C. K. (2010). Stress re-orientation along zones of weak fabrics in rifts: An explanation for pure extension in "oblique" rift segments? *Earth and Planetary Science Letters, 297*(3–4), 667–673.

Morton, A. C. (1985). A new approach to provenance studies: Electron microprobe analysis of detrital garnets from Middle Jurassic sandstones of the northern North Sea. *Sedimentology, 32*(4), 553–566.

Morton, A. C. (1985). Heavy minerals in provenance studies. In G. G. Zuffa (Ed.), *Provenance of arenites* (pp. 249–277). Springer.

Morton, A. C. (1991). Geochemical studies of detrital heavy minerals and their application to provenance research. *Geological Society, London, Special Publications, 57*(1), 31–45.

Morton, A. C., & Chenery, S. (2009). Detrital rutile geochemistry and thermometry as guides to provenance and thermal history of source terrains. *Journal of Sedimentary Research, 79*(7), 540–552.

Morton, A. C., & Hallsworth, C. R. (1994). Identifying provenance-specific features of detrital heavy mineral assemblages in sandstones. *Sedimentary Geology, 90*(3–4), 241–256.

Morton, A. C., & Hallsworth, C. R. (1999). Processes controlling the composition of heavy mineral assemblages in sandstones. *Sedimentary Geology, 124*, 3–29.

Morton, A. C., Hallsworth, C. R., & Chalton, B. (2005). Heavy mineral stratigraphy and provenance of the Brent Group (Middle Jurassic) sandstones, northern North Sea. *Marine and Petroleum Geology, 22*, 791–803.

Moussine-Pouchkine, A., & Bertrand-Sarfati, J. (1997). Tectonosedimentary subdivisions in the Neoproterozoic to Early Cambrian cover of the Taoudenni basin (Algeria-Mauritania-Mali). Journal of African Earth Sciences, 24(4), 425-443.

Nance, R. D., Murphy, J. B., & Santosh, M. (2014). The supercontinent cycle: A retrospective essay. *Gondwana Research, 25*(1), 4–29.

Nascimento, R. S., Sial, A. N., & Pimentel, M. M. (2007). C-and Sr-isotope systematics applied to Neoproterozoic marbles of the Seridó belt, northeastern Brazil. Chemical Geology, 237(1-2), 191-210.

Nebel, O. (2019). Advances and limitations in Rb–Sr geochronology. *Chemical Geology, 510*, 120–134.

Nelson, B. K., & DePaolo, D. J. (1984). 1,700-Myr greenstone volcanic successions in southwestern North America and isotopic evolution of Proterozoic mantle. Nature, 312(5990), 143-146.

Nelson, B. K., & DePaolo, D. J. (1988). Application of Sm–Nd isotopes to sedimentary provenance. *Geology, 16*(5), 408–411.

Nesbitt, H. W., & Young, G. M. (1982). Early Proterozoic climates and plate motions inferred from major element chemistry of lutites. *Nature, 299*(5885), 715–717.

Nesbitt, H. W., Markovics, G., & Price, R. C. (1980). Chemical processes affecting alkalis and alkaline earths during continental weathering. *Geochimica et Cosmochimica Acta, 44*(11), 1659–1666.

Nichols, G. (2009). *Sedimentology and stratigraphy* (2nd ed.). Wiley-Blackwell.

Norman, M. D., Garcia, M. O., & Bennett, V. C. (2003). Geochemistry of shield-building Hawaiian tholeiites: Implications for petrogenesis. *Geochimica et Cosmochimica Acta, 67*(19), 3149–3173.

Ogbahon, O. E., & Olujinmi, J. O. (2019). Provenance and tectonic setting of Cretaceous sediments in southwestern Nigeria. *Journal of African Earth Sciences, 151*, 31–42.

Oghenekome, C., Ojo, O. J., & Ola, P. S. (2018). Petrography and geochemistry of sandstones from the Benue Trough: Implications for provenance. *Journal of African Earth Sciences, 141*, 104–115.

O'nions, R. K., Hamilton, P. J., & Hooker, P. J. (1983). A Nd isotope investigation of sediments related to crustal development in the British Isles. Earth and Planetary Science Letters, 63(2), 229-240.

Osae, S., Asiedu, D. K., Banoeng-Yakubo, B., Koeberl, C., & Dampare, S. B. (2006). Provenance and tectonic setting of sediments from the Volta Basin, Ghana: Evidence from geochemistry and detrital zircon ages. *Journal of African Earth Sciences, 46*(3), 318–328.

Osae, S., Asiedu, D. K., Banoeng-Yakubo, B., Koeberl, C., & Dampare, S. B. (2006). Provenance and tectonic setting of Late Proterozoic Buem sandstones of southeastern Ghana: Evidence from geochemistry and detrital modes. Journal of African Earth Sciences, 44(1), 85-96.

Pandita, S. K., Ahmad, S. M., & Bhat, G. M. (2014). Geochemistry of sandstones from the Lesser Himalaya: Implications for provenance and tectonic setting. *International Journal of Earth Sciences, 103*(6), 1679–1694

Pandita, S., Bhat, S., Kotwal, S., Singh, Y., & Thakur, K. (2014). Provenance and tectonic settings of the lower siwalik subgroup, jammu, northwest himalaya. Journal of Palaeosciences, 63((1-2)), 17-23.

Pearce, J. A. (2014). Geochemical fingerprinting of oceanic basalts with applications to tectonic discrimination. *Annual Review of Earth and Planetary Sciences*, *42*, 105–134.

Pearce, J. A. (2014). Immobile element fingerprinting of ophiolites. *Elements, 10*(2), 101–108.

Pearce, J. A., Harris, N. B., & Tindle, A. G. (1984). Trace element discrimination diagrams for the tectonic interpretation of granitic rocks. Journal of petrology, 25(4), 956-983.

Pearce, J. A., Kempton, P. D., Nowell, G. M., & Noble, S. R. (1999). Hf–Nd element and isotope perspective on the nature and provenance of mantle and subduction components in Western Pacific arc-basin systems. *Journal of Petrology, 40*(11), 1579–1611.

Pearson, D. G. (1999). The age of continental roots. *Lithos*, *48*(1-4), 171–194.

Pearson, D. G., & Wittig, N. (2014). The formation and evolution of cratonic mantle lithosphere—Evidence from mantle xenoliths. In *Treatise on geochemistry* (2nd ed., pp. 255–292). Elsevier.

Pedrosa-Soares, A. C., Noce, C. M., Wiedemann, C. M., & Pinto, C. P. (2001). The Araçuaí–West Congo orogen in Brazil: An overview of a confined orogen formed during Gondwanaland assembly. *Precambrian Research*, *110*(1), 307–323.

Petersson, A., Elhers, J., & Amponsah, P. (2012). Petrographic and mineralogical studies of the Voltaian sandstones in the Northern Region, Ghana. *Journal of African Earth Sciences*, *64*, 97–110.

Petit, J.R., Jouzel, J., Raynaud, D., Barkov, N.I., Barnola, J.M., Basile, I., Bender, M., Chappellaz, J., Davis, M., Delaygue, G. and Delmotte, M., "Climate and atmospheric history of the past 420,000 years from the Vostok ice core, Antarctica." Nature 399, no. 6735 (1999): 429-436.

Petrelli, M. and Perugini, D. (2016). Solving petrological problems through machine learning: the study case of tectonic discrimination using geochemical and isotopic data. Contributions to Mineralogy and Petrology, 171(10).

Petrelli, M., & Perugini, D. (2016). Whole-rock geochemistry and magmatic processes: New approaches to igneous petrology. *Lithos*, *252–253*, 116–130.

Pettijohn, F. J. (1975). *Sedimentary rocks* (3rd ed.). Harper & Row.

Pettijohn, F. J., Potter, P. E., & Siever, R. (1987). *Sand and sandstone* (2nd ed.). Springer.

Piepgras, D. J., & Wasserburg, G. J. (1980). Neodymium isotopic variations in seawater. *Earth and Planetary Science Letters*, *50*(1), 128–138.

Pisarevsky , S. A., Murphy , J. B., Cawood , P. A. & Collins , A. S. 2008. Late Neoproterozoic and Early Cambrian palaeogeography: models and problems.In: Pankhurst , R. J., Trouw , R. A. J., De Briton Eves , B. B. & De Wit , M. J. (eds) West Gondwana:Pre-Cenozoic Correlation Across the South Atlantic Region. Geological Society, London, Special Publi-cations, 294, 9 -31

Potter, P. E. (1977). *Petrology of sedimentary rocks*. Springer.

Potter, P. E. (1978). Significance and uses of conglomerate clasts in sedimentology. *Journal of Sedimentary Petrology*, *48*(2), 497–505.

Potter, P. E., & Pettijohn, F. J. (1977). *Paleocurrents and basin analysis* (2nd ed.). Springer-Verlag.

Potts, P. J., & Webb, P. C. (1992). X-ray fluorescence spectrometry. *Journal of Geochemical Exploration*, *44*(1–3), 251–296.

Quick, J. C., Dott, R. H., & Witzke, B. J. (2019). Provenance analysis of conglomerates: New insights into basin evolution. *Sedimentary Geology*, *385*, 123–134.

Reading, H. G. (1996). *Sedimentary environments: Processes, facies, and stratigraphy* (3rd ed.). Blackwell Science.

Reading, H. G. (Ed.). (2009). Sedimentary environments: processes, facies and stratigraphy. John Wiley & Sons.

Reddy, S. M., et al. (2020). In-situ Rb–Sr dating: Applications to metamorphic minerals. *Journal of Metamorphic Geology*, *38*(8), 829–844.

Rollinson, H. (1993). *Using geochemical data: Evaluation, presentation, interpretation*. Longman.

Rollinson, H. (2021). *Early Earth systems: A geochemical approach* (2nd ed.). Wiley-Blackwell.

Rollinson, H. R. (2007). *Using geochemical data: Evaluation, presentation, interpretation* (2nd ed.). Pearson.

Rollinson, H., & Pease, V. (2021). *Using geochemical data: A guide for Earth scientists* (2nd ed.). Cambridge University Press.

Romans, B. W., Fildani, A., Graham, S. A., Hubbard, S. M., & Covault, J. A. (2016). Environmental signal propagation in sedimentary systems across timescales. *Earth-Science Reviews*, *153*, 7–29.

Rudnick, R. L., & Fountain, D. M. (1995). Nature and composition of the continental crust: A lower crustal perspective. *Reviews of Geophysics*, *33*(3), 267–309.

Rudnick, R. L., & Gao, S. (2014). Composition of the continental crust. In *Treatise on geochemistry* (2nd ed., pp. 1–51). Elsevier.

Sahraeyan, M. and Bahrami, M. (2012). Petrography and provenance of sandstones from the aghajari formation, folded zagros zone, southwestern iran. International Journal of Basic and Applied Sciences, 1(3).

Sahraeyan, M. and Bahrami, M. (2012) Petrography and Provenance of Sandstones from the Aghajari Formation, Folded Zagros Zone, Southwestern Iran. International Journal of Basic and Applied Sciences, 1, 283-298.

Sang, S., Xu, H., & Li, Z. (2018). Diagenetic modification of sandstones and its influence on provenance interpretation. *Marine and Petroleum Geology*, *97*, 115–130.

Sawakuchi, A. O., Bertotti, A., Mendes, V. R., & Almeida, R. P. (2020). Provenance of sands from South America: Constraints from heavy minerals and zircon U–Pb ages. *Sedimentary Geology*, *401*, 105650.

Sawakuchi, A. O., Rodrigues, F. C. G., Mineli, T. D., Mendes, V. R., Melo, D. B., Chiessi, C. M., & Giannini, P. C. F. (2020). Optically stimulated luminescence sensitivity of quartz for provenance analysis. Methods and Protocols, 3(1), 6.

Schmidberger, S. S., Simonetti, A., & Francis, D. (2002). Probing the mantle lithosphere of the North American craton using Lu–Hf and Sm–Nd isotope systematics of garnet and clinopyroxene peridotite xenoliths. *Geochemistry, Geophysics, Geosystems*, *3*(11), 1–20.

Scotese, C. R. 2009. Late Proterozoic plate tectonics and palaeogeography: a tale of two supercontinents, Rodinia and Pannotia. In: Craig , J., Thurow , J.,Thusu , B., Whitham , A. & A Butarruma , Y.(eds) Global Neoproterozoic Petroleum Systems: The Emerging Potential in North Africa. GeologicalSociety, London, Special Publications, 326, 67-83

Shackleton, N. (1967). Oxygen isotope analyses and Pleistocene temperatures re-assessed. Nature, 215(5096), 15-17.

Sharman, G. R., Graham, S. A., & Grove, M. (2019). Detrital zircon provenance studies of forearc and retroarc basins. *Earth-Science Reviews*, *197*, 102895.

Shirey, S. B., & Walker, R. J. (1998). The Re-Os isotope system in cosmochemistry and high-temperature geochemistry. *Annual Review of Earth and Planetary Sciences*, *26*(1), 423–500.

Sial, A. N., Karhu, J. A., & Ferreira, V. P. (2010). Insights from isotope stratigraphy. Precambrian Research, 182(4), v.

Smale, D. (1997). Provenance of Permian sandstones in Australia: Insights from heavy mineral analysis. *Sedimentary Geology*, *112*(1–2), 53–67.

Smith , A. G. 2009. Neoproterozoic timescales and strati-graphy. In: Craig , J., Thurow , J., Thusu , B.,Whitham , A. & Abutarruma , Y. (eds) Globa lNeoproterozoic Petroleum Systems: The Emerging Potential in North Africa. Geological Society, London, Special Publications, 326, 27-54

Smith, G. M., Miller, R. B., & White, J. D. (2014). Provenance of Eocene sediments in the Pacific Northwest: Implications for tectonics and climate. *Geosphere*, *10*(4), 768–785.

Spalletti, L. A., Limarino, C. O., & Colombo, F. (2008). Sedimentology, petrography, and provenance of Upper Paleozoic siliciclastic sequences from the Paganzo Basin, Argentina. *Sedimentary Geology*, *203*(1–2), 107–126.

Spandler, C., Arculus, R., Eggins, S., Mavrogenes, J., Price, R., & Reay, A. (2003). Petrogenesis of the greenhills complex, southland, new zealand: magmatic differentiation and cumulate

formation at the roots of a permian island-arc volcano. Contributions to Mineralogy and Petrology, 144(6), 703-721

Spandler, C., Hermann, J., Arculus, R., & Mavrogenes, J. (2003). Geochemical constraints on magma genesis in subduction zones. *Journal of Petrology*, *44*(6), 1031–1055.

Spear, F. S., & Pyle, J. M. (2010). The role of accessory minerals in metamorphic processes. *Reviews in Mineralogy and Geochemistry*, *72*(1), 105–147.

Spear, F. S., & Pyle, J. M. (2010). Theoretical modeling of monazite growth in a low-Ca metapelite. Chemical Geology, 273(1-2), 111-119.

Spencer, C. J., Kirkland, C. L., & Taylor, R. J. M. (2016). Strategies towards statistically robust interpretations of detrital zircon U–Pb datasets. *Earth-Science Reviews*, *156*, 1–21.

Stracke, A. (2012). Earth's mantle heterogeneity: Constraints from Sr–Nd–Pb–Hf isotopes. *Annual Review of Earth and Planetary Sciences*, *40*, 87–111.

Stuut, J. (2005). Provenance of present? day eolian dust collected off NW Africa. Journal of Geophysical Research Atmospheres, 110(D4).

Stuut, J. B. W. (2005). Provenance of desert dust: A review of mineralogical, geochemical, and isotopic approaches. *Earth-Science Reviews*, *72*(1–2), 1–20.

Sun, S. S., & McDonough, W. F. (1989). Chemical and isotopic systematics of oceanic basalts: implications for mantle composition and processes. Geological Society, London, Special Publications, 42(1), 313-345.

Sun, S., Li, X., & Yang, S. (2022). Provenance of East Asian River sands from heavy mineral analysis. *Sedimentary Geology*, *423*, 106025.

Sylvester, P. J. (1998). Post-collisional strongly peraluminous granites. *Lithos, 45*(1–4), 29–44.

Tang, D., Xu, W., Wang, Q., Pei, F., Xu, J., & Zhao, Q. (2016). Geochemistry of the late Paleozoic sediments in the southern North China Block: Implications for provenance, tectonic setting, and paleoweathering. *Sedimentary Geology, 335*, 88–101.

Tang, Y., Zhang, K., Zhang, Y., Wu, T., & Sun, S. (2016). Geochemical characteristics and provenance of late Paleozoic sandstones in the northwestern Junggar Basin, China. *Journal of Asian Earth Sciences, 117*, 273–288.

Tangari, D., Sharma, A., & Singh, M. (2024). Heavy mineral assemblages as indicators of provenance in Himalayan foreland basins. *Sedimentary Geology*, *435*, 106178.

Taylor S. R. and McLennan S. M. 1985. The continental crust: Its composition and evolution. Oxford: Blackwell. 312 p.

Taylor, P. N., Moorbath, S., & Leube, A. (1992). Radiogenic isotope studies on granitoid rocks from the Ghanaian Shield: Constraints on crustal evolution. *Precambrian Research*, *56*(1–2), 107–123.

Taylor, S. R., & McLennan, S. M. (1995). The geochemical evolution of the continental crust. *Reviews of Geophysics*, *33*(2), 241–265.

Taylor, S. R., & McLennan, S. M. (2001). Chemical composition and element distribution in the Earth's crust. Encyclopedia of physical science and technology, 312, 697-719.

Taylor, S. R., & McLennan, S. M. (2001). The composition of the continental crust: Geochemical constraints and models. *Geological Society, London, Special Publications*, *201*(1), 31–45.

Taylor, S. R., McLennan, S. M., & McCulloch, M. T. (1980). Geochemistry of loess, continental crustal composition and crustal model ages. *Geochimica et Cosmochimica Acta, 44*(6), 875–895.

Tegan, J. (2023). Sedimentary provenance analysis and tectonic reconstruction: A review. *Earth-Science Reviews*, *235*, 104289.

Tegan, N. (2023). Geochemical exploration of sediments in the Toumodi region: origin of metasediments, geological dynamics, and perspectives for regional geological history. Open Journal of Geology, 13(12), 1255-1270. https://doi.org/10.4236/ojg.2023.1312054

Tortosa, A., Arribas, J., & Critelli, S. (1991). Composition of sandstones from the Iberian Range (Spain): Relationships between paleogeography and tectonics. *Sedimentary Geology, 71*(1–2), 13–33.

Toteu, S. F., Fouateu, R. Y., Penaye, J., Tchakounte, J., Mouangue, A. C. S., Van Schmus, W. R., ... & Stendal, H. (2006). U–Pb dating of plutonic rocks involved in the nappe tectonic in southern Cameroon: consequence for the Pan-African orogenic evolution of the central African fold belt. *Journal of African Earth Sciences*, *44*(4-5), 479-493.

Totten, M. W., Hanan, M. A., & Stern, R. J. (2000). Geochemistry of clastic sediments in the Ouachita Mountains: Implications for the tectonic evolution of the southern margin of Laurentia. *Geological Society of America Bulletin, 112*(6), 1014–1029.

Totten, M. W., Hanan, M. A., & Weaver, B. L. (2000). Beyond whole-rock geochemistry of shales: The importance of assessing mineralogical effects on trace element behavior. *Sedimentary Geology, 133*(1–2), 5–20.

Tribovillard, N., Algeo, T. J., Lyons, T., & Riboulleau, A. (2006). Trace metals as paleoredox and paleoproductivity proxies: An update. *Chemical Geology*, *232*(1–2), 12–32.

Trompette, R., 1994. Geology of Western Gondwana (2000-500Ma), Pan-African Brasiliano Aggregation of South America and Africa. Balkema, Rotterdam, 350 pp.

Trompette, R., Carozzi, A. V., & Affaton, P. (1980). Lithostratigraphy and sedimentary history of the Volta Basin (Upper Proterozoic) of Ghana and Togo. *Precambrian Research*, *13*(2), 125–144.

Turner, D. C. (2009). *The geology of Ghana*. Geological Survey Department of Ghana.

Ueki, K., Hino, H., & Kuwatani, T. (2018). Geochemical discrimination and characteristics of magmatic tectonic settings: a machine?learning?based approach. Geochemistry Geophysics Geosystems, 19(4), 1327-1347.

Urrutia-Fucugauchi, J., Perez-Cruz, L., & Soler-Arechalde, A. (2021). Whole-rock geochemical studies: Applications to petrology and tectonics. *Boletín de la Sociedad Geológica Mexicana*, *73*(1), 1–16.

Urrutia-Fucugauchi, J., Pérez-Cruz, L., & Urrutia, A. (2021). Chicxulub museum, geosciences in mexico, outreach and science communication - built from the crater up. Geoscience Communication, 4(2), 267-280.

Van Grieken, R., & Markowicz, A. (2002). *Handbook of X-ray spectrometry* (2nd ed.). CRC Press.

Vance, D., & Thirlwall, M. F. (2002). An assessment of mass discrimination in MC-ICPMS using Nd isotopes. *Chemical Geology, 185*(3–4), 227–240.

Veizer, J. (1986). Evolution of the isotopic composition of seawater. In J. W. Valley, H. P. Taylor Jr., & J. R. O'Neil (Eds.), *Stable isotopes in high temperature geological processes* (pp. 595–662). Mineralogical Society of America, Reviews in Mineralogy, 16.

Veizer, J. (1986). Strontium isotopes in seawater through time. *Annual Review of Earth and Planetary Sciences, 14*(1), 527–567.

Veizer, J. (1988). The evolving continental crust: Evidence from isotopic and chemical signatures. *Reviews of Geophysics*, *26*(1), 1–23.

Veizer, J. (2005). Depositional and diagenetic history of limestones: stable and radiogenic isotopes. In Isotopic signatures and sedimentary records (pp. 13-48). Berlin, Heidelberg: Springer Berlin Heidelberg.

Veizer, J., Holser, W. T., & Wilgus, C. K. (1980). Correlation of 13C12C and 34S32S secular variations. Geochimica et Cosmochimica Acta, 44(4), 579-587.

Vermeesch, P. (2012). On the visualisation of detrital age distributions. *Chemical Geology*, *312–313*, 190–194.

Vermeesch, P. (2018). Statistical models for detrital zircon U-Pb geochronology. *Geochronology*, *1*(1), 1–23.

Vermeesch, P., & Garzanti, E. (2015). Making geological sense of 'big data' in sedimentary provenance. *Chemical Geology*, *409*, 20–27.

Vervoort, J. D., & Patchett, P. J. (1996). Behavior of hafnium and neodymium isotopes in the crust: Constraints from Precambrian crustally derived granites. *Geochimica et Cosmochimica Acta*, *60*(19), 3717–3733.

Vignoli, G., Dzikunoo, E., Jørgensen, F., Yidana, S., Banoeng-Yakubo, B., & Bai, P. (2020). Geophysical modelling of a sedimentary portion of the white volta basin (Ghana)., 891-902.

Vignoli, L., Abu, M., & Garzanti, E. (2020). Stratigraphic architecture and sediment provenance of the Volta Basin, Ghana. *Precambrian Research*, *345*, 105720.

Villa, I. M. (2016). The Rb–Sr isotope system: Principles and applications. *Geochemistry*, *76*(2), 91–111.

Villeneuve, M. (2005). Pan-African Orogeny: Structure and evolution of the West African Craton and adjoining mobile belts. *Journal of African Earth Sciences*, *43*, 195–224.

Villeneuve, M., & Cornée, J.-J. (1994). Structure, evolution and palaeogeography of the West African craton and bordering belts during the Neoproterozoic. *Precambrian Research, 69*(1–4), 307–326.

Villeneuve, M., & Dallmeyer, R. D. (1987). Geodynamic evolution of the Mauritanide and Rokelide orogens (West Africa): Evidence from 40Ar/39Ar mineral ages. *Tectonophysics, 139*(1–2), 167–211.

Vukmanovic, Z., et al. (2019). Rb–Sr systematics of magmatic systems. *Contributions to Mineralogy and Petrology*, *174*(6), 1–19.

Wang, H., Yang, S., & Li, C. (2018). Sediment provenance and weathering in East Asian river systems: Insights from geochemistry and zircon U–Pb dating. *Sedimentary Geology*, *375*, 21–36.

Wang, Y., Xu, W., Wang, F., & Li, X. (2018). New insights on the early Mesozoic evolution of multiple tectonic regimes in the northeastern north China craton from the detrital zircon provenance of sedimentary strata..

Weaver, B. L. (1989). Geochemistry of highly peraluminous granites, and the origin of monazite. *Contributions to Mineralogy and Petrology, 103*(4), 429–438.

Weaver, C. E. (1989). *Clays, muds, and shales*. Elsevier

Wei, J., & Algeo, T. J. (2020). Application of trace-element proxies to paleoenvironmental reconstruction. *Earth-Science Reviews*, *205*, 103203.

Weldeab, S., Siebel, W., Wehausen, R., & Emeis, K. C. (2003). Provenance of late Quaternary deep-sea sediments in the eastern Mediterranean: Evidence from Nd and Sr isotopes. *Marine Geology*, *202*(3–4), 183–195.

Weldeab, S., Siebel, W., Wehausen, R., Emeis, K. C., Schmiedl, G., & Hemleben, C. (2003). Late Pleistocene sedimentation in the Western Mediterranean Sea: implications for productivity changes and climatic conditions in the catchment areas. Palaeogeography, Palaeoclimatology, Palaeoecology, 190, 121-137.

Weltje, G. J. (2012). Quantitative models of sediment generation and provenance. *Sedimentary Geology*, *280*, 38–56.

Weltje, G. J., & von Eynatten, H. (2004). Quantitative provenance analysis of sediments: Review and outlook. *Sedimentary Geology, 171*(1–4), 1–11.

Williams, H. R., Thomas, R. J., & Boadi, B. (2015). The Pan-African reworking of the West African Craton in Ghana: New evidence from the northeast margin of the Volta Basin. *Geological Society, London, Special Publications*, *423*(1), 183–202.

Wilson, M. (1989). *Igneous petrogenesis: A global tectonic approach*. Springer.

Wilson, M. (Ed.). (1989). Igneous petrogenesis. Dordrecht: Springer Netherlands.

Winter, J. D. (2001). *An introduction to igneous and metamorphic petrology*. Prentice Hall.

Winter, J. D. (2010). *Principles of igneous and metamorphic petrology* (2nd ed.). Pearson.

Wong, F. L., Woodrow, D. L., McGann, M. L., Barnard, P. L., Foxgrover, A. C., Elias, E., Erikson, L. H., & Takesue, R. K. (2013). Heavy mineral analysis for assessing the provenance of sandy sediment in the San Francisco Bay coastal system. *Marine Geology*, *345*, 170–180.

Wong, W. H., & Tam, S. F. (1974). Sedimentary structures and depositional environments of the Lower Paleozoic sedimentary rocks of Hong Kong. *Journal of Sedimentary Petrology, 44*(2), 567–580.

Worden, R. H., & Burley, S. D. (2003). Sandstone diagenesis: The evolution of sand to stone. In R. H. Worden & S. D. Burley (Eds.), *Sandstone diagenesis: Recent and ancient* (pp. 3–44). Blackwell.

Yang, J., Li, X.-H., & Zhao, G. (2012). Geochemistry of late Neoproterozoic sediments from South China: Implications for weathering, provenance, and tectonic setting. *Precambrian Research, 212–213*, 223–236.

Yang, S., Li, C., & Li, X. (2009). Heavy mineral compositions of the Changjiang (Yangtze River) sediments and their provenance implications. *Sedimentary Geology*, *222*(1–2), 1–12.

Yang, S., Li, C., & Wan, S. (2009). Geochemical record of chemical weathering and monsoon climate change since the early Miocene in the South China Sea. *Paleoceanography, 24*(2), PA2209.

Yao, W. (2023). Trace element geochemistry of sedimentary basins: Paleoenvironmental and provenance implications. *Sedimentary Geology*, *440*, 106159.

Yao, Z. (2023). Provenance, depositional environment, and paleoclimatic conditions of a near-source fan delta: a case study of the Permian Jiamuhe formation in the Shawan sag, junggar basin. Minerals, 13(10), 1251.

Zachos, J., Pagani, M., Sloan, L., Thomas, E., & Billups, K. (2001). Trends, rhythms, and aberrations in global climate 65 Ma to present. science, 292(5517), 686-693.

Zhang, K. J., Zhang, Y. X., Li, B., & Zhong, L. F. (2007). Nd isotopes of siliciclastic rocks from Tibet, western China: Constraints on provenance and pre-Cenozoic tectonic evolution. Earth and Planetary Science Letters, 256(3-4), 604-616.

Zhao, Z. F., Zheng, Y. F., Gao, T. S., WU, Y. B., Chen, B., Chen, F. K., & Wu, F. Y. (2006). Isotopic constraints on age and duration of fluid-assisted high-pressure eclogite-facies recrystallization during exhumation of deeply subducted continental crust in the Sulu orogen. Journal of metamorphic Geology, 24(8), 687-702.

Zhu, H., & Zeng, L. (2021). Mineralogical and geochemical constraints on sediment provenance and tectonic setting of the Mesozoic–Cenozoic basins in South China. *Journal of Asian Earth Sciences, 205*, 104618.

Zhu, W., Zheng, B., Chen, J., & Wang, H. (1999). Geochemistry of clastic rocks of the Neoproterozoic Shisanlitai Formation, southern Anhui, China: Implications for provenance and tectonic setting. *Precambrian Research, 98*(3–4), 267–285.

Zindler, A., & Hart, S. (1986). Chemical geodynamics. IN: Annual review of earth and planetary sciences. Volume 14 (A87-13190 03-46). Palo Alto, CA, Annual Reviews, Inc., 1986, p. 493-571., 14, 493-571.

Zobah, T. N., Adenutsi, C. D., Amedjoe, G. C., Wilson, M. C., Boateng, C. D., Quaye, J. A., ... & Danuor, S. K. (2022). A review on the provenance of the Voltaian Basin, Ghana: Implications for hydrocarbon prospectivity. *Scientific African*, *18*, e01429.